THÈSE

En vue de l'obtention du

DOCTORAT DE L'UNIVERSITÉ DE TOULOUSE

Délivré par *l'Université Toulouse III - Paul Sabatier*
Discipline ou spécialité : *Physique de l'Atmosphère*

Présentée et soutenue par *Oscar Arnoud VAN DER VELDE*
Le *jeudi 21 février 2008*

Titre : *Morphologie de sprites et conditions de productions de sprites et de jets dans les systèmes orageux de méso-échelle*

JURY

Serge CHAUZY	*Professeur, Université Toulouse III*	*Président*
Martin FÜLLEKRUG	*Senior Scientist, Université de Bath (GB)*	*Rapporteur*
Pierre LAROCHE	*Ingénieur Chercheur, ONERA*	*Rapporteur*
Elisabeth BLANC	*Directrice de Recherche, CEA*	*Examinateur*
Torsten NEUBERT	*Senior Scientist, National Space Institute (DK)*	*Examinateur*
Joan MONTANYÀ	*Prof. associé, Univ. Polytechnique de Catalogne*	*Membre invité*
Serge SOULA	*Physicien OMP, Université Toulouse III*	*Directeur de thèse*

Ecole doctorale : *Sciences de l'Univers, de l'Environnement et de l'Espace (SDU2E)*
Unité de recherche : *Laboratoire d'Aérologie*
Directeur(s) de Thèse : *Serge SOULA*
Rapporteurs : *Martin FÜLLEKRUG et Pierre LAROCHE*

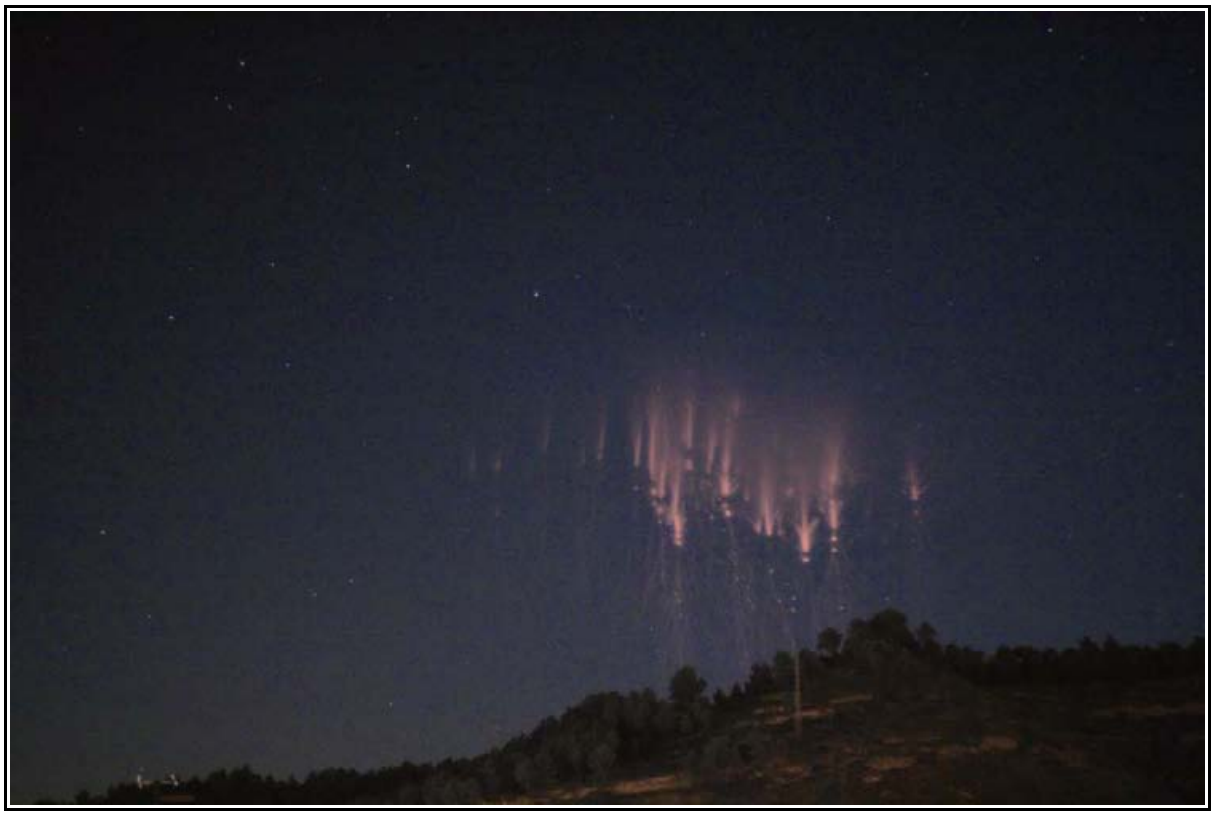

Photo: A "jellyfish" red sprite, photographed by the author with a Canon EOS 350D modified to pass infrared light. It occurred in the evening of 8 October 2009, at 21:43:54 UT and was triggered by a lightning flash 8 km ENE of Nant, southern France, at a distance of 290 km from the location of observation (Sant Vicenç de Castellet in northeastern Spain). Settings: ISO 1600, 0.3 seconds at f/1.6, 50 mm lens, RAW.

Remerciements

My first thanks go to Serge Soula, my Directeur de Thèse, for his support and patience (waiting for me to deposit the final thesis document, now three years after the Soutenance!). Thank you for everything Serge, and we sure will keep working together on new articles for the years to come! At the Laboratoire I enjoyed also the lunch conversations with Serge Chauzy, and I am thankful to my office-mate Marie-Pierre, who also was a great company for my cat at the office when I was on holiday! I really appreciate the help all three of you provided me.

Second, I'd like to acknowledge everyone who made possible the EU FP5 research training network “Coupling of Atmospheric Layers” (CAL), which provided us with an extremely interesting research topic and funding. In particular, thank you Torsten Neubert, not only for your organizing work which made it all possible but also for making it a big success and establishing a strong bond between European research groups, of which I still reap the benefits today (and surely not only me). I am grateful also to the rest of the Danish Space Center team for the observations infrastructure and resulting data which provided the basis of this dissertation.

The CAL community felt like a warm, comfortable home to me, with stimulating interactions and informal activities with “senior” scientists as well as my fellow “Young Scientists”, which were very welcome, because in Toulouse we were the only two persons investigating sprites! With the same joy I look back at the inspiring and fruitful interactions with my colleagues overseas, as well as the short term mission (COST P18 Lightning) in the Israeli sprite group. I'm already looking forward to meeting all of you again!

I'd like to take also the opportunity here to express my gratitude, gladly one more time, to the anonymous reviewers for their efforts of constructively reviewing (and thereby indeed improving) the submitted journal articles of my dissertation work.

Furthermore, I am grateful to Joan Montanyà for managing a smooth transition for me between Toulouse and my new position in the Lightning Research Group of the Technical University of Catalonia, as part of the new ESA Atmosphere-Space Interactions Monitor (ASIM) project, which follows up CAL.

And finally, a warm thank you to my friends, distant or by my side, who I have seen once a year or every day, and to my parents, brothers and other family in The Netherlands. A happy life with fun besides this thesis was not possible without you!

Greetings to you all and I hope you will enjoy reading.

Table des Matières

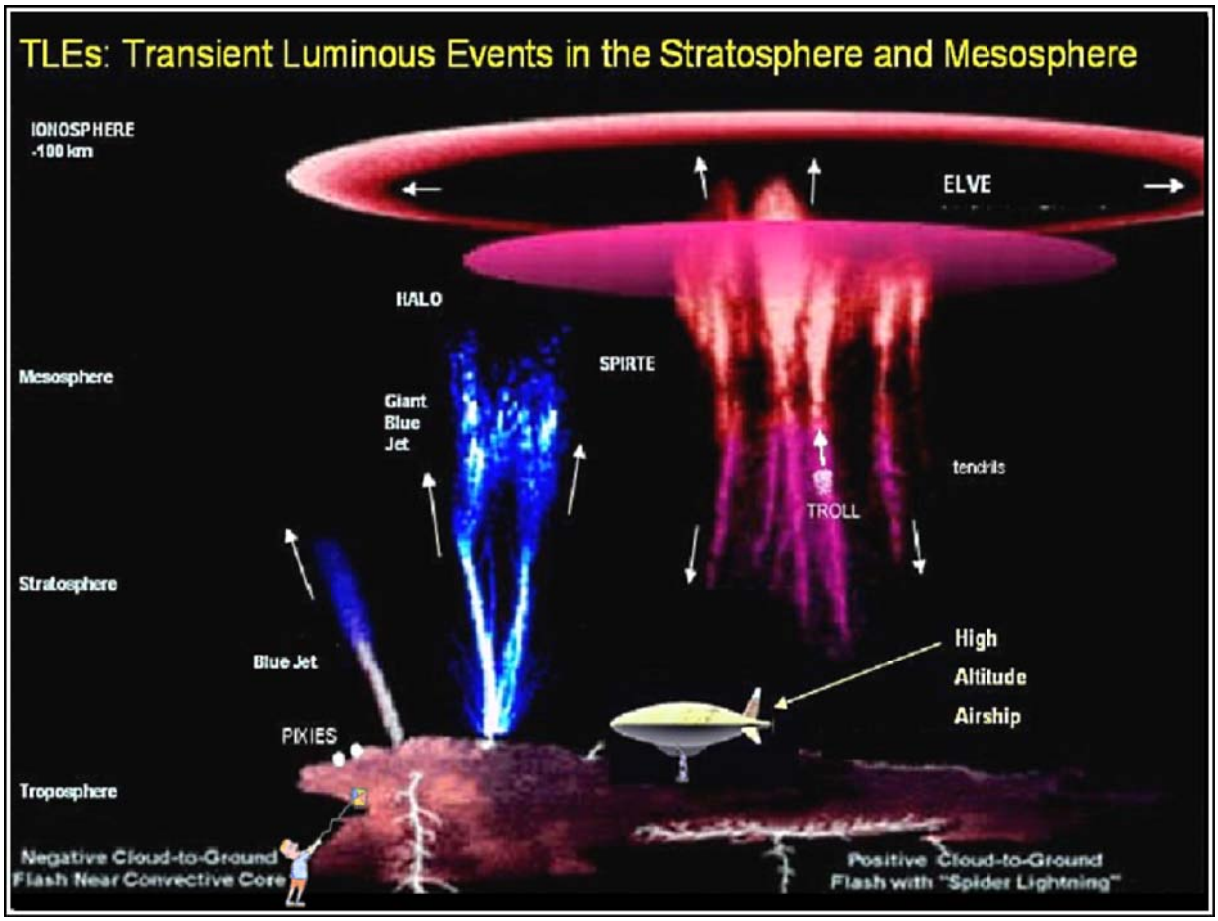

Figure 1. Overview of the family of Transient Luminous Events and their typical position over a thunderstorm: blue jets, gigantic jets, pixies, trolls, sprites, elves and halos. Image courtesy of Walter Lyons (except kite).

1 Introduction générale

Le terme TLE est maintenant évoqué couramment dans la communauté scientifique en physique de l'environnement. Littéralement de l'anglais Transient Luminous Event, il désigne des phénomènes lumineux transitoires qui se produisent au-dessus des orages sur plusieurs dizaines de km de hauteur et dont on connaît l'existence depuis environ 18 ans. C'est en effet en 1989 et en testant une caméra sensible, qu'une équipe de l'Université du Minnesota obtint une image montrant une émission lumineuse de courte durée dans la direction d'un orage qui se trouvait derrière l'horizon (Franz et al., 1990). Cette première observation d'une longue série était un cas de "red sprite", un de ces TLEs qui apparaît au-dessus des orages de grande taille et qui maintenant a été détecté dans toutes les régions du monde. Des témoignages, notamment de pilotes, avaient bien indiqué des brefs éclairs de forme et couleur très variées visibles à l'œil nu au-dessus des orages, mais le risque qu'ils pouvaient représenter pour leur crédibilité professionnelle fait qu'ils préféraient souvent ne rien déclarer du tout. Parmi toutes ces observations, certaines correspondaient aussi à des éclairs qui semblaient se développer verticalement à partir du nuage et qui allaient être confirmées un peu plus tard en 1994 avec la découverte des "blue jets" sous la forme de décharges coniques par une équipe de l'Université d'Alaska au cours de vols autour d'orages dans l'état de l'Arkansas aux USA (Wescott et al. 1995). Certains avaient même un tel développement vertical qu'ils ont pris le nom de "gigantic jets" découverts en 2002 pendant une campagne à Porto Rico (Pasko et al. 2002). En fait, ces phénomènes relient électriquement le sommet du nuage d'orage à la couche inférieure de l'ionosphère qui se trouve la nuit à une altitude d'environ 80 km. Les observations se sont étendues à partir d'engins spatiaux et en 1995, on a augmenté la diversité du phénomène avec un nouveau membre constitué par les "elves", sortes de cercle lumineux à la base de l'ionosphère plus facile à observer depuis l'espace aux limbes de la Terre (Fukunishi et al. 1996). Ces TLEs sont liés à des champs électriques ou à des impulsions électro-magnétiques générés par les orages. Il reste un certain nombre de questions sans réponse autour de ces phénomènes, notamment le taux de production global et la relation précise entre l'éclair et le sprite. Aussi, des campagnes d'observation depuis le sol, associant de plus en plus de moyens pour caractériser l'ensemble des processus mis en jeu, se font régulièrement sur plusieurs continents et à des saisons différentes de l'année. Plusieurs projets spatiaux d'étude de ces phénomènes sont soit en cours (ISUAL au Japon) soit en préparation (TARANIS, ASIM en Europe).

La découverte de ces TLEs mais aussi des Flashs Gamma d'origine Terrestres (TGFs) a révolutionné notre compréhension de l'environnement de la Terre en révélant une occurrence importante de transferts d'énergie impulsifs entre la troposphère et les couches supérieures de l'atmosphère. L'énergie totale dissipée par ces événements pris individuellement est de l'ordre de dizaines de Mégajoules et les puissances mises en jeu se comptent en Gigawatts. Les énergies des électrons intervenant dans les décharges électriques varient de quelques eV à des dizaines de MeV en produisant des émissions dans

l'ensemble du spectre électromagnétique. L'impact de ces phénomènes est loin d'être compris, ils affectent l'équilibre chimique de l'atmosphère (ozone et oxydes d'azote), le circuit électrique global de la Terre et perturbent les ceintures de radiation. Les mécanismes source font l'objet de nombreuses discussions, ils font intervenir des processus physiques qui n'avaient pas été envisagés jusqu'à présent et qui pourraient avoir des implications plus larges et se manifester dans d'autres environnements planétaires. Aussi la recherche sur ces phénomènes a rassemblé des scientifiques d'horizons divers (physique de la décharge, physique de l'atmosphère, chimie de l'environnement, physique du rayonnement, structure de l'ionosphère, etc.). Le projet européen CAL en est un exemple. De 2002 à 2006, il a réuni plusieurs équipes de scientifiques avec notamment des spécialistes de la décharge, des spécialistes de la physique de l'orage, des spécialistes de l'ionosphère, des chimistes de la haute-atmosphère, afin de mieux déterminer les mécanismes à l'origine des TLEs (Neubert et al., 2005). Les principaux objectifs du projet étaient de comprendre leurs conditions d'occurrence, de déterminer leurs taux, de caractériser les processus physiques de leur déclenchement et de préciser leur impact sur l'ionosphère et leur rôle dans la chimie de l'atmosphère. Le laboratoire d'Aérologie a participé aux travaux dans le cadre de ce projet, d'une part pour l'analyse des caractéristiques de l'orage et de son activité associés à la production de sprites et d'autre part pour leur observation avec des systèmes utilisant des caméras sensibles. Mon rôle a été de traiter les données de la première campagne faite en 2003 dans le cadre de CAL en associant des données radar météorologique pour la structure des orages, des données satellite météosat canal infrarouge pour la hauteur du sommet des nuages, des données de détection d'éclairs issues de plusieurs types de systèmes pour avoir une vue la plus complète possible sur l'activité d'éclair associée aux sprites. Mes premiers résultats ont été intégrés dans un article collectif présentant la campagne et ses résultats préliminaires. J'ai développé des collaborations lors de cette première étape qui a fait l'objet d'un article que l'on retrouvera dans le chapitre 3 de ce document. J'ai par la suite participé à l'organisation de nouvelles campagnes et j'ai développé un système complet pour l'enregistrement de signatures de phénomènes lumineux utilisé à partir de l'été 2006. Après de nouvelles observations, une étude particulière a porté sur un cas de sprite déplacé par rapport à son éclair parent afin de donner une explication à ces observations déjà commentées dans la littérature mais pas clairement interprétées. Le chapitre 5 du document expose cette étude sous la forme d'un article. L'article a été élargie avec une analyse approfondie des nouvelles observations en 2008. J'ai réalisé une étude statistique basée sur un nombre important de cas recensés sur plusieurs campagnes (2003, 2005 et 2006) et portant sur les caractéristiques des éclairs produisant des sprites et sur celles de ces mêmes sprites, abordant des aspects tout à fait nouveaux. Elle est incluse dans le chapitre 6 du document. Afin de caractériser la nature d'orages produisant des sprites, leur évolution et l'activité d'éclair typique à plusieurs échelles de temps, deux études de cas ont été développées de façon complète et sont présentées dans un article que l'on trouvera dans le chapitre 4 du document. Enfin, j'ai réalisé à mon initiative personnelle et en collaboration avec des chercheurs américains, l'étude des conditions de production d'un jet géant observé dans le Texas aux USA. Un article publié sur cette étude constitue le chapitre 7 du document. Le chapitre 2 du document est une large description des connaissances sur les TLEs, sur les

phénomènes en amont que sont les orages et sur les moyens d'observation dont les données ont été utilisées au cours de mon travail de thèse.

2 Scientific context

2.1 Introduction

The mysterious sounding "Red Sprites" are luminous phenomena high above thunderstorms in the mesosphere that have not been discovered until only recently. In 1989, a team of the University of Minnesota tested a new low-light camera system intended for research of the aurora, and recorded short-lasting pillars of light in the direction of a thunderstorm that was below the horizon (Franz et al, 1990).

This was a late discovery, considering that sprites are now observed as a common occurrence over large thunderstorm systems, that they are much brighter than for example the far dwarf planet Pluto (discovered in 1930!) and that they occur almost everywhere on our own planet!

Not surprisingly, eye-witness accounts of variously-shaped and colored brief flashes above storms have accumulated over more than a century, many of pilots who frequently fly in the clear air around thunderstorms – who were afraid they may not be taken seriously "seeing things". The reports also included strange upward lightning events, of which the first scientific proof was obtained in 1994, when a team of sprite researchers from the University of Alaska flew around thunderstorms in the state of Arkansas and found conical discharges escaping from the top of thunderclouds, now known as "blue jets" (Wescott et al. 1995). A similar but bigger new phenomenon dubbed "gigantic jet" was discovered in 2002 during an experiment in Puerto Rico (Pasko et al. 2002), and in the same year from Taiwan (Su et al. 2003). These events bridge the entire distance between the cloud tops and the lower regions of the ionosphere, around 80 kilometers altitude.

Not only from the ground or from airplanes, but also from spacecraft sprites and jet-like phenomena have been observed, as well yet another type of "Transient Luminous Event" (TLE): "elves", discovered in 1995 (Fukunishi et al. 1996). These are rings of light at the base of the ionosphere, and easier to detect from space over the Earth limb.

The entire family of known TLEs is related to electric fields and electromagnetic pulses generated in thunderstorms, and the conductivity between thunderstorm and ionosphere. They serve a yet unknown role in the electric circuit of the Earth and may also affect atmospheric layers chemically (NO_x and ozone production). Sprites are a real world example of low pressure streamer discharges, and have sparked the interest of scientists from many different disciplines.

During the pilot project *EuroSprite2000* (Neubert et al. 2001) sprites were captured over Europe for the first time by a camera installed on Pic du Midi de Bigorre (2877 m) in the Pyrenees. This success provided the basis for cooperation between various research groups in Europe interested in different aspects of sprites, united by the European Union Research Training Network "*Coupling of Atmospheric Layers*" (CAL) in 2002 for a period

of four years. The *EuroSprite* campaigns of 2003, 2005 and 2006 were a logical follow-up and provided the data used for the studies in this thesis. Neubert et al. (2005) presented an overview of the scope and the first results of the CAL network. Under CAL working program WP5, the objective of this thesis is to gain better understanding of the conditions in thunderstorms and processes in lightning that are at the basis of the occurrence of sprites and jets.

2.2 Earth-atmosphere electric circuit

The ionosphere is a region of the upper atmosphere where the air is ionized by radiation from the sun. It spans from the magnetosphere down to exosphere, thermosphere and into the upper half of the mesosphere. The height at which ionization is significant depends on diurnal, seasonal and 11-year solar activity cycles and is lower towards the poles. The ionosphere 'starts' around 50 km altitude during the day, and around 80 km at night.

As ion density decreases with altitude, the path length of free electrons increases before recombination of electrons (or negative ions) with positive ions occurs. This gives the ionosphere properties of a conductor for electric currents, and therefore functions together with the conducting surface of the Earth as capacitor plates in the Earth's electric circuit.

Within the circuit, thunderstorms fulfill the role of batteries, maintaining the difference of electric potential (Wilson, 1920). As the average thunderstorm top contains positive charge and the lower parts negative charge, brought to Earth by negative cloud to ground flashes and precipitation, the ionosphere is on average at a positive 250 kV potential compared to the Earth, but most of the potential difference is contained in the lowest kilometers of the troposphere, where positive space charge accumulates due to low mobility. So, while conductivity suggests that the ionosphere works as the outer shell of a spherical capacitor, with the surface of the Earth as inner shell, most of the charge in this circuit is present between these shells in the planetary boundary layer and in electrified precipitation.

The DC fair weather electric field near the surface is about -100 V/m, which exhibits diurnal fluctuations known as the Carnegie curve. It shows a peak during the local afternoons of the most thundery parts of the planet (Africa and South America) which have the strongest contribution in charging up the circuit by negative cloud-to-ground flashes. Conduction currents flow between the ionosphere and the surface, consisting of positive ions moving downwards and negative ions upwards.

2.3 Transient Luminous Events

2.3.1 Sprites

General characteristics

Sprites are streamer discharges occurring in the mesosphere above thunderstorms, lasting no longer than the blink of an eye. Sprites develop in tight connection to particularly intense lightning discharges which precede them by several milliseconds to more than two hundred milliseconds (Boccippio et al. 1995). Instead of rising out of a thunder cloud, they develop in mid-air usually between 50 and 90 kilometers altitude (Sentman et al. 1995), with the brightest part between 65 and 75 km. Individual streamers at the low pressures where sprites occur are tens of meters wide (Gerken et al. 2000) and a typical sprite element is 5-15 kilometers wide. Large sprites can span 50-100 km horizontally.

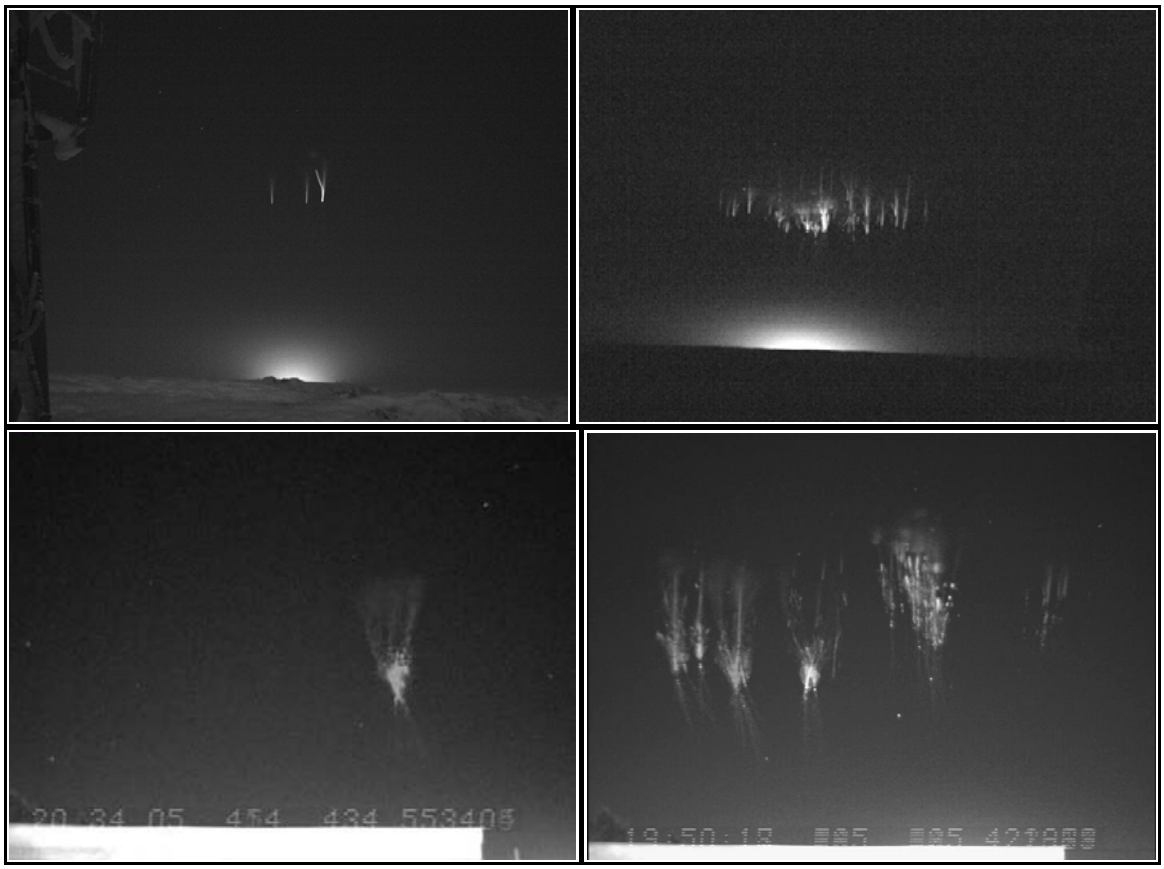

Figure 2. Examples of classic columniform sprites (top row) and carrot sprites (bottom row). Banding artifacts are caused by video interlacing.

There can be a lot of variation among sprites even within a few hours of observations, especially in vertical and horizontal dimensions, number of elements (groups), brightness and fine details. The most elementary sprite is a luminous column with a slightly diffuse top and abrupt bottom, from which dim streamers may stretch downward (Wescott et al., 1998a). They tend to cluster in groups, in rare cases as large as thirty elements. Carrot sprites have a bright body (or 'head') usually containing beads, from which long, usually dendritically shaped lower tendrils stretch out downward, and more wispy 'hairs' stretch out upward. Characteristic of most sprites are a diffuse region at the top, with streamers stretching downward (Pasko and Stenbaek-Nielsen, 2002).

Single elements develop within the time of a standard video frame (16 milliseconds), but a sprite event may consist of several elements that may dance above a thunderstorm occasionally for longer than 100 milliseconds (Lyons, 1994, 1996). The initial movement of streamers of normal sprites is downward (Stanley et al. 1999, McHargh et al. 2002, 2007). The upward-directed negative streamers appear to start from existing luminous structures from lower altitudes than the initial development, clearly visible in very-high speed (10 000 frames per second) imagery obtained by Stenbaek-Nielsen et al. (2007). The same recordings show that the streamers seen in normal images are just the traces of actually very bright streamer heads: wave fronts of ionization emitting light brighter than the planet Venus. Unfortunately, due to their fast movement (10^7 m s^{-1}) for a fraction of a second, sprites barely make a lasting impression to the eye.

Eye-witnesses reported different colors over the decennia, confirmed by observations of Lyons (1996) who found that people see sprites as green in 38% of cases, probably due to the poor color response of the human eye at low light intensities.

As image intensifiers and low-light CCD cameras commonly used to detect sprites show monochome images, little was known about the possible color of sprites before the first color image was obtained by Sentman et al. (1995) using a airborne TV camera, showing sprites to be red with tendrils stretching out to the cloud with a blueish color. The apparent brightness is comparable to a 'moderately bright aurora', more precisely an average 50-600 kilo-Rayleigh[1] (kR) (Sentman et al. 1995) up to 0.7-1.7 mega-Rayleigh (MR) when their short durations are taken into account (Yair et al. 2004).

[1] A Rayleigh is the number of photons integrated per second per cm^2, or $10^6/4\pi$ photons s^{-1} m^{-2} sr^{-1}

Figure 3. Color photograph of red sprites, taken by the author, Mont Aigoual, 21:10:26 UTC, 11 September 2006. Canon EOS 5D, 50 mm f/1.8, 4 seconds, ISO 1600. The sprite was also visible with the unaided eye, albeit colorless. Moonlight provided a blueish sky.

The light of sprites comes mainly from excited nitrogen atoms. Mende et al. (1995) and Hampton (1996) found the characteristic emissions of sprites to be caused by the first positive band of N_2 (665 nm and 886 nm, deep red and near-infrared) and the first negative band emission of N_2 (427.8 nm, blue) (Armstrong et al. 1998).

Sprites have been estimated to occur globally with rates of >30 sprites per hour (Sato and Fukunishi, 2003) up to 540 sprites per hour (Ignaccolo et al., 2006). A typical storm system during EuroSprite would produce sprites with 2-7 minute intervals during active periods, the duration of these periods may vary from short bursts to prolonged steady sprite production. From a meteorological point of view, the global rate estimates of Massimiliano correspond well with the 20-40 storms normally counted on global satellite images, that look large enough to be capable of producing sprites.

Sprite initiation mechanisms

History

Before the 1994 sprite observation campaign when sprites were for the first time triangulated (Sentman et al., 1995), only broad estimates could be made about the height of sprites. This led to terms as cloud-stratosphere lightning, or cloud-ionosphere lightning, illustrating an uncertainty of some 50 kilometers. The terms also were suggestive of the origin or direction of motion of these phenomena. Because of the uncertainty of what they really were, D. Sentman gave them the name "sprite", inspired by the mythical creatures. Later images and the measurements of Sentman et al. (1995) clearly showed sprites to occur between heights of 40 to 90 kilometers in the mesosphere, often lacking a direct connection with the thundercloud tops.

The first person to realize how electrical discharges may be produced high above thunderstorms was the Scottish scientist Charles Thomson Rees Wilson, who received in 1927 the Nobel Price for his work of the cloud chamber that visualizes the ionized trails of alpha and beta particles by condensation. He reasoned that the breakdown electric field threshold (needed for development of streamers) depends on air density and would decrease more rapidly with altitude than the intensity of electric fields caused by strong lightning discharges (Wilson, 1925). He speculated in 1956 that "it is quite possible that a discharge between the top of the cloud and the ionosphere is the normal accompaniment of a lightning discharge to earth…and many years ago I observed what appeared to be discharges of this kind from a thundercloud below the horizon. There were diffuse, fan-shaped flashes of greenish colour extending up into a clear sky." (Wilson, 1956, as quoted by Lyons, 1994)

High-altitude electric breakdown is controlled by the following properties, which vary with height:

- Electric field threshold for breakdown
- Relaxation time: the time it takes for ion fluxes to restore neutral electric fields
- Electric field changes caused by charging and discharging processes in the thunderstorm

Breakdown electric field threshold

According to Pasko (1996), one can assume the breakdown electric field to scale with height according to $E = E_0 N/N_0$, with $E_0 = 3.2 \times 10^6$ V/m at standard pressure (determined from laboratory experiments), N_0 and N are air molecule number density in m^{-3}, which we can take from the U.S. Standard Atmosphere 1976[2]. It can also be approximated by $E = E_0 \exp(-z/z_s)$ with z_s the atmospheric scale height, varying around 7 km.

To give an example, at a typical level of 8 kilometers in a thunderstorm the minimum required field for conventional breakdown is still a very large 1020 kV/m, but in the

[2] U.S. Standard Atmosphere website: http://www.aerospaceweb.org/design/scripts/atmosphere/

mesosphere at 80 kilometers streamers may develop already at much lower fields of 35 V/m.

Conductivity of air and relaxation time

The conductivity of air to electric currents (σ) depends on the number and mobility of ions, and scales with decreasing density of the air (increasing altitude). Here is an example of how fast ions may move, based on properties of the U.S. Standard Atmosphere: ion mobility $k(P,T) = k_0 \ P_0T/PT_0$ (MacGorman and Rust, 1998, formula 1.14) where the 0 subscript refers to standard conditions near the surface, $k_0 = 10^{-4}$ m/s per V/m. For an altitude of 80 km, k = 6.6 m/s per V/m, so ions may very briefly move at terminal speeds of 316 m/s under the influence of the local breakdown electric field (faster than the local speed of sound).

The local relaxation time τ depends on the conductivity by a simple $\tau = \varepsilon_0/\sigma$ (ε_0 is the permittivity of free space, 8.85 10^{-12} Faraday m^{-1}). It is the amount of time in which a charge (or an electric field) decreases to 1/e of its original value. A thunderstorm-induced electric field will last for a long time in and around a thunderstorm, because of the low conductivity of the cloudy air between the charges. As conductivity increases with altitude in clear air, the more mobile ions work more effectively to reduce electric fields, so that the fields can exist for less long. Taking the vertical profile of σ from figure 6b of Pasko et al. (1997), over a thunderstorm cloud top of 15 km τ = 2 seconds, at 50 km τ = 90 ms, and above 70 km τ < 1 ms. By 3τ, a disturbed electric field is restored back 95% to initial values by space charge fluxes.

Quasi-electrostatic fields due to thunderstorms

As Wilson (1925) noted, the electric fields generated by thunderstorm charges decrease with altitude z according to $1/z^3$ (assuming one simple point charge at a fixed altitude) while the breakdown threshold field, depending on air density, decreases exponentially with altitude (faster).

This yields a figure showing a region in the mesosphere where thunderstorm-generated electric fields would most easily surpass the breakdown threshold.

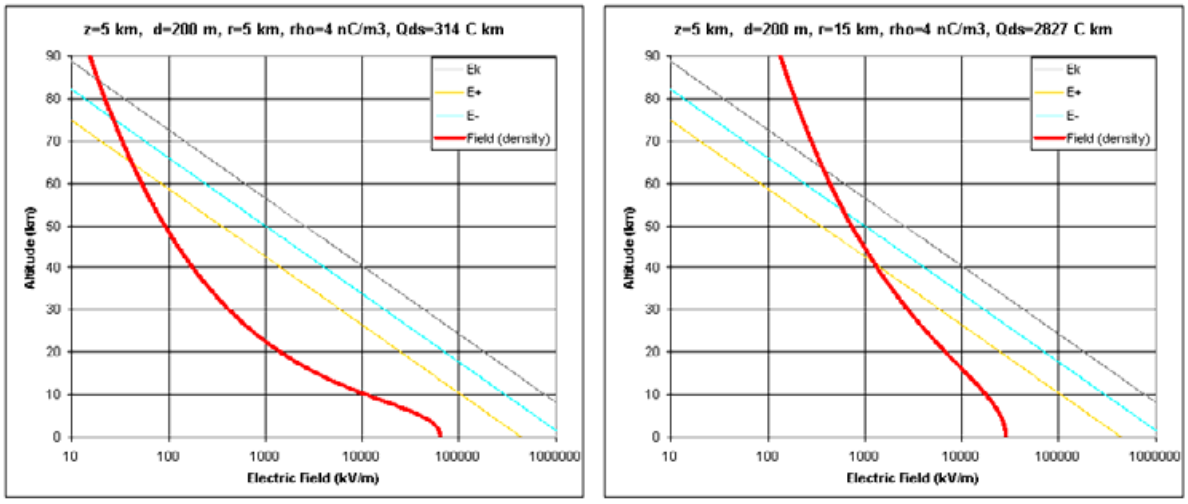

Figure 4. Electric field with height as a result of a lightning discharge based on a 200 m thick layer of charge of 5 km and 15 km radius, with a typical observed density of 4 nC m^{-3} at an altitude of 5 km. Computed for the vertical axis through the center of the disk. The grey line is the conventional breakdown threshold, the colored lines indicate minimum streamer propagation thresholds.

It must be noted that *static* electric fields resulting from a charge configuration in a thunderstorm are not causing the breakdown. Space charge redistributes itself under the influence of this electric field and eventually cancels it on the time scale of the relaxation time.

Problems arise if the electric field changes more rapidly than space charge fluxes can compensate. This may happen during a lightning discharge that moves charge to ground very quickly. We have seen that relaxation times are only a few milliseconds at altitudes above 60 km. As a typical cloud-to-ground return stroke lasts less than a millisecond, fields may indeed exist for a short time below 90 km altitude.

Because the space charge fluxes compensate for any slow building electric fields in the stratosphere and mesosphere, the layering of positive and negative charge in the storm does not matter. The magnitude of the quasi-electrostatic (short-lasting) field during a lightning discharge depends only on the amount of removed charge (Q) and the altitude from which the charges are removed (ds) – this is called a *charge moment change* (Qds) and expressed in Coulomb times kilometers (C km). Several studies have measured this parameter remotely by ELF radio waves, and found indeed that the higher the charge moment changes, the more likely it is that a sprite accompanies a lightning discharge (Hu et al, 2002; Cummer and Lyons, 2005).

If the removed charge is mostly of one polarity, the resulting high-altitude quasi-electrostatic field is higher than if two charge centers of opposite polarity are removed. Here the rule of thumb goes that removal of one charge does the same for the electric field as the insertion of an equal charge of opposite polarity at the same altitude. The resulting field from a lightning discharge can therefore simply be visualized by using only the charge configuration consisting of the charges removed during the discharge.

From the decrease of relaxation time with height can be inferred that longer-lasting lightning discharges may support initiation also at lower altitudes (60-70 km), but this requires higher charge moment changes. The same applies for the possibility of daytime

sprites, when conductivity values are increased at lower altitudes, limiting the height of a sprite and requiring higher charge moments.

While recent studies have attempted to define charge moment change thresholds (Huang et al. 1999, Hu et al. 2002, Cummer and Lyons, 2005), a fixed threshold has not been found so far. In this respect it has to be noted that there is a dependency on variations in conductivity profiles which are difficult to measure, and the same goes for the horizontal dimensions of charge active in a lightning discharge process. For example, for two disks of a given charge at a fixed height (i.e. the same charge moment change) but with different sizes, the distant effect on the electric field is the same along the vertical axis, but off-axis and low-altitude electric fields decrease more rapidly when the disk size is smaller even though the charge is more concentrated. Also, measuring currents from radio signals could provide more insight into the triggering and development of sprites than bulk time-integrated measures as charge moment changes (Cummer, 2003; Cummer and Stanley, 1999; Cummer and Füllekrug, 2001).

Streamer propagation

It must be noted that Pasko's initial modelling (Pasko et al. 1996, 1997) considered sprites as a result of electrostatic heating. With more clear images, notably telescopic close-ups (Gerken et al., 2000), it became obvious that sprites consist of streamers rather than a simple glow from excitation. The model does however a good job of representing the behavior of sprite halos, discussed in a later section.

A sprite is initiated when electrons are accelerated so much under the local electric field that when they collide with atoms in their path, some electrons of the atoms will be kicked out of their orbits, which then accelerate as free electrons, with the end result being an electron avalanche. The avalanche develops into a streamer tip with its own electric field. Some atoms have been excited by the collisions, and light is emitted when the electrons fall back to their original orbit. This makes the electron avalanches visible as streamers. The head works basically a ionization front, leaving a transient path of ions behind. A streamer can sustain itself as long as the local electric field remains higher than the minimum values E^{+}_{cr} = 4.4 kV/cm and E^{-}_{cr} = 12.5 kV/cm at standard pressure, for positive and negative streamer coronas respectively (used by Pasko et al., 2001). These scale with density as explained above. Within these bounds, the altitude and vertical size of sprites can be theoretically predicted given any charge moment change, but in reality the sprite itself works to cancel during its growth the surrounding electric fields. The removal of positive charge from a cloud means that the electric field vector above the cloud points temporarily downwards, so the downward streamers are positive and the upward streamers negative. The lower field threshold for positive streamers may explain their earlier occurrence. Positive streamer tips consist of series of electron avanches from their surroundings to the tip.

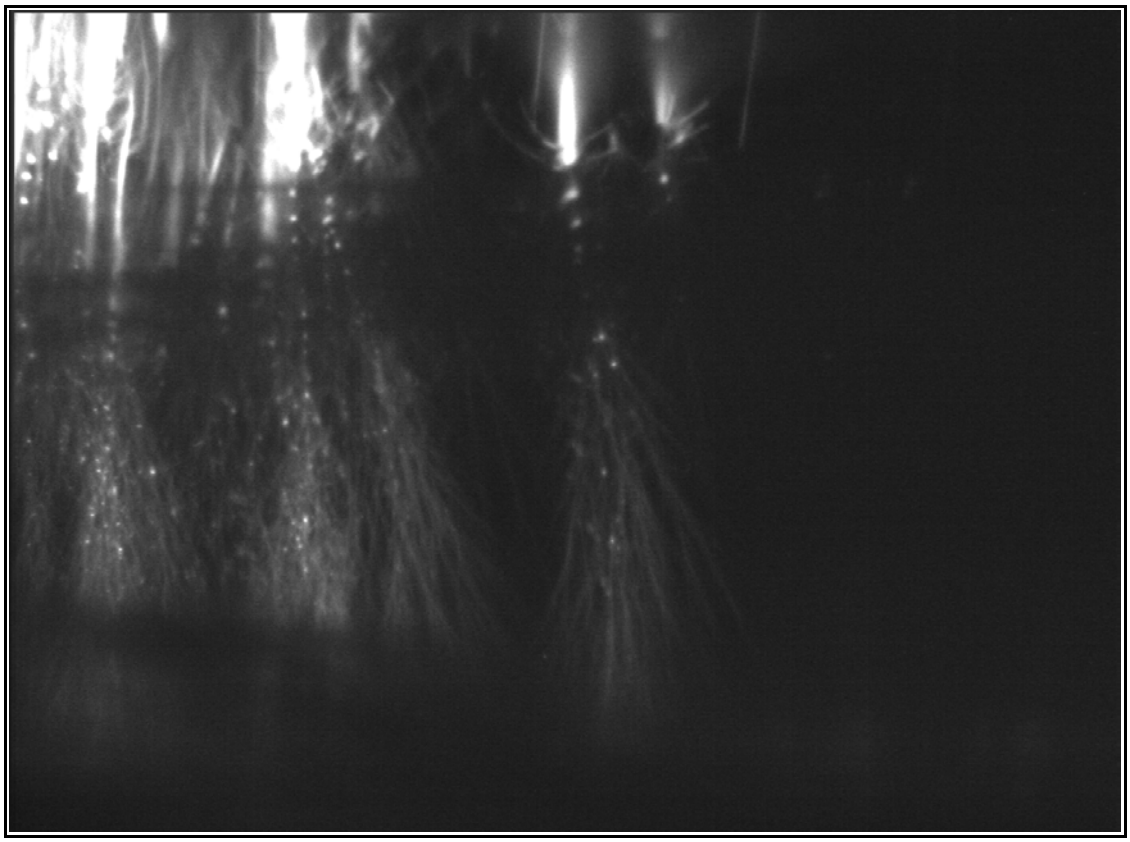

Figure 5. Close-up image obtained during EuroSprite 2005, July 28-29.

Sprites are often observed to have diffuse outlines near their top (>85 km), while streamers are clearly defined at lower levels (<75 km). Pasko et al. (1998) proposed an explanation by evaluating the characteristic time scales for electrostatic relaxation, electron/ion attachment, and streamer development from electron avalanches. Streamers can develop in altitude regions where the characteristic time needed for streamer formation is shorter than the relaxation time for electric fields (remember that the local duration of the quasi-electrostatic field produced by lightning is limited by the local relaxation time). Diffuse luminosity would be created by collective multiplication of electrons where the relaxation time for electric fields falls below the dissociative attachment timescale (lasting very short), so that more ions and electrons are becoming free than are recombined. Stenbæk-Nielsen et al. (2000) indeed confirmed this behavior.

Positioning and medium scale structure of sprites

Sprites occur in groups or single elements, and some are spaced at almost equal intervals from each other (Neubert et al., 2005). Some sprites obviously do not occur straight above the detected +CG lightning flash (Lyons, 1996; São Sabbas et al. 2003) but regularly more than 20 km away from it, or are offset to the lightning flash visible in the same image. Stanley (2000) observed, a number of cases in which the elements of grouped sprites to occur at the periphery of horizontal lightning discharges detected by the LDAR

system in Florida. Which processes could be responsible for the observed behavior? This is an interesting topic and studied in this thesis (chapters 3 and 5).

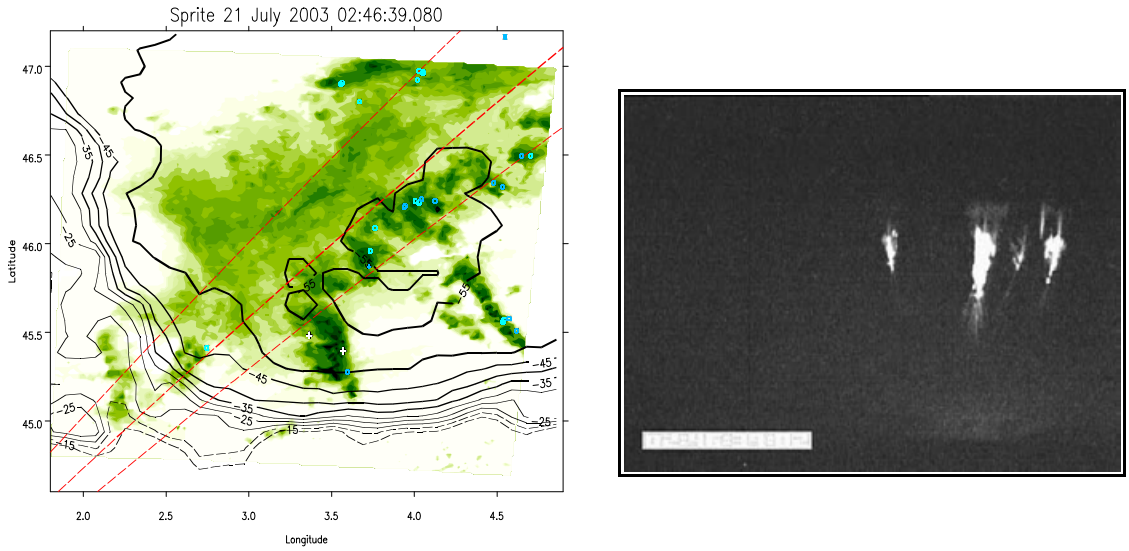

Figure 6. Example of a carrot sprite event whose tendrils point not to the triggering +CG (the rightmost white +, occurring at .079 ms) but a source of charge to the west of it. Azimuths from Pic du Midi to the main sprite elements plotted as dashed red lines, precipitation intensity in green.

Sprites horizontally displaced from their causative +CG often give away a clue about its apparent source of charge removal in the cloud, by their curved appearance. Neubert et al. (2005) showed a EuroSprite 2003 example of a sprite and possible electric field lines the sprite would be aligned with. This effect should be the strongest for a point source or towards the edges of a layer source of charge. During EuroSprite, it was often observed that the tendrils of carrot sprites pointed in the direction of the +CG. But there are a number of cases where the tendrils bent towards an area significantly displaced from the triggering +CG (figure 6), even when an element itself is straight above the +CG. Thus, it appears that the region of charge removal can be tens of kilometers far from the +CG, but connected to the CG via horizontal lightning channels. This concept is worked out in chapter 5.

However, it does not explain why sprites do not always occur directly above their apparent charge removal region in the cloud, where electric fields are supposedly the highest (if the removed charge would be uniformly distributed). Frequently suggested are ion density variations in the mesosphere, with locations of enhanced ion density serving as 'seeds' for sprite initiation. Meteoric dust has been hypothesized to influence this (Symbalisty et al., 2000; Zabotin and Wright, 2001), as well as upward-propagating gravity waves from thunderstorms (Snively and Pasko, 2003). Sentman et al. (2003) confirmed the existance of thunderstorm-generated gravity waves in the mesosphere, but alas, sprites occurred randomly and were not found to be any brighter if superposed on a gravity wave (visible by OH-Meinel emissions), nor did they have any noticeable effect on the gravity waves. Sprites do leave ionized traces (detectable by 'early/fast' events in VLF radio band,

Haldoupis et al. 2004; Mika et al., 2005) which may affect subsequent sprites within the same event (Stenbaek-Nielsen et al., 2000).

Cho and Rycroft (2001) suggested that radio pulses emitted by the horizontal part of a sprite-producing lightning discharge, reflected by the ground, may create interference patterns of minima and maxima in ion density, causing preferred locations for sprite initiation. However, their calculations involved radio waves of fixed frequencies. In reality the intracloud components generate a broad spectrum of noise (Very Low Frequency sferic clusters, e.g. Johnson and Inan, 2000; Ohkubo et al., 2005; Van der Velde et al., 2006), which do not seem favorable to create organized interference patterns.

A similar hypothesis was proposed earlier by Valdivia et al. (1997), who simulated sprites developing over extensive horizontal lightning discharges. Working as fractal antennas, such discharges produce focussed areas of enhanced ion density. They found initiation is possible for charge moments as low as 100 C km, and a horizontal structure of the resulting sprite appeared very similar to reality. Neubert et al. (2005) took this as a possibility for intracloud lightning to trigger sprites on its own, but no definitely convincing evidence has so far been found. The difficulty is in proving that a CG lightning stroke really was not present. It is common for a lightning detection system to detect only 80-90% of flashes, with the inherent chance to miss the triggering stroke. One such event was discussed in Van der Velde et al. (2006), included in chapter 3. It featured intense and more complex waveforms than typical events. Furthermore, charge moment changes are based on removal of a large quantity of charge of mostly one polarity. Bidirectional development of lightning, with a negative leader propagating into positive charge and a positive leader propagating into negative charge could imply that practically equal amounts of charge of both polarities are removed from the cloud, with a resulting charge moment change that is small.

New findings reported in an article belonging to this thesis show that thunderstorm conditions and processes in lighting do influence the morphology of sprites, as explained fully in chapters 3 and 6.

Runaway electron initiation hypothesis for sprites

An alternative or perhaps co-existing candidate mechanism for sprite triggering is that of avalanches of relativistic runaway electrons (Gurevich et al., 1992) generated by lightning flashes accelerated upwards under sufficiently strong electric fields so that the energy gained from the electric field exceeds the losses from collisions. The breakdown threshold for the runaway mechanism is an order of magnitude lower and thus more easily surpassed than that of conventional breakdown: $E = 218\ 10^3\ N/N_0$.

Runaway electrons are very energetic (~1 MeV range) and by colliding with atmospheric atoms 'bremsstrahlung' is created, in the form of gamma rays. The latter have first mysteriously been observed from space (Fishman et al., 1994) and are now known as Terrestrial Gamma-ray Flashes (TGF). They have been linked to thunderstorms and lightning discharges (Inan et al., 1996) and could possibly explain TLEs (Bell et al. 1995; Taranenko and Roussel-Dupré, 1996). Currently, satellite missions are planned with as

important objective to find out if TLEs are related to TGFs, such as the French TARANIS (Tool for the Analysis of RAdiations from lightNIngs and Sprites) microsatellite project, and the ASIM (Atmosphere-Space Interactions Monitor) lead by the Danish National Space Center.

The runaway breakdown mechanism might explain more easily sprite generation at the observed lower charge moment changes and lower altitudes, but encounters several difficulties, the main one being that a sprite is observed to develop also downwards after initiation, which would not be the case if triggered by runaway breakdown. Also, a small minority of sprites are reported to occur with negative CG discharges, which causes inverse electric fields and should cause any runaway breakdown to be downward-directed, thus making it impossible to produce a sprite.

However, Stolzenburg et al. (2007) found lightning flashes initiating at measured electric fields much lower than the conventional breakdown threshold, actually fitting well with the runaway breakdown threshold, surpassing it by 1.1 to 3.3 times. This may be useful at least for predicting lightning and jet initiation, although they note that surpassing the runaway threshold electric field may not be a sufficient requirement.

Negative sprites and the polarity asymmetry

While +CG flashes regulary produce sprites, only a few instances of –CG flashes have been described in literature to produce sprites. The best known is the observation by Barrington-Leigh et al. (1999) which involved large negative charge moment changes around -1600 C km. Williams et al. (2007) explored the reasons for the lack of –CG triggering of sprites (0.1% of sprites was triggered by -CG). For several continents, they calculated charge moment changes for all lightning flashes. The obtained distributions show that actually a significant part of –CGs do produce large charge moment changes typical of sprite-producing +CG flashes. So there must be a different explanation. Williams et al. (2007) suggest the impulsiveness of –CG lightning as opposed to the tendency of +CG lightning to produce continuing currents could possibly explain the asymmetry, reasoning that an electric field should exist longer in order to allow streamer development, which is not required for just the production of a halo. As described in section 2.3.2, halos are frequently observed for –CG flashes.

During EuroSprite 2006, the first confirmed negative sprite was recorded in the night of 11-12 September from Mont Aigoual over a storm over southwestern France. The triggering flash was the first -50.5 kA stroke of a three-stroked –CG according to the Météorage lightning detection network, to which the sprite was between 0-19 ms delayed. This sprite, the last one observed that night, appeared over the southern part of the stratiform precipitation region of a (at the time) poorly structured thunderstorm system that has previously only been producing sprites >30 km to the north. Within a second before this triggering –CG, also a few +CG flashes occurred in its vicinity closer to a convective core. The charge moment change of the triggering stroke has been calculated by Extremely Low Frequency radio recordings from Mitzpe Ramon in Israel and the NCK station in Hungary to be about -800 C km.

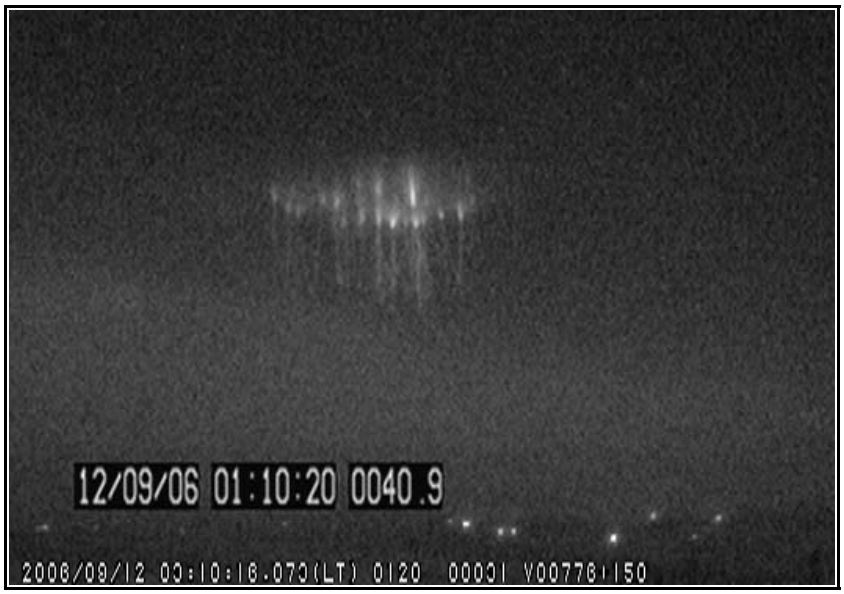

Figure 7. The only "negative sprite" observed during EuroSprite campaigns, caused by a -800 C km charge moment change –CG with a peak current of -50.5 kA.

2.3.2 Halos

Halos are generally amorphous glows that occur at about 75 km altitude and are delayed after the initiating CG stroke by 2–6 ms, and last for a few ms (Barrington-Leigh et al., 2001; Wescott et al., 2001). They are observed together with sprites for positive CGs, but a significant fraction of haloes occurs without being accompanied by sprites. In the observations by Bering et al. (2004), halos triggered by negative CGs were more numerous than all TLEs from positive flashes, although difficult to detect visually. Thus, the halo seems to be the fundamental response to lightning. Wescott et al. (2001) showed the haloes to occur centered over the causative positive CG flash, while sprites can be displaced for the same flash. Halos are reported to occur far more often in association with negative CG flashes than sprites themselves. Moudry et al. (2003) showed an example that halos are not necessarily uniform disks, but can exhibit structure and irregular shapes. This we see confirmed also for elves observed during the night of 15-16 November 2007 over the Mediterranean, which have irregularly shaped holes.

Figure 8. Four examples of halos accompanying a sprite: the diffuse disk of light on top. Halos also frequently appear without sprites.

2.3.3 Elves

Luminous patches of airglow near the top of the mesosphere above lightning discharges were first discovered in the Space Shuttle images by Boeck et al. (1992). During the SPRITES'95 observation campaign in Colorado, Fukunishi et al. (1996) obtained high-speed photometric data and image-intensified video showing that these events, now called elves, occur within about 160 microseconds after an intense cloud-to-ground lightning discharge at heights of 75-105 km. The observed horizontal dimensions typically range from 100-300 km, often manifesting itself as an expanding ring (Inan et al. 1997).

Elves are red-colored (but radiate also far-ultraviolet) and are brighter than sprites (1-10 MR), but last only a fraction of a millisecond which is too short to be detectable by the human eye, and also to be detected in normal video images with frame integration over >16 ms. Lightning flashes that produce elves may sometimes also produce sprites, and the reverse. The electromagnetic pulse (EMP) of the lightning return stroke is responsible for

Figure 9. Examples of elves during EuroSprite2007, all occurring over the Mediterranean Sea. Some elves occur together with sprites and occur at higher altitudes than the tops of those sprites. The sprite in such cases does not necessarily occur in the middle of the hole. The top left image appears to show some gravity waves in the elve brightness. Bottom left image shows also the associated lightning flash. The lower right image shows an elve with an irregular hole.

creating elves by heating of electrons near the base of the ionosphere, as found remarkably consistent with measurements by Inan et al. (1997). The simulations by Veronis et al. (1999) of very short duration lightning discharges suggest that elves dominate the optical emissions for strokes <100 microseconds, while quasi-electrostatic field-generated optical emissions dominate for strokes >1 milliseconds duration.

Elves may be expected for any lightning flash with strong EMP and usually are associated with lightning peak currents greater than 50 kA, regardless of lightning polarity. Barrington-Leigh and Inan (1999), using photometers, found 100% of CGs >57 kA to produce elves, while elve brightness also increased with electromagnetic pulse strength in VLF and lightning peak current. Rakov and Tuni (2003) predicted with a transmission line model of a CG return stroke that elves may be produced for peak currents >30 kA and very fast return stroke speeds $>2.5 \times 10^8$ m s^{-1}. More typically, peak currents greater than 100-120 kA are associated with elves (Huang et al., 1999). Larger peak currents have been observed by the North American Lightning Detection Network (NLDN) to occur more often over sea than over land (Lyons et al. 1998, Orville et al.,

2002), and the ISUAL instrument aboard the FORMOSAT-2 satellite has indeed observed a large majority (90%) of elves to occur over sea (Su et al., 2007).

Frey et al. (2005) noted that about half of the elves were accompanied by luminosity and VLF activity preceding that of the return stroke and elve by 2-5 ms, while the return strokes triggering sprites were not preceded by any luminosity. They suggested that a brighter, faster type of stepped leader ('beta') of negative ground flashes discussed in Rakov and Uman (2003) could be the cause.

Huang et al. (1999) considered it remarkable that a number of elve-producing CGs that had large enough charge moment changes to produce sprites (300 C km) failed to do so. They offer a possible explanation that elve-only discharges remove charge from smaller areas high in the storm, which gives an equal charge moment change as discharging a sheet of charge at lower altitudes, but the latter is more effective creating electrostatic fields at sprite altitudes as fields do not decrease (radially) as rapidly with height as for point charges. The higher potential of the higher source region must then explain the higher currents through the channel of the elve-producing lightning compared to that of most sprites, while the extensiveness of horizontal lightning could explain the longer delay for sprites. It must be noted that both for sprites and elves any observations of lightning structure have been very scarce or absent.

2.3.4 Jets

Characteristics

Blue jets, blue starters and gigantic jets form a family of TLE that appears to rise from high tops of certain thunderstorms and are characterized by blue and violet emissions. Blue jets and blue starters were first recorded over a storm in Arkansas during SPRITES'94 by color and black-and-white cameras observing from two airplanes (Wescott et al., 1995). These recordings remain one of the very few documented observations to date, emphasizing how rarely they are observed.

Blue jets are cones of streamers emerging from the overshooting top of the storm, moving upward with a speed of 112 ± 24 km/s, widening and fading with height, disappearing at altitudes of 37 ± 5 km (21 ± 5 km for blue starters), with durations of 200-300 ms. The cone angle varies between 6-32 degrees and the orientation varies. Wescott et al. suggested the first negative bands of N_2^+ are mainly responsible (391.4 nm, 427.8 nm and 470.9 nm in decreasing order of contribution) for the blue color while any red contributions are 'quenched' at these lower altitudes. The brightness of blue jets and starters had first been determined at 0.6 MR (Wescott et al., 1995), but with considerations of atmospheric transmission of light, Wescott et al. (1998) redetermined the brightness of these jets to higher values of 1 MR. The large Réunion island blue jet described in Wescott et al. (2001) even had a brightness of more than 6 MR.

Blue jets may occur at large rates. More than 50 blue jets were recorded in just 22 minutes, a much larger rate than is typical for sprites. The same storm produced also 30 blue starters (Wescott et al., 1996) and more than twenty upward lightning events during the same period. It was noted that the storm produced very frequent intracloud lightning flashes. While no lightning flash appeared to have directly triggered these jets, or the gigantic jet of Pasko et al. (2002) as inferred from radio sferic data, the images by Kuo et al. (2007) from the FORMOSAT-2 satellite definitely show that the cloud top delivering a gigantic jet remains lit throughout the event, though not as bright as a sprite (Steven Cummer, personal communication, 2007)

The first gigantic jet was a single event observed from Puerto Rico by Pasko et al. (2002). During the same year five events were observed also from Taiwan (Su et al., 2003), occurring in just a 20-minute time frame. Characteristic of most of the few gigantic jets reported till present (November 2007) is a leading jet rising from the cloud top to about 50-60 km with a speed of about 1000 km per second, then branching out to greater heights (70-90 km) as a tree, or a more compact luminosity like the body and hairs of carrot sprites. The upper branched part lasts about as long as a sprite. When it disappears, the lower jet remains visible while brighter parts ascend slowly along the top of the jet between 45-65 km, named the trailing jet by Su et al. (2003). The whole sequence can last as long as 200-800 ms and may feature a rebrightening. Pasko et al.'s event looks a bit different from the others in the sense that the upward speed of the leading jet could be followed by the camera, at only 100 km per second, features rebrightening, and it shows two main channels emerging from apparently one source in the cloud. It is probably due to the nanosecond gating of the image intensifier that a large amount of streamer detail is found in their images. While large ELF radio signals were detected in both cases, equal to positive downward or negative upward motions of charge, much smaller or absent ELF signals were found for the three cases studied by Van der Velde et al. (2007a, included in this work) and Van der Velde et al. (2007b).

Another class of jet-like events, named palm trees, embers or trolls (e.g. Heavner, 2000), was discovered in observations during the late 1990's. These events are upward single or grouped jets coming from the cloud and connecting to the lower tendrils of large sprite events, their tops may branch out like a tree. According to Heavner (2000) are of red color but a detailed study by Marshall and Inan (2007) found a blue emission. In their images, the events look different than jets: they do not fan out and may actually have a broad base near the cloud. The upward speed was about 1.5×10^6 m/s, quite similar to gigantic jets. The mechanism suggested by Marshall and Inan (2007) is that ionospheric electric potential can be carried along sprite bodies downward, increasing electric fields between the cloud and the sprite sufficiently to trigger the secondary, upward, event. A negative charge may be transported upward within the palm tree. Two palm tree events were recorded during *EuroSprite* from a thunderstorm near Mallorca, 25-26 September 2005. (Figure 10).

Figure 10. Two subsequent 40 ms images of the first palm tree (troll) observed from Pic du Midi over a Mediterranean thunderstorm, 25-26 September 2005, 1:22:04 UTC. About four upward structures can be identified, including the bright event to the right.

These palm trees appeared to follow a not very unusual sprite, and the left tree in the first sequence obviously grows after a sprite of only small vertical extent, so Marshall and Inan's (2007) hypothesis may not work well here, although the sprites during this period tended to be very extensive horizontally and vertically. Altitude calculations are pending.

Figure 11. Two 40 ms images (one not shown almost eventless frame in between) of the second palm tree (troll) observed 25-26 September 2005, 1:33:43 UTC. Clearly visible is the upward branching.

Jet mechanisms

Cloud tops have been estimated to be as high as 18 kilometers in cases of jets. Higher tops may aid initiation by bringing charged regions into altitudes where breakdown and streamer corona propagation thresholds are lower. The first theoretical models based on the conventional air breakdown mechanism, by Pasko et al. (1996) and Sukhorukov et al. (1996), suggested blue jets were large positive or negative streamers (waves of ionization) moving upward under the influence of the vertical electric field. They required discharging of the lower charge center or rapid charge accumulation to initiate the jet as result of a threshold electric field. Later modelling efforts (Pasko and George, 2002) supposed that jets consist of narrow fractal streamers. The jet continues to move upward as long as a minimum local electric field requirement is met. Multiple-streamer structure at the sides of jets was observed first in the Réunion island photograph studied by Wescott et al. (2001), which contained eight side branches from a main channel, as well as the gigantic jet by Pasko et al. (2002), and was predicted by Petrov and Petrova (1999). In

Pasko and George's work, the maximum height of the modelled event depends on the charge supplied by the storm cloud. Raizer et al. (2006, 2007) addressed the shortcomings of the fractal model. The charge inside the cloud must be gathered from the hydrometeors and supplied to the jet by conducting hot leaders, as opposed to cold streamers that are non-conducting at the time scale of the jet, so it is likely that a bi-leader process as in common lightning is involved. This has the advantage that less charge is needed because the leader channel carries the potential of the source region out of the cloud, providing high electric fields at the tip. The streamers that run ahead of the leader tip are still dependent on the existance of a minimum required field for their propagation.

Krehbiel et al. (2008) detected a blue jet in the data of the New Mexico Lightning Mapping Array. They suggest that the presence of screening layer charge at edges of electrified clouds, a requirement also for initiation of downward cloud-to-ground lightning (e.g. Mansell et al., 2002), is likely required as well for allowing outward growth of jets by increasing local fields.

Observational aspects

The observation of blue events is more difficult than red events, which is probably the reason that they are not observed more frequently. As Rayleigh scattering is inversely proportional to wavelength as λ^{-4}, the light of a blue-violet event (near 400 nm) event will be extincted at least ten times more with distance compared to a near-infrared event (700 nm), which decreases the odds that jets can be seen from long distances and low altitudes. Additionally, the cameras typically used are less sensitive for violet light (40-50% response at 390 nm) than for near-infrared light emitted by sprites (still 80% response near 700 nm). Together this means if a sprite appears as bright as a star with a visual magnitude of +3 at a typical observing distance of 300 km, a typical blue jet emitting light twice as bright as the sprite at the same distance should appear about 2.5 magnitudes dimmer ($2.512^{2.5}$ equals a factor of 10). For jets to appear as clearly in unintensified images as sprites with these cameras, typical observing distances need to be much closer than for sprites, preferably within 150 kilometers.

2.4 Thunderstorms

As large quasi-electrostatic electric fields are required for the occurrence of sprites and jets, thunderstorms (cumulonimbus clouds) are the prerequisite. There are more cloud types that can become electrified and create static electric fields, but a discharge is necessary to create the large field changes, as we have seen in the previous chapter. Besides thunderstorms, only volcanic ash plumes create lightning, but knowledge about volcanic plume electrification and discharges is just emerging. So far, sprites have only been recorded over thundery deep moist convection containing extensive charge layers. Blue jets and gigantic jets were observed from clustered intense convective cells in the tropics and mid-latitudes with very high tops.

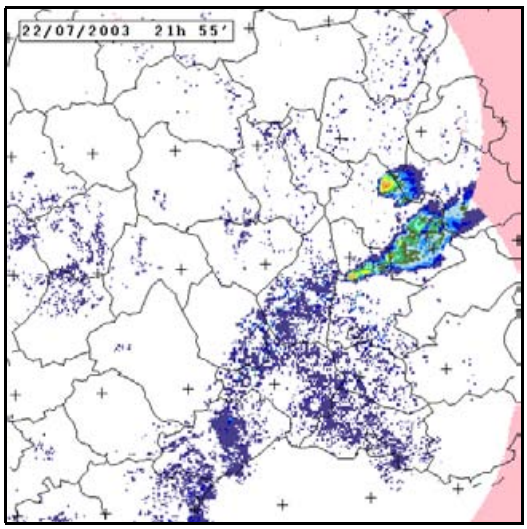

Figure 12. This radar image shows the southeastern corner of France near the time that two sprites occurred (the only ones for this thunderstorm). Sprites can already be observed over very small thunderstorm systems, provided there is at least a stratiform precipitation area of several tens of kilometers wide (depicted here as green colors). Crosses indicate the latitude-longitude grid at 1 degree spacing. The stratiform precipitation area resulted from a merger of the anvils of small supercells (which exhibited deviant motion relative to the average winds).

The topic of thunderstorms covers many aspects, such as convective processes, cloud microphysics and precipitation, electrification, and dynamics. I will provide only a rush through the basic backgrounds, and go into more detail for mesoscale convective systems, their structure, charge configuration and lightning activity as they are most relevant to sprites by their production of intense positive cloud-to-ground lightning.

2.4.1 Meteorology of deep moist convection

Instability of an airmass and its release

Thunderstorms are the result of atmospheric convection, which initiates when conditional instability is released. Conditional instability is a state often described by means of 'parcels' of air which are virtually moved in a vertical direction from their originating layer. These parcels change their properties which are then compared to their

new surroundings. Adiabatic processes – in which no energy is exchanged between the parcel and the surrounding air – dictate that temperature and pressure of a parcel are related by the ideal gas law for unsaturated air, so that temperature would decrease by about 10°C every vertical kilometer. Saturated air releases heat as water vapour condenses, and thus a saturated parcel cools less quickly (6°C per kilometer) when brought to a greater height than a parcel of dry air would. If the air at this new height is colder (heavier) than the parcel, the parcel would experience an upward buoyancy force and will continue to rise. This process is called moist convection and happens on a large scale in thunderstorms. It follows that chances for moist convection are determined by the amount of moisture and high temperature in the lowest kilometers of the atmosphere, together with strong decrease of temperature with height (colder air above) in the 2-5 kilometer layer. Additionally, atmospheric circulations need to be present which adiabatically (by lifting) cool down mid level layers and force parcels from low levels to ascend so that they become warmer than their surrounding air and will continue to rise by themselves (after having reached the Level of Free Convection). This gravitational instability, or 'buoyancy' is often expressed as a potential energy of a imaginary parcel of air, CAPE (Convective Available Potential Energy):

$$CAPE = \int_{LFC}^{EL} g\left(\frac{T_v^{\,parcel} - T_v}{T_v}\right)dz \qquad [\text{J kg}^{-1}]$$

where EL and LFC are equilibrium level and level of free convection, i.e. the heights between which a parcel is warmer than its surrounding air. T_v indicates the virtual temperature (temperature corrected for moisture content so that densities can be compared). CAPE can be converted to kinetic energy in the form of a convective updraft. The greater the CAPE, the greater the upward velocities in theory may become: $w = \sqrt{2 \cdot CAPE}$ [m s^{-1}]. In practice, entrainment of cooler or drier surrounding air and precipitation loading usually prevent the calculated upward velocities to be attained, although other factors like wind shear interactions with the updraft can increase updraft strength. Also, CAPE in a certain area will eventually be consumed if released, because effectively the troposphere is mixed towards a neutral thermal stratification. Thus, thunderstorm activity may last longer in areas with steeper lapse rates and higher CAPE.

Forecasting sprites is basically the same as forecasting thunderstorms[3] developing or lasting into the night (in order to see them). At night, the boundary layer usually stabilizes and convection may diminish quickly, except if a deep layer of steep lapse rates and moisture are present, which guarantees that CAPE can still be released from levels above the stable layer if also a source of lift is present. In fall and winter thunderstorm situations, CAPE is usually only small (<500 J kg^{-1}), but the warm sea water relative to the cold airmass keeps replenishing the boundary layer with heat and moisture causing new cells develop almost continuously, until convective overturning has mixed the airmass to a neutral profile.

[3] A large set of model-derived parameters assisting thunderstorm forecasting is presented on my Convective Weather Maps website: www.lightningwizard.com/maps

In Europe, CAPE values are usually lower than those over the Great Plains of the United States (Brooks et al., 2003; Romero et al. 2007). This appears to result in a smaller average size and shorter duration of storm systems. Observations indicate that the most sprites are produced by systems that regenerate convective cells continuously adjacent to a region of more 'stratiform' (i.e. uniformly layered) precipitation. From our experience in France, this region only needs to measure a few tens of kilometers across to produce a few sprites. Regeneration of cells requires a continuous supply of low level heat and moisture, and is focussed by mesoscale circulations (low level convergence) and organized by vertical variations in the speed and directions of horizontal winds, known as vertical wind shear.

Influence of wind shear on thunderstorm cells and their organization

The basic element of convection, a cell, consists of an updraft, where warm moist air rises, water vapour condenses into cloud particles from which may grow precipitation-sized particles; and a downdraft, where precipitation falls and drags the surrounding air downward, helped by evaporative cooling of cloud and precipitation particles near the top and sides of the cloud. Dynamical forces resulting from the interaction of vertical wind shear with buoyant bubbles are responsible for enhancing updraft and downdraft velocities and longevity of the convective cell. A typical cell lives for about 30-60 minutes, including its growth stage as towering cumulus, mature stage, and dissipation as cool outflow cuts off the base of the updraft from its supply of warm air. In the cases of strong vertical shear (>15 m/s shear vector between 0-6 km altitude) and clockwise turning of layer shear vectors with height within the lower kilometers, a storm cell may acquire rotation as it ingests vorticity via the winds it ingests. These special cases of cells are called 'supercells' and typically produce large hail (2-6 cm or even larger) as evidence of their exceptional updraft strength, as well as tornadoes, and downbursts of damaging winds. More commonly, if there is at least moderate vertical wind shear, the life cycle of cells can be extended because of better updraft-downdraft separation: inflow of new air relative to the storm is better matched to the speed of the expanding pool of outflow air at low levels, so that an updraft will last longer. Increasing vertical shear will favor more continuously propagating cells over discrete (stepwise) propagation of cells.

This dependence of storm cell behavior on vertical wind shear is not only reported anecdotically. Especially the idealized simulations of Weisman and Klemp (1982, 1984) have revealed the important contribution of wind shear, and later publications focussed on the dynamical details and applications in operational meteorology. Besides wind shear and instability, the previously discussed degree of capping and nature of the forcing mechanism are of large influence to the resulting type of storm. Determining the likely 'convective mode' (single cells, multicell clusters, supercells, mesoscale convective systems) into which storms will develop after their initiation is an important aspect of severe weather forecasting today.

2.4.2 Thunderstorm electrification

Non-inductive ice-ice charging mechanism

One of the longest-standing questions is how convective clouds become electrified and produce lightning. Over the last decennia, studies of electric field mills, balloon launches and lightning structure have generally indicated that an average isolated thunderstorm contains a main positive charge reservoir above a main negative charge reservoir which resides mostly between -10°C and -25°C (at about 3-6 km height) in the updraft region (MacGorman and Rust, 1998). This is known as a positive dipole. Usually this dipole is accompanied by an extra positive charge low in the cloud (thus a tripole) and a negative screening charge layer at the top. However, distributions of charge in the horizontal dimension are not uniform, some storms may develop more than six layers of charge or inverted dipoles (e.g. Stolzenburg et al., 1998)

Of all charging mechanisms proposed during decades of research, the mechanism considered to be the most capable of reproducing such vertical layering and amount of electrification involves rebounding collisions between ice crystals and graupel pellets (small porous hail), which are growing as small supercooled cloud droplets freeze to their surface (riming). This mechanism does not need an external electric field or capturing of ions to polarize charge on a particle and is therefore called the noninductive graupel-ice mechanism.

As it is difficult to study interactions of cloud and precipitation particles inside the clouds and measure their charges, laboratory experiments are executed to shed light on the different aspects of electrical properties of particles in a controlled environment. Takahashi (1978) found that according to the temperature and the liquid water content, riming particles charged positively for higher temperatures and for either very high or low cloud water content, while the cold mid range of cloud liquid water causes riming particles to acquire negative charge. This yields figure 12.

A British group (e.g. Jayaratne et al. 1983, Saunders et al. 1991, Saunders and Peck, 1998) conducted similar experiments, but could not reproduce well Takahashi's results. Saunders et al. did conclude that there indeed seems to be a charge reversal temperature below which the riming particle acquires negative charge, but this threshold temperature decreased in their case as effective cloud water content increased, meaning that positive charging becomes more likely. Note that we speak of 'effective cloud liquid water', because it is the collision rate of cloud droplets with the riming particle that matters (Jayaratne and Saunders, 1985). The largest difference with Takahashi's results (1978) was at low effective water content, where they found negative charging of the riming particle. Researchers from Argentina (Pereyra et al., 2000, Avila and Pereyra, 2000) obtained results much closer to Takahashi (1978).

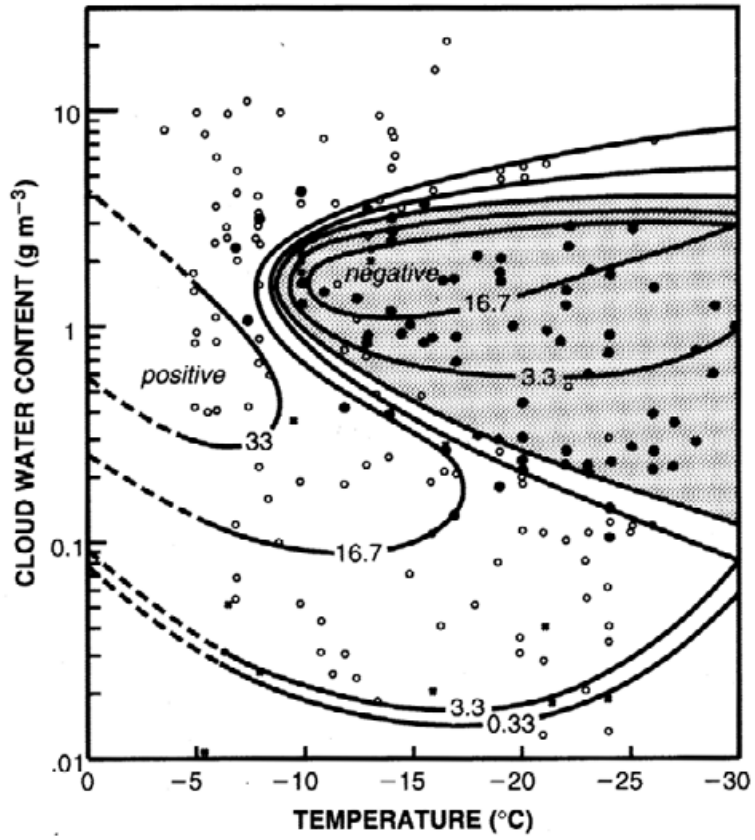

Figure 13. Results from Takahashi (1978) for charging of a riming particle, as a function of cloud liquid water and temperature.

They concluded the different experimental setups are indeed the major cause for the different laboratory results: the use of a single cloud of water and ice particles, or mixing two separate clouds of water and of ice particles shortly before encountering the riming target. In the single cloud experiment employed by the British researchers, small ice particles grow at the cost of cloud droplets and the saturation (relative humidity) will be smaller with respect to liquid water. Relative humidity, a factor not considered separately in previous works, was confirmed in a new experimental wind tunnel setup by Berdeklis and List (2001) to be of strong importance especially in the temperature range around -15°C. Lower relative humidity in this range means higher saturation with respect to ice than to water, which leads to depletion of vapor from liquid surfaces towards ice, and a more neutral to positive charge on the riming target. Berdeklis and List see this effect as a confirmation of the observation of Reynolds et al. (1957) that the sign of the charge transfer changed from negative to positive when the number concentration of ice crystals was increased to greater than that of the cloud droplets. But note that in the atmosphere the formation of cloud droplets is easier compared to the formation of ice crystals, because of the relative lack of ice condensation nuclei (aerosols with structure similar to the molecule raster of ice crystals). This means that concentrations of different aerosols may affect the resulting charge for a given temperature-humidity regime. Lyons et al. (1998) observed anomalously high percentages of positive ground flashes over a large region in the Plains, which they found possibly attributable to high aerosol concentrations from

forest fires in Mexico. However, only mixed support for this was evident in a smoke case study by Lang and Rutledge (2006), with more likely explanations in the near-storm meteorological characteristics (as discussed in the next section).

The possible theoretical explanations for the observed charging behavior as result of particle-particle interactions, the droplets freezing on growing graupel and transfer of water vapor are complex and go beyond the meteorological scope of this section. It is now interesting to translate the average laboratory results to the macroscopic distribution of thunderstorm charge.

Electrical aspects of thunderstorm cells

The overall level of electrification increases with higher concentrations of cloud particles and stronger updrafts, because of the increased collision efficiency. The concentrations depend on the supply of water vapor to the storm (boundary layer absolute humidity, i.e. dewpoints) and the presence of sufficient cloud condensation nuclei. Stronger updrafts are a result of higher CAPE (instability) in the environment of the storm, which for a given amount of low-level water vapor is increased by stronger (dry adiabatic) temperature lapse rates between the boundary layer and middle levels of the troposphere. Note however that non-hydrostatic pressure components induced by significant vertical shear, if present, could become more important in determining updraft speeds than CAPE.

Recently, Williams and Stanfill (2002), seeking explanations for the global land-sea lightning activity differences, hypothesized that high cloud bases and high aerosol concentrations could generate stronger updrafts and water supply in the mixed-phase region. Warm rain formation by coalescence of large cloud droplets increases if there are fewer aerosols available for nucleation. This would cause existing cloud droplets to grow larger and fall out of the cloud when their gravitational force exceeds the updraft drag force. A lower cloud base creates a larger cloud depth to the mixed phase temperature region, producing more warm rain. This depletes water from the updraft that otherwise would have reached the mixed phase region and contribute to charging.

If we translate the laboratory factors to the field, we should look at 1) ice particle and supercooled droplet concentrations, 2) temperature, 3) relative humidity (saturation), 4) differential fall speeds of particles (updraft strength) and 5) dry or wet growth regimes.

Williams (1995) classified three types of thunderstorms according to updraft and microphysical characteristics.

Normal thunderstorm (warm airmass storm): Graupel tends to charge negatively at temperatures below -10°C at intermediate (0.5-2 g m^{-3}) effective cloud water contents. Lighter ice crystals are advected to greater heights and form a positive charge center on top of this. The lower positive charge of the tripole exists because of the warmer temperatures and perhaps because screening layer charge at the bottom of the cloud is ingested.

Thunderstorm with broad, strong updrafts: Graupel tends to charge positively at increasingly colder temperatures when high (>2 g m^{-3}) effective cloud water contents are present. At the same temperatures in low to middle levels now a positive charge center is found instead of negative. Oppositely charged ice crystals form a negative charge center in the anvil to form an 'inverted' dipole. There is usually no lower negative charge. Since the presence of a small lower charge center under the main dipole is suspected of being crucial to the triggering of cloud-to-ground flashes (e.g. Mansell et al. 2002, 2005; Wiens et al. 2005; Tessendorf et al. 2007), resulting CG lightning activity may be very low or absent, whereas intracloud activity is very high (e.g. Lang et al., 2000). The effect of a stronger updraft means also that particles of a certain size may be found at greater heights than in the case of weaker updrafts and shift the entire dipole upwards. This favors intracloud lightning over cloud-to-ground lightning as well – an "elevated charge" mechanism (MacGorman et al. 1989). Lightning mapping systems and internal electric field measurements with balloons, obtained during the STEPS field campaign in 2000, showed indeed that charge layers were shifted upwards in a strong updraft, and that an inverted polarity charge structure was present (Rust and MacGorman, 2002, Lang et al., 2004, Wiens et al. 2005, MacGorman et al., 2005). Earlier, NLDN (National Lightning Detection Network) studies have shown that a small subset of storms exhibits anomalously large positive ground flash rates. These storms were usually taller and a high percentage of them produced severe weather (hail, tornadoes), compared to negative-dominant storms (e.g. Stolzenburg, 1994, Branick and Doswell, 1992, MacGorman and Burgess, 1994, Smith et al., 2000). Many hailstorms, however, are of normal lightning polarity (e.g. Changnon, 1992), so rather than being directly related, large hail and inverted polarity charge structures have some factors in common. Hail is a result of collisions of graupel with supercooled droplets. They freeze eventually onto the graupel, but in cases of excessive collisions a permanent coating of liquid water can be maintained at the surface of the graupel particle. In this situation, called wet growth, collisions with solid particles may not be rebouncing as the particles become sticky. So, wet growth as result of too large liquid water content could reduce the charging process and intracloud lightning (MacGorman et al., 2003).

A favored region for the development of positive-dominant storms are the High Plains of the United States. It was recognized by Knapp (1994) that regions in the United States where the troposphere tends to be relatively moist (e.g., the east and south) experienced significantly fewer positive storms. Williams et al. (2005) attempted to explain the flash rate and the polarity distribution by examining convective cloud base heights and instability (both are highest in the western Great Plains). Basis was the speculation of Lucas et al. (1994), who observed lower vertical speeds and smaller cores over the ocean, that boundary layer thermal width and cloud updraft width scale with convective cloud base height, a function of temperature and dewpoint ($T-T_d$) obtained from measurements at the surface. In the storm simulations of McCaul and Cohen (2002) it was indeed shown that wider and stronger updrafts occurred for higher cloud bases for equal CAPE. Carey and Buffalo (2007) found a strong separation between warm cloud depth (freezing level – cloud base height) in areas with positive- versus negative-dominant storms (positive: WCD <2300 m). This is strong evidence for the earlier explained detrimental effects of

warm rain formation to the updraft speed and vapor delivery to the mixed phase region in storms, and the non-inductive charging polarity dependency on cloud water content. In contrast, no difference in CAPE, Level of Free Convection (LFC) and deep layer shear (0-6 km) was present between environments of positive and negative storms. They do note that negative storms grew in an environment allowing larger adiabatic liquid cloud water content, but apparently other factors compensate for this in positive storms. In-situ observations are needed to quantify the assertion that more liquid cloud water in the mixed-phase region is indeed the cause for positive charging.

Winter thunderstorm: The mixed-phase temperature region is found lower in the cloud, and so is the main dipole. Updrafts are weaker and water content is lower due to the lower possible absolute humidity at low temperatures, causing the lower negative charge to be weaker (Saunders), or positive instead (Takahashi). This increases the chances that positive cloud-to-ground lightning will dominate (some lower negative charge necessary to trigger them). Flash rates will be low as result of the relative lack of hydrometeors, weak updrafts, and higher breakdown thresholds at lower altitudes. The positive flashes that do occur can be very impulsive (high peak currents) and can produce sprites, as confirmed in Japan (e.g. Hayakawa et al. 2004; Adachi et al. 2005), Israel (Ganot et al. 2007), and Spain (our *EuroSprite* observations) and likely also over the Atlantic Gulf Stream east of Canada (Price et al. 2002). Winter thunderstorms are almost uniquely tied to large water bodies and their coastal regions, as they provide the necessary buoyant energy when cold airmasses are advected over their relatively warm surfaces. Land surfaces are cold in winter when incoming radiation is weak.

2.4.3 Mesoscale Convective Systems and their electrical aspects

Types of Mesoscale Convective Systems

Clusters of thunderstorm cells often transform into systems organized on the mesoscale, with large circulations induced by their common cold pool of outflow and forced ascent with the strongest convection to the side of the main precipitation shield. The heaviest precipitation occurs near the strongest updrafts and is often arranged linearly, called the convective region, while a broad area of moderate to light, uniform precipitation falls from the anvil canopy adjacent to the convection: the stratiform region. Thunderstorms with maintain this configuration are called Mesoscale Convective Systems (MCS). Their dynamically organized nature can make these systems persist for many hours, much longer than the individual convective elements inside. Under special circumstances MCSs can become very large (>250 km) or can cluster together and form very large, nearly circular cloud shields named Mesoscale Convective Complexes (MCC, Maddox, 1980).

MCSs exhibit recurring precipitation structures. Houze et al. (1990) identified symmetrical, asymmetrical and amorphous systems, based on the relative positioning of stratiform precipitation to the convective line, and the presence or absence of a linear convective region. Parker and Johnson (2000) expanded the terminology with trailing stratiform, leading stratiform, and parallel stratiform configurations. The symmetrical trailing stratiform case has been the most studied over the years, also known as the classic squall line structure. Because the dynamics of mesoscale updrafts and downdrafts differ for each type, and their implications for the charge distribution within these systems are probably important. Parker and Johnson (2000) found the following tendencies for the environment in which the different types of MCS formed:

- Trailing stratiform (TS): strongest cold pool, strongest front-to-rear storm-relative winds*
- Parallel stratiform (PS): weaker cold pool, strong mid/upper level line-parallel storm-relative winds
- Leading stratiform (LS): weakest cold pool, weaker line-parallel winds, strongest rear-to-front upper level storm-relative winds

*Storm-relative winds are wind vectors at a given level from which the storm motion vector has been subtracted.

Figure 14. Trailing Stratiform MCSs often feature an impressive shelf cloud structure at their passage, marking the forced ascent over the leading edge of the cold pool. Top row: examples from the Great Plains, USA. Bottom row: examples from Toulouse, France.

Most characterical to MCSs are their extensive stratiform precipitation areas adjacent to convective cells. The area develops usually within a few hours of clustered convection from particles advected away from the convection in upper levels, and is accompanied by mesoscale downward motions at lower levels towards the convective region associated with cool, drier air and a rear inflow into the convective mesolow (pressure), and mesoscale upward motions at middle and upper levels associated with ascent over the cold pool. Between the convective and stratiform areas, a transition zone is sometimes present with weak precipitation. During the life cycle of an MCS (Zipser, 1982), the mesoscale downdrafts increase towards the mature stage, while the dissipating stage is entered when the total flux of mesoscale updrafts decreases.

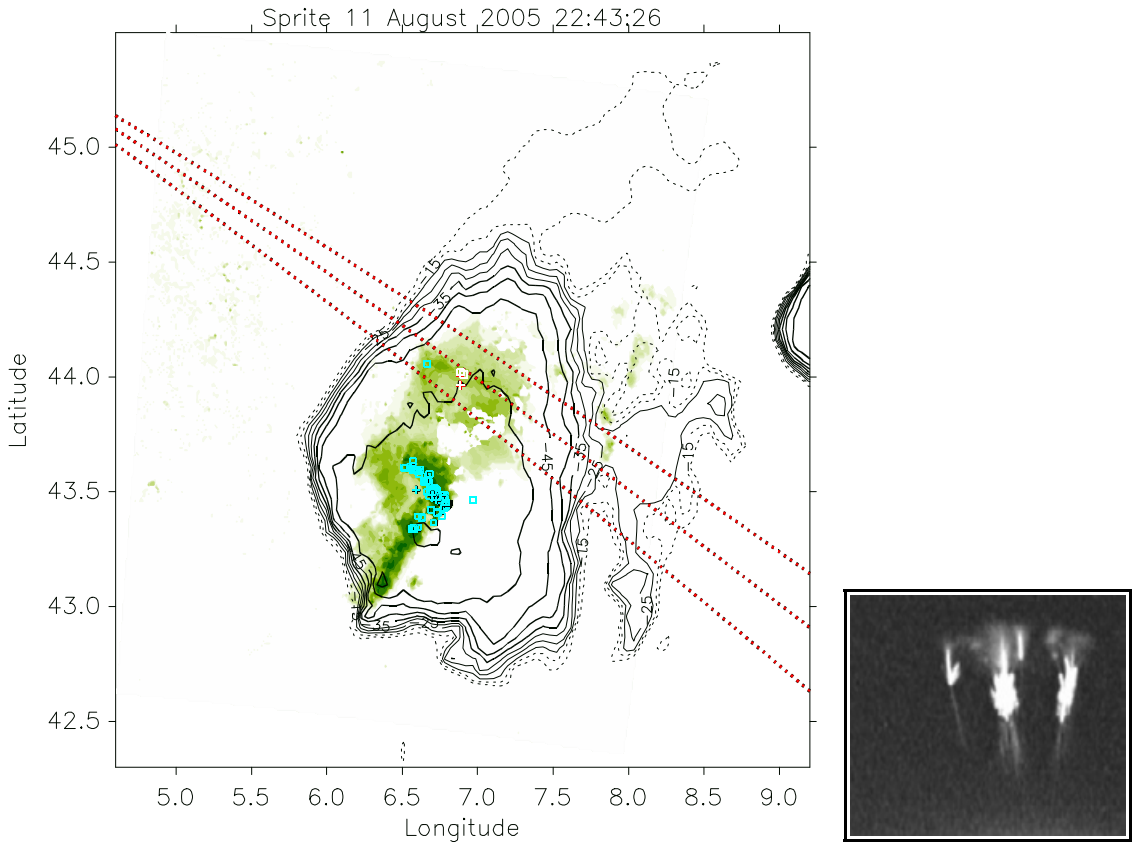

Figure 15. A group of classic carrot sprites observed from Puy de Dôme over a small parallel-stratiform MCS near the Alps in southeastern France. Green is precipitation; black lines are satellite cloud top temperature contours, red dotted lines indicate azimuth from the camera. Blue marks are –CGs, highlighting convective parts, while plotted in white are the sprite-triggering and following flashes. The sprites are oriented along the electric field lines from the source region in the cloud (e.g. Neubert et al., 2005), which appears related to the band of enhanced reflectivity.

Charge structure of the stratiform region

In the following, we summarize the most important findings with relation to MCS electrification, lightning and sprites.

Electric field measurements from balloons have shown that the stratiform region consists of several layers of charge of alternating polarity. Marshall and Rust (1993) noticed that profiles among different MCSs could be consistently categorized into two types: A, where five or six charge layers are more or less regularly distributed with height (first observed by Chauzy et al. 1985), and B, where two major oppositely charged layers reside near the melting level. For type B profiles the charge layer near 0°C tended to narrow (250 m) and be positive, while for type A, negative. The lowest charge layer at/below the cloud base and melting level is usually of negative charge (e.g. Stolzenburg et al. 1998), except in bands of intense rain.

Charge densities can be derived from measured vertical electric field profiles by a 1-dimensional approximation of Gauss' law: $\rho = \varepsilon (\Delta E_z/\Delta z)$ C m^{-3}, with $\varepsilon = 8.86\times10^{-12}$ F m^{-1}, under the assumption of infinite layers, but shown by Stolzenburg and Marshall (1994) to work reasonably well even for 4×4 km^2 layers. Schuur and Rutledge (2000a) reported

charge densitities of up to 5 nC m^{-3} inside the stratiform regions of symmetric and asymmetric MCSs. Hunter et al. (1992) found similar values in a LS-MCS. Such charge densities are similar to that found in convective regions. A 250 m thin layer extending over 80 by 200 km would contain 20 000 Coulombs or charge (Marshall and Rust, 1993). It is for this reason that lightning tapping from this reservoir low in the cloud (3-6 km) has a higher chance of producing sprites than the much smaller regions of positive charge at the higher altitudes in thunderstorm cores (Williams, 1998).

Marshall et al. (2001) observed a type A profile that supplied positive charge for powerful +CG flashes from altitudes a few kilometers *above* the freezing level. It was not known if these indeed produced sprites. However, in the storm studied by Lyons et al. (2003) the source positive charge reservoir for sprites in their storm was found near the freezing level, as evident from causative lightning heights, which would be most consistent with a type B charge configuration. It is still unknown if a specific type of profile would be particularly favorable for sprite production, but if large charge moment changes are needed to trigger a sprite, horizontal extensiveness of the discharging of charge layers could easily become more important than a few kilometers difference in charge layer height.

Long standing is the question where the charge in the stratiform region originates from. The region receives cloud and precipitation particles from the convective cores advected by mid and upper level storm-relative flow, but contains also larger and smaller scale upward motions and mixed-phase particles that allow local non-inductive charging.

The charge at the 0°C level may be attributed to several candidate mechanisms: non-inductive melting processes described by Drake (1968); inductive charging by drop breakup (Simpson, 1909), or to the non-inductive ice-ice charging mechanism discussed before as general charging mechanism for convective storms. Schuur and Rutledge (2000b) tested different mechanisms by modelling and showed that in-situ non-inductive charging with the Takahashi (1978) scheme contributed most effectively inside the stratiform region of a TS-MCS, accounting for 70% of the charge distribution, while charge advection from cores accounted for the remaining 30%. They remarked that this is consistent with the results of Rutledge and Houze (1987) that mesoscale updrafts were responsible for 80% of condensate production in the stratiform region. Observations documented in Schuur and Rutledge (2000a) confirm the importance of mesoscale updrafts and higher cloud liquid water content for charge production in the stratiform region, again consistent with in-situ non-inductive charging inside the stratiform region. While the observations of narrow charge layers near the 0°C level may rather be explained by melting processes (Shepherd et al, 1996), the simulations of Schuur and Rutledge indicated factors limiting the effectiveness of the Drake (1968) melting process charging, besides that it produces the opposite charging as observed. It can be concluded that the observed narrow stratiform charge layers indeed hint at least at the presence of a local charging process, but the kinematic and microphysical mechanisms are still unexplained.

Positive and intracloud lightning in the stratiform region

Since the employment of large lightning detection networks which measure polarity and peak currents of CG lightning flashes, it has been noticed that CG flashes tend to exhibit horizontal bipolar patterns, with flashes of mostly negative polarity in the convective parts of an MCS and a positive lightning maximum displaced at a few tens of kilometers distance from the convective line in the stratiform region (e.g. Rutledge and MacGorman, 1988; Rutledge et al, 1990; Engholm et al., 1990). The +CG flashes in the stratiform region had higher average peak currents than the other flashes (e.g. Rutledge and Petersen, 1994, MacGorman and Morgenstern, 1998). Among these are the +CG flashes that trigger sprites (Boccippio et al., 1995). In parallel stratiform MCSs especially, +CG flashes have frequently been observed to concentrate near local reflectivity maxima (Parker et al., 2001, Rutledge et al. 1990), as shown in the figure below.

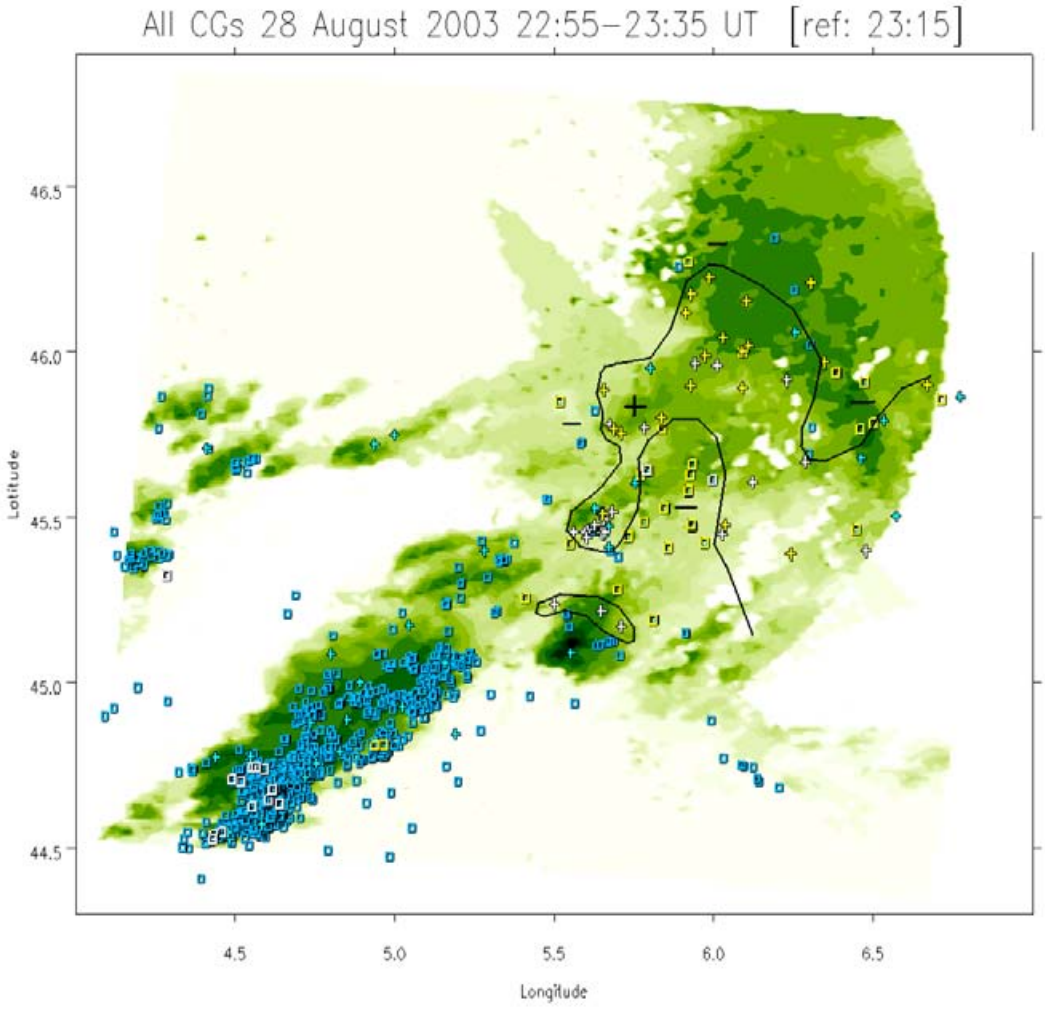

Figure 16. Accumulated 40-minute lightning activity using Lagrangian correction for plotting relative to the radar reflectivity features of a moving storm system. Yellow are all CGs occurring within one second of a sprite, white are those which triggered sprites, squares are negative and plusses positive CGs. This PS-MCS featured regions where +CGs and –CGs preferred to occur. The black line is drawn to highlight lightning polarity regions. Light green indicates reflectivities <30 dBZ, dark green >40 dBZ.

Stanley (2000) and Lyons et al. (2003) observed sprites and the details of cloud lightning processes using high resolution intracloud lightning mapping systems, confirming the speculations of Boccippio et al. (1995), among others, that there is an extensive intracloud component to the +CG flashes that trigger sprites. Recent observations with three-dimensional lightning mapping systems have shown that +CGs in the stratiform region are connected to large, highly branched discharges known as 'spider lightning' (e.g. Mazur et al., 1998) which crawl at speeds of 10-100 km s^{-1} over large distances, often visible at the base of stratiform clouds of MCSs. Their vertical dimensions are limited to less than a kilometer, travelling apparently through thin layers of charge.

Figure 17. Example of a spider lightning flash at the base of the stratiform region of a MCS. Photographed in Nebraska, May 23rd 2006.

Spider lightning flashes often start at the rear side of the convective region and slope 4 km downwards into the stratiform region over about 40 km distance (Carey et al. 2005), the same slope as convection-originated ice particle (snow) trajectories (Rutledge and MacGorman, 1988). The downward sloping behavior was also present for the sprite-producing flashes of Lyons et al. (2003). By comparison of electric field soundings and 3D lightning observations in thunderstorm cells by Coleman et al. (2003), it was found that lightning indeed typically travels through the largest charge densities within a layer. So the observations of sloping lightning paths suggest that snow particles of high convective origins carry positive charge that settles in the stratiform region, pointing at the advective charging mechanism, although it seems likely that also local mechanisms near the melting level are present. Lang et al. (2004) found that 77% of the stratiform region +CG flashes in

the TS-MCS they investigated originated in the convective line. The other flashes occurred within stratiform region only, which contained reflectivity values greater than 40 dBZ. They showed that spider lightning flashes can cause multiple +CGs along their path.

According to Coleman et al. (2003), charge varies a lot over horizontally small distances. They concluded that intracloud lightning flashes deposit charge of opposite polarity in narrow regions, rather than that they neutralize exactly the amount of charge of the region they travel through. When extrapolated to horizontal flashes in a stratiform region, this suggests that the simple model for charge removal by a +CG for calculation of mesospheric electrostatic fields from a circular disk of charge is overestimating largely the efficiency of the lightning process (and of course also the simplicity of the shape of the calculated electric field).

2.5 Lightning

A lightning *flash* or *discharge* is the entire set of electrical processes from its initiation to its extinction. Lightning *activity* usually refers to the presence or frequency of lightning flashes. In lightning physics the terms 'leader' and 'streamer' frequently appear. A leader is a conducting channel of hot plasma, while a streamer is a cold filament of corona discharge, an ionized channel.

2.5.1 Lightning initiation

The inititation of a natural lightning discharge is one of the most difficult to verify in the field, because local measurements in clouds are almost unavailable. As discussed in section 2.3.1, pages 15 and 21, there exist several experimentally determined breakdown electric field thresholds based on different processes, which decrease with decreasing atmospheric number density (altitude). It was shown by Marshall et al. (1995) that electric field soundings show fields bounded by the breakeven breakdown threshold (which is the same as runaway breakdown, though the value used at that time was somewhat lower). Lightning occurred when measured fields were near the threshold values. Recently, Stolzenburg et al. (2007) reinvestigated electric field soundings that were obviously in proximity to lightning (some measuring balloons got struck). They discovered that the electric fields at the moment of the discharge were lower than the conventional breakdown threshold (i.e. when a spark develops in a gap of a certain electric field), but surpassed the runaway breakdown threshold by about 1-3 times its value.

These measurements provide credible evidence that the runaway breakdown mechanism, discussed in section 2.3.1 (page 21) could have initiated lightning discharges. The runaway breakdown mechanism relies on an energetic electron (1 MeV) creating an avalanche of electrons accelerating under strong enough electric fields more than they are

slowed down by collisions. The source of such energetic electrons are hypothesized to be cosmic rays.

Without the help of energetic electrons, lightning has been hypothesized to initiate when hydrometeors emit corona discharge under locally strong cloud electric fields, which then could develop into streamers and leaders. For this, particles need to be large and rather elongated, their orientation aligned with the electric field vector so that induction causes positive and negative charge to accumulate at opposite ends. Modelling studies indicate that at observed electric fields corona can develop from rain droplets (e.g. Coquillat et al. 2003). But it is not known if and how the predicted corona indeed can develop into a lightning flash, or if it may instead act to reduce the electric field.

Observations of TGFs are now commonly linked to CG lightning (e.g. Inan et al., 2006, 76% of TGFs) and recently Dwyer et al. (2003) observed strong bursts of X-rays at short distances from triggered lightning. These must be a sign of bremsstrahlung occurring when energetic particles lose energy by collisions in the atmosphere. So, while lightning may be triggered by runaway electron processes from energetic particles, it may also provide energetic particles itself, which on its turn might set off another lightning discharge or a TLE along the electric field lines. This may be interesting perhaps in the context of 'communicating' lightning flashes within a group of separate storms observed from space by Yair et al. (2006), who sought explanations for this synchronicity in electromagnetic wave propagation effects or redistribution of static electric fields after flashes.

A hybrid mechanism consisting of energetic particles and hydrometeor corona mechanisms was proposed by Cooray and Rakov (2007). They suggest that energetic particles can leave traces of ions which cause instant condensation if in a saturated environment, equivalent to the workings of Wilson's cloud chamber. This would create long hydrometeor chains, with their opposite ends aquiring opposite charges by induction if the chain is aligned with the local electric field. From this, lightning might initiate at observed electric fields.

2.5.2 Intracloud flashes

Processes

Lightning flashes are commonly divided into intracloud (IC) and cloud-to-ground (CG) flashes. IC flashes do not connect to the ground and lack an impulsive return stroke.

Almost all of what we know about IC lightning (as well as a significant part of CG lightning) comes from data obtained from Very High Frequency (VHF) lightning mapping systems. VHF lightning mapping shows IC to develop as a bidirectional leader process (Kasemir, 1960; Mazur, 1989, 2002), often depicted as a double-ended tree, from a region between charge centers where electric fields are largest: a negative end and a positive end, propagating into regions of charge of a polarity opposite to that of the respective leader.

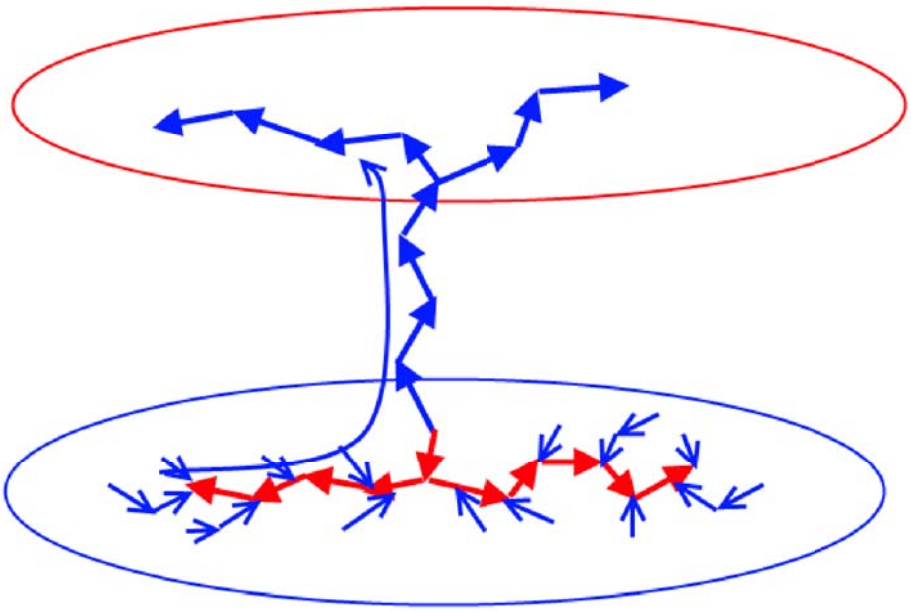

The net charge over the bidirectional leader is zero. Negative leaders propagate in a stepwise manner at speeds of 0.75×10^5 m s^{-1} (above 7.4 km, Proctor, 1997) to 1.3×10^5 m s^{-1} (Proctor, 1981). Others report speeds of $1\text{-}3 \times 10^5$ m s^{-1} (Shao and Krehbiel, 1996) and these are about the same as reported for stepped leaders in –CG flashes (Proctor et al., 1988). Positive leaders, on the other hand, travel continuously but usually at lower speeds, $0.4 - 0.75 \times 10^5$ m s^{-1} if we take the difference obtained from visual measurements in natural upward-propagating leaders from a tower by Berger (cited by Williams, 2006) as representative also for cloud flashes. Berger noted also that positive streamers were less luminous. The differences result from the direction of electrons from or towards leader tips: electrons diverge into weaker fields at negative tips, which takes more energy than electrons converging towards positive tips, according to Williams (2006). At the same time, the threshold electric field for propagation of negative streamers is larger than that of positive streamers.

Figure 18. Typical development of a bi-level cloud discharge. A bidirectional leader grows with its negative end (blue arrows) upward into positive charge (red ellipse) where it spreads out, and with the positive end into negative charge (blue ellipse). As the negative leader activity stops, negative recoil leaders connect to the positive end and backwards (upwards) into the existing channels. Positive recoil leaders are not observed at the negative leader end of the tree.

In the VHF frequency band, negative leader heads radiate much stronger than positive heads (e.g. Shao and Krehbiel, 1996; Mazur et al., 1998), making it possible to determine also the polarity of the charge center from lightning mapping data, confirmed by Rust et al. (2005) by electric field data. In a typical thunderstorm cell, most IC lightning activity occurs by connecting the upper positive and central negative charge regions. The flashes often exhibit a bi-level horizontal structure with a bridge between the two levels (like the letter 'H' on its side, but with the layers not necessarily co-aligned). The direction of 'recoil streamers' observed by VHF lightning mapping systems (also called 'K' streamers,

associated with 'K' changes in the electric field) equally depends on the configuration of the charge centers involved.

Recoil streamers are actually *leaders* (Mazur, 2002) of negative polarity moving along previously conducting channels, which often retrace the entire extent of the channel near the end of a flash (Shao and Krehbiel, 1996). In a normal IC flash, recoil leaders would develop where the positive leader ended in the negative charge region and go backwards along the channel and upward into the positive charge region. The radiative sources are more scattered than those of the negative leader during the active stage. At the same time the recoil leaders start, the negative leader activity in the other charge center ceases. Thomas et al. (2000) compared VHF locations and satellite-detected lightning brightness, and found the recoil events at the end of a flash to be the brightest of the entire flash. The negative recoil leaders are fast ($10^6 – 10^7$ m s^{-1}) and extend the existing channels at ~10^4 m s^{-1}, (Mazur et al., 1997; Shao and Krehbiel, 1996).

A positive equivalent of recoil leaders has so far not been observed, perhaps again because of their low VHF radio emissions, but evidence is so far also absent in other measurements (Mazur, 2002). In chapters 3 and 5 we speculate about possible recoil processes at the negative leader end in lightning associated with a +CG flash, for which VLF sferic power becomes much stronger after the +CG return stroke onset. These high frequency components appear to originate from the lightning processes which supply continuing current, which itself shows only slow changes and can be detected in the Ultra Low to Extremely Low Frequency range. It is quite possible that this lightning process is simply a highly energetic expansion of existing negative leaders inside the positive charge region. This is discussed further in the CG lightning section, 2.5.3.

Spider lightning

A remarkable type of intracloud lightning is 'spider lightning', visible as it crawls along the cloud base. These long highly branched horizontal discharges have already been described to occur by Ligda (1956) in radar observations. The longest reached over 150 km in length. More typically they are tens of kilometers long and may span very large areas (>5000 m^2, Lyons et al. 2003). As explained in section 2.4.3, they are usually confined to vertically narrow layers. The duration of these events last into seconds. Mazur et al. (1998) determined the visible channels to be negative polarity leaders, travelling though positive charge layers. Their speed of propagation is similar to other cloud lightning and stepped leaders of CG flashes. Mazur et al. (1998) discuss two events that also produced a +CG during their development. They could not detect the radiation from positive leaders, but it was found that, assuming bidirectional leader development, the +CG struck at a time and location relative to the initiation point of the flash corresponding to a slow positive leader speed of 2×10^4 m s^{-1}. If on the other hand the positive leader moved much faster (2×10^6 m s^{-1}), it must have developed later during the flash after significant development of negative leaders. Lang et al. (2004) confirmed that also stratiform –CG flashes may be initiated by spider lightning.

Narrow Bipolar Events

A yet different and relatively newly discovered type of intracloud flash is a 'Narrow Bipolar Event' (NBE)[4]. It was recognized as a separate class by Smith et al. (1999) but observed earlier by LeVine (1980) and Willett et al. (1989). NBEs are very powerful discharges of very short duration (2-5 μs). These flashes typically transfer 0.3 C of charge with average peak currents of 16 kA (Eack, 2004). However, an extreme example provided by Betz et al. (2004) to demonstrate the pseudo-3D capabilities of a VLF lightning detection network exhibited a -243 kA peak current and was located at a height of 15.7 km, which was explained as an NBE. Such peak currents are considered rare even for CG return strokes. Eack (2004) reported that the discharges responsible for NBE propagate at an average velocity of 1.5×10^8 m s^{-1} (similar to return strokes) over an average length of 3.2 km, and appear to occur without streamers or leaders. The typical durations varied mostly between 10-20 μs, with some events displaying continuing current for 400 μs (still much shorter than for +CG discharges). Suszcynsky and Heavner (2003) identified the range of heights and cloud regime of NBEs. The highest occurrence was found between 10 and 15 km, in convective updrafts, their frequency possibly links to convective updraft strength. Lightning at high altitudes is candidate for emission of runaway electrons detected in space as TGF.

2.5.3 Cloud-to-ground flashes

CG flashes (or just 'ground' flashes) are classified by their polarity and the origin of movement of their stepped leaders, from a tall object on Earth or inside the cloud. The polarity denominator refers to the polarity of the charge in the cloud that is brought to ground, most usually (~90%) negative (–CG). +CG flashes are more unusual and in some storms almost absent. For this reason it has not received as much attention as it can take a considerable amount of time to gather statistically useful measurements. Besides +CG and –CG flashes, a bipolar category exists, in which subsequent return strokes through the same channel are of opposite polarity. Such flashes apparently tap from very different charge regions in the storm. I shall focus on the typical –CG and +CG processes.

Much of what we know about CG discharges comes from electric field measurements at the ground, optical and direct current measurements on towers and wired rockets, and remote sensing of their electromagnetic signals. Return strokes broadcast strong pulses in radio frequencies, detectable from long distances in ELF through LF range. Leader and 'K' processes show up as longer lasting sferic noise. At MF frequencies the energy of return strokes and leader processes are comparable and hard to differentiate, while at HF through UHF frequencies the leader processes dominate and return strokes mark interruptions in the activity (Malan, 1958). My own MF sferic recordings obtained from a nearby thunderstorm over Toulouse, April 29th 2007, simultaneous with video recordings, show a typical duration of about 150 milliseconds for a –CG flash, including its preceding and following activity inside the cloud. This offers some reference for the VLF and SAFIR

[4] or Narrow Positive/Negative Bipolar Pulse, NPBP or NNBP

measurements and sprite delay times encountered in the articles of chapters 3 and 5. From more remote locations, much of the leader activity registers barely over the noise floor of a VLF system, making it hard to determine the true duration of a flash. For more information about detection systems, see sections 2.6.3-2.6.5.

Processes

Ground flashes have been observed to start in the same way as cloud flashes, as a bidirectional leader tree, of which the lower end travels outside of the cloud. A layer of charge opposite to that of the main charge center has been found instrumental to the propagation of the lower part of the leader tree out of the cloud, usually downwards but sometimes even upwards (e.g. Krehbiel et al., 2008, see also section 2.3.4 about jets). A model for vertical propagation of bidirectional leaders and their properties was described by Mazur and Ruhnke (1993, 1998). It is based on the electric potential profile in the cloud, which is a function of its charge distribution. A bi-leader initiates where the field is highest, and stays at the net potential of its initiation point. It can then develop in both directions for as long as there is a difference between the cloud potential and each of the leader tips at their location. A similar conceptual model is used by Raizer et al. (2007) to explain the development of a blue jet.

As this (stepped) leader approaches the ground, a contact streamer completes the connection between the cloud and the ground and an intense upward return stroke follows, draining the charge from the cloud. Mazur and Ruhnke (1993) regard the return stroke as a ground potential wave and can therefore only move upwards, at a speed $>10^8$ m s^{-1}. At the time of the return stroke, recoil leaders start occurring in the cloud. These are usually followed by a dart leader that traces the existing path which then is followed by a new return stroke upon reaching the ground. This process may repeat itself and is typical for –CG flashes, which on average have 2-3 return strokes, in rare cases even more than 15 strokes (Saba et al. 2006a). The strokes are separated by a few tens to a few hundreds of milliseconds. Multiple ground contact points within a few kilometers are quite common for –CGs.

In +CG flashes, only one return stroke occurs, but the current usually does not cut off after the initial return stroke but can last over a long time compared to the typical microsecond-scale duration of –CG strokes. This 'continuing current' (CC) can last more than 150 milliseconds (e.g. Fuquay, 1982) during which the current remains 5-10 kA (e.g. Cummer and Füllekrug, 2001, assuming a discharge altitude of 4 km). This difference may explain why sprites are triggered almost exclusively by +CG flashes (Williams et al., 2006, 2007), and why some sprites are long-delayed to the detected causative +CG. The long duration of CC can be seen as evidence for the bidirectional leader process: if no additional charge would be continuously deposited by leader or recoil processes on the cloud end of the channel in contact with the ground, a ground potential wave through the channel would discharge even a long channel in less than a few milliseconds.

Saba et al. (2006b) found –CG strokes to have low peak currents when they also had long continuing current. For +CG strokes this did not apply. However, it is found that

longer-delayed sprites (suggesting a longer continuing current) do occur with lower average +CG peak currents (e.g. Van der Velde et al. 2006, included in chapter 3).

An explanation for the multistroked character of –CG lightning was given by Heckman (1992, described in Williams et al., 2006). Lightning channels lose their conductivity as they cool down. This can be assumed to be a time constant τ. This must balance with the electrical time constant represented by RC, resistance times capacitance. Capacitance increases with channel length. Instability results when $RC > \tau$, so for longer and more resistive channels. The interstroke recoil activity and redistribution of charge on channels inside the cloud determines if there will be a new stroke to ground. It is reasoned by Mazur (2002) that the much greater branching and larger distances covered by negative in-cloud leader activity keeps the current higher in +CG flashes, making it less prone to cut-off than most –CG flashes.

Besides originating from within the cloud, lightning can also initiate from tall objects on the ground. For a –GC [+GC] discharge[5] a positive [negative] leader grows upward into the clouds and is followed by a negative [positive] upward return stroke upon connection (Mazur and Ruhnke, 1993). So for each polarity CG, the flash can initiate either from within the cloud or from tall (man-made) objects. It is not known if these differences have consequences for the triggering of sprites.

[5] CG versus GC distinction cannot be made by lightning detection networks, so that in our studies using Météorage or NLDN data some CG flashes may actually have been GC flashes.

2.6 Instrumentation

2.6.1 Sprite observation systems

The main operational camera system during the EuroSprite campaigns of 2003–2007 was installed by the team of the Danish Space Research Institute at the observatory from Observatoire Midi-Pyrénées (OMP) at Pic du Midi de Bigorre (42°56′12.0″N ; 0°0′34.16″E) a mountain top of 2877 m height in the French Pyrenees. It profits very clear skies when local weather conditions are favorable. Within a range of about 1000 km, TLEs can be observed over most of France, the Alps, northern Italy, the western Mediterranean Sea and the Iberian peninsula. During the campaigns the system is remotely controlled via a SSH terminal over the internet. The system runs software written by Thomas Allin[6] for automatic detection of transient events. The station consisted of two JAI CV- S3200 low-light CCD cameras in 2003, based on the Sony ICX248AL 1/2" monochrome ExView HAD sensor. These cameras were used in later campaigns on Puy de Dôme (2005) and in a special system on a mountain on Corsica (2007). The cameras were equipped with 16 mm F/1.4 lenses (field of view 20°). An image consists of two interlaced frames of 20 ms each.

Since the campaign of 2005, two JAI CV-M4+ progressive scan cameras with 2/3” Sony ICX285AL CCD sensors of 1.45 megapixel resolution and 40 ms-duration (slower) frames are used. This camera is less sensitive, rated at 0.1 lux, but its 10-bit A/D conversion and lower gain provides a large dynamic range with excellent tonality in bright parts and much better details. One camera is fitted with a lens providing a close-up view, while the other provides a wide view (31° horizontal field of view).

The camera settings, such as the gain, shutter and integration period could be adjusted over serial RS232 links. The cameras were mounted in a weatherproof housing on top of a QuickSet 20 motorized pan/tilt unit. The pan/tilt unit featured a two-axis control interface, which was accessible through a serial RS232 link to a control PC one floor below. The unit allowed for the pointing of the camera within 360° of azimuth, and from –35° to +35° of elevation.

Every minute during operation, pan images were uploaded to the Danish webserver for inspection of viewing angle and conditions by the operator. After detection, triggered event images were uploaded in JPEG format. The next day the raw files would be uploaded, including the ten frames before and after the trigger.

All images and video files were time stamped using the PC system time, that was synchronized to UTC time through the Network Time Protocol (NTP) connected to a GPS receiver next to the camera with Pulse Per Second (PPS) output. The PC clock was synchronized every 10 minutes. The time in the file names then only needs a fixed correction related to the way the images are grabbed from the camera into the computer.

In principle, the system time was supposed to be correct within 0.006 seconds, with an almost constant drift of 0.012 seconds per 10 minutes.

[6] Spritewatch software is available freely from http://www.allinux.dk

Since EuroSprite 2006 our team in Toulouse began operating our own camera at Mont Aigoual (1567 m), supplemented by a remotely operable system at a laboratory just outside Lannemezan in 2007. These are Watec 902H and 902H2 Supreme cameras with 1/2" Sony ICX429ALL ExView CCDs (rated at 0.0003 lux at f/1.4 and high gain), operated with 16mm F1.4 or 12mm F0.8 lenses. The latter must be used with a accessory IR focus correction lens, but due to the narrow space inside the CS mount, it cannot be used except on the 902H2 Ultimate model (operated by me personally since 2007). The cameras have an internal switch for automatic gain control (AGC) which needs to be set to LO, at which they are still very sensitive but less noisy. The Ultimate version allows gain to be set manually (e.g. lower than 'LO') and different gamma (brightness) settings to eliminate even more image noise and control the rendition of bright parts of sprites.

For manual operation, the system would be set up at a location with a good view that has a connection to the internet, in order to be able to make decisions for aiming the camera (by compass and map) based on the latest satellite, radar and lightning information. The camera is mounted on a tripod, its output fed to a time inserter[7] connected to a GPS receiver, which outputs the time-stamped image via a USB 2.0 Pinnacle video capture card (frame grabber) into the laptop computer. The Japanese software UFOCapture[8] is used to record AVI movies of events. It allows many settings for trigger thresholds and masks against scintillation noise and unwanted slow-moving objects. I also connect one or two AM radios to the sound input to simultaneously record sferics (crackles) produced by the sprite-triggering lightning flash. The whole system usually takes 10-20 minutes to set up, focus and aim properly.

Event azimuths, elevations, and great circle paths

The obtained images are stripped of any black sidebars resulting from capturing in 720x576 PAL format and resized to fit the 4:3 video standard to obtain the correct aspect ratio of the image. This is necessary to obtain correct star fits in the software "Cartes du Ciel" (SkyCharts)[9]. This software allows us to overlay calculated stars over an image, given a certain time, location and part of the sky. The matching of stars with those in the image needs to be done by hand, but works very well if the camera direction and time are known and enough stars are visible. The accuracy of the azimuths for an event depends on the focal length of the lens and resolution of the camera. A sprite is usually much wider than the read-out of azimuth, which varies typically only within 10 arcminutes. The error at 300 km distance is less than 1 km. However for cases in which the image has been enlarged and the event is narrow, as was the case in the Marfa gigantic jet event discussed in an included article (chapter 7), the pixels of the image are blown up and for example stars, which have an infinitely small width in reality, are found to be several arcminutes wide. One has to be careful in such cases. When triangulating events, errors add up so that

[7] GPS time inserter from PFD Systems, http://www.pfdsystems.com
[8] UFOCapture, http://sonotaco.com/e_index.html
[9] SkyCharts/Cartes du Ciel can be freely obtained under the GNU Public Licence at: http://www.ap-i.net/skychart/index.php (we used v. 2.76)

for too narrow angles between the individual azimuths of the cameras, as demonstrated in the Marfa GJ case, a very large range of uncertainty is the result.

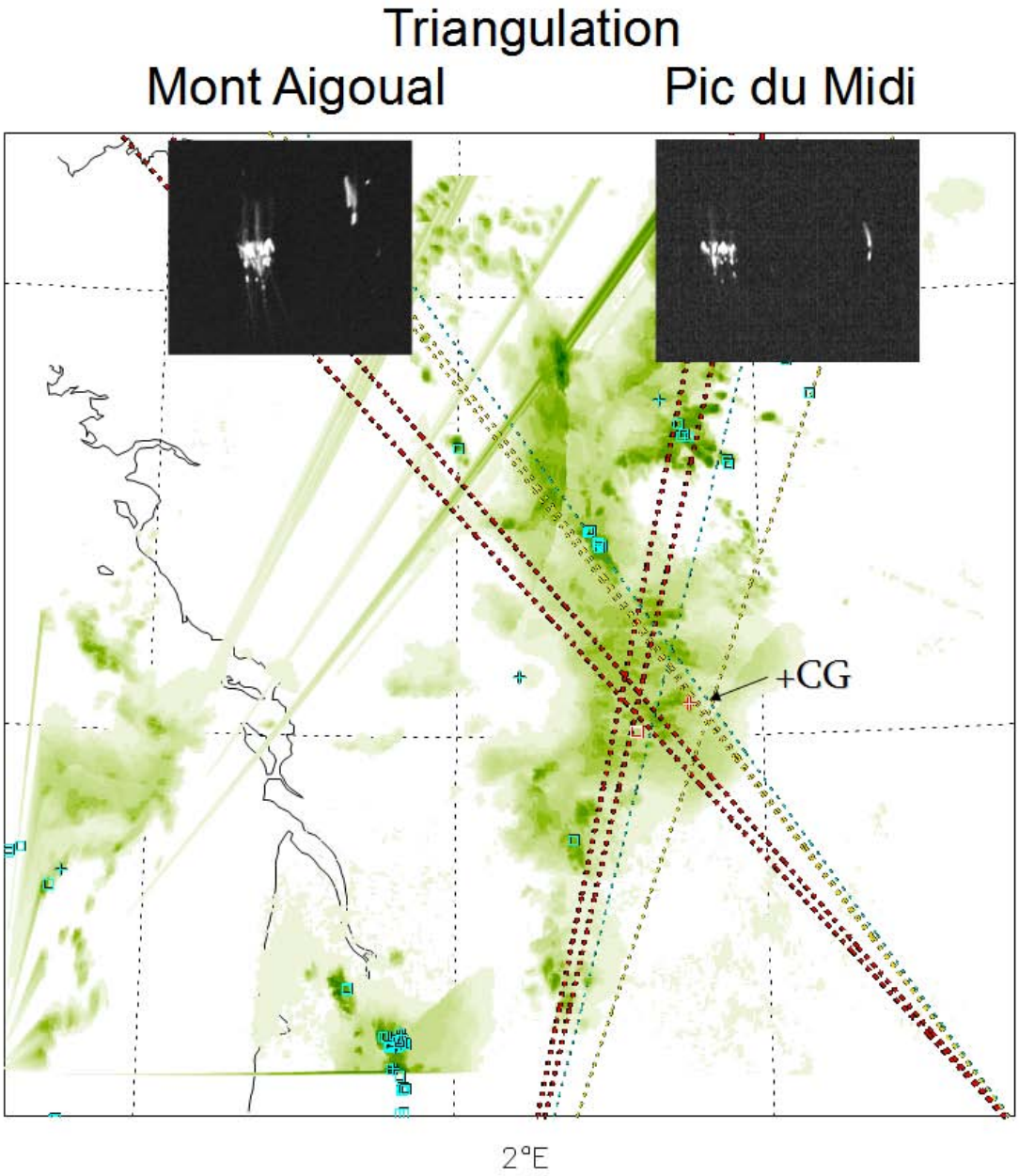

Figure 19. Triangulation of a sprite observed simultaneously from two camera stations. The sprite elements occurred where the corresponding great circle paths for the same element cross. The triggering +CG is indicated in white (+). Clearly, the large carrot element is displaced from the +CG and its tendrils appear to point to the +CG, as also described by Neubert et al. (2005).

With the azimuth and exact camera location a great circle path to the event can be calculated using the method of haversines (explained in chapter 2.7). The elevation can be used together with a known distance to the event (triangulated or approximated by detected lightning) to calculate precisely the height of a feature above the Earth's surface.

2.6.2 Radar

The French territory is covered by the meteorological radar network ARAMIS (Application Radar À la Météorologie Infra-Synoptique), operated by Le Centre de Météorologie Radar (CMR) of Météo-France. It consisted in 2004 of 18 conventional radars, of which 10 are C-band radars (λ = 5 cm) and 8 are S-band radars (λ = 10 cm). Each radar has a range of approximately 250 km and produces images every 5 minutes. In order to compose one Plan Position Indicator image, the radar beam makes two complete scans with an elevation of respectively 1.4° (for low distance) and 0.8° (for large distance). Taking into account the curvature of the Earth, a cloud is scanned, if at the maximum distance from the radar, at a height of about 8 km. The parameter provided by the radar is the reflectivity factor directly related to the precipitation rate. Composite images are created with a resolution of 1.5 × 1.5 km, increased to 1 × 1 km after 2004.

2.6.3 Météorage CG Lightning Detection Network

The French detection network for cloud-to-ground lightning, Météorage, covers the entire country as well as parts of the adjacent territories. It comprises 17 regularly spaced (200-250 km) sensors that work in conjunction with sensors in neighbouring countries. The Météorage stations use a technology called IMPACT (IMProved Accuracy from Combined Technology) that combines the advantages of a magnetic direction finding system (LLP) and a time of arrival system (LPATS), (Cummins et al., 1998).

The oldest and most widely used location system is the LLP, named after its original manufacturer, *Lightning Location and Protection Inc*. Each station is equipped with a direction finder (DF) and a flat plate antenna that determines the field polarity. The DF consists of two crossed magnetic loop antennas which detect the north-south and west-east component of the magnetic field radiated by the return stroke of the CG flash, the most energetic phase in terms of low frequency electromagnetic fields (1-300 kHz).

By trigonometry each station provides the direction of the electromagnetic wave generated by the source, i.e. the direction from the station to the ground-strike point. When the same signal is detected by several stations, the location of the ground-strike point can be estimated by triangulation. A shape recognition procedure identifies the signal waveform generated by the return stroke in order to distinguish between CG discharges and other signals like intra- and intercloud lightning. (Soula and Chauzy, 2001). The quality of detection of the magnetic signal is sensitive to distortions of the magnetic field by obstacles and metallic objects. Hence, the installation site must be carefully chosen. The detection range for lightning signals is about 200 km or more. LPATS (Lightning Position and Tracking System) measures the time of arrival (TOA) of the leading edge of the lightning impulse. Using bandwidths extending to a few megahertz, the leading edge can be determined to within 1 μs or better. The exact time of the signal's arrival at the antenna stations is compared for the different locations. The

position of the signal source is given by the intersection of the hyperbolas for equal time differences. To determine the 3 unknown parameters (time, longitude, latitude) of the signal source, at least 3 independent measurements are necessary. Due to the ambiguity of the intersection of 2 hyperbolas, in the general case 4 measurements of arrival time are needed. The uncertainty in the determination of the time is in the order of the time uncertainty of the single sensor (Δt_i). The location uncertainty inside the network is in the order of $\Delta t_i \cdot c$. Hence for location uncertainty lower than 1 km, a time resolution higher than 3 μs is necessary. To avoid reception of the skywave (the propagation of radio waves by reflection against the inner surface of the ionosphere), receiver sites must be less than a few hundred kilometers apart.

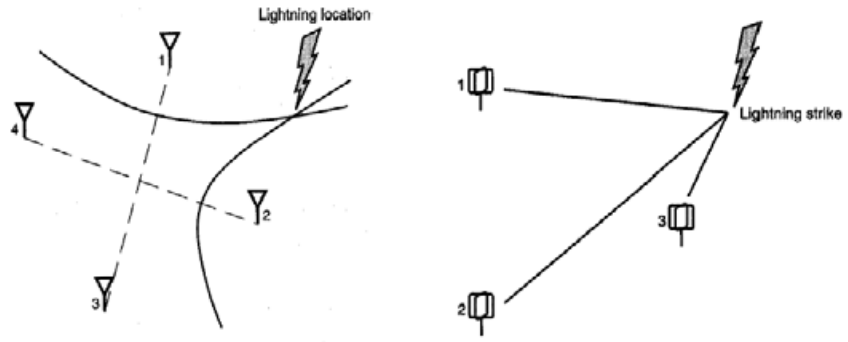

Figure 20. Lightning location principles : TOA - Time Of Arrival (left), DF – Direction Finding *(right) (from MacGorman and Rust, 1998).*

Since 1997, the Météorage uses both these techniques of detection. The IMPACT system combines magnetic and electric field measurements in the frequency range 0.4 kHz - 400 kHz. The basic principle is the same as before, but IMPACT is synchronized by GPS signals, which keeps the absolute timing error between sensors smaller than 300 ns. The system provides information of the location in 2-D, the time of occurrence, the polarity, the multiplicity, and the peak current of each individual return stroke. The detection efficiency is around 90% (Morel and Sénési, 2000), and about 70% of the locations are determined with an accuracy of < 4km (Seity, 2003).

2.6.4 SAFIR Intracloud Lightning Detection System

The SAFIR (Surveillance et Alerte Foudre par Interférométrie Radioélectrique) lightning location system was originally developed by a research group of the French National Aerospace Research Agency (ONERA) in a research and development program about lightning prevention and storm forecasting for aeronautics, defence and aerospace applications. SAFIR operates in the VHF frequency band of 110-118 MHz. This high frequency allows to detect signals from the single step of the leader process and from recoil streamers of cloud discharges. These processes emit series of pulses in the high frequency range. A consequence of the VHF range is the line-of-sight propagation of the

lightning signals. The Earth curvature, mountains and obstacles limit the detection range of the antennas, especially for low altitudes. A ray arriving at a detection station from 200 km distance was emitted from an altitude of at least 3 km. The antenna represents an array of 5 electric dipoles comprising an interferometer. Additionally to the VHF registration, a second antenna at LF (300 Hz – 3 MHz) is used for the detection of return stroke signals[10] The combination of both antennas enables the discrimination between intracloud and cloud-to-ground lightning.

For total coverage, a minimum of three stations is required. Each station detects, by interferometric technique (based on the phase difference between waves received by several antennas) the direction of the electromagnetic wave generated by the leader phases of any cloud discharges. In the 2D configuration used for the permanent networks installed in France, the detection of the same signal by several stations leads to the location in the horizontal plane of the radiation sources. The time resolution is 100 μs.

The mean distance of stations in SAFIR networks is at about 80-100 km. With the angular resolution of 0.25°, this yields a location accuracy better than 1 km. The detection efficiency is around 90% for ICs and CGs for distances smaller than about 150 km. The detection capacity is limited currently to 100 events per second. Since SAFIR detects many signals from a single lightning channel, this limit can be reached easily during intense storms. This low value was chosen to meet the slow data transmission lines.

Initially, there were three SAFIR systems working over the French territory, one over the Paris region, one on the Atlantic Coast, and one in the southeast. Since 2005, only the Atlantic system is still operational in France. Additionally, the regional weather service of Catalonia operates a SAFIR system covering northeastern Spain.

In our experience, the reliability of the system is quite poor. Of a typical flash rarely more than a few consecutive points are sampled (at the 0.1 millisecond time resolution of the system), leaving large parts of a flash undetected. Spatially, the reliability is by far not as good as in theory, at least not with the typical low spatial density of receiving stations. Very frequently, traces of sources are aligned towards/from one of the antennas. Long traces may look like a long intracloud lightning flash, but are just artifacts most of time. In the studies included in this work we only used SAFIR sources as a proxy for the presence of activity before sprite-producing return strokes, in combination with broadband VLF waveforms and a critical analysis of apparent horizontal lightning speeds and receiver positions where applicable.

[10] However, it appears that somehow the SAFIR-detected return strokes, when compared to Météorage, are poorly detected and sometimes of different polarity and time.

2.6.5 ELF/VLF electromagnetic measurements

Transient signals in the range of ELF (3 – 30 Hz) through VLF (Very Low Frequency : 3 kHz – 30 kHz) are generated by various natural phenomena, but the far most significant source of "noise" in these frequencies is lightning activity. Lightning discharges radiate the bulk of their electromagnetic energy in these low frequencies, with a broad peak around 10 kHz. The discharge currents generate radio pulses and noises termed "atmospherics" or "sferics". The attenuation suffered by globally propagating electromagnetic waves is extraordinarily small at these frequencies, amounting to only 0.3 dB/1000 km at 10 Hz, increasing with frequency to about 1 dB/1000 km at 60 Hz, which allows the waves to propagate a few times around the globe before dissipating.

Between the conducting terrestrial surface and the lower boundary of the D-region of the ionosphere, a resonating cavity is formed, a spherical parallel-plate waveguide, commonly referred to as the Earth-ionosphere waveguide. The sferics are "trapped" in this waveguide by multiple reflections from the ground and the lower ionosphere, and at certain frequencies, constructive interference occurs, which generates quasi standing electromagnetic waves, called Schumann Resonances (SR). As the circumference of the Earth is about 40 000 km, and the speed of electromagnetic radiation 300 000 km/s, the fundamental frequency should be roughly $f = c/\lambda$ = 7.5 Hz. In practice, SR depends on many factors, and the actually observed fundamental frequency is approximately 7.8 Hz, with the following higher order resonances occurring at 14.2, 19.6, 25.9 and 32 Hz. The low attenuation rate of frequencies in the ELF range allows the SR to be prominent in sferic noise spectra and enables the radiation from intense individual lightning flashes to be detected at global ranges.

ELF measurements can be used to derive the charge moment change of the lightning discharge that caused a pulse in the waveform. This is a complex calculation for which several methods exist (Huang et al. 1999) which involves fitting the waveform with a modelled waveform (with several tuneable variables) and requires the source to observer distance to be known. Charge moment changes for lightning flashes during EuroSprite can be calculated on request by colleages in Hungary and Israel.

During EuroSprite 2003-2007, the University of Stanford operated a broadband VLF receiver in Nançay, central France. The details are described in the article included in chapter 3. Because of its proximity to our sprite-producing thunderstorms, it offers the advantage that also a good amount of intracloud lightning signals show up in waveforms and spectrograms, visible as long lasting sferic clusters rather than pulses. Signals emitted by horizontal lightning do not carry as well over long distances as CG return stroke pulses, because their horizontal polarization cannot profit from the Earth-ionospheric waveguide. Expect a maximum usable range of 500-800 km.

2.7 Geometrical calculations

2.7.1 Altitude of a TLE above the Earth's surface

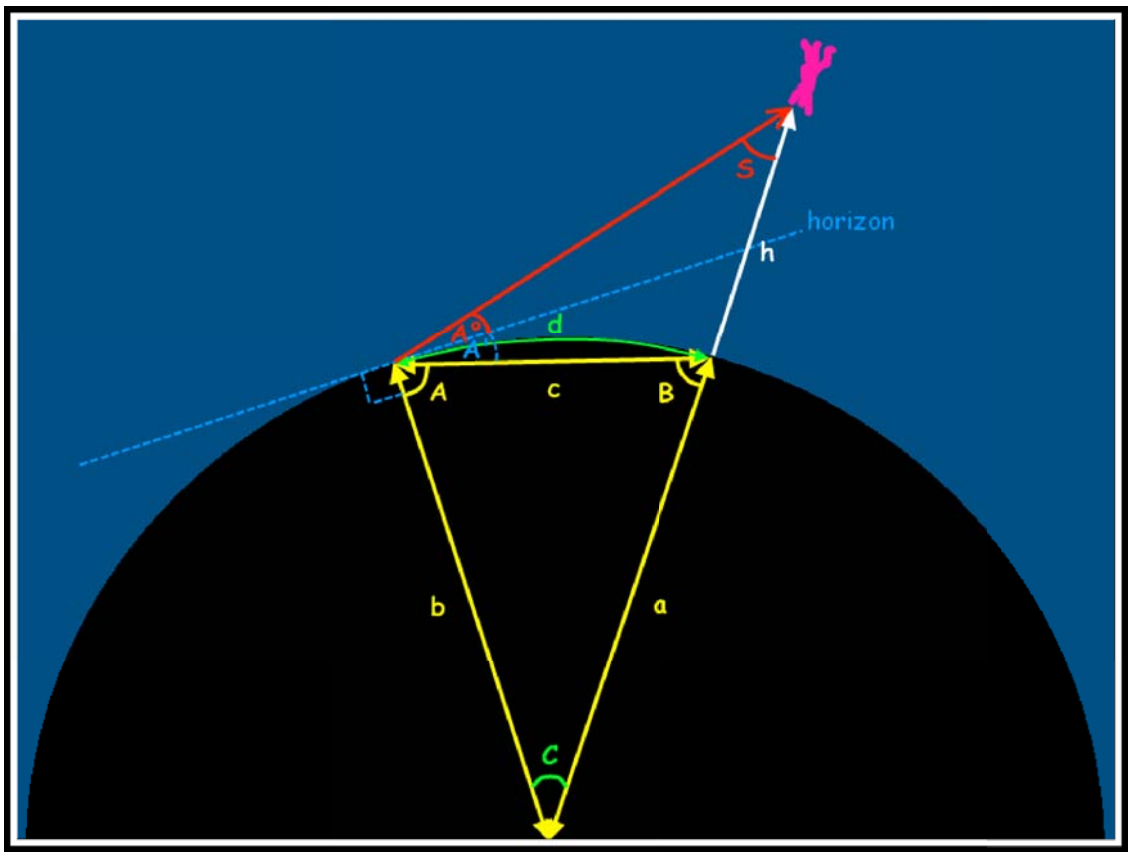

In order to calculate the altitude of a sprite or blue jet above the Earth's curved surface, its great circle distance d must be known, and from the images and star fitting method the elevation angle A^0 is derived. The Earth is an oblate sphere with a radius 6356 km < R < 6378 km. For the calculations we assume it is a true sphere, which is, given the only <0.3% differences, good enough for the comparatively short distances of TLEs. The above schematic picture exaggerates the height and distance of the sprite compared to the Earth. The sprite occurs in the zenith above point B at a great circle distance d from the camera in A. The astronomical software yields the elevation angle A^0 to the sprite above the astronomical horizon, which is tangent to the Earth's curved surface in A. If an elevation angle was instead derived from a visible horizon from a mountain or balloon camera location, one would have to consider this (a calculation different from described here, though perhaps not with significantly different results).

We can now construct a triangle ABC. Corner C (in degrees) follows simply from d:

$$C = \frac{180}{\pi}\frac{d}{a} \quad \text{with} \quad a = R$$

The cosine rule for triangle *ABC* with sides *abc* opposite to the corresponding corners *ABC* goes:

$$c^2 = a^2 + b^2 - 2ab\cos C$$

so if *a*=*b* it simplifies to

$$c = \sqrt{2a^2 - 2a^2\cos C}$$

which can be used for determining the second triangle: *ABS*. We happen to know more about the corners of this triangle, because the sum of *A* and *A'* is 90°, and the sum of *ABC* is 180°. So:

$$A = B = \frac{180° - C}{2} = 90° - \tfrac{1}{2}C \qquad \text{and} \qquad A' = 90° - A = \tfrac{1}{2}C$$

While corner S can be derived from the large triangle *ACS*:

$$S = 180° - C - (90° + A^0) = 90° - C - A^0$$

We can now solve the triangle ABS with the sine rule:

$$\frac{\sin A}{a} = \frac{\sin B}{b} = \frac{\sin C}{c}$$

Filling this out with the corresponding sides and angles gives:

$$\frac{\sin(A^0 + A')}{h} = \frac{\sin S}{c}$$

and the height of the TLE is found:

$$h = \frac{c\sin(A^0 + \tfrac{1}{2}C)}{\sin(90° - C - A^0)}$$

If h_{cam} is not zero, we have to deal with this from the first step.

$$a = R + h_{cam}$$

Points A and B are then above the Earth's surface, which requires a correction of great circle distance d which was measured over the surface itself. The corrected d' is:

$$\frac{d'}{2\pi(R+h_{cam})} = \frac{d}{2\pi R} \qquad \text{so} \qquad d' = \frac{(R+h_{cam})}{R} d$$

By using the corrected a and d' the same calculation is performed, and h_{cam} is added to the final answer h.
Running a test calculation for typical TLE distances, it becomes obvious that the differences between d and c, as well as d and d', are really small: less than 0.1 km, which is perhaps only a half percent of the distance. The uncertainty in the precise distance is larger than that imposed by the calculation when angle C is small (commonly less than 6° of latitude/longitude for sprites observed from ground).
It is therefore possible to simplify the calculation to:

$$h = \frac{d \sin(A^0 + \frac{1}{2}C)}{\sin(90° - C - A^0)} + h_{cam}$$

avoiding the calculation of c, and involves only an initial calculation of angle C.
For example, the altitude above the Earth's surface (not the local terrain but approximately the geoid) of the "fork" feature of the gigantic jet discussed in chapter 7, measured at an angle $A° = 7.75°$ at an assumed distance of d = 305 km, and h_{cam} = 1.4 km gives: $C = 2.74°$,

$$h = \frac{305 \cdot \sin(7.75° + 1.37°)}{\sin(90° - 2.74° - 7.75°)} + 1.4 = 50.6 \text{ km}$$

which corresponds with the value in Table 1, Van der Velde et al. (2007).
Similarly one could calculate the altitude of the beam of a weather radar with distance, for example a low elevation of 0.8° scans the precipitation at a distance of 100 km at 2.2 km height. Normally, however, the radar beam height calculation needs to consider the refractive properties of air, a result of the temperature stratification. This goes also for TLE observations. The increasing speed of light with altitude causes light from beyond the horizon to be visible. In effect, the TLE will be observed to occur at a slightly higher elevation angle than it actually was if there would be no atmosphere. Fortunately, the software SkyCharts calculates the refraction and scales its elevation grid accordingly.

2.7.2 Great Circle Paths

A "great circle" is a circle over the surface of a sphere such that the center of the circle coincides with that of the sphere. It is the shortest way to connect between two points over the surface of a sphere. A sprite orients itself perpendicular to the Earth's surface, which means always on the line through the center of the Earth, so that the great circle distance indicates where the sprite occurs in the zenith (i.e. its location on a map).
In order to calculate a great circle path, we need a reference coordinate system and the astronomical azimuth of the observed phenomenon relative to the meridian through the camera location. Meridians (lines of longitude) are great circles, whereas lines of latitude are not, except the equator (0°).
We can use the trigonometrical laws valid for spherical triangles to solve a great circle path. Our spherical triangle consists of the observation site *C*, north pole A, and a point *B* along our desired great circle path which crosses the local longitude line at the angle determined from the star fix.

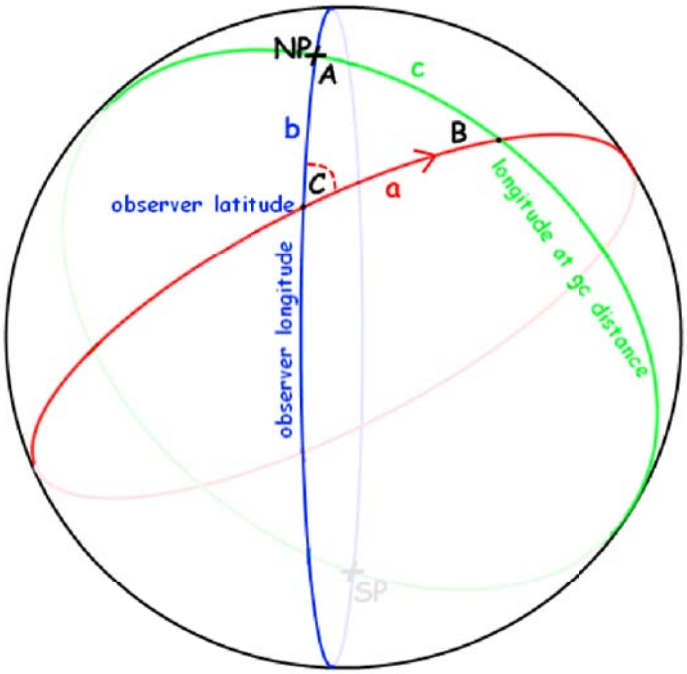

The law of haversines is applicable to the triangle *ABC*:

$$hav(c) = hav(a-b) + \sin(a)\sin(b)hav(C) \quad \text{where} \quad hav(\theta) = \sin^2\left(\frac{\theta}{2}\right)$$

Haversine means 'half the versed sine', a 'versed sine' is $1-\cos\theta$. Navigators used tables of haversines and their inverses to be able to calculate great circle distances and angles easily.

In this calculation, great circle parts *a, b, c* and azimuth C are expressed as angles in radians from the center of the sphere (i.e. *a/R*). We can now take *a* as any great circle distance, free to choose, as the great circle is mathematically defined (a numerical calculation using the previous latitude-longitude effectively corresponds to 'dead reckoning' by which the azimuth is kept constant, which is not what we want). To calculate a path, we take a series of *a* with increments of e.g. 10 kilometers. *b* is known: the great circle distance from the observation site to the north pole:

$b = \frac{\pi}{180} \cdot (90° - Lat_{cam})$ where *Lat* is latitude in degrees.

Now *hav(c)* can be solved. The inverse of this haversine gives *c*, which relates directly to the latitude of the point along the circle (just like *b*):

$c = 2\arcsin\left(\sqrt{hav(c)}\right)$ and $Lat_{GC} = 90° - \frac{180}{\pi} \cdot c$

The longitude relative to the observation site of the great circle point Lon_{GC} is angle A, basically determined by *a.* Using again the law of haversines:

$$hav(a) = hav(b-c) + \sin(c)\sin(b)hav(A)$$

$$hav(A) = \frac{hav(a) - hav(b-c)}{\sin(c)\sin(b)}$$

The angle A we find from the inverse haversine is relative to that of the observation site, and because it is always positive, we need to build in a test for initial angle C >180° in order to add or subtract A from Lon_{cam} :

$Lon_{GC} = Lon_{cam} - 2\arcsin\left(\sqrt{hav(A)}\right)$ for $\sin C < 0$
$Lon_{GC} = Lon_{cam} + 2\arcsin\left(\sqrt{hav(A)}\right)$ for $\sin C \geq 0$

2.7.3 Triangulation of Great Circle Paths

Finding the great circle distance between two known points on a sphere, *a* in the figure, we use angle A as the difference in longitudes of the points, and its legs b and c as the distances in radians from the North Pole as found from the latitude difference from the pole. Then, the Law of Haversines can be applied as above,

$$hav(a) = hav(b-c) + \sin(c)\sin(b)hav(A)$$

$$hav(A) = \frac{hav(a) - hav(b-c)}{\sin(c)\sin(b)}$$

or the simpler alternative, the Spherical Law of Cosines:

$$\cos(a) = \cos(b)\cos(c) + \sin(b)\sin(c)\cos(A)$$

$$\cos(A) = -\cos(B)\cos(C) + \sin(B)\sin(C)\cos(a)$$

and one of the main laws in spherical trigonometry:

$$\sin(a)\cos(B) = \cos(b)\sin(c) - \sin(b)\cos(c)\cos(A)$$

(where ABC are arranged anti-clockwise)
Triangulation of a sprite or lightning flash from two azimuths measured by observation sites or antennas can be done subsequently. These three points form a new spherical triangle SB'C'. First, the great circle distance *a* (baseline, in radians) between the sites is found, as well as the azimuths of the sites with respect to each other, using the North Pole as one of the corners (A). Then the difference between azimuth to the other observation site and the azimuth of the event is determined for each site, which yields angles B' and C'. Then distances b' or c' from the cameras to the sprite are calculated to determine the final position using a spherical triangle S, B or C, and North Pole (A).

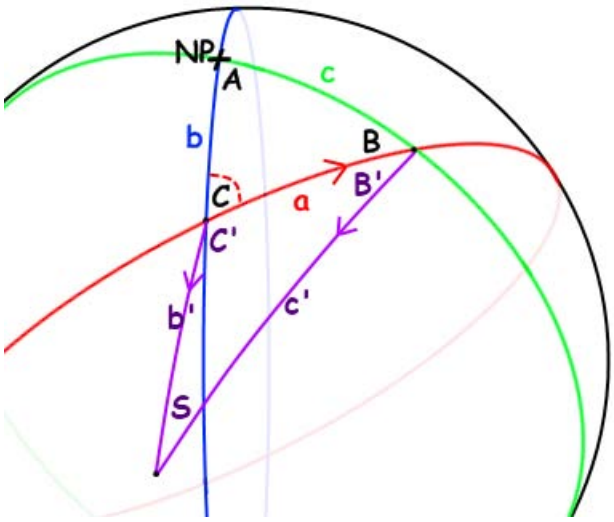

Let's demonstrate this with an example.

North Pole is **A**.

Camera in **B**: 44°N 5°E.
Camera in **C**: 43°N, 0°E.
Azimuth θ_B to Sprite: 230.3°
Azimuth θ_C to Sprite: 194.6°

Sprite at **S**: unknown °N, unknown °E

While here degrees are used for simplicity, in the formulas they are converted to radians. The number of numerical conversions between radians and degrees or kilometers should be minimized, since rounding errors will accumulate.
The baseline length in radians from the center of the Earth:

a = arccos(cos(90°-43°) cos(90°-44°) + sin(90°-43°) sin (90°-44°) cos(|5°-0°|))
a = 0.06565 (distance B-C is a*R = 418 km)

The bearing (azimuth) from C to B could be calculated using the rule:

$$\sin(a)\cos(C)=\cos(c)\sin(b)-\sin(c)\cos(b)\cos(A)$$

for a spherical triangle where ABC are arranged clockwise;
or using the Spherical Law of Sines:

$$\frac{\sin(A)}{\sin(a)}=\frac{\sin(B)}{\sin(b)}=\frac{\sin(C)}{\sin(c)}$$

However, in both cases ambiguity of quadrants is a problem. Since the atan2() function automatically sorts out the quadrants, the following method is commonly adopted to find the azimuths (initial bearing):

$x = \sin(lon_2-lon_1)\cos(lat_2)$
$y = \cos(lat_1)\sin(lat_2) - \sin(lat_1)\cos(lat_2)\cos(lon_2-lon_1)$
$\theta_1 = \mathrm{mod}(\mathrm{atan2}(x,y),2\pi)$

Which returns 256.32° for corner B, and 72.87° for corner C.
Angles C' and B' of the triangulation triangle can now be found with the azimuths of the observed event:

C' = | mod((C-θ_C)+180, 360)-180 | in degrees,
C' = | mod((C-θ_C)+π, 2π) - π | in radians,

and similarly for B'. Here the modulo makes sure we get the inside angles of the triangle.

The angle S:

S = arccos(-cos(B')cos(C')+sin(B')sin(C')cos(a)) = 32.34°

is the angle at which the directions from the cameras intersect. The optimal angle is 90°. At too small or too wide intersection angles (a few degrees from 0° or 180°) the position error can become large, since error in the measured angle in Sky Charts for each camera

can amount up to 10' for the most typical lenses used for TLE observations (6-16 mm). For reference, the full moon appears about 30' wide from Earth.

The distance of the sprite to B and C:

b' = asin(sin(B')/(sin(S)/sin(a))) and c' = asin(sin(C')/(sin(S)/sin(a)))
b' = 342.7 km, c' = 665.4 km

The final step is to complete the dashed line shown in the next figure to obtain latitude and longitude of the event. They can be calculated from either spherical triangle SAB or SAC.

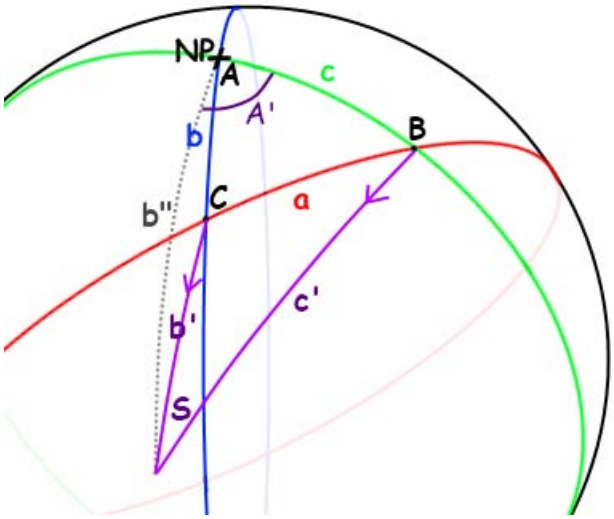

Here A' (the longitude difference) and b'' (latitude) are drawn only for the SAB triangle. We apply the Spherical Law of Cosines to find side b'':

$\cos(b'') = \cos(c)\cos(c')+\sin(c)\sin(c')\cos(\theta_B)$
$b'' = \text{acos}(\cos(c)\cos(c')+\sin(c)\sin(c')\cos(\theta_B))$
$Lat_S = 90°-b'' = 40.0117°$

Note that the azimuth can be the outside angle (>180°). In this case it does not matter, because the cosine is symmetrical around 180° (sign does not change).
Finally, the longitude is found from:

$\sin(A')/\sin(c') = \sin(\text{inside\_angle}_B)/\sin(b'')$
$A' = \arcsin(\sin(c') \sin(\text{inside\_angle\_B}) / \sin(b''))$
where $\text{inside\_angle}_B = |\text{mod}(\theta_B + \pi, 2\pi) -\pi|$

Depending on whether the event occurred more to the west, or to the east of the camera longitude, the A' should be subtracted or added:

if $\theta_B > 180°$: $Lon_S = Lon_B - A'$
if $\theta_B \leq 180°$: $Lon_S = Lon_B + A'$
$Lon_S = -1.0143°E$

S = 40°N, -1°E was the intended result for testing the algorithm but can only be obtained with exact input azimuths. The triangulation can be checked by comparing the outcomes of the two different triangles, SAB and SAC. If the input is incorrect (e.g. the azimuths are swapped so that no intersection of great circle paths occur), the outcomes are not equal.

2.8 Bibliography

Adachi, T., H. Fukunishi, Y. Takahashi, Y. Hiraki, R.-R. Hsu, H.-T. Su, A. B. Chen, S. B. Mende, H. U. Frey, and L. C. Lee (2006), Electric field transition between the diffusese and streamer regions of sprites estimated from ISUAL/array photometer measurements, Geophys. Res. Lett., 33, 17803, doi: 10.1029/2006GL026495.

Armstrong, R. A., J. A. Shorter, M. J. Taylor, D. M. Suszcynsky, W. A. Lyons, L. S. Jeong, Photometric measurements in the SPRITES '95 and '96 campaigns: nitrogen second positive (399.8 nm) and the first negative (427.8 nm) emission, J. Atm. Terr. Phys., 60, 787, 1998.

Avila, E. A., and R. G. Pereyra (2000), Charge Transfer During Crystal-Graupel Collisions for Two Different Cloud Droplet Size Distributions, Geophys. Res. Lett., 27(23), 3837–3840.

Barrington-Leigh, C. P., U. S. Inan, M. Stanley, and S. A. Cummer (1999), Sprites triggered by negative lightning discharges, Geophys. Res. Lett., 26(24), 3605–3608.

Barrington-Leigh, C. P., U. S. Inan, and M. Stanley (2001), Identification of sprites and elves with intensified video and broadband array photometry, J. Geophys. Res., 106(A2), 1741–1750.

Bell, T. F., V. P. Pasko, and U. S. Inan, "Runaway electrons as a source of Red Sprites in the mesosphere", Geophys. Res. Lett., 22, p. 2127, 1995.

Bell, T. F., S. C. Reising, and U. S. Inan (1998), Intense continuing currents following positive cloud-to-ground lightning associated with red sprites, Geophys. Res. Lett., 25(8), 1285–1288.

Berdeklis, P., and R. List, 2001: The ice crystal–graupel charging mechanism of thunderstorm electrification. J. Atmos. Sci., 58, 2751–2770.

Bering, E. A., III, J. R. Benbrook, L. Bhusal, J. A. Garrett, A. M. Paredes, E. M. Wescott, D. R., Moudry, D. D. Sentman, H. C. Stenbaek-Nielsen, and W. A., Lyons (2004), Observations of transient luminous events (TLEs) associated with negative cloud to ground (_CG) lightning strokes, Geophys. Res. Lett., 31, L05104, doi:10.1029/2003GL018659.

Betz, H.-D., K. Schmidt, P. Oettinger, and M. Wirz (2004), Lightning detection with 3-D discrimination of intracloud and cloud-to-ground discharges, Geophys. Res. Lett., 31, L11108, doi:10.1029/2004GL019821.

Blanc, E., T. Farges, R. Roche, D. Brebion, T. Hua, A. Labarthe, and V. Melnikov (2004), Nadir observations of sprites from the International Space Station, J. Geophys. Res., 109, A02306, doi:10.1029/2003JA009972.

Boccippio, D. J., E. R. Williams, S. J. Heckman, W. A. Lyons, I. T. Baker, and R. Boldi (1995), Sprites, ELF transients, and positive ground strokes, Science, 269, 1088-1091.

Boeck, W. L., O. H. Vaughn Jr., R. Blakeslee, B. Vonnegut, and M. Brook (1992), Lightning induced brightening in the airglow layer, Geophys. Res. Lett., 19(2), 99–102.

Branick, M.L., and C.A. Doswell,III, An observation of the relationship between supercell structure and lightning ground strike polarity, Weather and Forecasting, 7, 143-149, 1992.

Brooks, H. E., J. W. Lee, and J.P. Craven, (2003), The spatial distribution of severe thunderstorm and tornado environments from global reanalysis data. Atmospheric Research, 67-68, 73-94.

Carey, L.D., and K.M. Buffalo, (2007) Environmental Control of Cloud-to-Ground Lightning Polarity in Severe Storms, Monthly Weather Review, 135, 1327–1353.

Carey, L. D., M. J. Murphy, T. L. McCormick, and N. W. S. Demetriades (2005), Lightning location relative to storm structure in a leading-line, trailing-stratiform mesoscale convective system, J. Geophys. Res., 110, D03105, doi:10.1029/2003JD004371.

Changnon, S.A. (1992), Temporal and spatial relations between hail and lightning, J. Appl. Meteor., 31, 587-604.

Chauzy, S., M. Chong, A. Delannoy, and S. Despiau (1985), The June 22 tropical squall line observed during the COPT 81 experiment: Electrical signature associated with dynamical structures and precipitation, J. Geophys. Res., 90, 6091-6098.

Cho, M. and M.J. Rycroft (2001), Non-uniform ionisation of the upper atmosphere due to the electromagnetic pulse from a horizontal lightning discharge, Journal of Atmospheric and Solar-Terrestrial Physics 63, pp. 559–580.

Coleman, L. M., T. C. Marshall, M. Stolzenburg, T. Hamlin, P. R. Krehbiel, W. Rison, and R. J. Thomas, Effects of charge and electrostatic potential on lightning propagation, J. Geophys. Res., 108(D9), 4298, doi:10.1029/2002JD002718, 2003.

Cooray, V. and V. Rakov, (2007), Does Wilson's cloud chamber offer clues on lightning initiation in thunderclouds? Eos Trans. AGU, 88(52), Fall Meet. Suppl., Abstract AE31A-0021

Coquillat, S., B. Combal, and S. Chauzy, Corona emission from raindrops in strong electric fields as a possible discharge initiation: Comparison between horizontal and vertical field configurations, J. Geophys. Res., 108(D7), 4205, doi:10.1029/2002JD002714, 2003.

Cummer, S. A. (2003), Current moment in sprite-producing lightning, J. Atm. and Sol.-Terr. Phys., 65, 499

Cummer, S. A. and M. Füllekrug, (2001), Unusually intense continuing current in lightning produces delayed mesospheric breakdown. Geophys. Res. Lett. 28, 3, 495-498

Cummer, S.A. and W.A. Lyons, 2005: Implications of lightning charge moment changes for sprite initiation. J. Geophys. Res., 110, A04304, doi:10.1029/2004JA010812.

Cummer, S. A., and M. Stanley (1999), Submillisecond Resolution Lightning Currents and Sprite Development: Observations and Implications, Geophys. Res. Lett., 26(20), 3205–3208.

Cummer, S. A., N. Jaugey, J. Li, W. A. Lyons, T. E. Nelson, and E. A. Gerken (2006), Submillisecond imaging of sprite development and structure, Geophys. Res. Lett., 33, L04104, doi:10.1029/2005GL024969.

Cummins, K. L., M. J. Murphy, E. A. Bardo, W. L. Hiscox, R. B. Pyle, and A. E. Pifer (1998), A Combined TOA/MDF Technology Upgrade of the U.S. National Lightning Detection Network, J. Geophys. Res., 103(D8), 9035–9044.

Drake, J. C. (1968), Electrification accompanying the melting of ice particles, Q.J.R. Meteorol. Soc., 94, 176-191.

Dwyer, J. R., et al., Energetic radiation produced during rocket-triggered lightning, Science, 299, 694–697, 2003

Eack, K. B. (2004), Electrical characteristics of narrow bipolar events, Geophys. Res. Lett., 31, L20102, doi:10.1029/2004GL021117.

Eack K. B., Beasley W. H., Rust W. D., Marshall T. C. and Stolzenburg M. (1996), Initial results from simultaneous observations of X-rays and electric fields in a thunderstorm J. Geophys. Res. 101 29637–40

Engholm, C. D., E. R. Williams, and R. M. Dole, 1990: Meteorological and electrical conditions associated with positive cloud-to-ground lightning. Mon. Wea. Rev., 118, 470–487.

Fishman, G. J., P. N. Baht, R. Mallozzi, J. M. Horack, T. Koshut, C. Kouveliotou, G. N. Pendleton, C. A. Meegan, R. B. Wilson, W. S. Paciesas, S. J. Goodman, and H. J. Christian, Discovery of intense gamma-ray flashes of atmospheric origin, Science, 164, 1313, 1994.

Franz, R. C., R. J. Nemzek, and J. R. Winckler, Television image of a large upward electrical discharge above a thunderstorm system, Science, 249, 48, 1990.

Frey, H. U., S. B. Mende, S. A. Cummer, A. B. Chen, R.-R. Hsu, H.-T. Su, Y.-S. Chang, T. Adachi, H. Fukunishi, and Y. Takahashi (2005), Betatype stepped leader of elve-producing lightning, Geophys. Res. Lett., 32, L13824, doi:10.1029/2005GL023080.

Fukunishi, H., Y. Takahashi, M. Kubota, K. Sakanoi, U. S. Inan, and W. A. Lyons (1996), Elves: Lightning-induced transient luminous events in the lower ionosphere, Geophys. Res. Lett., 23(16), 2157–2160.

Fuquay, D. M. (1982), Positive Cloud-to-Ground Lightning in Summer Thunderstorms, J. Geophys. Res., 87(C9), 7131–7140.

Ganot, M., Y. Yair, C. Price, B. Ziv, Y. Sherez, E. Greenberg, A. Devir, and R. Yaniv (2007), First detection of transient luminous events associated with winter thunderstorms in the eastern Mediterranean, Geophys. Res. Lett., 34, L12801, doi:10.1029/2007GL029258.

Gerken, E., U. Inan, and C. Barrington-Leigh, Telescopic imaging of sprites, Geophys. Res. Lett., 27, 2637-2640, 2000.

Gurevich, A. V., G. M. Milikh, and R. A. Roussell-Dupré, Runaway electron mechanism of air breakdown and preconditioning during a thunderstorm, Phys. Lett. A, 165, 463, 1992.

Haldoupis, C., T. Neubert, U. S. Inan, A. Mika, T. H. Allin, and R. A. Marshall (2004), Subionospheric early VLF signal perturbations observed in one-to-one association with sprites, J. Geophys. Res., 109, A10303, doi:10.1029/2004JA010651.

Hampton, D. L., M. J. Heavner, E. M. Wescott, and D. D. Sentman (1996), Optical spectral characteristics of sprites, Geophys. Res. Lett., 23(1), 89–92.

Hayakawa, M., T. Nakamura, Y. Hobara, and E. Williams (2004), Observation of sprites over the Sea of Japan and conditions for lightning-induced sprites in winter, J. Geophys. Res., 109, A01312, doi:10.1029/2003JA009905.

Heavner, M. (2000), PhD dissertation, University of Alaska Fairbanks, USA.

Heckman, S. 1992. Why does a lightning flash have multiple strokes? Ph.D. Dissertation, Mass. Inst. of Technol., Cambridge.

Houze, R. A. Jr., B. F. Smull, and P. Dodge (1990), Mesoscale organization of springtime rainstorms in Oklahoma, Mon. Wea. Rev., 118, 613-654.

Hu, W., S. A. Cummer, W. A. Lyons and T. E. Nelson, 2002, Lightning charge moment changes for the initiation of sprites, Geophys. Res. Lett., 29 (8), 1279.

Huang, E., E. Williams, R. Boldi, S. Heckman, W. Lyons, M. Taylor, T. Nelson, and C. Wong (1999), Criteria for sprites and elves based on Schumann resonance observations, J. Geophys. Res., 104(D14), 16,943–16,964.

Hunter, S. M., T. J. Schuur, T. C. Marshall, and W. D. Rust, 1992: Electrical and kinematic structure of the Oklahoma mesoscale convective system of 7 June 1989. Mon. Wea. Rev., 120, 2226–2239.

Ignaccolo, M., T. Farges, A. Mika, T. H. Allin, O. Chanrion, E. Blanc, T. Neubert, A. C. Fraser-Smith, and M. Füllekrug (2006), The Planetary rate of sprite events, Geophys. Res. Lett., 33, L11808, doi:10.1029/2005GL025502

Inan, U. S., S. C. Reising, G. J. Fishman, and J. M. Horack (1996), On the association of terrestrial gamma-ray bursts with lightning and implications for sprites, Geophys. Res. Lett., 23(9), 1017–1020.

Inan, U. S., C. Barrington-Leigh, S. Hansen, V. S. Glukhov, T. F. Bell, and R. Rairden (1997), Rapid lateral expansion of optical luminosity in lightning-induced ionospheric flashes referred to as 'elves', Geophys. Res. Lett., 24(5), 583–586.

Inan, U. S., S. C. Reising, G. J. Fishman and J. M. Horack, "On the association of terrestrial gamma-ray bursts with lightning and implication for sprites", Geophys. Res. Lett., 23, p. 1017, 1996.

Inan, U. S., M. B. Cohen, R. K. Said, D. M. Smith, and L. I. Lopez (2006), Terrestrial gamma ray flashes and lightning discharges, Geophys. Res. Lett., 33, L18802, doi:10.1029/2006GL027085.

Jayaratne, E. R., and C. P. R. Saunders (1985), Thunderstorm electrification: The effect of cloud droplets, J. Geophys. Res., 90(D7), 13,063– 13,066.

Jayaratne, E. R., C. P. R. Saunders, and J. Hallett, 1983: Laboratory studies of the charging of soft-hail during ice crystal interactions. Quart. J. Roy. Meteor. Soc., 109, 609–630.

Johnson, M. P., and U. S. Inan (2000), Sferic clusters associated with early/fast VLF events, Geophys. Res. Lett., 27(9), 1391–1394.

Kasemir, H. W. (1960), A Contribution to the Electrostatic Theory of a Lightning Discharge, J. Geophys. Res., 65(7), 1873–1878.

Knapp, D.I., 1994. Using cloud-to-ground lightning data to identify tornadic thunderstorm signatures and nowcast severe weather. Natl. Weather Dig. 19, 35– 42.

Krehbiel, P. R., J. A. Riousset, V. P. Pasko, R. J. Thomas, W. Rison, M. A. Stanley, and H. E. Edens (2008), Upward electrical discharges from thunderstorms, Nat. Geosci., 1(4), 233–237, doi:10.1038/ngeo162.

Kuo, C.-L., et al. (2007), Modeling elves observed by FORMOSAT-2 satellite, J. Geophys. Res., 112, A11312, doi:10.1029/2007JA012407.

Lang, T.J., Rutledge, S.A., Dye, J.E., Venticinque, M., Laroche, P., Defer, E., 2000. Anomalously low negative cloud-to-ground lightning flash rates in intense convective storms observed during STERAO-A. Mon. Weather. Rev. 128, 160–173.

Lang, T.J., L.J. Miller, M. Weisman, S.A. Rutledge, L.J. Barker, V.N. Bringi, V. Chandrasekar, A. Detwiler, N. Doesken, J. Helsdon, C. Knight, P. Krehbiel, W.A. Lyons, D. Macgorman, E. Rasmussen, W. Rison, W.D. Rust, and R.J. Thomas, 2004: The Severe Thunderstorm Electrification and Precipitation Study. Bull. Amer. Meteor. Soc., 85, 1107–1125.

Lang, T. J., S. A. Rutledge, and K. C. Wiens, 2004, Origins of positive cloud-to-ground lightning flashes in the stratiform region of a mesoscale convective system, Geophys. Res. Lett., 31, L10105, doi:10.1029/2004GL019823.

Lang, T. J., and S. A. Rutledge (2006), Cloud-to-ground lightning downwind of the 2002 Hayman forest fire in Colorado, Geophys. Res. Lett., 33, L03804, doi:10.1029/2005GL024608.

LeVine, D. M. (1980), Sources of strongest RF radiation from lightning, J. Geophys. Res., 85, 4091– 4095.

Ligda, M. G. H., The radar observations of lightning, J. Atmos. Sol. Terr. Phys., 9, 329–346, 1956.

Lucas, C., E. J. Zipser, and M. A. LeMone, 1994: Vertical velocity in oceanic convection off tropical Australia. J. Atmos. Sci., 51, 3183–3193.

Lyons, W. A. (1994), Characteristics of luminous structures in the stratosphere above thunderstorms as imaged by low-light video, Geophys. Res. Lett., 21(10), 875–878.

Lyons, W. A. (1996), Sprite observations above the U.S. High Plains in relation to their parent thunderstorm systems, J. Geophys. Res., 101(D23), 29,641–29,652.

Lyons, W. A., M. Uliasz, and T. E. Nelson (1998), Climatology of large peak current cloud-to-ground lightning flashes in the contiguous United States, Mon. Weather Rev., 126, 2217–2233.

Lyons, W.A., T.E. Nelson, E.R. Williams, S.A. Cummer and M.A. Stanley (2003), Characteristics of Sprite-Producing Positive Cloud-to-Ground Lightning during the 19 July 2000 STEPS Mesoscale Convective Systems, Mon. Wea. Rev., 131, (10), pp. 2417–2427.

Lyons, W. A., L.M. Andersen, T.E. Nelson and G.R. Huffines, (2006), Characteristics of sprite-producing electrical storms in the STEPS 2000 domain. On line summary and CD, 2nd Conf. on Meteorological Applications of Lightning Data, AMS, Atlanta, 19 pp.

MacGorman, D.R., D.W. Burgess, V. Mazur, W. D. Rust, W. L. Taylor, and B. C. Johnson, 1989: Lightning rates relative to tornadic storm evolution on 22 May 1981. J. Atmos. Sci., 46, 221–250.

MacGorman, D.R., and D.W. Burgess (1994), Positive cloud-to-ground lightning in tornadic storms and hailstorms, Mon. Weather Rev., 122, 1671-1697.

MacGorman, D. R., and C. D. Morgenstern (1998), Some characteristics of cloud-to-ground lightning in mesoscale convective systems, J. Geophys. Res., 103(D12), 14,011–14,024.

MacGorman, D. R. and Rust, W. D. 1998 The electrical nature of storms. Oxford University Press, New York, USA.

MacGorman, D., D. Rust, O. van der Velde, M. Askelson, P. Krehbiel, and R. Thomas, 2003, Lightning Relative to Precipitation and Tornadoes in a Supercell Storm, Preprints, 12th International Conference on Atmospheric Electricity, Versailles, France, June 2003.

MacGorman, D.R., W.D. Rust, P. Krehbiel, W. Rison, E. Bruning, and K. Wiens, 2005: The Electrical Structure of Two Supercell Storms during STEPS. Mon. Wea. Rev., 133, 2583–2607.

Maddox, R. A. (1980), Mesoscale convective complexes, Bull. Am. Meteorol. Soc., 61, 1374-1387.

Malan, D.J. 1958. Radiation from lightning discharges and its relation to the discharge processes. In Recent Advances in Atmospheric Electricity, ed. L.G. Smith, pp. 557-563, London: Pergamon.

Mansell, E. R., D. R. MacGorman, C. L. Ziegler, and J. M. Straka (2002), Simulated three-dimensional branched lightning in a numerical thunderstorm model, J. Geophys. Res., 107(D9), 4075, doi:10.1029/2000JD000244.

Mansell, E. R., D. R. MacGorman, C. L. Ziegler, and J. M. Straka (2005), Charge structure and lightning sensitivity in a simulated multicell thunderstorm, J. Geophys. Res., 110, D12101, doi:10.1029/2004JD005287.

Marshall, T. C., and W. D. Rust, 1993: Two types of vertical electrical structures in stratiform precipitation regions of mesoscale convective systems. Bull. Amer. Meteor. Soc., 74, 2159–2170.

Marshall, R. A., and U. S. Inan (2007), Possible direct cloud-to-ionosphere current evidenced by sprite-initiated secondary TLEs, Geophys. Res. Lett., 34, L05806, doi:10.1029/2006GL028511.

Marshall, T. C., W. D. Rust, and M. Stolzenburg (1995), Electrical structure and updraft speeds in thunderstorms over the southern Great Plains, J. Geophys. Res., 100(D1), 1001–1015.

Marshall, T. C., M. Stolzenburg, W. D. Rust, E. R. Williams, and R. Boldi (2001), Positive charge in the stratiform cloud of a mesoscale convective system, J. Geophys. Res., 106(D1), 1157–1163.

Marshall, R. A., U. S. Inan, and W. A. Lyons (2007), Very low frequency sferic bursts, sprites, and their association with lightning activity, J. Geophys. Res., 112, D22105, doi:10.1029/2007JD008857.

Mazur, V., Triggered lightning strikes to aircraft and natural intracloud discharges, J. Geophys. Res., 94(D3), 3311-3325, 10.1029/88JD03884, 1989.
Mazur, V., 2002. Physical processes during development of lightning flashes. C.R. Physique 3, 1393– 1409.
Mazur, V., and L. H. Ruhnke (1993), Common Physical Processes in Natural and Artificially Triggered Lightning, J. Geophys. Res., 98(D7), 12,913–12,930.
Mazur, V., and L. H. Ruhnke (1998), Model of electric charges in thunderstorms and associated lightning, J. Geophys. Res., 103(D18), 23,299–23,308.
Mazur, V., P. R. Krehbiel, and X.-M. Shao (1995), Correlated high-speed video and radio interferometric observations of a cloud-to-ground lightning flash, J. Geophys. Res., 100(D12), 25,731–25,754.
Mazur, V., X. Shao, and P. R. Krehbiel (1998), "Spider" lightning in intracloud and positive cloud-to-ground flashes, J. Geophys. Res., 103(D16), 19,811–19,822.
Mazur, V., E. Williams, R. Boldi, L. Maier, and D. E. Proctor (1997), Initial comparison of lightning mapping with operational Time-of-Arrival and Interferometric systems, J. Geophys. Res., 102(D10), 11,071–11,086.
McCaul E. W. Jr., and C. Cohen, 2002: The impact on simulated storm structure and intensity of variations in the mixed layer and moist layer depths. Mon. Wea. Rev., 130, 1722–1748.
McHarg, M. G., R. K. Haaland, D. Moudry, and H. C. Stenbaek-Nielsen (2002), Altitude-time development of sprites, J. Geophys. Res., 107(A11), 1364, doi:10.1029/2001JA000283.
McHarg, M. G., H. C. Stenbaek-Nielsen, and T. Kammae (2007), Observations of streamer formation in sprites, Geophys. Res. Lett., 34, L06804, doi:10.1029/2006GL027854.
Mende, S. B., R. L. Rairden, G. R. Swenson, and W. A. Lyons (1995), Sprite spectra; N2 1 PG band identification, Geophys. Res. Lett., 22(19), 2633–2636.
Mika, A., C. Haldoupis, R. A. Marshall, T. Neubert, and U. S. Inan (2005), Subionospheric VLF signature and their association with sprites observed during EuroSprite-2003, J. Atmos. Sol. Terr. Phys., 67, 1580
Morel, C., Sénési, S. (2000), SAF NWC scientific report for MTR on PGE11 rapid developing thunderstorms, METEOFRANCE CNRM, web report.
Moudry, D., H. Stenbaek-Nielsen, D. Sentman, and E. Wescott, Imaging of elves, halos and sprite initiation at 1 ms time resolution, J. Atmos. Solar-Terr. Phys., 65, 509-518, 2003.
Neubert, T., T. H. Allin, H. Stebaek-Nielsen, and E. Blanc, sprites over Europe, Geophys. Res. Lett., 28, 3585, 2001.
Neubert T., et al. (2005), Co-ordinated observations of transient luminous events during the EuroSprite2003 campaign, J. Atm. and Sol.-Terr. Phys., 67, 807-820.
Ohkubo, A., H. Fukunishi, Y. Takahashi, and T. Adachi (2005), VLF/ELF sferic evidence for in-cloud discharge activity producing sprites, Geophys. Res. Lett., 32, L04812, doi:10.1029/2004GL021943.
Orville, R. E., G. R. Huffines, W. R. Burrows, R. L. Holle, and K. Cummins (2002), The North American Lightning Detection Network (NALDN)-First results: 1998–2000, Mon. Weather Rev., 130, 2098–2109.
Parker, M.D., and R.H. Johnson (2000), Organizational Modes of Midlatitude Mesoscale Convective Systems. Mon. Wea. Rev., 128, 3413–3436.
Parker, M.D., S.A. Rutledge, and R.H. Johnson (2001), Cloud-to-Ground Lightning in Linear Mesoscale Convective Systems. Mon. Wea. Rev., 129, 1232–1242.
Pasko, V. P., U. S. Inan, and T. F. Bell (2001), Mesosphere-troposphere coupling due to sprites, Geophys. Res. Lett., 28(19), 3821–3824.
Pasko, V. P., M. A. Stanley, J. D. Mathews, U. S. Inan, and T. G. Wood, Electrical discharge from a thundercloud top to the lower ionosphere. Nature, 416, 152 - 154, 2002.
Pasko, V. P., and J. J. George, Three-dimensional modeling of blue jets and blue starters, J. Geophys. Res., 107(A12), 1458, doi:10.1029/2002JA009473, 2002.
Pasko, V. P., and H. C. Stenbaek-Nielsen (2002), Diffuse and streamer regions of sprites, Geophys. Res. Lett., 29(10), 1440, doi:10.1029/2001GL014241.
Pasko, V. P., U. S. Inan, and T. F. Bell (1996), Sprites as luminous columns of ionization produced by quasi-electrostatic thundercloud fields, Geophys. Res. Lett., 23(6), 649–652.
Pasko, V. P., U. S. Inan, T. F. Bell, and Y. N. Taranenko (1997), Sprites produced by quasi-electrostatic heating and ionization in the lower ionosphere, J. Geophys. Res., 102(A3), 4529–4562.

Pereyra, R.G., Avila, E.E., Castellano, N.E., Saunders, C.P.R., 2000. A laboratory study of graupel charging. J. Geophys. Res. 105, 20803– 20813.

Price, C., W. Burrows, and P. King, The likelihood of winter sprites over the Gulf Stream, Geophys. Res. Lett., 29(22), 2070, doi:10.1029/2002GL015571, 2002.

Proctor, D. E. (1981), VHF Radio Pictures of Cloud Flashes, J. Geophys. Res., 86(C5), 4041–4071.

Proctor, D. E., R. Uytenbogaardt, and B. M. Meredith (1988), VHF RADIO PICTURES OF LIGHTNING FLASHES TO GROUND, J. Geophys. Res., 93(D10), 12,683–12,727.

Proctor, D. E. (1997), Lightning flashes with high origins, J. Geophys. Res., 102(D2), 1693–1706.

Raizer, Y. P., G. M. Milikh, and M. N. Shneider (2006), On the mechanism of blue jet formation and propagation, Geophys. Res. Lett., 33, L23801, doi:10.1029/2006GL027697.

Rakov, V. A., and W. G. Tuni, Lightning electric field intensity at high altitudes: Inferences for production of elves, J. Geophys. Res., 108(D20), 4639, doi:10.1029/2003JD003618, 2003.

Rakov, V. A., and M. A. Uman (2003), Lightning—Physics and Effects, 687 pp., Cambridge Univ. Press, New York.

Rust, W. D., D. R. MacGorman, and W. L. Taylor (1985), Photographic verification of continuing current in positive cloud-to-ground flashes, J. Geophys. Res., 90, 6144-6146.

Rust, W.D., MacGorman, D.R., 2002. Possibly inverted-polarity electrical structures in thunderstorms during STEPS. Geophys. Res. Lett. 29 (No. 12).

Rutledge, S. A., and R. A. Houze, Jr. (1987), A diagnostic modeling study of the trailing stratiform region of a midlatitude squall line, J. Atmos. Sci., 44, 2640-2656.

Rutledge, S.A., and D.R. MacGorman, 1988: Cloud-to-Ground Lightning Activity in the 10–11 June 1985 Mesoscale Convective System Observed during the Oklahoma–Kansas PRE-STORM Project. Mon. Wea. Rev., 116, 1393–1408.

Rutledge, S. A., C. Lu, and D. R. MacGorman (1990), Positive cloud-to-ground lightning in mesoscale convective systems, J. Atmos. Sci., 47, 2085-2100.

Rutledge, S.A., and W.A. Petersen, (1994), Vertical Radar Reflectivity Structure and Cloud-to-Ground Lightning in the Stratiform Region of MCSs: Further Evidence for In Situ Charging in the Stratiform Region. Mon. Wea. Rev., 122, 1760–1776.

Romero, R., M. Gayà, C. A. Doswell III, 2007: European climatology of severe convective storm environmental parameters: A test for significant tornado events. Atmospheric Research 83, 389–404

Saba, M. M. F., M. G. Ballarotti, and O. Pinto Jr. (2006a), Negative cloud-to-ground lightning properties from high-speed video observations, J. Geophys. Res., 111, D03101, doi:10.1029/2005JD006415.

Saba, M. M. F., O. Pinto Jr., and M. G. Ballarotti (2006b), Relation between lightning return stroke peak current and following continuing current, Geophys. Res. Lett., 33, L23807, doi:10.1029/2006GL027455.

São Sabbas, F. T., D. D. Sentman, E. M. Wescott, O. Pinto, Jr. Odim Mendes, Jr. and M. J. Taylor, 2003, Statistical analysis of space–time relationships between sprites and lightning, J. Atm. and Sol.-Terr. Phys., 65, 5, 525-535.

Sato, M., and H. Fukunishi, Global sprite occurrence locations and rates derived from triangulation of transient Schumann resonance events, Geophys. Res. Lett., 30(16), 1859, doi:10.1029/2003GL017291, 2003.

Saunders, C. P. R., and S. L. Peck (1998), Laboratory studies of the influence of the rime accretion rate on charge transfer during crystal/graupel collisions, J. Geophys. Res., 103, 13,949–13,956.

Saunders, C. P.R. , W. D. Keith, and R. P. Mitzeva, 1991: The effect of liquid water on thunderstorm charging. J. Geophys. Res., 96, 11 007–11 017.

Schuur, T.J. and S. A. Rutledge, 2000a: Electrification of stratiform regions in mesoscale convective systems. Part I: An observational comparison of symmetric and asymmetric MCSs. J. Atmos. Sci., 57, 1961–1982.

Schuur, T.J. and S. A. Rutledge, 2000b: Electrification of Stratiform regions in Mesoscale Convective Systems. Part II: Two-dimensional numerical model simulations of a symmetric MCS. J. Atmos. Sci., 57, 1983–2006.

Seity, Y., S. Soula, P. Tabary and G. Scialom (2003), The convective storm system during IOP 2a : Cloud-to-Ground lightning flash production in relation with dynamics and microphysics, Q. J. R. Meteorol. Soc, 129, Part B (MAP) No. 588, 523-542.

Sentman, D. D., E. M. Wescott, D. L. Osborne, D. L. Hampton, and M. J. Heavner (1995), Preliminary results from the Sprites94 aircraft campaign: 1. Red sprites, Geophys. Res. Lett., 22(10), 1205–1208.

Sentman, D. D., E. M. Wescott, R. H. Picard, J. R. Winick, H. C. Stenbaek-Nielsen, E. M. Dewan, D. R. Moudry, F. T. São Sabbas, M. J. Heavner, and J. Morill, Simultaneous observations of mesospheric gravity waves and sprites generated by a Midwestern thunderstorm, J. Atmosph. Solar-Terr. Phys., 65, 537-550, 2003.

Shao, X. M., P. R. Krehbiel, R. J. Thomas, and W. Rison (1995), Radio interferometric observations of cloud-to-ground lightning phenomena in Florida, J. Geophys. Res., 100(D2), 2749–2784.

Shao, X. M., and P. R. Krehbiel (1996), The spatial and temporal development of intracloud lightning, J. Geophys. Res., 101(D21), 26,641–26,668.

Shepherd, T. R., W. D. Rust, and T. C. Marshall, 1996: Electric fields and charges near 08C in stratiform clouds. Mon. Wea. Rev., 124, 919–938.

Simpson, G. C., 1909: On the electricity of rain and its origin in thunderstorms. Proc. Roy. Soc. London, A209, 379–413.

Smith, D. A., X. M. Shao, D. N. Holden, C. T. Rhodes, M. Brook, P. R. Krehbiel, M. Stanley, W. Rison, and R. J. Thomas (1999), A distinct class of isolated intracloud lightning discharges and their associated radio emissions, J. Geophys. Res., 104, 4189–4212.

Smith, S.B., J.G. LaDue, and D.R. MacGorman, 2000: The Relationship between Cloud-to-Ground Lightning Polarity and Surface Equivalent Potential Temperature during Three Tornadic Outbreaks. Mon. Wea. Rev., 128, 3320–3328.

Snively, J. B., and V. P. Pasko (2003), Breaking of thunderstorm-generated gravity waves as a source of short-period ducted waves at mesopause altitudes, Geophys. Res. Lett., 30(24), 2254, doi:10.1029/2003GL018436

Stanley, M.A., 2000: Sprites and their parent discharges. PhD. Dissertation, New Mexico Institute of Mining and Technology, Socorro, NM, 163 pp.

Stanley, M., P. Krehbiel, M. Brook, C. Moore, W. Rison, and B. Abrahams (1999), High speed video of initial sprite development, Geophys. Res. Lett., 26(20), 3201–3204.

Stanley, M. A. (2000), Sprites and their parent discharges, Ph.D. dissertation, 163 pp., N. M. Inst. of Mining and Technol., Socorro, N. M.

Stenbaek-Nielsen, H. C., D. R. Moudry, E. M. Wescott, D. D. Sentman, and F. T. Sâo Sabbas (2000), Sprites and possible mesospheric effects, Geophys. Res. Lett., 27(23), 3829–3832.

Stenbaek-Nielsen, H. C., M. G. McHarg, T. Kanmae, and D. D. Sentman (2007), Observed emission rates in sprite streamer heads, Geophys. Res. Lett., 34, L11105, doi:10.1029/2007GL029881.

Stolzenburg, M., and T. C. Marshall, Testing models of thunderstorm charge distributions with Coulomb's law, J. Geophys. Res., 99, 25921-25932, 1994.

Stolzenburg, M., T. C. Marshall, W. D. Rust, and B. F. Smull, 1994: Horizontal distribution of electrical and meteorological conditions across the stratiform region of a mesoscale convective system. Mon. Wea. Rev., 122, 1777–1797.

Stolzenburg, M., W. D. Rust, and T. C. Marshall, Electrical structure in thunderstorm convective regions, 3. Synthesis, J. Geophys. Res., 103, 14,097– 14,108, 1998.

Stolzenburg, M., T. C. Marshall, W. D. Rust, E. Bruning, D. R. MacGorman, and T. Hamlin, Electric fields observed near lightning flash initiations (2007), Geophys. Res. Lett., 34, L04804, doi:10.1029/2006GL028777

Su, H. T., R. R. Hsu, A. B. Chen, Y. C. Wang, W. S. Hsiao, W. C. Lai, L. C. Lee, M. Sato, and H. Fukunishi, Gigantic jets between a thundercloud and the ionosphere, Nature, 423, 974, 26. June, 2003.

Su, H.-T., A. B. Chen, C.L. Kuo, Y.J. Lee, R.R. Hsu ; J.L. Chern, H. U. Frey, S. B. mende, Y. Takahashi, H. Fukunishi, L. C. Lee, 2007: Global Occurrence of TLE's and their effects. ICAE 2007, Beijing.

Sukhorukov, A. I., E. V. Mishin, P. Stubbe, and M. J. Rycroft (1996), On blue jet dynamics, Geophys. Res. Lett., 23(13), 1625–1628.

Suszcynsky, D. M., and M. J. Heavner (2003), Narrow bipolar events as indicators of thunderstorm convective strength, Geophys. Res. Lett., 30(17), 1879, doi:10.1029/2003GL017834.

Takahashi, T., 1978: Riming electrification as a charge generation mechanism in thunderstorms. J. Atmos. Sci., 35, 1536–1548.

Taranenko, Y., and R. Roussel-Dupré, High altitude discharges and gamma-ray flashes: a manifestation of runaway air breakdown, Geophys. Res. Lett., 23, 571, 1996.

Tessendorf, S. A., L. J. Miller, K. C. Wiens, and S. A. Rutledge, 2005: The 29 June 2000 supercell observed during STEPS. Part I: Kinematics and microphysics. J. Atmos. Sci., 62, 4127–4150.

Thomas, R. J., P. R. Krehbiel, W. Rison, T. Hamlin, D. J. Boccippio, S. J. Goodman, and H. J. Christian (2000), Comparison of Ground-Based 3-Dimensional Lightning Mapping Observations with Satellite-Based LIS Observations in Oklahoma, Geophys. Res. Lett., 27(12), 1703–1706.

Valdivia, J. A., G. Milkh, and K. Papadopoulos, 1997, Red sprites: Lightning as a fractal antenna, Geophys. Res. Lett., 24, 3169–3172.

Van der Velde O. A., Á. Mika, S. Soula, C. Haldoupis, T. Neubert, U. S. Inan (2006), Observations of the relationship between sprite morphology and in-cloud lightning processes, J. Geophys. Res., 111, D15203, doi:10.1029/2005JD006879.

Van der Velde, O. A., W. A. Lyons, T. E. Nelson, S. A. Cummer, J. Li, and J. Bunnell (2007a), Analysis of the first gigantic jet recorded over continental North America, J. Geophys. Res., 112, D20104, doi:10.1029/2007JD008575.

Van der Velde, O. A., W. A. Lyons, S. A. Cummer, S, M. B. Cohen, D. D. Sentman, N. Jaugey, T. E. Nelson, R. Smedley (2007b), Electromagnetical, Visual and Meteorological Analyses of two Gigantic Jets Observed Over Missouri, USA. Eos Trans. AGU, 88(52), Fall Meet. Suppl., Abstract, abstract AE23A-0895.

Veronis, G., V. P. Pasko, and U. S. Inan (1999), Characteristics of mesospheric optical emissions produced by lighting discharges, J. Geophys. Res., 104(A6), 12,645–12,656.

Weisman, M. L., and J. B. Klemp, 1982: The dependence of numerically simulated convective storms on vertical wind shear and buoyancy. Mon. Wea. Rev., 110, 504–520.

Weisman, M. L., and J. B. Klemp, 1984: The structure and classification of numerically simulated convective storms in directionally varying shears. Mon. Wea. Rev., 112, 2479–2498.

Wescott, E. M., D. Sentman, D. Osborne, D. Hampton, and M. Heavner (1995), Preliminary results from the Sprites94 aircraft campaign: 2. Blue jets, Geophys. Res. Lett., 22(10), 1209–1212.

Wescott, E. M., D. D. Sentman, M. J. Heavner, D. L. Hampton, D. L. Osborne, and O. H. Vaughan Jr. (1996), Blue starters: Brief upward discharges from an intense Arkansas thunderstorm, Geophys. Res. Lett., 23(16), 2153–2156.

Wescott, E. M., H. C. Stenbaek-Nielsen, D. D. Sentman, M. J. Heavner, D. R. Moudry, and F. T. S. Sabbas (2001), Triangulation of sprites, associated halos and their possible relation to causative lightning and micrometeors, J. Geophys. Res., 106(A6), 10,467–10,478.

Wescott, E.M., D. D. Sentman, M. J. Heavner, D. L. Hampton, W. A. Lyons and T. Nelson, (1998), Observations of `Columniform' sprites, J. Atm. and Sol.-Terr. Phys., 60, 733-740.

Wiens, K. C., S. A. Rutledge, and S. A. Tessendorf, 2005: The 29 June 2000 supercell observed during STEPS. Part II: Lightning and charge structure. J. Atmos. Sci., 62, 4151–4177.

Willett, J. C., J. C. Bailey, and E. P. Krider (1989), A class of unusual lightning electric field waveforms with very strong high-frequency radiation, J. Geophys. Res., 94, 16,255– 16,267.

Williams, E. R., 1998, The positive charge reservoir for sprite-producing lightning, J. Atm. and Sol.-Terr. Phys., 60, 689-692.

Williams, E. and S. Stanfill, C. R. Physique 3 (2002) 1277–1292.

Williams, E. R. (2006), Problems in lightning physics—The role of polarity asymmetry, Plasma Sources Sci. Technol., 15, S91–S108.

Williams, E. R., V.C. Mushtak, D. Rosenfeld, S.J. Goodman and D.J. Boccippio, (2005), Thermodynamic conditions favorable to superlative updrafts, mixed phase microphysics and lightning flash rate, Atmos. Res.

Williams, E., E. Downes, R. Boldi, W. Lyons, and S. Heckman (2007), Polarity asymmetry of sprite-producing lightning: A paradox?, Radio Sci., 42, RS2S17, doi:10.1029/2006RS003488.

Wilson, C.T.R. The electric field of a thunderstorm and some of its effects, Proc. Roy. Soc. London, 37, 32D, 1925.

Yair, Y., P. Israelevich, A. D. Devir, M. Moalem, C. Price, J. H. Joseph, Z. Levin, B. Ziv, A. Sternlieb, and A. Teller (2004), New observations of sprites from the space shuttle, J. Geophys. Res., 109, D15201, doi:10.1029/2003JD004497.

Yair, Y, R. Aviv, G. Ravid, R.Yaniv, B. Ziv, C. Price, (2006), Evidence for synchronicity of lightning activity in networks of spatially remote thunderstorms. J. Atm. and Sol.-Terr. Phys. 68, 1401–1415

Zabotin, N. A., and J. W. Wright (2001), Role of meteoric dust in sprite formation, Geophys. Res. Lett., 28(13), 2593–2596.

Zipser, E.J. (1982), Use of a conceptual model of the life-cycle of mesoscale convective systems to improve very-short-range forecasts. In Nowcasting, K.A. Browning ed., Academic Press, London, pp. 191-204.

Figure 21. Spider lightning over Toulouse. August 23, 2004.

3 Observation des relations entre la morphologie des sprites et les processus intra-nuageux de l'éclair parent

3.1 Résumé

Ce chapitre reprend une étude qui a fait l'objet d'un article publié au Journal of Geophysical Research – Atmosphere :

- Van der Velde, O. A., Á. Mika, S. Soula, C. Haldoupis, T. Neubert, and U. S. Inan (2006), Observations of the relationship between sprite morphology and in-cloud lightning processes, J. Geophys. Res., 111, D15203, doi:10.1029/2005JD006879.

L'article est présenté intégralement dans le chapitre et il est précédé d'une introduction qui en décrit le contexte, les objectifs, la démarche, les résultats et les interprétations à la lumière d'éléments bibliographiques sur le sujet. Par ailleurs, ce travail a également fait l'objet de communications lors de Conférences ou de réunions intermédiaires dans le cadre du projet CAL :

- Van der Velde, O., A. Mika, S. Soula, C. Haldoupis, T. Neubert, U. Inan, 2006. Lightning discharge processes generating carrot and column sprites. European Geosciences Union, General Assembly 2006, Vienna, Austria, 2-7 April 2006.

- Van der Velde, O. Characteristics of sprite-generating thunderstorms. CAL third-year meeting, Cambridge, UK, January 9-11 2006.

I- Objectif de l'étude

Les sprites sont des "Transient Luminous Events" (TLEs) qui sont observés entre 40 et 90 km au-dessus d'orages de type Mesoscale Convective System (MCS), avec des durées de quelques ms à quelques dizaines de ms, et presque toujours produits après un éclair nuage-sol positif (CG+). L'intervalle de temps entre le CG+ et le processus de décharge sous forme de sprite est en général inférieur à 100 ms mais il est variable, d'au moins un ordre de grandeur, et les raisons de cette variabilité ne sont pas bien comprises.

Le lien fort qui lie la production d'un sprite à la présence d'un éclair CG+ conduit à expliquer la décharge d'altitude par l'existence d'un champ électrique quasi statique suffisamment intense après l'arc-en-retour positif. Cette possibilité de décharge avait d'ailleurs été évoquée par Wilson en 1925, mais les premières observations ne seront faites que quelques décennies plus tard, en 1989 exactement. Dans certaines théories sur la génération des sprites, un rôle important est donné aux champs créés par les courants de propagation horizontale de certaines phases de l'éclair. De plus, tous les éclairs CG+ ne produisent pas de telles décharges et les particularités de ceux qui en produisent n'ont pas encore été clairement mises à jour. Il est donc important de bien identifier le mécanisme global de l'éclair associé au sprite et les phases qui ont un rôle important dans la génération des conditions favorables à la production du sprite. Dans ce travail nous analysons les signatures électromagnétiques, dans plusieurs gammes de fréquences, d'éclairs associés à des sprites de plusieurs types et observés au cours de la campagne EuroSprite 2003. Les caractéristiques morphologiques et temporelles des sprites sont considérées.

II- Moyens d'observation

Dans le cadre du projet CAL (Coupling of Atmospheric Layers) qui était un projet européen de type RTN (Research Training Network) et qui a réuni 11 équipes pour l'étude des TLEs (Neubert et al., 2004), des campagnes d'observation de sprites et autres TLEs sont organisées en France tous les étés depuis 2003. Ainsi au cours de l'été 2003, une centaine de sprites ont été observés par une caméra placée au Pic du Midi (42,93° N ; 0,14°E) à 2877 mètres d'altitude. Cette caméra CCD (type JAI CV–S3200 et depuis 2005 aussi JAI CV-M4+ de haute résolution) noir et blanc très sensible pouvait être pilotée par internet et un logiciel de détection de variation de luminosité dans le champ de la caméra permettait de faire des enregistrements sur événements uniquement. Le temps d'exposition de la caméra était de 20 ms et avec un recoupement de 2 temps de pose pour faire une image nous avions un taux de 25 images par seconde. L'optique de la caméra, du type grand angle avec un objectif de focale 16 mm et d'ouverture f/1,4, donnait un champ de 23° environ. Les données enregistrées en plus des séquences vidéo étaient des informations sur l'orientation de la caméra. Les images de sprite sont analysées avec un logiciel qui les superpose à la carte du ciel représentative de l'instant de l'observation au moyen des étoiles qui y sont visibles. Ainsi la direction du sprite peut être déterminée précisément.

La caractérisation des systèmes orageux à l'origine des sprites a pu se faire à partir des données issues du réseau de radars français ARAMIS (Application Radar À la Météorologie Infra-Synoptique) pour la structure des systèmes précipitants. Ce réseau qui couvre le territoire français comprend 18 radars conventionnels, dont 10 dans la bande C (λ = 5 cm) et 8 dans la bande S (λ = 10 cm). Chaque radar a une portée d'environ 250 km et produit des images en mode PPI (Plan Position Indicator) toutes les 5 minutes avec le facteur de réflectivité radar et à une résolution de 1.5 × 1.5 km. Pour composer une image, l'antenne radar fait 2 tours complets à une élévation de 1.4° (courte distance) et 0.8° (grande

distance). Ainsi, en prenant en compte la rotondité de la Terre, le nuage sera scanné à une altitude maximale d'environ 8 km.

La température des sommets des nuages a été déterminée grâce aux données des satellites Météosat de première génération. L'Europe était vue par 3 des 8 satellites Météosat (n° 6-8) localises près du meridian de Greenwich. Le principal instrument qui est un radiomètre fonctionne dans trois bandes :

- 0.4 to 1.0 μm visible band (VIS)
- 5.7 to 7.1 μm water vapour absorption band (WV)
- 10.5 to 12.5 μm thermal infrared band (IR)

C'est la dernière bande qui a été utilisée pour les informations utiles à la description des systèmes orageux.

Le territoire français est couvert par un réseau de stations de détection des éclairs nuage-sol qui est opéré par la société Météorage. Ce réseau est une application de la technique LLP mise au point aux Etats-Unis. Il est constitué de 18 stations réparties sur toute la France. Chacune d'elles est équipée d'une double antenne croisée qui détecte le champ magnétique rayonné par l'arc-en-retour de l'éclair CG dans la gamme BF. Le signal est identifié comme tel grâce à une reconnaissance de forme correspondant à celui émis par un canal vertical près du sol. Chacune des stations fournit la direction de la source rayonnante qui correspond à la direction du point d'impact de l'éclair. Une triangulation sur ces différentes directions permet d'obtenir la localisation du point source en 2D. Actuellement, le système utilise la technologie IMPACT qui prend en compte les différences de temps d'arrivée et la précision de la localisation est comprise entre 0 et 4 km pour 70% des cas détectés. Ainsi, ce système fournit la date et les coordonnées de chaque éclair CG avec le nombre d'arcs-en-retour ainsi que leur pic d'intensité de courant.

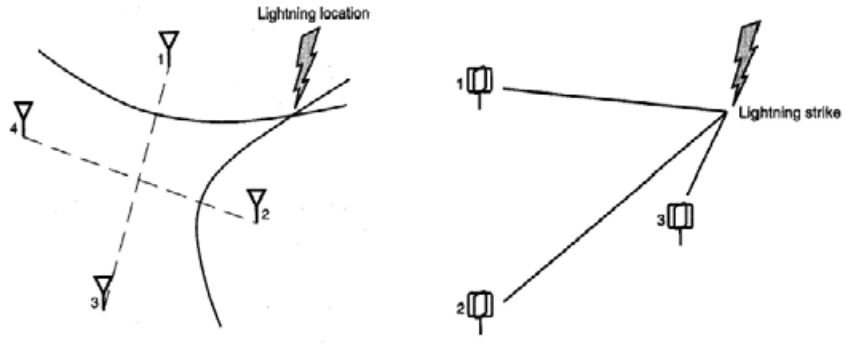

Principe de la détection des éclairs CG : TOA - Time Of Arrival (gauche), DF – Direction Finding (droite) (tiré de *MacGorman and Rust*, 1998).

L'activité totale d'éclair (éclair intranuage (IC) + nuage-sol (CG)) pouvait être détectée grâce au système SAFIR (Surveillance et Alerte Foudre par Interférométrie Radioélectrique) dans certaines régions au cours de l'été 2003. Il en existait notamment un dans le Sud-Est de la France avec 3 stations. SAFIR détectait les émissions de rayonnement électromagnétique en VHF dans la gamme de fréquence 110-118 MHz. Cette valeur de

fréquence permet de détecter des signaux issus des phases leader d'éclairs nuage-sol ou intranuage, essentiellement des leaders négatifs. La propagation rectiligne des ondes à cette fréquence élevée limite la portée des stations du système SAFIR à cause de la rotondité de la Terre. Ainsi la portée d'un seul système de 3 stations reste limité à une centaine de km de rayon. Le principe utilisé pour la détermination de la direction repose sur l'interférométrie à partir de plusieurs antennes sur une station. Pour la localisation 2D effectuée par le système utilisé dans le cas de notre étude, c'est la triangulation qui est appliquée entre plusieurs stations. De plus, les stations SAFIR sont équipées d'antennes LF (Low Frequency) pour identifier des arcs-en-retour et permettre ainsi la discrimination de éclairs nuage-sol. Les données fournies par SAFIR sont des séries de points source datés et localisés que l'on peut associer ensuite dans un même éclair en utilisant des critères spatio-temporels. La résolution de la détection restait limitée à 100 microsecondes et la capacité de traitement des points sources était également limitée sur des créneaux temporels d'1 seconde.

Des observations large-bande ELF/VLF étaient réalisées à partir d'une antenne de réception située en France à Nançay (47,38 °N ; 2,19 °E). Ce système est constitué de 2 boucles magnétiques triangulaires qui détectent les composantes N-S et E-W dans la bande 350 Hz – 45 kHz. L'échantillonage se fait à une fréquence 100 kHz et le temps GPS est enregistré. Ce type de signal permet de détecter les arcs-en-retour des éclairs CG avec une très bonne efficacité et dans un rayon de 500 km, les signaux issus de certaines phases des éclairs intra-nuage ont de grandes chances d'être détectés.

III- Etude de cas

Les cas de sprites analysés dans cette étude ont été produits par un orage de type MCS au cours de la nuit du 23 au 24 juillet 2003. Ce système orageux s'était formé en fin d'après-midi au Nord des Pyrénées sous la forme d'un amas de cellules convectives tout d'abord, évoluant ensuite vers une forme plus organisée avec une région stratiforme à l'avant. Le système s'est déplacé dans la région des Alpes et avait produit 15 sprites entre 2111 TU et 0033 TU répartis en 3 périodes distinctes correspondant à des phases de développement du système convectif. Ces phases sont décrites dans une première partie de l'article en s'appuyant sur l'analyse des images radar, de façon qualitative quant à la forme et de façon quantitative quant à la surface nuageuse avec des valeurs données de réflectivités radar. On a pu constater que les sprites étaient produits au-dessus de régions où les réflectivités moyennes (< 40 dBZ) occupaient une grande partie du nuage. D'autre part, la réflectivité autour de l'éclair CG+ qui avait produit un sprite (dans un rayon de 10 km) était en général relativement uniforme.

Les sprites ont été classés en 3 groupes selon leur morphologie : sprite en forme de colonne (5), sprite en forme de carotte (8) et forme indéfinissable (2). Les caractéristiques de délai entre l'éclair CG+ et le sprite, d'activité en rayonnements VHF avant l'éclair CG+ et ELF/VLF après l'éclair CG+ ont été examinées. Ainsi, les délais entre CG+ et sprite sont

plus courts pour les formes "colonne" que pour les formes "carotte" (en moyenne 12 ms contre 69 ms). En général les types "carotte" sont produits après un CG+ précédé d'une activité VHF plus importante que dans les cas de type "colonne" et de même, ils sont également précédés par des "sferics" en rayonnement ELF/VLF qui démarrent après le CG+. Un cas de sprite de forme "carotte" n'était pas associé à un éclair CG+ détecté par Météorage mais à une forte production de rayonnement VHF environ 50 ms avant. Une forte activité ELF/VLF était également enregistrée avant le sprite ce qui pouvait laisser penser qu'un éclair CG+ avait pu être manqué par le système de détection Météorage en raison d'une trop grande complexité du signal.

IV- Discussion

Les observations faites à partir des cas de sprites considérés permettent de retrouver certaines tendances proposées dans la littérature, de proposer de nouveaux concepts et de poser quelques questions sur le mécanisme de déclenchement des sprites. D'une part, la relation entre l'évolution de la structure orageuse et la production de sprites est assez conforme aux résultats publiés pour des orages dans d'autres régions du monde. D'autre part, la relation entre le type de sprite et la chronologie des différents événements associés au processus permet d'établir un nouveau schéma. Les sprites de type "colonne" sont produits après des CG+ d'assez forts pics de courant et dans un délai court tandis que les sprites de type "carotte" sont produits après un CG+ de plus faible pic de courant et dans un délai plus long. Les 2 types de sprites sont associés à du rayonnement ELF/VLF mais dans le cas des "carottes" ce rayonnement est beaucoup plus long. L'activité intranuageuse des éclairs pourrait avoir un rôle important dans la génération des sprites, notamment des "carottes", et donc sur la forme qu'ils auront. Les cas d'éclairs CG+ dont l'arc en retour est suivi d'un courant continu relativement long pourrait être identifié à ce schéma. L'absence de détection de rayonnement VHF après l'arc en retour du CG+ qui produit le "carrot" sprite va effectivement dans le sens de cette explication, mais on doit être sûr que le système de détection utilisé est capable de détecter suffisamment de signaux de faible amplitude.

Cette discussion met également en avant des perspectives d'études futures à partir d'autres événements de sprites mais aussi en analysant des cas d'éclairs ne produisant pas de sprite. Un point important serait également de pouvoir analyser l'activité VHF avec des systèmes de détection ayant une ligne de base plus courte, comme le LMA, afin d'être sûr que les différentes stations peuvent détecter des signaux de faible amplitude en même temps.

3.2 Article

JOURNAL OF GEOPHYSICAL RESEARCH, VOL. 111, D15203, doi:10.1029/2005JD006879, 2006

Observations of the relationship between sprite morphology and in-cloud lightning processes

Oscar A. van der Velde,[1] Ágnes Mika,[2] Serge Soula,[1] Christos Haldoupis,[2] Torsten Neubert,[3] and Umran S. Inan[4]

Received 10 November 2005; revised 30 March 2006; accepted 25 April 2006; published 4 August 2006.

[1] During a thunderstorm on 23 July 2003, 15 sprites were captured by a LLTV camera mounted at the observatory on Pic du Midi in the French Pyrénées. Simultaneous observations of cloud-to-ground (CG) and intracloud (IC) lightning activity from two independent lightning detection systems and a broadband ELF/VLF receiver allow a detailed study of the relationship between electrical activity in a thunderstorm and the sprites generated in the mesosphere above. Results suggest that positive CG and IC lightning differ for the two types of sprites most frequently observed, the carrot- and column-shaped sprites. Column sprites occur after a short delay (<30 ms) from the causative +CG and are associated with little VHF activity, suggesting no direct IC action on the charge transfer process. On the other hand, carrot sprites are delayed up to about 200 ms relative to their causative +CG stroke and are accompanied by a burst of VHF activity starting 25–75 ms before the CG stroke. While column sprites associate with short-lasting (less than 30 ms) ELF/VLF sferics, carrot sprites associate with bursts of sferics initiating at the time of the causative +CG discharge and persisting for 50 to 250 ms, indicating extensive in-cloud activity. One carrot event was found to be preceded by vigorous IC activity and a strong, long-lived cluster of ELF/VLF sferics but lacking a +CG. The observations of ELF/VLF sferic clusters associated with lightning and sprites form the basis for a discussion of the reliability of lightning detection systems based on VHF interferometry.

Citation: van der Velde, O. A., Á. Mika, S. Soula, C. Haldoupis, T. Neubert, and U. S. Inan (2006), Observations of the relationship between sprite morphology and in-cloud lightning processes, *J. Geophys. Res.*, *111*, D15203, doi:10.1029/2005JD006879.

1. Introduction

[2] Sprites are transient luminous events (TLE) of less than ~100 ms duration ocurring above active thunderstorms in the mesosphere in the 40–90 km altitude range [e.g., *Neubert*, 2003]. Although predicted 80 years ago [*Wilson*, 1925] it is only during the last 15 years that TLEs have been known to the scientific community [*Franz et al.*, 1990]. On the basis of simultaneous observations of cloud-to-ground (CG) lightning activity and sprites it is now generally accepted that positive cloud-to-ground flashes (+CG) trigger sprites [*Boccippio et al.*, 1995; *Lyons et al.*, 2003a] provided they are characterized by sufficiently large charge moment changes (typically 200–1500 C km) [*Williams*, 1998; *Hu et al.*, 2002; *Lyons et al.*, 2003b; *Cummer and Lyons*, 2005].

[3] The most commonly accepted theories of sprite generation invoke the quasi-electrostatic field generated in the stratosphere and mesosphere following a +CG discharge [*Pasko et al.*, 1997]. However, alternative theories suggest an important role for the field generated by horizontal lightning currents [*Valdivia et al.*, 1997; *Rycroft and Cho*, 1998].

[4] In this paper, the term intracloud (IC) lightning activity is not meant to describe a separate class of flashes as opposed to cloud-to-ground (CG) flashes, but refers to all phases of lightning in the cloud or air involved during one flash event, including leader activity accompanying a CG flash. While the importance of IC lightning in the sprite generation process is little known, primarily due to lack of measurements by lightning detection networks, indirect evidence suggests that it may also play a part. For instance, the time delays between the causative +CG and the sprite may extend to beyond 100 ms [*Bell et al.*, 1998; *Füllekrug and Reising*, 1998; *Mika et al.*, 2005], suggesting that the electric field in the mesosphere builds up over time as a result of the charge redistribution mediated by the continuing current of the +CG and the IC currents feeding it. Furthermore, sprites may be horizontally displaced up to 50 km from the +CG discharge [*Wescott et al.*, 2001; *São Sabbas et al.*, 2003] possibly as a result of horizontally extended IC lightning channels.

[5] In recent years, three-dimensional lightning mapping systems have aided greatly in identifying processes of sprite-generating lightning flashes. In a storm system in Florida, sprites were found to occur at the periphery of

[1] Université Paul Sabatier, Toulouse, France.
[2] University of Crete, Department of Physics, Heraklion, Crete, Greece.
[3] Danish National Space Center, Copenhagen, Denmark.
[4] STAR Laboratory, Stanford University, Stanford, California, USA.

0148-0227/06/2005JD006879$09.00

expanding horizontal cloud discharges ('spider lightning'), shortly after a +CG was produced [*Stanley*, 2000]. The intracloud discharge in these cases continued after the +CG to last up to several seconds and spanned tens of kilometers. The height of charge removal was at 7–8 km, higher than was found for High Plains storms [*Lyons et al.*, 2003b] during the STEPS field campaign [*Lang et al.*, 2004a] in the summer of 2000, when the +CGs only produced sprites when the maximum of VHF sources at 8 km weakened and a secondary, lower-level (2–5 km) maximum started to develop.

[6] Further observational evidence comes from very low frequency (VLF) and extremely low frequency (ELF) observations suggesting that strong IC activity may be associated with sprites [*Ohkubo et al.*, 2005].

[7] In this paper we present one of the first direct observations of intracloud lightning simultaneously with optical observations of sprites. We explore the association between sprites and the lightning activity and find distinct differences between activity related to column and carrot sprites. Finally, the data set forms the basis for a discussion of the differences (and difficulties) in IC lightning registration by a very high frequency (VHF) lightning detection system and a nearby ELF/VLF broadband receiver.

2. Instrumentation

[8] During July and August 2003, the EuroSprite 2003 campaign brought together several instruments in order to investigate the origin and effects of sprites [*Neubert et al.*, 2005]. Sprites were detected with a light-sensitive camera system mounted at the Observatoire Midi-Pyrénées on Pic du Midi in the French Pyrenees (42.93° N, 0.14° E) at 2877 m altitude. The system was controlled remotely over the Internet and included automated event detection for reduction of the data volume. The frame integration time was 20 ms and the system time was correct to within 12 ms.

[9] Data from two different lightning detection systems were used to obtain accurate positions and timing of CG and IC lightning. The large French lightning detection network run by Météorage adopts 17 sensors using both direction finding and time of arrival techniques to determine the location of positive and negative CG strokes over the entire country [*Cummins et al.*, 1998]. The detection efficiency is ~90 % and the network provides the location, time, stroke multiplicity, and peak current of each detected CG flash. The second lightning detection system, SAFIR, can detect the total (CG and IC) lightning activity over a limited area in southeastern France. It consists of three stations in a triangular configuration with a baseline of a few hundred kilometers, each station detecting the direction of VHF radio emissions from lightning flashes by interferometry. SAFIR provides the two-dimensional (2-D) source location (horizontal only) by triangulation methods with a 100 μs time resolution [*Richard and Lojou*, 1996].

[10] Sprite-producing thunderstorms traversed the area covered by the SAFIR system on three nights. The best-quality data were obtained during the night of 23–24 July 2003, when the sprite-producing region of a mesoscale convective system (MCS) was in the range of detection. During this night, SAFIR had only two operational antennas, which caused lightning signals originating from a small area between the antennas not to be accurately determined and therefore dismissed by the system. This detection gap of the SAFIR network could have affected events 10, 11, and 12 (Table 1), with +CG strokes occurring near the edges of the gap. SAFIR sources were detected for some of these strokes, but the sprite-producing second +CG strokes of events 11 and 12 must have occurred in this gap.

[11] Observations of broadband ELF/VLF activity were available from a receiver located at Nançay (47.38°N, 2.19°E), near Orleans, France. The system uses two large triangular magnetic loop antennas measuring the N-S and E-W components in the band ~350 Hz to 45 kHz. The analog outputs of the two channels are sampled at 100 kHz and the system uses GPS-based timing. It has been shown that the detection efficiency of broadband ELF/VLF receivers is 100% for CG discharges [*Wood and Inan*, 2002]. The ELF/VLF measurements are therefore useful for identification of CG flashes possibly missed by the lightning detection networks. In addition, at short distances from the receiver (within about 500 km) one would expect the ELF/VLF system to detect sferics originating from IC lightning [*Johnson and Inan*, 2000; *Ohkubo et al.*, 2005].

3. Observations

[12] During the night of 23–24 July 2003, 15 sprite events were captured by the camera at Pic du Midi. For the events of this night we had minimal difficulty classifying the type of a sprite: they almost all obeyed the classic shapes of columns (narrow, straight, short, mostly uniform elements) or carrots (taller, irregular shapes, usually with very visible streamers extending upward and downward from a bright core). Examples of observed sprites are shown in Figure 1. On the left there is a cluster of three sprites of the carrot type, with tendrils extending downward and upward, in the middle a cluster of column type sprites of single column emissions, and on the right one carrot sprite event for which no causative +CG could be identified. The three cases in Figure 1 are discussed in more detail in the following.

3.1. Meteorological Development

[13] A mesoscale convective system developed in the early evening of 23 July 2003 north of the Pyrenees, around 1600 UTC. Initially the system was a mere clustering of cells surrounded by stratiform precipitation regions, but as a cold pool formed the system developed more of a leading line–trailing stratiform configuration, but not very steady. About 2 hours before the first sprite the system developed a northern and a southern convective region. The first sprite was observed at 2111 UTC as portions of the northern convective region started to weaken quickly. A radar image of this part of the storm is shown in Figure 4. During this episode, which lasted for an hour, events 1–8 occurred. Events 9–12 happened when the southern convective region weakened, around 2300 UTC. The system assumed a spiral shape (developing a Mesoscale Convective Vortex) at this time, with the higher reflectivities and sprites near the center. At a stronger portion of the eastern arm of remaining reflectivity, three sprites (13–15) happened an hour later, just before the system had completely dissolved.

[14] The size of the northern portion of the storm system with radar reflectivities greater than >10 dBZ was about

Table 1. Sprites Observed on 23–24 July 2003 and Their Parent Lightning Activity Characteristics Inferred From the Météorage and SAFIR Systems and a Nearby Broadband VLF Receiver[a]

Event	Time, UTC	Delay Sprite to +CG, ms	Delay Sprite to VHF Sources, ms	Initial Small ELF/VLF Signal Before +CG, ms	ELF/VLF Cluster Duration, ms	Number of VHF Sources	+CG, kA	+CG Reflectivity, dBZ	+CG Cloud Top, °C
				Carrot Sprites					
1	2111:32. 336	38	–	25	70	–	60.4	33.0	−44.0
3	2134:58. 160	no CG	59–50	-	80 (150)	71		33.5	−51.8
4	2152:11. 214	136	173–136	25 + VHF	210	37	33.6	34.9	−53.3
5	2156:28. 462	265	265–203	-	175	17	63.9	36.2	−52.6
		205					27.3	36.0	−52.9
7	2205:35. 720	41	367–36	25 + VHF	80	21	53.3	36.3	−49.9
9	2251:02. 268	169	-	45	75	-	42.5	30.0	−43.9
		46					75.5	22.9	−44.8
12	2321:41. 127	18	18–9	-	45	88°	147.5	35.1	−45.3
	2321:41. 267	−6					22.5	30.6	−46.9
15	0033:01. 565	27	–	75	50	–	45.1	14.3	−38.0
				Column Sprites					
2	2121:55.*	(+CG 55.454)	(55.054 to 55.116)	50	5	3	122.7	31.8	−41.0
10	2300:27.*	(+CG 27.707)	(27.256 to 27.706)	-	30	5 °	96.3	36.3	−45.2
11	2312:34. 810	−3	554–543	-	30	8 °	54.8	29.0	−46.8
13	0023:28. 347	27	105–103	70 + VHF	30	5	70.4	12.2	−36.9
14	0028:27. 495	11	101-99	80 + VHF	(60) 20	4	59.5	13.5	−40.6
				Undefined Sprites (See Section 3.5)					
6	2159:03. 486	159	-	-	220	0	44.4	36.5	−52.7
	2159:03. 506								
8	2209:06. 806	123	-	-	175	0	25.4	34.9	−49.2
	2209:06. 826								

[a]Here asterisk indicates precise time unknown; long dash indicates likely lacking VHF detection at longer range; open circle indicates may have been affected by SAFIR gap (see instrumentation section). ELF/VLF cluster (strongest part) duration time in parenthesis means there exists an uncertainty about the relevant cluster duration (in event 3 about the end, in event 14 about the start). Reflectivities and cloud top temperatures are taken as an average within a radius of 10 km from the parent +CG stroke.

20,000 km^2 during the occurrence of sprites, while at the same time reflectivity areas greater than 40 dBZ in the convective region amounted only to 1000–1500 km^2. The maximum reflectivity in the storm decreased from 63 dBZ at the time of the first sprite to 48 dBZ at the time of the last sprite. The total reflectivity area reached about 40,000 km^2 already before sunset at 1923 UTC. The total shield of cloud tops colder than −30°C reached an area of 50,000 km^2, while the area colder than −50°C reached its maximum of 17,000 km^2 at 2130 UTC. Compared to sprite-producing storms over the High Plains of the United States [*Lyons et al.*, 2006], our storm system had relatively small horizontal and vertical dimensions but met the minimum parameter preconditions observed there.

[15] The coldest cloud tops during the sprite occurrences around −54 °C (the tropopause level according to the soundings), while sprites appeared over areas of cloud tops warmer by 2–16 degrees, consistent with the findings of *Lyons et al.* [2006]. The average reflectivity values in a circle with a radius of 10 km around a sprite-producing +CG were very uniform among the sprites, generally between 30 and 35 dBZ. There appear to be no meaningful differences in reflectivity or cloud top temperature values between carrot and column sprites in the data set of this paper. An upcoming paper will discuss in more detail the statistics on meteorological properties and CGs of sprite-producing storms in France.

3.2. Column Sprite Events

[16] The observed sprites and the associated lightning as recorded by the various systems are listed in Table 1. Events with the least associated VHF IC sources detected by the

Figure 1. Examples of observed sprites: (left) Carrots 2205:35 UTC; (middle) columns 2312:34 UTC; (right) carrot without detected parent +CG, 2134:58 UTC.

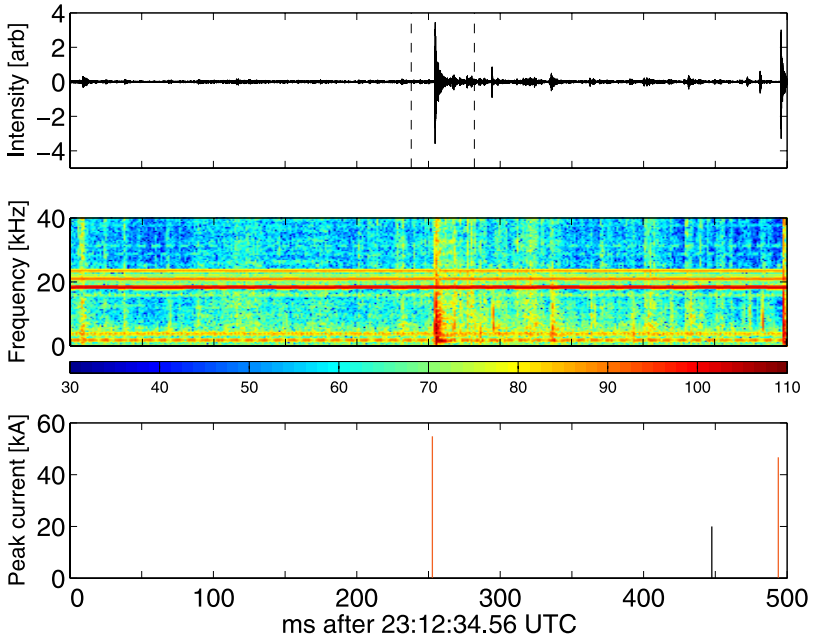

Figure 2. Broadband ELF/VLF waveforms (top) and the corresponding spectrum (middle, dB), 250 ms before and after the column sprite event of 23 July 2003, 2312:34 UTC (Figure 1, middle). Displayed is the east-west component of the signal. The two vertical dashed lines indicate the sprite observation time, accounting for the video frame integration time of 20 ms plus the time uncertainty of 12 ms. The bottom panel shows Météorage cloud-to-ground strokes (red) and SAFIR VHF lightning sources (black). The vertical scale indicates the +CG peak current (kA). The lengths of the black lines representing the SAFIR data are scaled arbitrarily. The units of the top panel waveforms are arbitrary after filtering out noise.

SAFIR system (3 to 8 sources: events 2, 10, 11, 13, and 14) were all column sprites. In these cases, the spatially clustered sources occurred up to several hundred milliseconds before the causative +CG flashes. On the other hand, the lag times between +CGs and the column sprites were short, between −3 and +27 ms (average 12 ms) relative to the start of the video frame integration time of 20 ms. Events 2 and 10 were retrieved from the video files with less temporal accuracy. However, the parent +CG flash and the sprite of event 10 was visible in the same video frame, so the delay must have been smaller than 20 ms. Event 2 followed in the first frame after a bright flash, so this delay ranged anywhere between ∼1 and 40 ms.

[17] The approximate average and median duration of ELF/VLF sferic clusters was about 25–30 ms for column sprites. The clusters started with the +CG return stroke and the waveform amplitudes decreased exponentially with time for nearly all the events. The single small column event at 2121 UT did not have a clearly recognizable long-lasting sferic cluster. Figure 2 shows the ELF/VLF-broadband sferic cluster and the VHF sources associated with event 11 (2312 UTC; Figure 1, middle). Here, the burst of ELF/VLF sferic energy is short (about 30 ms) while the delay between the +CG and the sprite is of the same order. The Météorage network detected a +CG stroke (54.8 kA) within the 20 ms video frame integration time that contained the sprite, and, as shown in Table 1, this appears to be typical of all observed column sprites. In this case, SAFIR only detected a small cluster of 8 sources about 550 ms before the sprite, which may be too early to be associated with the charge transfer process that triggered the sprite.

3.3. Carrot Sprite Events

[18] The events with the largest number of associated VHF IC sources, (17 to 88 sources: events 3, 4, 5, 7, and 12) were all carrot sprites. The VHF sources were clearly related in time to the sprite-causative +CG flash, except for event 3 where no +CG flash was identified. It is remarkable that the delay between the +CGs and the sprites was 18–205 ms, which is much longer than for column sprites, with an average value of 63 ms (median: 39.5 ms). The duration of the ELF/VLF sferics was also longer with averages of 100–110 ms (median 75–80 ms).

[19] Figure 3 shows the ELF/VLF broadband sferic cluster and the VHF sources associated with event 7 (2205 UTC; Figure 1, left), which occurred in the same portion of the storm as events 4–8. It was accompanied by a burst of 21 VHF sources, all happening before the causative +CG discharge. The return stroke is well defined in the ELF/VLF waveforms as a brief pulse of strong power particularly intense at the lowest frequencies (<5 kHz). The isolated cluster of VHF sources, at about 20 ms prior to the +CG discharge, occurred simultaneously with a weak burst of broadband ELF/VLF noise. On the other hand, the ELF/VLF sferics following the return stroke are not accompanied by any lightning detected by the Météorage and the SAFIR systems. The carrot sprite was triggered during the period of high sferic activity at least 30 ms after the +CG.

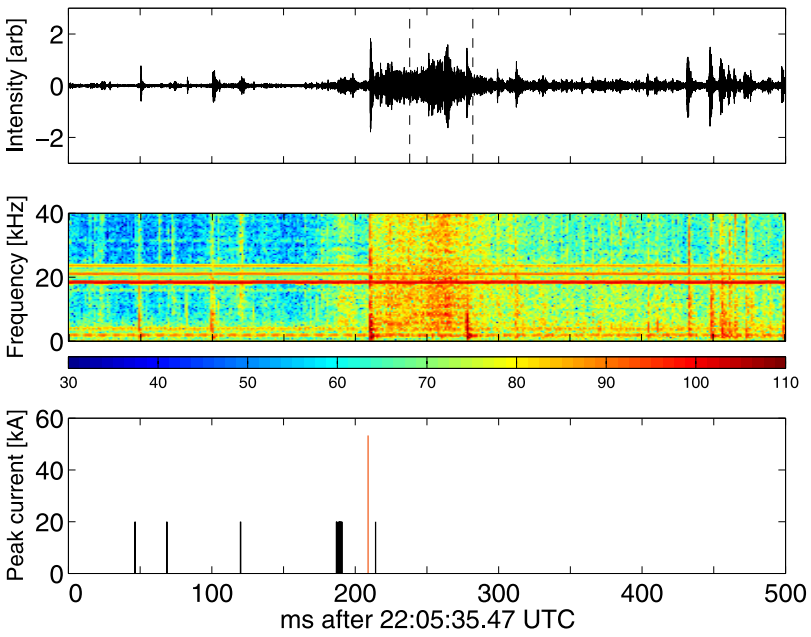

Figure 3. Same as in Figure 2 but for the carrot sprite event of 23 July 2003, 2205:35 UTC (Figure 1, left). Displayed is the east-west component of the signal.

The situation described above was typical for most of the carrot events of Table 1.

[20] We remark that we classified event number 12 with certainty as a carrot sprite, but a regular pattern of straight vertical elements in the top parts of the carrots occurs as well, especially in the second frame, which is somewhat reminiscent of columns. This event also features the shortest delay among the carrot sprites, and the sprites in the two frames were produced by two separate +CGs.

3.4. A Sprite Without a Causative CG Flash

[21] The two carrot sprites of event 3 (2134:58 UTC; Figure 1, right) could not be associated with a CG flash by either of the two lightning detection systems. However, the SAFIR system recorded a burst of 71 VHF sources prior to the event, the second-largest VHF burst seen on that night. Figure 4 shows the locations of all detected sources during the one second period centered around the event overlaid on a map of weather radar reflectivity and infrared cloud-top temperature. Also shown is the direction of the two sprites as seen from Pic du Midi. The direction toward the larger sprite passes near the VHF cluster (white diamonds) which has a spatial extent of $\leq$12 km. The smaller sprite curves at the bottom toward the clouds illuminated by IC activity and probably traces the direction of the electric field from the source region in the clouds [*Neubert et al.*, 2005]. The sources are located near the highest cloud tops in a portion of the stratiform region with relatively high radar reflectivity, due to a decay of a part of the convective region in this area half an hour before the sprite. The burst of VHF sources lasted for 9 ms and ended 50 ms before the sprite. Two −CG strokes (white squares) occurred about 500 ms before the sprites at ∼15 km distances from the VHF source region. This time difference is probably too long for the flashes to be related to the sprites, besides the overall unlikelihood of sprite-generation by −CGs. Other studies

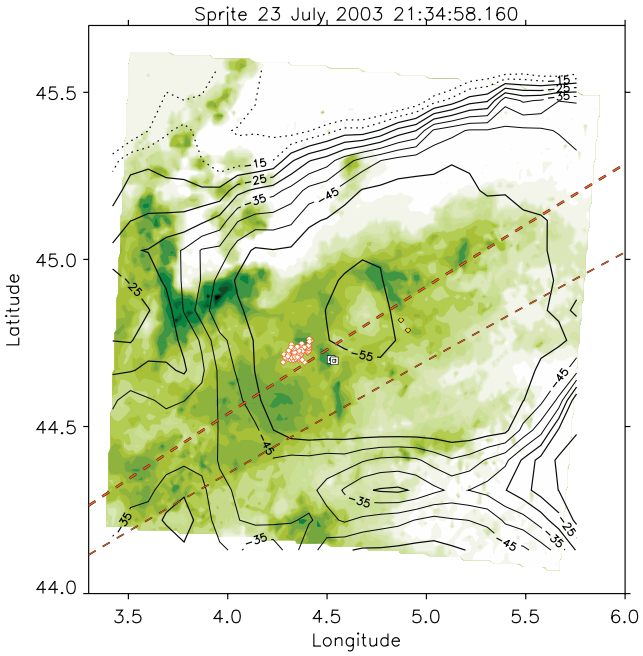

Figure 4. Thunderstorm conditions during the carrot sprite event observed on 23 July 2003, 2134:58 UTC (Figure 1, right). Directions of the two sprites seen from the Pic du Midi (dashed lines) are overlaid on radar reflectivity (shaded in green), infrared cloud top temperature (contour lines, °C) and 1 s of lightning activity (squares: −CG; diamonds: VHF sources). Lightning activity highlighted in white occurred within 500 ms before the sprite, and lightning activity displayed in yellow occurred within 500 ms after the sprite.

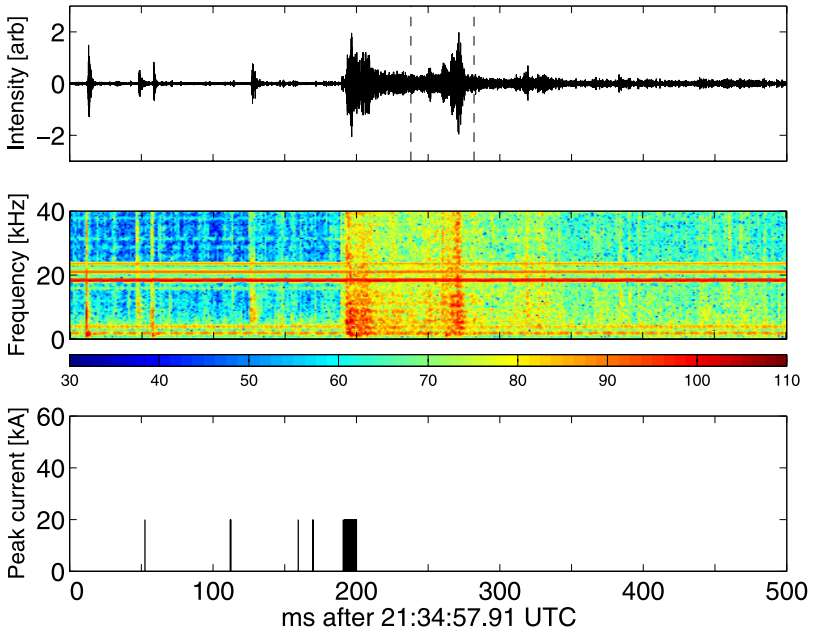

Figure 5. Same as in Figure 2 but for the sprite event of 23 July 2003, 2134:58 UTC, for which Météorage did not detect any causative +CG stroke (Figure 1, right). Displayed is the east-west component of the signal.

report maximum delays of about 200 ms [*São Sabbas et al.*, 2003] and 280 ms [*Mika et al.*, 2005].

[22] The ELF/VLF and VHF activity for this event is shown in Figure 5. The lower panel shows the cluster of VHF lightning sources (black column) occurring nearly simultaneously with the onset of a strong cluster of ELF/VLF sferics. The ELF/VLF activity was not associated with any cloud-to-ground lightning detected by the two networks and the question is if a +CG stroke (and IC activity) was missed because the waveforms were too complex [*Reising et al.*, 1996]. The presence of strong ELF/VLF sferic activity may support this suggestion. In addition, the impulsive rise in the north-south ELF/VLF signal at the onset of the event is possibly due to an undetected return stroke, whereas the smoother rise observed in the east-west component (Figure 5) is rather characteristic for cloud flashes. While we cannot exclude that an undetected +CG return stroke triggered the sprites, the data underscore the importance of IC lightning activity in sprite generation.

3.5. Other Events and Nonevents

[23] VHF sources were not detected for events 1, 6, 8, 9, and 15. For events 1 and 15 this was likely due to decreased detection efficiency since the storm was located rather far from the SAFIR antennas.

[24] The delays between the causative +CGs and events 6 and 8 were rather long (159 ms and 123 ms) with no accompanying VHF activity in spite of being located at optimum detection range. However, the ELF/VLF band did show long-lasting sferic clusters (around 200 ms) after the +CG, similar to those observed with carrots. We could not easily identify the type of these two sprites: event 6 consisted of three grouped small carrot-like elements. They seemed to occur closer to the camera than the preceding sprites, or alternatively, higher in altitude. The second frame showed many small elements shaped like a fan. Event 8 looked somewhat similar, more blobby, and clouds may have obscured part of this sprite.

[25] The two non-sprite-producing +CG flashes (at 2154:19.114 UTC and 2158:08.133 UTC) that occurred in the same region and period as events 4–8 showed no signature of sferic clusters. This result may indicate that extensive IC breakdown did not occur and that the process of supply of continuing current of charge to ground was not present [*Bell et al.*, 1998].

4. Discussion

[26] The general characteristics of the observations, valid for the events of this particular storm system, can be summarized as:

[27] 1. The IC and CG lightning characteristics, reflected in both the VHF and ELF/VLF bands, have different characteristics for column and carrot sprites.

[28] 2. Column sprites are triggered by +CG discharges with relatively high peak currents and with short delays between the +CG and the sprite (on average ∼12 ms relative to the start of the video frame integration time of 20 ms). In contrast, carrot sprites are triggered by +CG discharges with smaller peak currents and longer delays (∼20 to 200 ms). We did not find a relationship between the +CG peak current and the number of columns observed [*Adachi et al.*, 2004]

[29] 3. Column sprites are associated with little or no IC lightning activity while carrot sprites are associated with bursts of IC activity. For carrot sprites, the VHF sources are observed ∼25 to 75 ms prior to the causative +CG discharge. For both sprite categories, ELF/VLF sferic activity is observed following the causative +CG flash. Sferic

activity is short-lived (<30 ms) for column sprites and long lasting (~45 to 250 ms) for carrot sprites.

[30] 4. The SAFIR system rarely observed VHF sources after the sprite-related +CG stroke. However, ELF/VLF sferics, persisting up to several hundred milliseconds, were always observed after the +CG return stroke.

[31] 5. Observations suggest that some carrot sprites may be caused exclusively by IC discharges.

[32] The data presented herein show that the intracloud phase of a lightning flash plays an important role in the generation of carrot sprites but appears relatively unimportant for column sprites. This result may indicate that carrot sprites are provoked by larger total charge moment changes, whereas column sprites are provoked by larger instantaneous charge moment changes during a +CG discharge. We hypothesize that these discharge characteristics cause the mesospheric electric field to reach higher values for column sprites, but exceeding the breakdown threshold only for a shorter duration compared to carrot sprites. This might explain the short, straight shape of column sprites, compared to the taller and more complex shape of carrot sprites that have more time to grow in vertical and horizontal directions. The results further confirm the suggestion that ELF/VLF sferic clusters are indicative of sprite-producing discharges [*Johnson and Inan*, 2000; *Ohkubo et al.*, 2005], although the data do not allow a clear distinction between +CG- and IC activity.

[33] It is striking that lightning sources detected by the VHF interferometer are only seen preceding the causative +CG while there is also a strong ELF/VLF signature beginning at the +CG and persisting for up to several hundred milliseconds. We suppose that in our sprite-producing +CGs the characteristics of the in-cloud lightning processes are different after the +CG stroke than before. It is possible that the electromagnetic radiation caused by an abundance of in-cloud leaders renders the electromagnetic signal so complex that our SAFIR VHF interferometer system fails to identify IC lightning locations, or that the VHF radiation is too weak to be detected simultaneously at multiple stations having a long baseline. The relative insensitivity of VHF interferometers to signals from positive leaders is known [*Mazur et al.*, 1998]. However, negative leaders propagate across positively charged regions in the cloud and supply this charge to a +CG, so this cannot be a valid explanation in this case. The VHF sources preceding some of the sprite-producing +CGs must therefore associate with negative leader activity, either inside the clouds or between the earth and the cloud. This allows for a speculation about possible lighting processes: in the case of negative in-cloud leaders, the origin must be a negatively charged region, horizontally or vertically close to the positively charged region that delivers the +CG. In the case of negative leaders between earth and cloud, these leaders must originate from a mountain or tall man-made construction in reaction to the electric field created by the positive charge inside the cloud. When these leaders connect to the positive charge region, one or more positive return strokes may follow, in fact a ground-to-cloud (GC) flash [e.g., *Berger and Vogelsanger*, 1965]. In another way a +CG is created when a positive leader grows from the cloud to the ground, after which a return stroke follows. In both cases the positive charge region would be neutralized by negative leaders during/after the return stroke, leading to a continuing current, which has been observed in some cases by *Proctor et al.* [1988]. This process would be responsible for the observed ELF/VLF sferic clusters following the +CG stroke. For further studies it would certainly be interesting, if not necessary, to identify exactly which lightning processes are going on, beyond the detection of a +CG with its peak current and its charge moment change.

[34] Systems such as the Lightning Mapping Array (LMA) and the Lightning Detection and Ranging (LDAR II) systems, also operating in the VHF range but utilizing short baselines and time-of-arrival location, are capable of showing extensive horizontal channels, known as spider lightning [e.g., *Mazur et al.*, 1998; *Lang et al.*, 2004b; *Carey et al.*, 2005]. It appears worthwhile to compare these systems with broadband ELF/VLF observations to test if long-duration sferic clusters are indeed signatures of spider lightning. We found the ELF/VLF clusters to last only up to 0.2–0.3 s, which is much shorter than the 1–3 s duration of a spider lightning discharge observed in the referred studies above. It may indicate smaller horizontal extension of the intracloud flashes in our storm, which may be related to the relatively small size compared to the average storm in the High Plains region of the United States [*Lyons et al.*, 2006]. A long-lasting low-amplitude signal, not present before the +CG, is sometimes seen to extend for longer than our graphs show (>300 ms). We may speculate that either intracloud lightning may have continued in a differently radiating phase, or the ionospheric environment was modified, possibly caused by the sprite or electromagnetic pulse, which changed the propagation of radio waves. Nevertheless, the first consistent signal received from the sprite-generating discharge in our events was the +CG, or a weak signal preceding the +CG by only 25–75 ms, whereas in the work of *Stanley* [2000] an initial cloud discharge was already starting 0.5–1.5 s before the +CG. Since our SAFIR data do not show extensive horizontal discharges and signals after the time of the +CGs, we could not verify the phenomenon of sprites occurring at the periphery of a developing cloud discharge.

[35] A study of ELF/VLF sferic characteristics for the events of other sprite-producing storm systems, and also of the +CG discharges that did not produce sprites, is on the way. Further studies of IC lightning detection measurements with nearby broadband ELF/VLF recordings will certainly be useful in validating the detection efficiency of lightning locating systems like SAFIR which employ VHF-band interferometry or time-of-arrival techniques.

[36] **Acknowledgments.** This study was supported by the Research Training Network "Coupling of Atmospheric Layers" (CAL), sponsored by the EU FP5 program. We thank Thomas Allin for his efforts in recording the 2003 sprite data. The lightning detection data came from two different companies. We thank Stephane Pedeboy of Météorage for the extended network data and Jean-Yves Lojou of Vaisala for the SAFIR data. The authors are grateful to Météo France for providing weather radar data. Stanford participation is supported by the National Science Foundation.

References

Adachi, T., H. Fukunishi, Y. Takahashi, and M. Sato (2004), Roles of the EMP and QE field in the generation of columniform sprites, *Geophys. Res. Lett.*, *31*, L04107, doi:10.1029/2003GL019081.

Bell, T. F., S. C. Reising, and U. S. Inan (1998), Intense continuing currents following positive cloud-to-ground lightning associated with red sprites, *Geophys. Res. Lett.*, *25*, 1285.

Berger, K., and E. Vogelsanger (1965), Messungen und Resultate der Blitzforschung der Jahre 1955–1963 auf dem Monte San Salvatore, *Bull. Schweiz. Elektrotech.*, *56*, 2–22.

Boccippio, D. J., E. R. Williams, S. J. Heckman, W. A. Lyons, I. T. Baker, and R. Boldi (1995), Sprites, ELF transients, and positive ground strokes, *Science*, *269*, 1088.

Carey, L. D., M. J. Murphy, T. L. McCormick, and N. W. S. Demetriades (2005), Lightning location relative to storm structure in a leading-line, trailing-stratiform mesoscale convective system, *J. Geophys. Res.*, *110*, D03105, doi:10.1029/2003JD004371.

Cummer, S. A., and W. A. Lyons (2005), Implications of lightning charge moment changes for sprite initiation, *J. Geophys. Res.*, *110*, A04304, doi:10.1029/2004JA010812.

Cummins, K. L., M. J. Murphy, E. A. Bardo, W. L. Hiscox, R. B. Pyle, and A. E. Pifer (1998), NLDN'95, A combined TOA/MDF technology upgrade of the US National Lightning Detection Network, *J. Geophys. Res.*, *103*, 9035.

Franz, R. C., R. J. Nemzek, and J. R. Winckler (1990), Television image of a large upward electrical discharge above a thunderstorm system, *Science*, *249*, 48.

Füllekrug, M., and S. C. Reising (1998), Excitation of Earth-ionosphere cavity resonances by sprite-associated lightning flashes, *Geophys. Res. Lett.*, *25*, 4145.

Johnson, M. P., and U. S. Inan (2000), Sferic clusters associated with Early/Fast VLF Events, *Geophys. Res. Lett.*, *27*, 1391.

Hu, W., S. A. Cummer, W. A. Lyons, and T. E. Nelson (2002), Lightning charge moment changes for the initiation of sprites, *Geophys. Res. Lett.*, *29*(8), 1279, doi:10.1029/2001GL014593.

Lang, T. L., et al. (2004a), The Severe Thunderstorm Electrification and Precipitation Study (STEPS), *Bull. Am. Meteorol. Soc.*, *85*, 1107.

Lang, T. J., S. A. Rutledge, and K. C. Wiens (2004b), Origins of positive cloud-to-ground lightning flashes in the stratiform region of a mesoscale convective system, *Geophys. Res. Lett.*, *31*, L10105, doi:10.1029/2004GL019823.

Lyons, W. A., T. E. Nelson, R. A. Armstrong, V. P. Pasko, and M. A. Stanley (2003a), Upward electrical discharges from thunderstorm tops, *Bull. Am. Meteorol. Soc.*, *84*, 445.

Lyons, W. A., E. R. Williams, S. A. Cummer, and M. A. Stanley (2003b), Characteristics of sprite-producing positive cloud-to-ground lightning during the 19 July 2000 STEPS mesoscale convective systems, *Mon. Weather Rev.*, *131*, 2417.

Lyons, W. A., L. M. Andersen, T. E. Nelson, and G. R. Huffines (2006), Characteristics of sprite-producing electrical storms in the STEPS 2000 domain, paper presented at 2nd Conference on Meteorological Applications of Lightning Data, Am. Meteorol. Soc., Atlanta.

Mazur, V., X.-M. Shao, and P. R. Krehbiel (1998), "Spider" lightning in intracloud and positive cloud-to-ground flashes, *J. Geophys. Res.*, *103*, 19,811.

Mika, A., C. Haldoupis, R. A. Marshall, T. Neubert, and U. S. Inan (2005), Subionospheric VLF signatures and their association with sprites observed during EurosSprite 2003, *J. Atmos. Sol. Terr. Phys.*, *67*, 1580.

Neubert, T. (2003), On sprites and their exotic kin, *Science*, *300*, 747.

Neubert, T., et al. (2005), Co-ordinated observations of transient luminous events during the EuroSprite2003 campaign, *J. Atmos. Sol. Terr. Phys.*, *67*, 807.

Ohkubo, A., H. Fukunishi, Y. Takahashi, and T. Adachi (2005), VLF/ELF sferic evidence for in-cloud discharge activity producing sprites, *Geophys. Res. Lett.*, *32*, L04812, doi:10.1029/2004GL021943.

Pasko, V. P., U. S. Inan, T. F. Bell, and Y. N. Taranenko (1997), Sprites produced by quasi-electrostatic heating and ionization in the lower ionosphere, *J. Geophys. Res.*, *102*, 4529.

Proctor, D. E., R. Uytenbogaardt, and B. M. Meredith (1988), VHF radio pictures of lightning flashes to ground, *J. Geophys. Res.*, *93*, 12,683.

Reising, S. C., U. S. Inan, and T. F. Bell (1996), Evidence for continuing current in sprite-producing cloud-to-ground lightning, *Geophys. Res. Lett.*, *23*, 3639.

Richard, P., and J. Y. Lojou (1996), Assessment of application of storm cell electrical activity monitoring to intense precipitation forecast, paper presented at 10th International Conference on Atmospheric Electricity, Int. Comm. of Atmos. Electr., Osaka, Japan.

Rycroft, M. J., and M. Cho (1998), Modelling electric and magnetic fields due to thunderclouds and lightning from cloud-tops to the ionosphere, *J. Atmos. Terr. Phys.*, *60*, 889.

São Sabbas, F. T., D. D. Sentman, E. M. Wescott, O. Pinto Jr., O. Mendes Jr., and M. J. Taylor (2003), Statistical analysis of space–time relationships between sprites and lightning, *J. Atmos. Sol. Terr. Phys.*, *65*, 525.

Stanley, M. A. (2000), Sprites and their parent discharges, Ph.D. dissertation, 163 pp., N. M. Inst. of Mining and Technol., Socorro, N. M.

Valdivia, J. A., G. Milkh, and K. Papadopoulos (1997), Red sprites: Lightning as a fractal antenna, *Geophys. Res. Lett.*, *24*, 3169.

Wescott, E. M., H. C. Stenbaek-Nielsen, D. D. Sentman, M. J. Heavner, and F. T. São Sabbas (2001), Triangulation of sprites, associated halos and their possible relation to causative lightning and micro-meteors, *J. Geophys. Res.*, *106*, 10,467.

Williams, E. R. (1998), The positive charge reservoir for sprite-producing lightning, *J. Atmos. Sol. Terr. Phys.*, *60*, 689.

Wilson, C. T. R. (1925), The electric field of a thundercloud and some of its effects, *Proc. Phys. Soc. London*, *37*, 32D.

Wood, T. G., and U. S. Inan (2002), Long-range tracking of thunderstorms using sferic measurements, *J. Geophys. Res.*, *107*(D21), 4553, doi:10.1029/2001JD002008.

C. Haldoupis and Á. Mika, Department of Physics, University of Crete, Iraklion, Crete, GR-71003 Greece.

U. S. Inan, STAR Laboratory, Stanford University, Stanford, CA 94305-9515, USA.

T. Neubert, Danish National Space Center, Juliane Maries Vej 30, DK-2100 Copenhagen, Denmark.

S. Soula and O. A. van der Velde, Laboratoire d'Aérology, Observatoire Midi-Pyrénées (CNRS/UPS), 14 Avenue Edouard Belin, F-31400 Toulouse, France. (vdvo@aero.obs-mip.fr)

4 Analyse d'orage et d'activité d'éclair associés à des sprites observés pendant la campagne EuroSprite: 2 cas d'étude

4.1 Résumé

Ce chapitre reprend une étude qui a fait l'objet d'un article publié à la revue Atmospheric Research:

- Soula, S., O. van der Velde, J. Montanya, T. Neubert, O. Chanrion, and M. Ganot (2009), Analysis of thunderstorm and lightning activity associated with sprites observed during the EuroSprite campaigns: Two case studies, *Atmos. Res.* 91, 514-528

L'article est inséré dans le chapitre après une synthèse qui en fait une présentation en décrivant la démarche de l'article, et en résumant chaque partie de l'article.

Par ailleurs, une partie de ce travail a fait l'objet d'une communication lors de la Conférence Internationale d'Electricité Atmosphérique (ICAE 2007):

- Soula, S., O. van der Velde, J. Montanya, Á. Mika, C. Haldoupis, T. Neubert, M. Ganot, 2007, Analysis of thunderstorm systems and lightning activity associated with sprites observed during the EuroSprite campaigns 2- Case studies, International Conference of Atmospheric Electricity, Pékin, Chine, August 13th-17th, 2007.

I- Contexte de l'étude

Les sprites et les orages qui les produisent ont été analysés principalement sur les continents américain et asiatique. Il existe peu d'étude à partir d'observations sur le continent européen et le contexte des campagnes Eurosprite nous permet de faire des études de conditions de production des sprites, en particulier sur les types d'orages concernés, sur les phases de développement de l'orage favorables à la production des sprites, sur l'activité d'éclair associée à la production de sprites à plusieurs échelles

temporelles. Le taux de production de sprites à l'échelle de la Terre n'est pas encore connu. Des misions spatiales permettent de faire des observations parcellaires avec le satellite Taiwanais FORMOSAT et l'expérience ISUAL, et des nouvelles missions spatiales sont en préparation en Europe (TARANIS, ASIM). Il est donc important de faire des observations sol et d'en analyser les résultats. Ainsi, si certaines caractéristiques sur les conditions de production des sprites ont déjà été bien établies, il reste encore à préciser les relations entre les configurations de charge dans le nuage d'orage au moment des sprites, les relations entre taux de sprites et type/taille d'orage, les mécanismes précis des éclairs associés aux sprites.

Avec les données fournies par une ou plusieurs caméras lors des campagnes Eurosprite, nous avons a pu avoir certaines situations orageuses avec une activité bien documentée et correspondant à des conditions favorables d'observation nocturne des sprites sur une période assez longue. Cet article présente deux études de cas d'orages de type MCS et de taille comparable qui correspond en plus à celle d'un certain nombre de cas d'étude trouvés dans la littérature pour des régions différentes, notamment aux Etats-Unis ou au Brésil. La démarche sera d'analyser la situation météorologique et le développement du système orageux

II- Moyens d'observation

Une partie des moyens d'observation dont les données ont été utilisées dans ce cas ont été décrits par ailleurs dans ce document. Ainsi nous nous sommes appuyés sur l'analyse des données météosat pour la hauteur des nuages, des données du réseau radar pour la structure de réflectivité des systèmes orageux, des données météorage pour l'activité d'éclairs nuage-sol. Ces moyens ont été décrits dans la partie 3.1-II. La localisation des orages décrits ici n'ont pas permis de bénéficier des données Safir pour l'activité totale d'éclair.

Pour l'observation des sprites, nous avons utilisé les images de la caméra du Pic du Midi pour un cas et les images de 2 caméras CCD pour l'autre cas, localisées au Mont Aigoual (44.121N 3.576E, 1565 m d'altitude) durant la campagne EuroSprite 2006. Il faut noter que j'ai pris une grande part à la mise au point d'un de ces deux systèmes d'observation de sprites, mis au point au laboratoire pour l'été 2006. Ce système comprenait une caméra Watec 902H avec un objectif optique 16mm à ouverture f/1.4, installée sur un théodolite monté sur un tripode pour l'orientation. Cette caméra était reliée à PC portable et ses prises de vue étaient analysées avec le logiciel UFOCapture qui permet de faire une sélection des événements lumineux par détection des variations de luminosité et une acquisition de séries d'images courtes (1 seconde environ) et centrées sur l'événement déclencheur. L'autre système avait été apporté par Michal Ganot, étudiante à l'Université de Tel-Aviv (TAU), qui a fait un séjour de 2 semaines au laboratoire en Septembre 2006 dans le cadre d'une mission courte durée à travers le COST P18 "Lightning". Il comprenait une caméra Watec 100N avec un objectif de 12mm et une ouverture f/0.8 montée sur un tripode. Elle était connectée à PC portable et ses images

étaient également gérées par un logiciel UFOCapture. Pour cette caméra un GPS et un système d'insertion du temps sur les images permettait d'avoir une datation précise des images. La première figure de l'article montre la configuration des regions concernées par les 2 systèmes orageux et l'emplacement des cameras d'observation.

III- Etude de cas

Dans la partie III de l'article, nous analysons les phases de formation, de développement, et d'activité des deux orages. Dans cette partie, nous nous limitons à une description tirée directement des observations. Ainsi, à partir d'une série d'images radar bien choisies, nous montrons qualitativement les étapes caractéristiques de l'évolution des deux orages de type MCS. Nous constatons que l'un des deux orages a eu une évolution en deux périodes actives bien distinctes. La hauteur des nuages et l'évolution des surfaces différentielles de nuage à certaines hauteurs des sommets sont analysées quantitativement et on peut voir également le type d'évolution en deux périodes pour l'un des systèmes MCS et on peut constater que nos cas répondent assez bien aux critères de taille évoqués dans certaines études. Les sprites apparaissent répartis sur des périodes bien distinctes de l'évolution du système orageux, et suivent assez bien les cycles de développement dans le cas de l'orage qui en présente plusieurs. Le nombre de sprites parait assez compatible avec des cas d'études trouvés dans la littérature. La production de sprites n'est pas du tout en phase avec la production d'éclairs, cela pour les deux orages étudiés. Ils sont produits en fin d'activité d'éclairs nuage-sol dans une période de forte proportion de CG+.

IV- Analyse et discussion

Cette section est une analyse des deux cas qui met en avant les similitudes et les différences observées, les analogies avec les études disponibles dans la littérature et qui permet de proposer des interprétations. Elle est divisée en 2 parties qui correspondent à deux aspects de l'activité orageuse, la structure orageuse et l'activité précipitante pour l'une et l'activité d'éclairs pour l'autre.

Dans la première partie de la discussion, nous développons une comparaison avec d'autres cas de systèmes MCS ayant produit des sprites et nous constatons que nos deux cas de taille similaire sont comparables sur de nombreux aspects à des MCS classés de taille modeste aux Etats-Unis. Ils sont nettement plus réduits que les grands systèmes MCC des régions de grande plaine des US qui sont les producteurs par excellence des sprites avec parfois quelques centaines d'événements en quelques heures. Les délais entre maximum de développement de la région convective et début de la période de production sont cohérents avec la plupart des cas trouvés dans la littérature, mais comme nous le montrons, dans certains cas où il est noté une reprise d'activité dans une région du système, l'activité doit être différentiée entre les différentes régions du système orageux. En terme de production de précipitation, nous avons réalisé une analyse quantitative supplémentaire de l'évolution de la quantité produite par zones de réflectivité radar

différente et on montre clairement que les sprites sont produits lorsque la proportion de précipitation issue des réflectivité moyennes (30-40 dBZ) augmentait rapidement. Pour ce qui est du taux de production de sprites, un de nos cas en présentait des valeurs nettement supérieures et ce cas avait également des flux de précipitations de type convectif plus importants, ce qui pourrait laisser penser que l'activité convective du système est un facteur précurseur important de production de sprites. Cet aspect doit être analysé dans plus de cas.

Le deuxième aspect développé dans cette analyse est l'activité d'éclair associée et ses caractéristiques. Un tableau a été réalisé avec un certain nombre de paramètres pour caractériser les éclairs CG+ qui ont produit des sprites (S-CG+). Ces paramètres sont calculés en valeur moyenne et médiane, leurs valeurs extrêmes sont données, et toutes ses valeurs sont comparées à celles des autres CG+. Les pics de courant de ces S-CG+ sont en moyenne plus intenses que ceux qui n'ont pas produit de sprites, d'un facteur 2 environ. Par contre la dispersion est très grande dans l'ensemble des valeurs, ce qui indique bien que le pic de courant n'est pas un critère absolument déterminant pour déclencher le processus. Mais les différences relevées sont suffisamment significatives pour pouvoir dire que les pics de courant des CG+ parents sont souvent plus forts et qu'il y a un lien avec la production de sprites. Il est noté un fait remarquable, c'est une valeur moyenne récurrente autour de 60 kA pour ces S-CG+ pour les 3 périodes de production relevées et en plus cette valeur correspond assez bien à d'autres résultats d'études sur ce paramètre. D'autres paramètres sur les CG+ ont été analysés, la multiplicité par exemple. Ce paramètre ne permet pas de distinguer une propriété particulière des S-CG+. Les deux autres paramètres considérés sont l'intervalle de temps entre un CG+ et l'éclair CG suivant, qu'il soit positif ou négatif. C'est le comptage pratiqué par les critères de Météorage qui est dans ce cas considéré, c'est-à-dire qu'un arc-en-retour sera considéré comme un nouvel éclair CG s'il se produit à plus de 5 km ou à plus de 0,5 seconde du précédent. On note que cet intervalle de temps est beaucoup plus faible en général pour les éclairs S-CG+, notamment quand on examine les valeurs médianes. De plus, ces valeurs médianes sont très faibles dans le cas des S-CG+, de 0,28 à 0,41 seconde suivant les périodes de production, alors qu'elles valent de 1,49 à 5,49 secondes pour les autres CG+. Il faut noter en plus que les taux d'éclairs CG étaient plus faibles lors des pérodes de production de sprites. Il y a donc beaucoup plus d'événements d'éclairs CG successifs parmi les S-CG+. Une autre façon d'étudier cette propriété a été de considérer plus directement le phénomène de répétition d'éclairs CG en comptant le nombre d'éclairs CG (+ et -) dans la seconde suivant un CG+. La différence est encore notable entre les deux groupes de CG+, avec des valeurs de 3 à 4 fois plus grandes pour les S-CG+. Le pourcentage de S-CG+ suivis par au moins 1 CG dans la seconde va de 67 à 87 % suivant les périodes et celui des autres CG+ ne dépasse pas 40 %. Afin de voir une éventuelle relation entre la distance et le temps, séparant respectivement le CG+ et le CG suivant, pour des temps inférieurs à 0,5 seconde c'est-à-dire lorsqu'il est susceptible d'appartenir au même processus d'éclair. Le résultat obtenu sous forme de distribution montre bien une relation plutôt linéaire avec une augmentation en phase des 2 paramètres. Cette augmentation évoquerait donc une propagation de l'éclair entre les 2 CG successifs, c'est-à-dire un processus du type "spider" lightning. Les

éclairs S-CG+ sont donc plus souvent associés à un processus d'éclair qui comprend plusieurs CGs. Pour présenter ce résultat nous avons choisi une dernière représentation graphique qui permet de visualiser cette tendance au cours de l'évolution de l'activité d'éclair. Nous avons donc montré l'évolution du nombre d'éclairs cumulé pour un cas d'orage où les processus multi éclairs CG se traduisent par des petits sauts de la courbe et mettant un symbole sur la courbe aux instants des sprites. La plupart de ces petits sauts correspondent à des sprites, et lorsque ce n'est pas le cas, une analyse montre que la distance entre les différents CG du processus ne sont pas aussi éloignés. Donc c'est bien une propagation du type "spider" qui favorise la production de sprites.

V- Conclusion

La conclusion décrit les conditions de cette étude et reprend quelques résultats tirés des parties "études de cas" et "analyse et discussion". Les résultats marquant concernant la structure et l'activité précipitante montrent bien le rôle du développement de la partie stratiforme dans la production de sprites. Pour l'activité d'éclair CG associée, on voit un plus grand nombre de résultats. Certains concernent directement les caractéristiques de l'éclair S-CG+ et d'autres concernent l'activité CG immédiate après le S-CG+. Les S-CG+ ont un pic de courant plus fort, et sont plus facilement associés à d'autres éclairs CG dans un processus de type "spider".

4.2 Article

Atmospheric Research 91 (2009) 514–528

Contents lists available at ScienceDirect

Atmospheric Research

journal homepage: www.elsevier.com/locate/atmos

Analysis of thunderstorm and lightning activity associated with sprites observed during the EuroSprite campaigns: Two case studies

Serge Soula [a,b,*], Oscar van der Velde [a,b], Joan Montanyà [c], Torsten Neubert [d], Olivier Chanrion [d], Michal Ganot [e]

[a] Université de Toulouse; UPS; LA (Laboratoire d' Aérologie); 14 avenue Edouard Belin, F-31400 Toulouse, France
[b] CNRS; LA (Laboratoire d' Aérologie); F-31400 Toulouse, France
[c] Electrical Engineering Department, Technological University of Catalonia, Colon, 1, 08222, Terrassa, Spain
[d] National Space Institute, Technical University of Denmark, Juliane Maries Vej 30, 2100 Copenhagen O, Denmark
[e] Department of Geophysics and Planetary Sciences, Tel-Aviv University, Tel-Aviv 69978, Israel

ARTICLE INFO

Article history:
Received 30 November 2007
Accepted 11 June 2008

Keywords:
Sprite
Lightning
Ground flash
Mesoscale Convective System
Electric discharge
Mesosphere

ABSTRACT

During the summers of 2003 to 2006 sprites were observed over thunderstorms in France by cameras on mountain tops in Southern France. The observations were part of a larger coordinated effort, the *EuroSprite* campaigns, with data collected simultaneously from other sources including the French radar network for precipitation structure, Meteosat with images of cloud top temperature and the *Météorage* network for detection of cloud-to-ground (CG) flash activity. In this paper two storms are analyzed, each producing 27 sprite events. Both storms were identified as Mesoscale Convective Systems (MCS) with a trailing stratiform configuration (ST) and reaching a maximum cloud area of ~120,000 km^2. Most of the sprites were produced while the stratiform area was clearly developed and during periods of substantial increase of rainfall in regions with radar reflectivity between 30 and 40 dBZ. The sprite-producing periods followed a maximum in the CG lightning activity and were characterized by a low CG flash rate with a high proportion of +CG flashes, typically around 50%. All sprites were associated with +CGs except one which was observed after a −CG as detected by the Météorage network. This −CG was estimated to have −800 C km charge moment change. The peak current of sprite-producing +CG (SP+CG) flashes was twice the average value of +CGs and close to 60 kA with little variation between the periods of sprite activity. The SP+CG flashes were further characterized by short time intervals before a subsequent CG flash (median value <0.5 s) and with clusters of several CG flashes which suggest that SP+CG flashes often are part of multi-CG flash processes. One case of a lightning process associated with a sprite consisted of 7 CG flashes.

1. Introduction

Sprites are electric discharges in the Mesosphere above thunderstorms. They are so-called Transient Luminous Events (TLEs) which include the "blue jet" from thunderstorm cloud tops into the stratosphere and the "elve" at the base of the ionosphere. Sprites are the TLEs most commonly observed from the ground, usually by TV-frame rate, light sensitive optical imagers. They come in a variety of forms that have given names such as "column", "carrot" or "angel" sprites. Sprites are thought to be positive streamers. They initiate around 70 km altitude, then propagate downward – at times with a branched structure – and occasionally continue with upward propagating elements and more diffuse luminosity (Pasko et al., 2002). After the first observation of sprites (Franz et al., 1990), it was soon realised that the large majority are induced by positive cloud-to-ground (+CG) flashes (Boccippio et al., 1995; Lyons, 1996). To date, only a few cases of sprites

* Corresponding author. Laboratoire d'Aérologie, OMP, 14 Avenue Edouard Belin, 31400 France. Tel.: +33 5 61 33 27 74; fax: +33 5 61 33 27 90.
E-mail address: sous@sero.obs-mip.fr (S. Soula).

0169-8095/$ – see front matter © 2008 Elsevier B.V. All rights reserved.
doi:10.1016/j.atmosres.2008.06.017

induced by −CG flashes have been reported (Barrington-Leigh et al., 1999) as discussed in Williams et al. (2007). It is also suggested that sprites are associated with "spider lightning", which is extended horizontal lightning in clouds that may feed several CG flashes (Mazur et al., 1998). Whereas the peak current in +CGs are not well correlated with sprite occurrences (Lyons et al., 2003) the charge moment change (CM) (defined as the product of the mean altitude of the charge reservoir in the cloud and the amount of charge lowered to ground by a CG flash) is a much better predictor, as first suggested by Wilson (1925). Recent work suggests that higher CM changes increase the probability of sprite generation (Huang et al., 1999; Hu et al., 2002) which becomes significant for CM changes above 600 C km (Cummer and Lyons, 2005).

As initially observed over the Great U.S. Plains (Lyons, 1994) and confirmed by later observations (Yair et al., 2004; Hayakawa et al., 2004; Pinto et al., 2004; Neubert et al., 2005) the storms which produce sprites are often mesoscale convective systems (MCSs). The Mesoscale Convective Complex (MCC) is the largest MCS with strong convective activity, horizontal dimensions from 150 to 1000 km and cloud top temperatures lower than −32 °C (Maddox, 1980). The MCC is the most sprite-productive storm with several hundred sprites within 4–5 h (Lyons et al., 2003). However, sprites can also be produced by the non-MCSs observed in Europe (Neubert et al., 2001) or in Japan (Hayakawa et al., 2004). Thus, in most case studies reported in the literature, the production rate is one sprite every few minutes. It is then difficult to establish a threshold in the size or strength of a storm system needed for producing sprites.

A recent study by Lyons et al. (2006) describes the characteristics of storms producing sprites observed during the STEPS 2000 experiment conducted in the U.S.A. More than 2000 TLEs (mainly sprites) were observed from 3 dozen storms. The use of the Lightning Mapping Array (LMA) in the VHF range allowed identification of location and characteristics of lightning activity associated with the sprites. However, the analysis of sprite-producing storms has not been exhausted. During the EuroSprite campaigns, several smaller (relative to the U.S.) storms in France were identified as sprite producers, especially during the summers of 2003 with 101 sprite events observed (Neubert et al., 2005) and 2006 with 123 sprites observed from either of two sites. Among them, two MCS-type storms with 27 recorded sprite events each have been selected for analysis in this paper. First, the radar reflectivity distribution, the cloud top temperature and the structure, size and development of the storms are analyzed. Then, the cloud-to-ground (CG) lightning activity is discussed in relation to sprite production. The characteristics of the two storms are compared and several quantitative aspects are derived and compared with similar studies reported in the literature.

2. Observation system and data

Two camera systems at two different locations were fielded during the campaigns. One was located at the

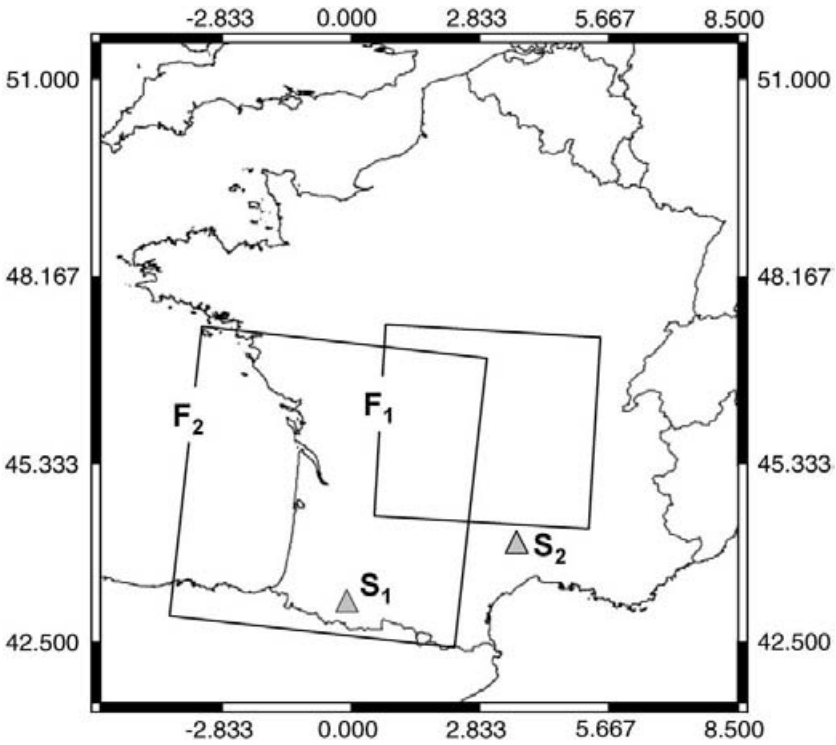

Fig. 1. Location of the French observation sites S_1 and S_2, at Pic du Midi and Mont Aigoual, respectively. Frames F_1 and F_2 display two domains used in the following figures to show the radar images of both storms which produced sprites, on 21 July, 2003, and on 11 September, 2006, respectively. F_1 and F_2 have dimensions of 300 km×300 km and 500 km×500 km, respectively.

Observatoire Midi Pyrenées at Pic du Midi at 2877 m altitude (Neubert et al., 2005). It includes two low-light, TV-frame rate CCD cameras mounted on a pan-tilt unit remotely controlled over the internet. The camera used here was equipped with a 16 mm, f/1.4 lens with 22.5° field-of-view (FOV). The video frames consist of two interlaced fields, with exposure time of 20 ms (PAL video system). The system time was synchronized to UT time through the Network Time Protocol (NTP) and correct to within 12 ms. The events were detected and stored by automated trigger software in order to reduce the data volume. For the summer of 2006 two additional cameras were used at Mont Aigoual (44.121N 3.576E, 1565 m). One camera was a Watec 902H with a 16 mm, f/1.4 lens (FOV=23°), mounted on a tripod, and connected to a laptop equipped with trigger software. The second camera, operated by Tel-Aviv University (TAU), was a Watec 100 N with a 12 mm f/0.8 lens (FOV=30.5°) also mounted on a tripod system and connected to a laptop with the same trigger software and a GPS and time-inserter unit. Fig. 1 shows the locations of the camera systems labelled S_1 and S_2, respectively. Also shown are two square-shaped frames F_1 and F_2 which bound the regions where the sprite-producing MCSs occurred and which will be used in the following figures for the description of the storms based on radar images. In order to accurately determine the direction of a sprite detected by a camera, we use freeware software which allows the superposition of the camera image of the sprite and the stellar background with the sky chart for any date and time from this observation site. The distance of the event, and therefore its location, cannot be determined directly from a single site as is the case for all our observed sprites. However, the sprites considered here can be assigned without any ambiguity to their causative CGs for which the locations are known from the Météorage lightning detection network.

For the description of the structure of the storms we use data from the meteorological radar network ARAMIS of 18 conventional radars (10 C-band and 8 S-band) covering France. Each radar has a range of approximately 250 km and produces images every 5 min. The Plan Position Indicator-type images were made with a constant and low elevation of respectively 1.4° (for low distance) and 0.4° (for large distance) and therefore display the reflectivity factor at low altitude in the cloud systems. The cloud top temperature data are provided by the Meteosat satellites from EUMETSAT, placed in a geostationary orbit at 36,000 km altitude. This temperature is deduced from the 10.5 to 12.5 μm thermal infrared band (IR) of the radiometer equipping each Meteosat satellite.

Data from a lightning detection network are used to obtain accurate positions and timing of CG lightning flashes. This French network run by Météorage adopts 17 sensors using both direction finding and time of arrival techniques to determine the location of positive and negative CG strokes over the entire country (Cummins et al., 1998). Its detection efficiency for CG flashes is ~90% and about 70% of the locations are determined with accuracy better than 4 km. It provides the location, time, and peak current of each detected CG stroke. Strokes are considered associated with the same CG flash event provided they occur within 0.5 s and within 4 km.

3. Case studies

3.1. Case of 21 July 2003

On 21 July 2003 a large region of low pressure located over North-Ireland with a trough over the Atlantic Ocean west of the Iberian Peninsula, organized a strong south-westerly flow over France. A convergence associated with warm air at low level and a cold anomaly in altitude created favourable conditions for storm development over Central France. The maximum value of CAPE on 20–21 July at 0000 UT was 1800 J kg^{-1} as found from a sounding made from the Nîmes station (43.86N; 4.40E). Fig. 2 shows the distribution of the radar reflectivity factor in the area F_1 (300 km×300 km) at 0100 UT, 0200 UT, and 0300 UT during the night of 20–21 July 2003. Convective cells started to develop before 0100 UT over southwestern France by forming a linear convective zone moving longitudinally north-eastwards with large reflectivity values (>60 dBZ) in several parts of the convective zone. The system entered F_1 before 0000 UT and at 0100 UT several cells with high reflectivity were visible. Between 0100 and 0200 UT the convective cells gathered to form a 50-km line of high reflectivity reaching 65 dBZ. At the same time, a stratiform area developed to form a 250 km×125 km zone of relatively uniform reflectivity between 30 and 40 dBZ. This system exhibited the characteristics of a trailing stratiform MCS. Around 0300 UT the stratiform area remained relatively extended and several convective cells appeared along the right side of this zone. The red dotted lines in Fig. 2 show the FOV (22.5°) of the camera in S_1.

The cloud top temperature determined from Meteosat images gives an estimation of the cloud top altitude and the associated vertical convection inside the clouds. The coldest temperature indicates the highest altitude. Fig. 3 displays the area of cloud cover in different temperature ranges as a function of time between 0030 and 0430 UT. The maximum cloud top height (temperatures from −65 °C to −60 °C) was observed at 0130 UT when most of the convective cells gathered together to form a line. While the surface with high values of the cloud top height increased until 0200 UT to then decrease, the surface with intermediate values (−55 °C to −45 °C) increased appreciably from 0130 to 0300 UT. According to the soundings made in Nîmes at 0000 UT the temperature of −55 °C was at 13 km altitude, which indicates a very strong vertical development of the convective cells. Between 0205 and 0313 UT 27 sprites were observed over this system. Fig. 4 shows 6 of the brighter ones as observed at a distance from S_1 of around 450 km. The period of sprite production lasted 1 h and 8 min, which gave an average time interval between the sprites of 2 min 37 s. The time interval between two successive sprites ranged from 9 s to 6 min 25 s, which means that this period of sprite production was relatively continuous and clearly identified in the lifetime of the MCS.

Fig. 5 displays the time series of the CG flash rates (+CG and −CG) and that of the sprite rate, calculated over 5-minute periods between 0000 and 0400 UT. The plot does not start at the beginning of the lightning activity, but at 0000 UT when the CG flash rates were high for the MCS located in the surrounding regions of F_1. The −CG flash rate reached 25.2 min^{-1} at 0015 UT and then decreased until 0205 UT to below 5 min^{-1}. It remained low for a 30-minute period (0205–0235 UT). It increased again after this period due to the development of new convective

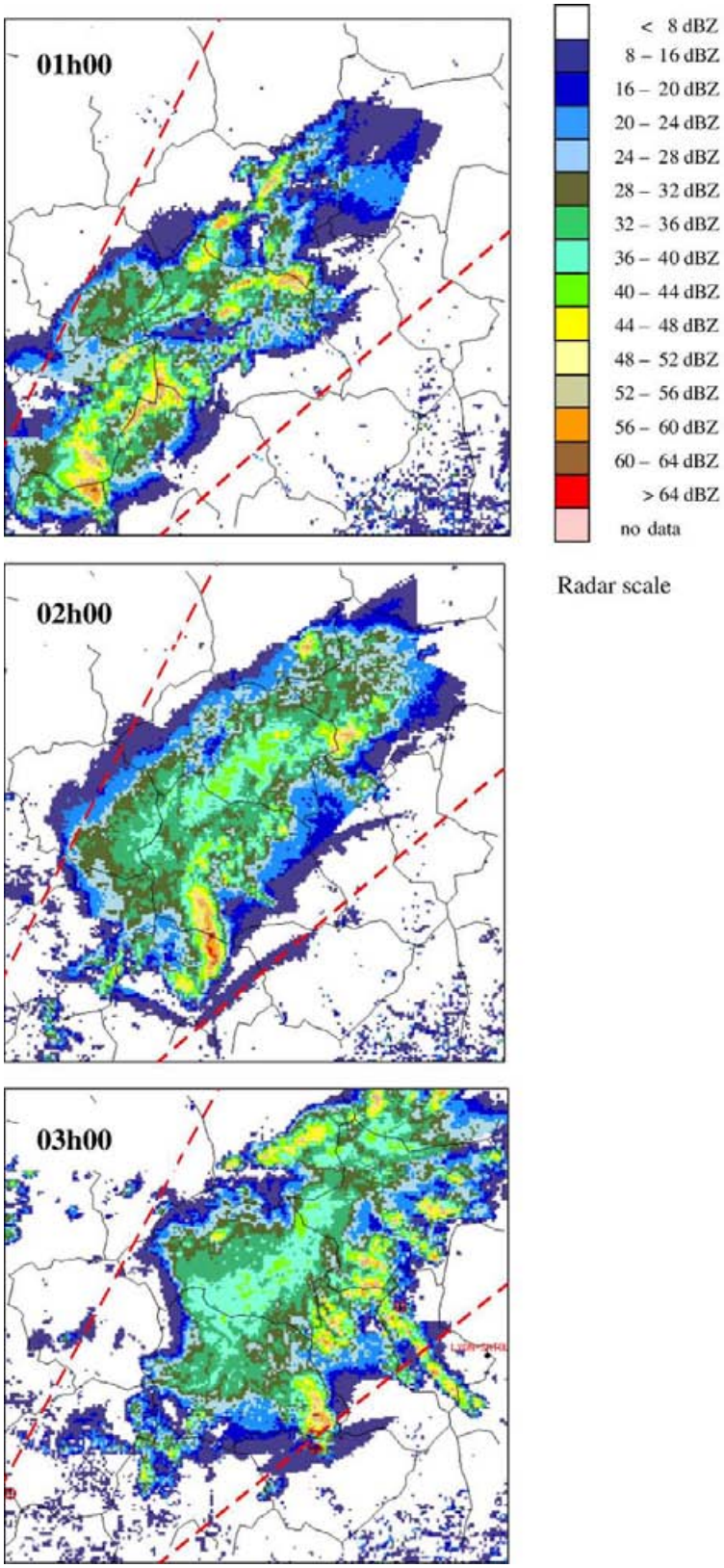

Fig. 2. PPIs (Plan Position Indicator) of the radar reflectivity factor in the MCS which produced 27 sprite events on 21 July, at 0100 UT, 0200 UT, and 0300 UT. The domain corresponds with the frame F_1 (300 km × 300 km). The red dotted lines indicate the FOV of the camera in S_1 (22.5°).

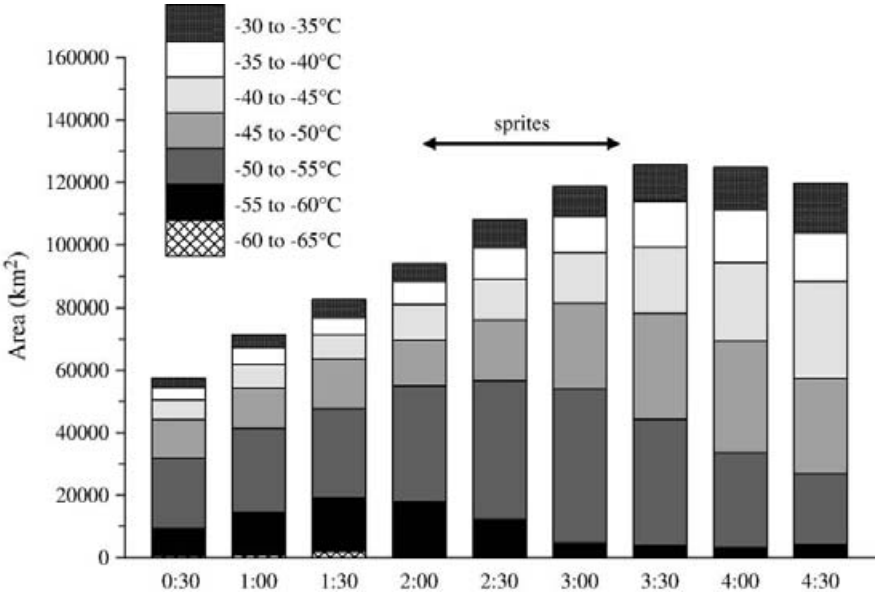

Fig. 3. Time series of the area of the cloud canopy at different atmospheric temperature intervals for the cloud top temperature: case of the MCS on 21 July.

cells, to a maximum of 13.4 min^{-1} reached at 0340 UT. In contrast, the +CG flash rate remained rather constant between 0.4 and 3.6 min^{-1}. The proportion of +CG flashes was then larger than 30% during the 30-minute period 0205–0235 UT, with a maximum value of 63% at 0215 UT. The sprite-producing period is well defined and corresponds to the period of low −CG flash rate and consequently, to the period of a high +CG rate. The maximum sprite rate was 3 in the considered 5-minute intervals, with only one interval without any sprite. After the last sprite was observed at 0313 UT, daylight started to appear and prevented sustained observation. However, chirps in infrasound identified as sprite signatures were observed until ~05 UT presumably from the same active region (Farges et al., 2005). The distribution in time of the events shows that there is a preferential period in the lifetime of the storm for sprite production.

3.2. Case of September 11th, 2006

On 11th of September, a pronounced and elongated trough of low pressure was present over the nearby Atlantic Ocean north of Spain. The CAPE deduced from the sounding in Bordeaux at noon was 800 J kg^{-1}. Such CAPE values and instability in the atmosphere remained all the day over France. The flow pattern over France was approximately southerly, advecting warm air into the area near the surface. Several thunderstorms producing strong rainfall developed in the evening, especially close to the Atlantic Ocean. Finally,

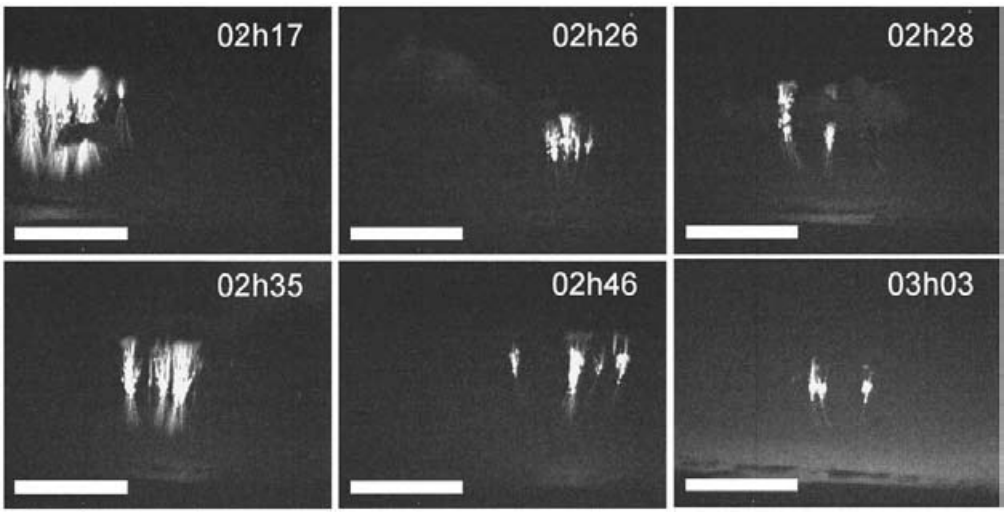

Fig. 4. Images of sprites observed from S_1 over the MCS on 21 July (FOV = 22.5°).

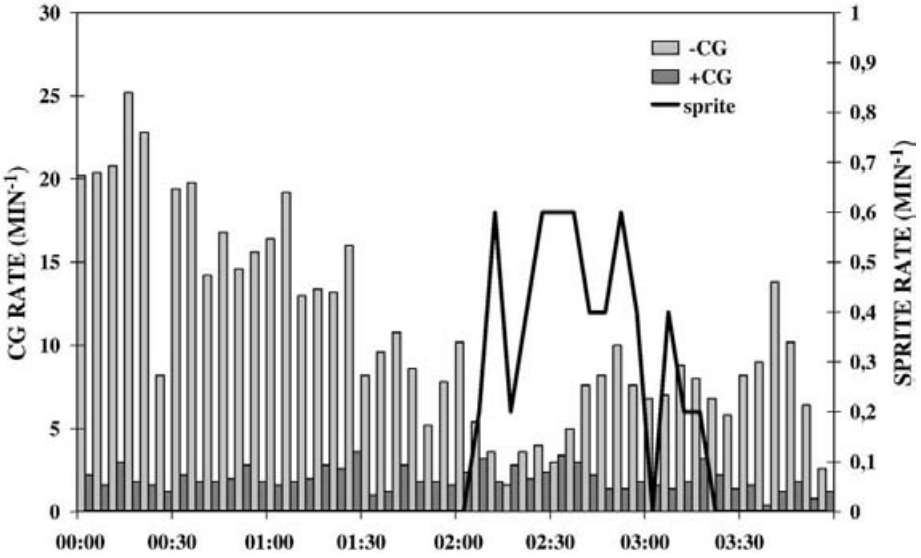

Fig. 5. Time series of the rates (5-minute averaged) for +CG and −CG lightning flashes, and sprites, produced by the MCS on 21 July.

a very large part of the country was affected by thunderstorms during that day and cumulative local precipitation attained values close to 100 mm in many areas. Fig. 6 displays the evolution of the radar reflectivity field in the 500 km × 500 km area F_2 in southwestern France, crossed by a convective system during the night of 11–12 September, for the period 1930 UT to 0115 UT. The beginning of the period is the time when the system first began generating sprites, as observed by the cameras, and the end of the period was marked by the last recorded sprite event. The system was a TS-type MCS moving northwards with a velocity of about 30 km h^{-1} with a convective line or cluster at its northern side. The size reached roughly 200 km × 150 km at the time of maximum development at about 2030 UT. The system exhibited first a stratiform zone extending transversely to the northward direction of movement (1930–2200 UT) then the stratiform zone developed longitudinally during the later part (0000–0115 UT). The radar reflectivity values did not exceed 60 dBZ between 1930 and 0115 UT and the largest ones were observed in the first period, with several convective cells imbedded in the system. By considering the evolution of the system, it follows that the convective area slightly decreased during the first period (1930–2200 UT), then was reinforced between 2200 and 2300 UT and finally decreased after 2315 UT. On the other hand, the stratiform area substantially decreased after 2200 UT to be strongly reduced at 2300 UT and then developed again until 0115 UT when the convective area disappeared totally.

Fig. 7 shows the variation with time of the area of cloud top temperatures between 1800 UT and 0200 UT. According to the sounding made on 11 September in Saragossa (Spain), south of the area F_2, the temperature −60 °C was found at about 12 km. The area of cloud top temperatures below −60 °C (altitudes above 12 km) was large and continued to increase until 1900 UT where it reached ~33% of the area of the whole system (~10,000 km^2). After 1930 UT, the area of this convective region substantially decreased while that of the whole system continuously increased until 2130 UT, essentially for the benefit of the intermediate temperature values, between −60 °C and −40 °C.

During that night 27 sprites were observed between 2018 and 0111 UT, from station S_2 indicated in the map of Fig. 1. The sprites appeared in three distinct periods of relatively continuous production, 2018–2149 UT, 2317–2337 UT, and 0009–0111 UT, with 12, 5 and 10 events, respectively. The average time interval between two consecutive sprites was 8 min 12 s, 5 min and 6 min 46 s for the three periods, respectively. These average values were relatively close and higher than in the first storm. The maximum and minimum values of this interval were observed in the first period, 19 min 17 s and 2 min 28 s, respectively. The last two periods were close in time and can be considered as one with a 32-minute gap of production, for the analysis in the following section. The sprites were observed with one or both cameras located at S_2 and at a distance around 350 km. Fig. 8 displays 6 of these sprites exhibiting a large diversity of shape, size and structure. Contrary to the first case, the sprites produced by this storm could be very different from one to the other. Some events were extensive, with a width of about 30 km, for example the event detected at 2110 UT.

By considering the evolution of the storm structure in terms of convective and stratiform areas and the location of CG flashes, it is possible to distinguish two areas of lightning activity for this system. Fig. 9 shows the location of all +CG flashes generating sprites (SP+CG flashes) with different symbols for the three periods. They were well separated spatially, from south to north corresponding to the displacement of the system allowing separate analysis of the regions or periods. The CG flashes are therefore spatially divided into two groups, and Fig. 10 displays the rates of CG flashes and sprites for each group. The upper panel shows the lightning activity of the system when it was in the south of the region displayed in Fig. 6. The −CG flash rate reached the largest values around 1945 UT, up to 14.6 min^{-1}, and then abruptly decreased after 2000 UT to a few min^{-1}. The first period of sprites corresponds with the low −CG flash rates. The +CG

flash rate did not undergo any similar strong decrease since it remained close to 2 min^{-1} and therefore the relative +CG rate was high reaching 50%, when the first sprites were produced. The lower graph corresponds with the second phase of the MCS when it was within the northern parts of region F_2. The sprite production started when the −CG flash rate substantially decreased and was about 5 min^{-1}, which was similar to the first period. Most sprites were produced when the −CG flash rate was low and the +CG proportion was high.

4. Analysis and discussion

4.1. Cloud structure, precipitation activity and sprite production

The two cases of MCS have almost the same size as estimated from infrared cloud top temperatures (1.25×10^5 km^2 and 1.3×10^5 km^2) and the same number of observed sprites (27). For both systems the maximum area was reached during the sprite production period. These characteristics compare well with those of moderate MCS reported over the U.S. with areas of 1.2×10^5 km^2 producing 15 sprites (Lyons et al., 2003) and 0.3×10^5 km^2 (radar reflectivity area) producing 36 sprites (Lyons, 1996). Another study reported a long lifetime MCC over Kansas reaching 2.3×10^5 km^2 with more than 50 sprites observed (São Sabbas and Sentman, 2003).

However, the number of sprites observed in our two cases is low compared to the numbers generally observed in the U.S. (Lyons et al., 2000, 2006). This is consistent with the size of the systems being just above the threshold of onset at 1×10^5 km^2 estimated by Lyons et al. (2003) for MCCs that may eventually produce several hundreds of sprites. Another criteria suggested for sprite production is that the area of radar reflectivity must be above 20,000 km^2 (Lyons, 1996), which was also exceeded.

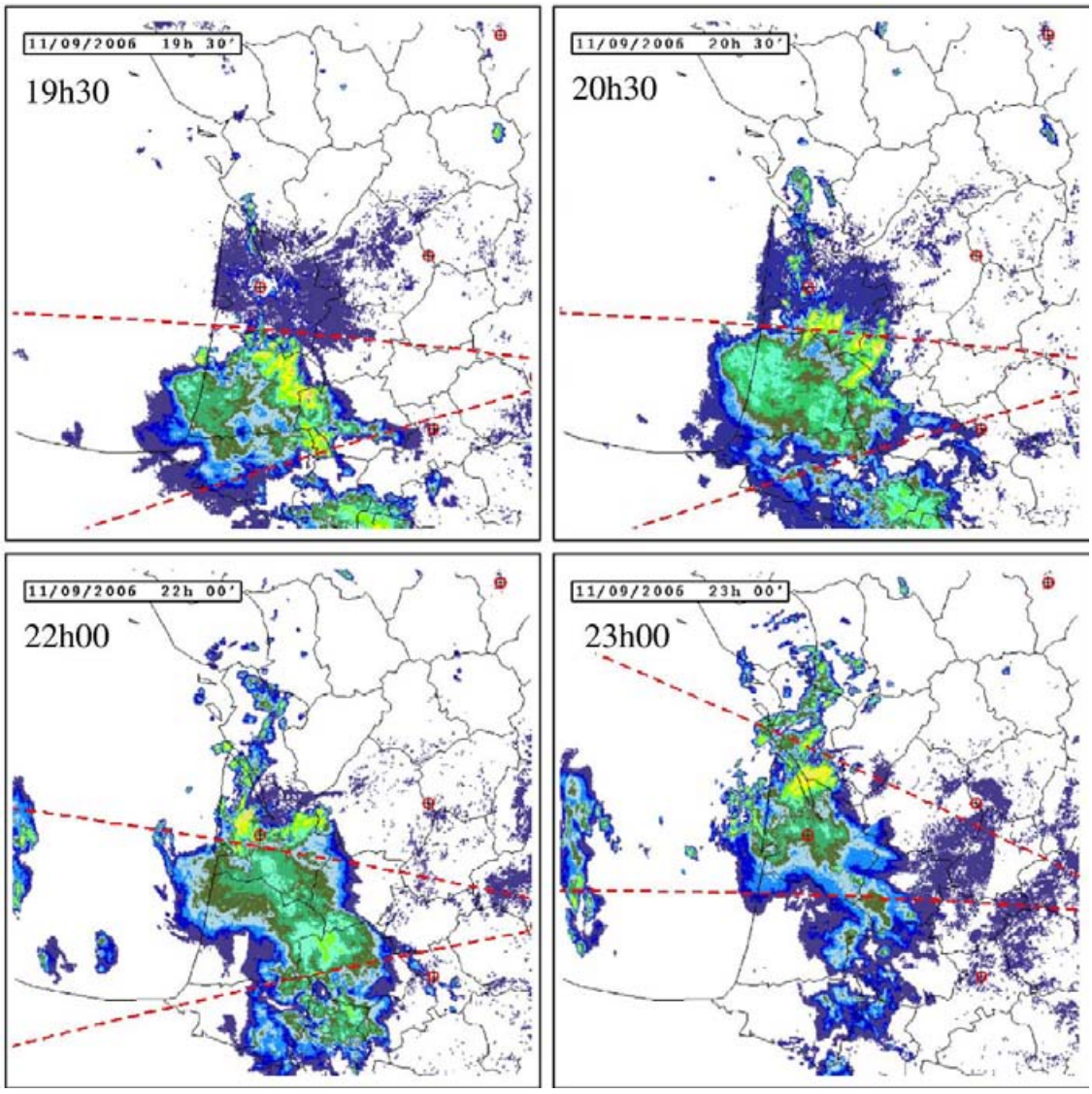

Fig. 6. PPIs (Plan Position Indicator) of the radar reflectivity factor in the MCS which produced 27 sprite events on 11 September, at 1930 UT, 2030 UT, 2200 UT, 2300 UT, 2315 UT, 0000 UT, and 0115 UT. The domain corresponds with F2 (500 km×500 km) and the radar scale is that of Fig. 2.

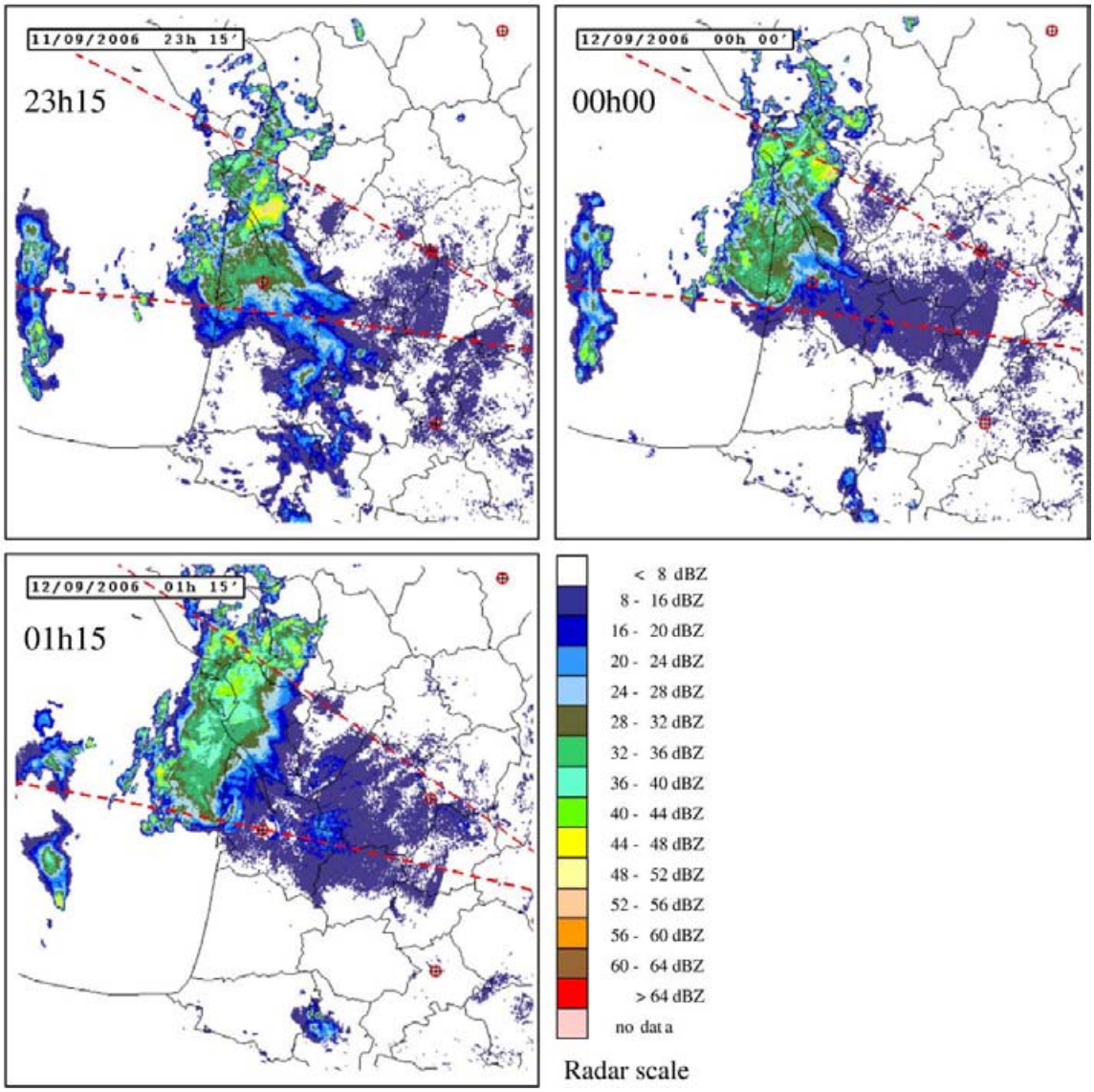

Fig. 6 (*continued*).

During both storms we found distinct periods of sprite production which clearly indicates that some special conditions are required. This conclusion is consistent with those based on storms elsewhere (e.g. São Sabbas and Sentman, 2003). For the second storm several periods of production could be identified which could be related to the two cycles of evolution of the storm seen for instance in the size of the system. In our cases sprite production started about 30 min and 1 h after the maximum area of coldest temperatures was reached. This is different from the case studied by São Sabbas and Sentman (2003) where the maximums in sprite production and cloud cover area of coldest top temperature were reached simultaneously. We suggest that the storm over Kansas was more severe (minimum temperature was below −70°), larger and with a longer lifetime and that the onset for sprite production was reached before the end of the development of the storm. In our cases sprite production is better correlated with the cloud area with top temperature between −55 °C and −50 °C. This is consistent with the study of Lyons (1996) of a modest-size MCS where the majority of sprites were observed above the stratiform area of the MCS.

Based on the radar observations we made a quantitative analysis of the rainfall activity during the lifetime of the storms to search for signatures associated with the phase of the storm where sprites are generated. For this purpose the reflectivity factor was converted into a rainfall rate. Radar reflectivity Z, typically expressed in dBZ, is related to a factor Z_0 expressed in $mm^6\ m^{-3}$ by: $Z = 10 \log Z_0$, where Z_0 is proportional to the density of particles n and their diameter D in the scanned radar beam volume ($Z_0 \propto n D^6$). For non-critical use as in this study, reflectivity Z_0 can be converted to the rainfall rate R by the commonly used empirical relationship for the drop size distribution: $Z_0 = 200\ R^{1.6}$ (Z_0 in $mm^6\ m^{-3}$ and R in $mm\ h^{-1}$) (Marshall-Palmer, 1948). Fig. 11 shows the

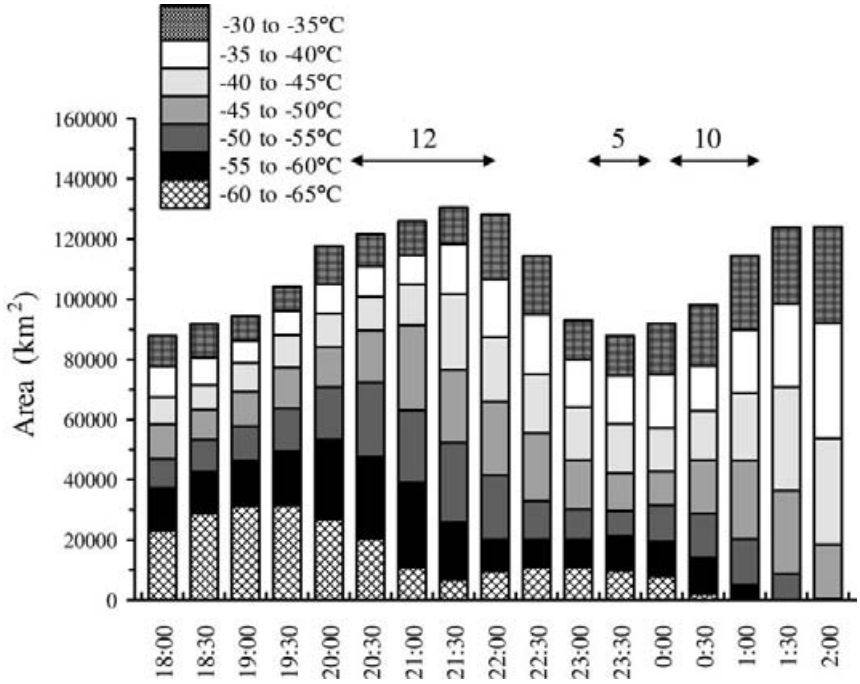

Fig. 7. Time series of the area of the cloud canopy at different atmospheric temperature intervals for the cloud top temperature: case of the MCS on 11 September. The arrows indicate the periods of sprite production with the number of sprites.

precipitation mass as a function of time for different intervals of radar reflectivity in the two storms. The best correlation between sprite production periods and precipitation is with the precipitation mass produced by the 35–40 dBZ and 30–35 dBZ intervals. The value of the mass is around 1×10^7 kg s^{-1} for the first storm at the onset of sprite production. The largest mass was reached for the 35–40 dBZ interval during periods of sprite generation at 1.7×10^7 and 1.2×10^7 kg s^{-1} corresponding to 2.7 and 11.5 mm h^{-1}, respectively.

Most sprites were observed when the stratiform areas developed rapidly. Although the storms were of comparable size, the storm on 11 September produced lower convective precipitation mass values compared to the storm on 21 July as seen in reflectivity values larger than 40 dBZ. On the other hand, the sprite production rate was larger in the 21 July storm. This suggests that the production rate of sprites is related to the decay of the convective region which influences the electrical conditions inside the stratiform region, most likely through the rearward deposition of precipitation particles. This scenario is consistent with estimates of charge sources in the stratiform region with advection from convective parts amounting to 30% and local processes to 70% (e.g. Schuur and Rutledge, 2000). Local charging inside the stratiform region has been attributed mostly to the non-inductive charging process of particles in the mesoscale updraft, rather than charging processes associated with melting (Schuur and Rutledge, 2000). The role played by the advection process is observationally supported by the downward sloping path of spider lightning along apparent snowfall trajectories (e.g. Carey et al., 2005, Ely et al., 2008). Advection and local stratiform charging may both be linked to the intensification of a front-to-rear mesoscale updraft. In our observations, the collapse of convective regions indicated by the decreasing −CG flash rates was followed by expanding stratiform precipitation and the occurrence of sprites. In both MCSs, sprites continued approximately 'till the moment that the 30–40 dBZ precipitation mass started to decrease. This suggests that the mesoscale updraft weakened and/or that the rearward advection of precipitation from the convective region decreased.

4.2. Lightning activity and sprite production

In both storms considered in this study, sprites were observed during a period beginning up to 2 h after the maximum rate of −CG flashes was reached and during an electric phase of the storm where the −CG flash rate was low and the relative proportion of +CG flashes was high. These characteristics are consistent with the findings of Lyons (1996) who reported that sprite production by an MCS was not correlated with the total CG flash activity and that most of the 36 sprites observed occurred at least 1 h after the maximum −CG flash rate was reached. In contrast, São Sabbas et al. (2003) found a good temporal correlation between −CG flash activity and sprite production in a very active storm over Kansas. This storm was so powerful that the number of −CG flashes reached close to 100 min^{-1} compared to 14 min^{-1} in the European storms analyzed here (Figs. 6 and 11). We suggest that the system was so large that several separate regions were electrically active and that only those in the sprite-producing region should have been included in the analysis. Lyons et al. (2003) considered a storm case documented during the STEPS experiment, which produced 15 sprites. In this case the maximum sprite rate

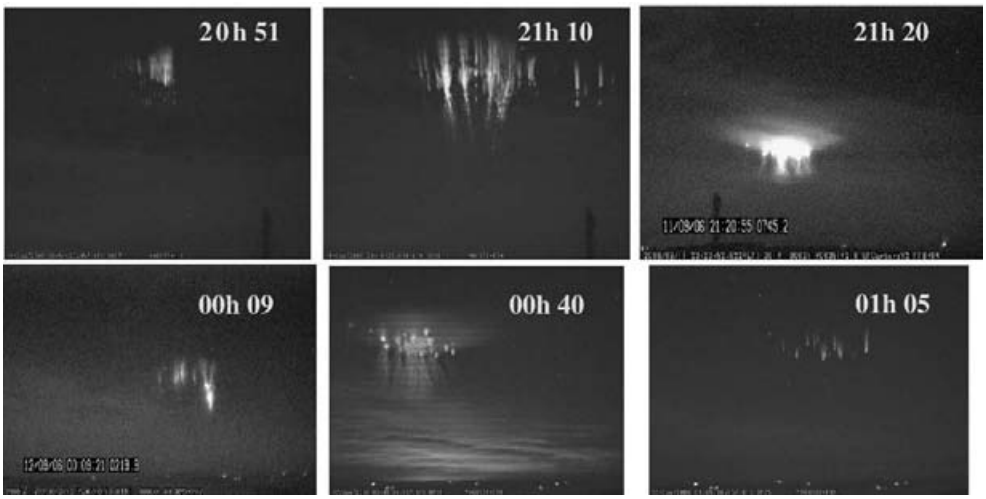

Fig. 8. Images of sprites observed from S_2 over the MCS on 11 September (FOV=23°).

was observed around 0600 UT with 6 events in less than 5 min. They gave the CG flash numbers in 1-hour intervals and it was relatively low during the interval 0500–0600 UT. Another paper by Pinto et al. (2004) considered case studies of 6 sprite-producing storms observed in Brazil with a total of 16 sprites. Only one of these storms was an MCS and all storms appeared of moderate size and with moderate CG flash rates. During the periods of sprite production, they noted a high percentage of +CG flashes which generally corresponds to a low −CG flash rate and is also observed in our cases. Before the two MCSs produced sprites, the −CG flashes were strongly dominant as is observed in normal polarity thundercells.

Now we turn to the CG flash activity related to individual sprites. All sprites observed from the two storms were preceded by a detected +CG flash, except one which was produced 0–19 min after the first stroke (−50.5 kA) of a three-stroke −CG flash. The charge moment change of this negative

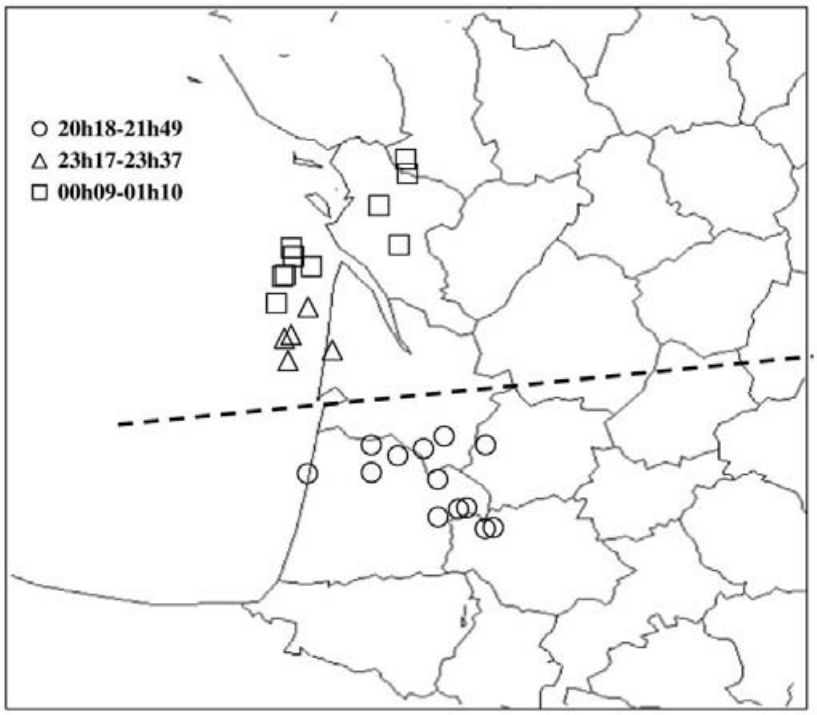

Fig. 9. Location of the SP+CG flashes on 11 September in the domain F_2, for the three periods of production considered in the description of the system. The dotted line is used for separating two groups of CG lightning flashes.

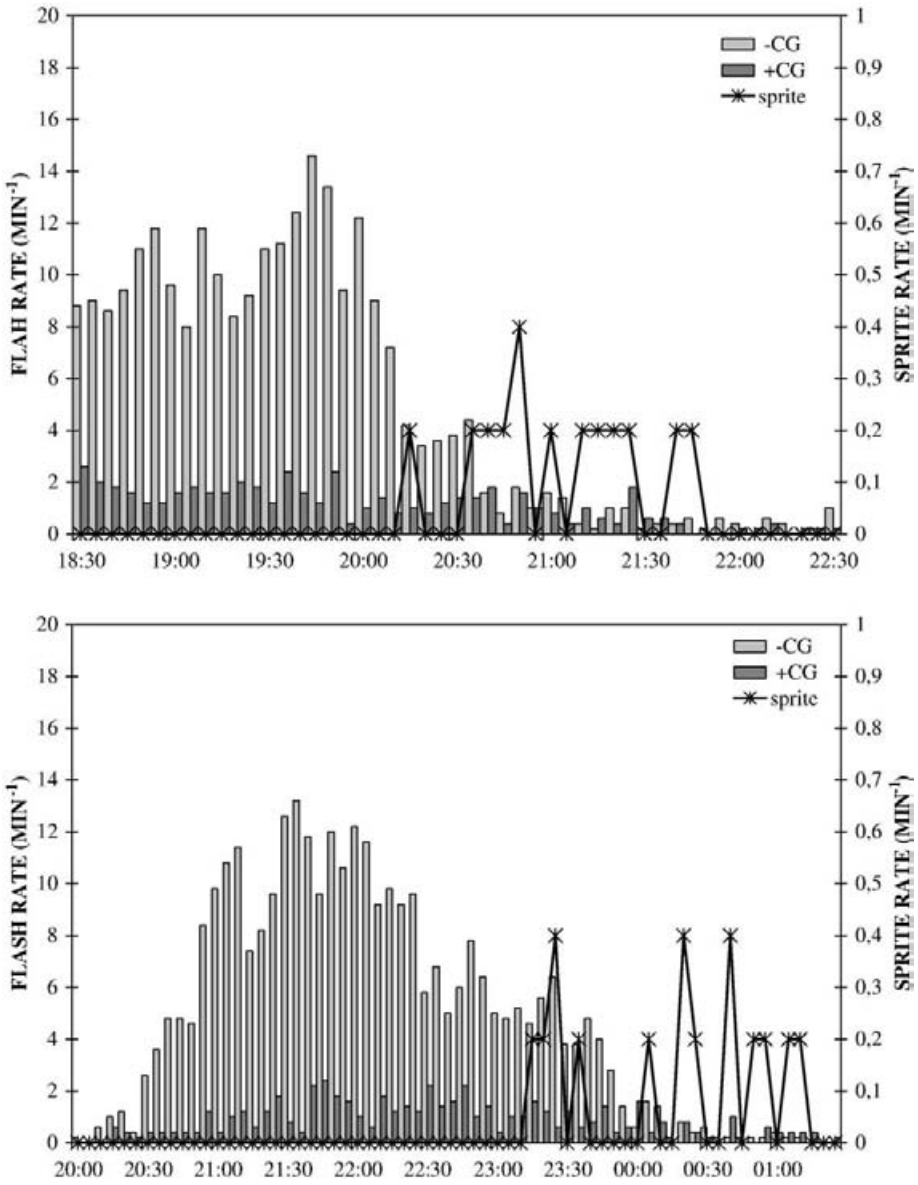

Fig. 10. Time series of the rates (5-minute averaged) for +CG and −CG lightning flashes, and sprites, produced by the MCS on 11 September, separating two periods of activity.

triggering stroke has been estimated from Extremely Low Frequency (ELF) electromagnetic wave observations from Mitzpe Ramon in Israel and the NCK station in Hungary to be about −800 C km.

In order to characterize the 53 +CG flashes involved in a sprite trigger, some parameters have been extracted from the data provided by the Météorage network. They are listed in Table 1. The +CG flashes are separated into two groups according to trigger (SP+CG) or no trigger (+CG) of a sprite. Four parameters are considered: the peak current (I), the multiplicity (M), the time interval between a +CG flash and the following CG flash which can be positive or negative and which was produced in the same MCS (dt), and the number of CG flashes produced by the MCS within 1 s after a +CG flash (N). For each parameter, the average, maximum, minimum and median values are calculated. The CG flashes are determined based on data from Météorage which considers two successive strokes as different CG flashes when they are separated by at least 4 km in distance or/and by at least 0.5 s in time. The percentage in the last column of the table represents the proportion of +CG flashes which are followed by another CG flash within 1 s.

First we note that the average value for the SP+CG is around 60 kA and about twice the average value of +CG flashes. This is very close to the value of 59.7 kA found by Lyons et al. (2006) by considering a large number of cases and São Sabbas et al. (2003) estimating 60 kA and with currents in the 40–50 kA range. The average value for the currents of +CG

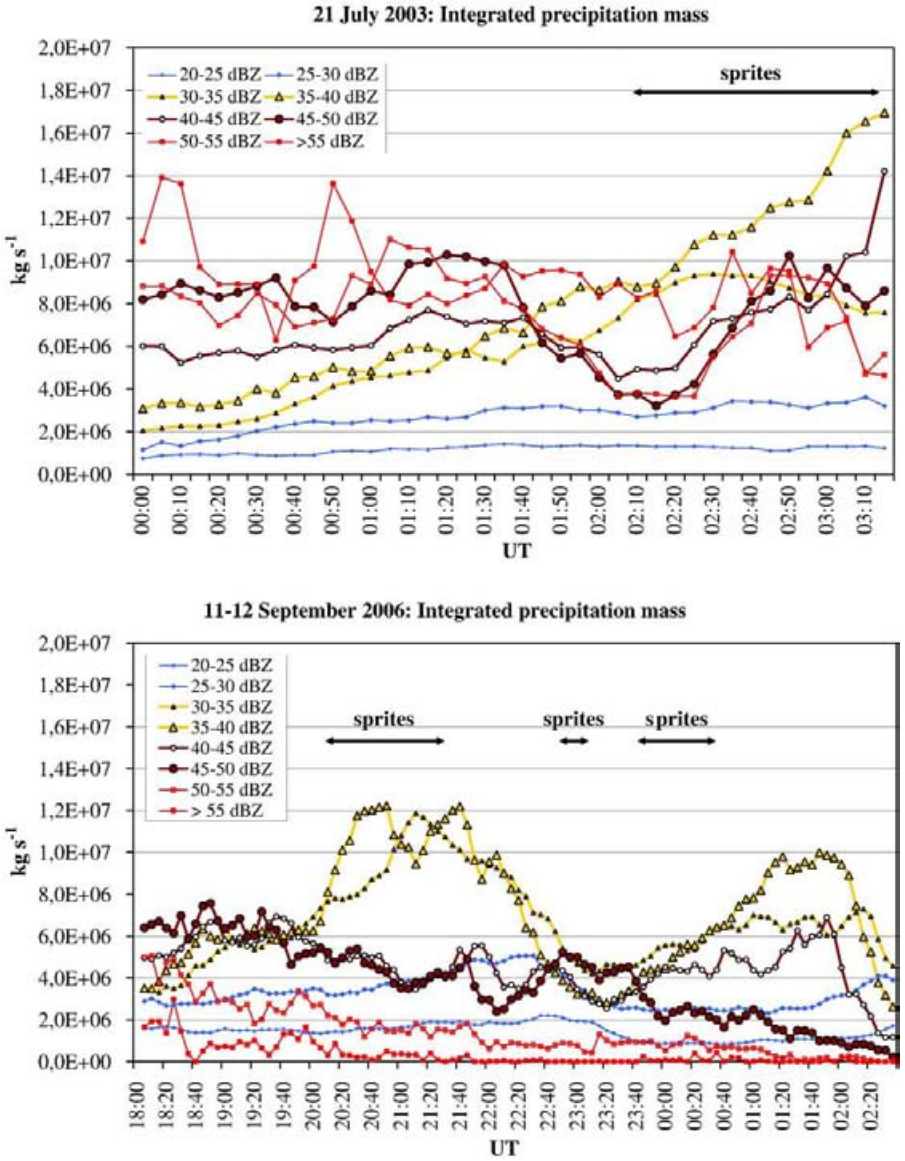

Fig. 11. Time series of the precipitation mass for different intervals of value of radar reflectivity in the thundercloud for 21 July (upper graph) and for 11 September (lower graph).

flashes without sprites was very close to 30 kA for each of the three storm periods. Pinto et al. (2004) also found this ratio of 2 with a significant number of events. The values of the peak current for both types of +CG flashes were found within a large range. For each case, the ratio between the maximum and minimum values was larger than 10. The minimum value for +CG flashes was 10 kA, the filtering value adopted for avoiding the misclassification of intracloud flashes (Cummins et al., 2006). Also in Lyons et al. (2003) and in Huang et al. (1999), the range of the peak current of the SP+CG flashes was large, with about one order of magnitude. It indicates the peak current is not a robust predictor for sprite triggering. The median values of the peak current were also much larger for SP+CG flashes, between 46.0 and 53.2 kA, compared to 18.8–25.2 kA for +CG flashes. For the multiplicity, no significant difference between SP+CG flashes and +CG flashes can be noted. In both groups of +CG flashes it remained low on average. However, the maximum value was always larger for the +CG flashes.

The time dt was always lower for the group of SP+CG flashes, for all storms considered and for most of its values, i.e. either average or maximum or median value. The minimum values were close to zero for both types of +CG flashes. The average values were clearly lower for the SP+CG flashes, for example 2.25 s compared to 5.13 s in the case of 21 July, and 1.64 s compared to 31.26 s in the case of the second period of 11 September. This difference is remarkable since the sprites were produced during periods with low CG flash rates and therefore with average time intervals between CG flashes larger than during the whole period of the storm. It indicates

Table 1
Characteristics of the +CG lightning flashes produced by both MCSs, triggering a sprite (SP+CG), and not triggering a sprite (+CG)

Storm	Value	*I* (kA)		*M*		dt (s)		*N*	
		SP+CG	+CG	SP+CG	+CG	SP+CG	+CG	SP+CG	+CG
21/07/2003	Average	59.3	31.0	1.1	1.1	2.25	5.13	1.85	0.45
27 SP+CG	Max	185.8	175.3	2.0	5.0	15.99	47.89	5	5
392 +CG	Min	17.5	10.0	1.0	1.0	0.01	0.00	0	0
	Median	46.0	24.2			0.41	2.40		
								85.2%	30.2%
11/09/2006	Average	58.9	31.3	1.2	1.2	8.73	9.31	1.92	0.71
Cell 1	Max	151.0	215.7	2	6	35.40	236.51	5	5
12 SP+CG	Min	8.0	10.0	1	1	0.00	0.00	0	0
221 +CG	Median	53.2	18.8			0.28	1.49		
								66.7%	39.7%
11/09/2006	Average	68.0	30.5	1.6	1.2	1.64	31.26	1.4	0.32
Cell 2	Max	178.0	127.7	3	5	10.69	424.34	3	5
14 SP+CG	Min	14.8	10.0	1	1	0.07	0.00	0	0
206 +CG	Median	48.9	25.2			0.35	5.49		
								85.7%	26.5%

I, *M*, dt, and *N* are the peak current of the +CG flash, the multiplicity of the +CG flash, the time interval between a +CG flash and the following CG flash (+ or −), and the number of CG flash (+ and −) within 1 s after a +CG flash, respectively. The percentage in the last column is the proportion of +CG flashes which are followed by at least 1 CG flash within 1 s.

the SP+CG flashes could have a specific feature. For the median value of this time dt, the difference between both groups of +CG flashes appears still larger. As a matter of fact, it was always lower than 0.5 s: 0.41, 0.28, and 0.35 s, for the three periods in Table 1, respectively. It means dt was often very low since the median value shares the group into two halves. Such low values indicate the following CG flash could be associated with the SP+CG flash in the same lightning process in many cases. However, the detection system counted them as new CG flashes because the distance was too large to be considered as a stroke of the same CG flash. So, these following CG flashes could be remote strokes involved in the same lightning process with long-distance propagation. Observations of multi-stroke +CG flash parents were reported by Lyons (1996) for several cases of sprite but we can wonder if the criteria for associating strokes in a same CG flash were different for the study by Lyons. Fig. 12 displays a distribution of the distance between the striking points of the SP+CG flash and of the following CG flash versus dt for the three storm periods and for the cases with dt lower than 0.5 s (31 cases over the 53 SP+CG flashes). Dt exceeded 1 s for 10 SP+CG flashes. The distance tends to increase with dt, which suggests a propagation of a lightning process between both CG flashes involved. A linear curve fitting provides a coefficient of about 10^5 m s^{-1} for the ratio between distance and time. This value corresponds with the velocity of the negative leader propa-

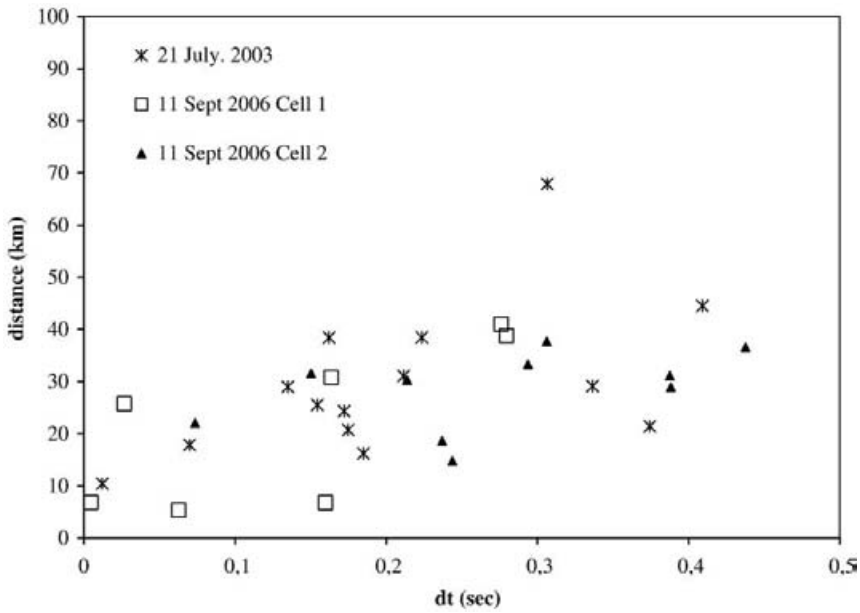

Fig. 12. Diagram of the distance versus time interval dt between an SP+CG flash and the following CG flash for the cases with dt lower than 0.5 s. The three periods are considered in the graph.

gating toward or within a positive charge region (Mazur et al., 1998). In support of this view, other authors observed sprites to be associated with lightning discharges horizontally propagating over long distances, Stanley (2000) in Florida and Lyons et al. (2003) during STEPS.

The number *N* of CG flashes following a +CG flash within 1 s (last column of Table 1) supports this assumption. So, for the SP+CG flashes *N* was 2–4 times larger than for the other +CG flashes. Even if the SP+CG flashes occurred during periods with low CG flash rates, *N* for this type of flash was always larger than 1 on average. The proportion of the SP+CG flashes with at least 1 CG flash produced within 1 s was 66.7%, 85.2%, and 85.7%, for the three storm periods, respectively. It was always lower than 40% for the other +CG flashes. Fig. 13 displays the evolution of the cumulative CG flash number for the first sprite production period of the 11 September MCS, between 2000 and 2200 UT. The time is expressed in hours and zero corresponds to 2000 UT. The 12 sprites produced after an SP+CG flash are indicated with circles superimposed on the curve. Multiple CG flashes are well visible under the form of small jumps of the CG flash number and several sprites were produced simultaneously to such jumps. However, not all jumps corresponded with a sprite as for example at 1.135 and 1.425 h. At 1.135 h, the detection system counted 6 different CG flashes within 0.5 s, all −CG flashes and some of them with several strokes. Furthermore, the distance between two consecutive CG flash striking points was lower than 10 km, except for the two last ones with 40 km. For the lightning process at 1.425 h, the number of CG flashes was 5, including 4 +CG and 1 −CG, and the distance between the striking points of two consecutive CG flashes was lower than 30 km. For comparison, at 1.449 h, a lightning sequence associated with a sprite involved 7 CG flashes, 5 +CG with a peak current close to 130 kA for two of them, and 2 −CG. The distances between the striking points of these 7 CG flashes ranged up to 40 km. The presence of several CG flashes during the lightning process associated with the sprite can indicate a long-propagating lightning but we cannot conclude that this feature is necessary for sprite triggering. In some cases of sprites without the presence of multiple CG flashes, VHF detection should be necessary to check this kind of propagation which can be assigned to the negative leader moving towards positive charge within the cloud.

5. Conclusion

Two MCSs in France each with 27 recorded sprite events have been analyzed in terms of cloud structure, precipitation, and lightning activity. The main characteristics of these storms are described with data from the French radar network operated by the French weather service MétéoFrance and from the French CG flash detection network managed by the company Météorage. Both MCSs were of similar size (120,000 km^2), and they produced sprites during distinct periods, one for the storm of 21 July and two for that of 11 September. The sprites were produced when the stratiform area was clearly developed and when the amount of precipitation produced by regions with reflectivity values between 30 and 40 dBZ, was increasing and becoming dominant. A significant decrease of the −CG flash rate preceded the sprite periods, while the +CG flash rate remained constant. So, +CG flashes constituted around 50% of all CG flashes during the sprite periods. All sprites detected were associated with an SP+CG flash, except one which was observed after a −CG flash as detected by the Météorage network. The charge moment change of this −CG flash was estimated at −800 C km, according to ELF radiation detections. The SP+CG flashes had peak currents about two times larger on average than the other +CG flashes, around 60 kA for each period of sprite production. This average is very close to

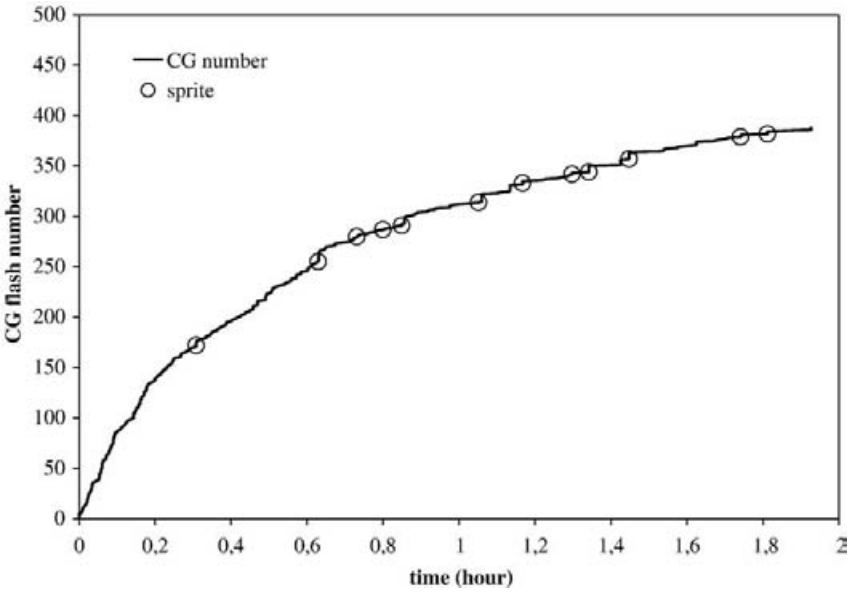

Fig. 13. Evolution of the cumulative CG flash number during the first period of sprite production (2000–2200 UT) for the MCS on 11 September, 2006. The circles indicate the occurrence of the 12 sprites.

several values found in previous studies (Lyons et al., 2006; São Sabbas et al., 2003) but the range of the currents was very large for each period, roughly of one order of magnitude.

The CG lightning activity following the SP+CG flashes has been analyzed and compared with that following other +CG flashes not linked with sprites. It appears the SP+CG flashes were characterized by a shorter average time interval with the following CG flash. The median value of this time interval was less than 0.5 s for the three active periods studied from the two MCSs, which means the SP+CG flash could often be part of a multi-CG flash lightning process.

Acknowledgements

This study was partly supported by the Research Training Network 'Coupling of Atmospheric Layers' (CAL), sponsored by the EU FP5 program under contract n° HPRN-CT-2002-00216. The authors would like to thank Météorage, for providing the data on the CG lightning flashes and Météo-France, the French weather service, for providing the data from the radar network. The authors thank Joszef Bor from the Geodetic and Geophysical Research Institute in Hungary, and Eran Greenberg from Tel-Aviv University, for providing a charge moment change value.

References

Barrington-Leigh, C.P., Inan, U.S., Stanley, M., Cummer, S.A., 1999. Sprites triggered by negative lightning discharges. Geophys. Res. Lett. 26 (24), 3605–3608.

Boccippio, D.J., Williams, E.R., Heckman, S.J., Lyons, W.A., Baker, I.T., Boldi, R., 1995. Sprites, ELF transients, and positive ground strokes. Science 269, 1088.

Carey, L.D., Murphy, M.J., McCormick, T.L., Demetriades, N.W.S., 2005. Lightning location relative to storm structure in a leading-line, trailing-stratiform mesoscale convective system. J. Geophys. Res. 110, D03105. doi:10.1029/2003JD004371.

Cummer, S.A., Lyons, W.A., 2005. Implications of lightning charge moment changes for sprite initiation. J. Geophys. Res. 110, A04304. doi:10.1029/2004JA010812.

Cummins, K.L., Murphy, M.J., Bardo, E.A., Hiscox, W.L., Pyle, R.B., Pifer, A.E., 1998. NLDN'95, a combined TOA/MDF technology upgrade of the US National Lightning Detection Network. J. Geophys. Res. 103, 9,035–9,044.

Cummins, K.L., Cramer, J.A., Biagi, C., Krider, E.P., Jerauld, J., Uman, M.A., Rakov, V.A., 2006. The U.S. National Lightning Detection Network: post-upgrade status, paper presented at 2nd Conf. on Meteorological Applications of Lightning Data, Amer. Meteorol. Soc., Atlanta. paper 6.1.

Ely, B.L., Orville, R.E., Carey, L.D., Hodapp, C.L., 2008. Evolution of the total lightning structure in a leading-line, trailing-stratiform mesoscale convective system over Houston, Texas. J. Geophys. Res. 113, D08114. doi:10.1029/2007JD008445.

Farges, T., Blanc, E., Le Pichon, A., Neubert, T., Allin, T.H., 2005. Identification of infrasound produced by sprites during the Sprite2003 campaign. Geophys. Res. Lett. 32, L01813. doi:10.1029/2004GL021212.

Franz, R.C., Nemzek, R.J., Winckler, J.R., 1990. Television image of a large upward electrical discharge above a thunderstorm system. Science 249, 48–51.

Hayakawa, M., Nakamura, T., Hobara, Y., Williams, E., 2004. Observation of sprites over the Sea of Japan and conditions for lightning-induced sprites in winter. J. Geophys. Res. 109, A01312. doi:10.1029/2003JA009905.

Hu, W., Cummer, S.A., Lyons, W.A., Nelson, T.E., 2002. Lightning charge moment changes for the initiation of sprites. Geophys. Res. Lett. 29 (8), 1279. doi:10.1029/2001GL014593.

Huang, E., Williams, E., Boldi, R., Heckman, S., Lyons, W., Taylor, M., Nelson, T., Wong, C., 1999. Criteria for sprites and elves based on Schumann resonance observations. J. Geophys. Res. 104 (D14), 16,943–16,964.

Lyons, W.A., 1994. Characteristics of luminous structures in the stratosphere above thunderstorms as imaged by low-light video. Geophys. Res. Lett. 21 (10), 875–878.

Lyons, W.A., 1996. Sprite observations above the U.S. High Plains in relation to their parent thunderstorm systems. J. Geophys. Res. 101 (D23), 29641–29652. doi:10.1029/96JD01866.

Lyons, W.A., Armstrong, R.A., Bering III, E.A., Williams, E.R., 2000. The hundred year hunt for the sprite, Eos Trans. AGU 81 (33), 373.

Lyons, W.A., Nelson, T.E., Williams, E.R., Cummer, S.A., Stanley, M.A., 2003. Characteristics of sprite-producing positive cloud-to-ground lightning during the 19 July 2000 STEPS mesoscale convective systems. Mon. Weather Rev. 131, 2417–2427.

Lyons, W.A., Andersen, L.M., Nelson, T.E., Huffines, G.R., 2006. Characteristics of sprite-producing electrical storms in the STEPS 2000 domain. On line summary and CD, 2nd Conf. on Meteorological Applications of Lightning Data. AMS, Atlanta. 19 pp.

Maddox, R.A., 1980. Mesoscale convective complexes. Bull. Am. Meteorol. Soc. 61, 1374–1387. doi:10.1175/1520-0477.

Marshall, J.S., Palmer, W.M., 1948. The distribution of raindrops with size. J. Meteorol. 5, 165–166.

Mazur, V., Shao, X., Krehbiel, P.R., 1998. "Spider" lightning in intracloud and positive cloud-to-ground flashes. J. Geophys. Res. 103 (D16), 19,811–19,822.

Neubert, T., Allin, T.H., Stenbaek-Nielsen, H., Blanc, E., 2001. Sprites Over Europe. Geophys. Res. Lett. 28 (18), 3585–3588.

Neubert, T., Allin, T.H., Blanc, E., Farges, T., Haldoupis, C., Mika, A., Soula, S., Knutsson, L., van der Velde, O., Marshall, R.A., Inan, U.S., Sátori, G., Bór, J., Hughes, A., Collier, A., Laursen, S., Rasmussen, I.L., 2005. Co-ordinated observations of transient luminous events during the EuroSprite2003 campaign. J. Atmos. Sol.–Terr. Phys. 67, 807–820.

Pasko, V.P., Stanley, M.A., Mathews, J.D., Inan, U.S., Wood, T.G., 2002. Electrical discharge from a thundercloud top to the lower ionosphere. Nature 416, 152–154. doi:10.1038/416152a.

Pinto Jr., O., Saba, M.M.F., Pinto, I.R.C.A., Tavares, F.S.S., Naccarato, K.P., Solorzano, N.N., Taylor, M.J., Pautet, P.D., Holzworth, R.H., 2004. Thunderstorm and lightning characteristics associated with sprites in Brazil. Geophys. Res. Lett. 31, L13103. doi:10.1029/2004GL020264.

São Sabbas, F.T., Sentman, D.D., 2003. Dynamical relationship of infrared cloudtop temperatures with occurrence rates of cloud-to-ground lightning and sprites. Geophys. Res. Lett. 30 (5), 1236. doi:10.1029/2002GL015382.

São Sabbas, F.T., Sentman, D.D., Wescott, E.M., Pinto Jr., O., Mendes Jr., O., Taylor, M.J., 2003. Statistical analysis of space–time relationships between sprites and lightning. J. Atmos. Sol.–Terr. Phys. 65 (5), 525–535.

Schuur, T.J., Rutledge, S.A., 2000. Electrification of stratiform regions in mesoscale convective systems. Part II: two-dimensional numerical model simulations of a symmetric MCS. J. Atmos. Sci. 57, 1983–2006.

Stanley, M.A., 2000. Sprites and their parent discharges, Ph.D. dissertation, 163 pp., N. M. Inst. of Mining and Technol., Socorro, N. M.

Williams, E., Downes, E., Boldi, R., Lyons, W., Heckman, S., 2007. Polarity asymmetry of sprite-producing lightning: a paradox? Radio Sci. 42, RS2S17. doi:10.1029/2006RS003488.

Wilson, C.T.R., 1925. The electric field of a thunderstorm and some of its effects. Proc. Royal Soc. London 37, 32D.

Yair, Y., Israelevich, P., Devir, A.D., Moalem, M., Price, C., Joseph, J.H., Levin, Z., Ziv, B., Sternlieb, A., Teller, A., 2004. New observations of sprites from the space shuttle. J. Geophys. Res. 109, D15201. doi:10.1029/2003JD004497.

5 Evolution spatio-temporelle de décharges de grande extension horizontale et associées à des éclairs positifs producteurs de sprite dans le Nord de l'Espagne

5.1 Résumé

Ce chapitre reprend une étude qui a fait l'objet d'un article publié dans la revue Journal of Geophysical Research :

- van der Velde, O. A., J. Montanyà, S. Soula, N. Pineda, and J. Bech (2010), Spatial and temporal evolution of horizontally extensive lightning discharges associated with sprite-producing positive cloud-to-ground flashes in northeastern Spain, *J. Geophys. Res.*, 115, A00E56, doi:10.1029/2009JA014773.

Cet article est une mise à jour de notre analyse initiale d'un "sprite déplacée" dans la même région, qui est résumé dans un chapitre (2.2) d'un synthèse des résultats des campagnes d'EuroSprite:

- Neubert, T., et al. (2008), Recent Results from Studies of Electric Discharges in the Mesosphere, *Surveys in Geophysics*, 29, 2, 71-137, doi: 10.1007/s10712-008-9043-1

L'article plus recent utilise de meilleures données de détection d'éclairs (système LS8000) et un plus grand nombre de sprites: 17. L'article est mis dans ce chapitre après une synthèse qui en fait une présentation en décrivant le contexte de l'article, les données utilisées et la démarche suivie, les études de cas et les particularités des observations utilisées, et en développant une discussion et une conclusion de cette étude.

I- Contexte de l'étude

On sait maintenant qu'une écrasante majorité des sprites observés sont associés à un éclair nuage-sol positif (+CG) tout en se produisant de quelques ms à quelques dizaines de ms après lui. Plusieurs études montrent que les valeurs typiques pour cet intervalle de temps sont autour de 10 ms et que seulement dans une très faible proportion de cas il peut

atteindre ou dépasser 100 ms. Les sprites sont dus à l'existence d'un champ électrique transitoire au-dessus du nuage après un éclair +CG ayant neutralisé une grande quantité de charge, notamment grâce à un courant continu souvent observé dans ce type d'éclair (Rust et al., 1985). D'autre part, la localisation horizontale du sprite au-dessus du système orageux, quand elle est connue, ou la direction du sprite, quand elle seule est disponible, ne coïncident pas toujours avec la position de l'éclair +CG et on parle dans ce cas de sprite déplacé. Un exemple d'étude de nature statistique faite par Sao Sabbas et al. (2003) montrait que pour un tiers des cas de sprites considérés, la distance entre la projection verticale du TLE et la position de l'éclair +CG était supérieure à 50 km.

Ces déplacements horizontaux pourraient être dus à des canaux de longueur et de propagation importantes dans le nuage d'orage, notamment dans la partie stratiforme, d'après certains auteurs comme Lyons (1996) ou Wescott et al. (2001). On sait d'ailleurs que les sprites sont produits le plus souvent au-dessus des zones stratiformes des MCS. Il est donc important de pouvoir caractériser de la façon la plus complète possible l'activité totale du processus de l'éclair qui précède les sprites et notamment les phases leader qui montrent son étendue spatiale et la localisation des zones susceptibles d'avoir été déchargées par le processus de l'éclair. La détection du rayonnement VHF qui est surtout propre au traceur (ou leader en anglais) négatif peut être d'un grand intérêt dans cette problématique. En effet, puisque les éclairs associés aux sprites sont des éclairs nuage-sol positifs, les traceurs négatifs ont un rôle important et indiqueront bien la zone de charge positive déchargée. De plus, même si l'on sait que le processus d'éclair à l'origine des sprites comprend au moins un arc positif, sa caractérisation complète n'est pas connue, et il n'existe pas de seuil de pic de courant, par exemple, à attribuer à cet arc pour expliquer la production d'un sprite. On sait d'autre part que les éclairs nuage-sol positifs peuvent comporter une composante continue importante et donc sa signature électromagnétique est intéressante à analyser dans le cas des éclairs associés aux sprites.

Les cas de sprites observés dans une zone couverte par un système de détection en VHF ne sont pas nombreux et donc peu d'analyses ont pû être faites sur ces cas-là. Nous avons analysé dans cette étude trois cas de sprites, observés dans la région Nord-Est de l'Espagne qui est couverte par un système SAFIR (LS8000) géré par le service météorologique catalan Météocat. Ainsi, nous avons fait une caractérisation multifréquence de la signature du processus d'éclair associé à trois sprites vus depuis Sant Vicenç de Castellet (catalogne) au cours de l'été 2008.

II- et III- Données utilisées et méthodologie

Les observations ont été faites le 6 août 2008 au cours d'un orage qui a produit 17 sprites détectés. Il se trouvait dans le domaine d'un interféromètre VHF exploité par le service météorologique catalan (MeteoCat) dans le Nord-Est de l'Espagne (Montanya et al., 2006). Ce système (XDDE) comporte deux stations SAFIR classiques et deux stations du type LS8000 qui permettent de cartographier en 2D les sources VHF de tous les éclairs avec une résolution temporelle de 100 µs dans un rayon d'environ 250 km. Les sources VHF sont groupées en « burst » dans l'analyse car la précision de localisation ne permet pas

de suivre la propagation exacte d'un traceur. D'autre part une méthode de « lissage » par le calcul d'une position moyenne de plusieurs sources consécutives n'est pas toujours applicable, notamment si plusieurs traceurs sont détectés simultanément.

Les caractéristiques des éclairs nuage-sol (temps, localisation 2D, polarité et pic de courant) sont issues du réseau Linet (Betz et al., 2004) qui a été récemment renforcé dans la région. Les stations de ce réseau détactent le rayonement VLF émis par l'arc en retour de l'éclair nuage sol. Un radar en bande C couvre la région de l'orage considéré. Les images utilisées pour l'étude sont en mode PPI avec une élévation de 0.6° et une fréquence d'une toutes les 6 minutes.

La caméra qui a fourni les images de sprites est une Watec 902H2 Ultimate équipéé d'un objectif 12 mm et d'ouverture f/0.8 avec un champ horizontal de 31°. Le mode de capture des événements par cette caméra utilise le logiciel UFOCapture. Les images utilisées correspondent à des intervalles de temps de 20 ms (PAL standard).

Le premier sprite était enregistré à 2056 TU et les autres événements étaient produits pendant un peu plus d'une heure à une distance comprise entre 95 et 180 km de la caméra. La distance relativement courte de l'orage a pu entrainer une obturation partielle du champ de vision au-dessus de l'orage à cause du développement de l'enclume nuageuse. D'autres événements non détectés ont pu se produire. L'azimuth des éléments des sprites a été déterminé grâce à la position des étoiles visibles dans les images et reporté sur les champs de réflectivité radar grâce à la méthode des grands cercles.

IV- Analyse de l'orage

L'orage scanné par le radar autour de 2000 TU présente une structure multicellulaire orientée nord-ouest/sud-est. Les réflectivités à ce moment-là indiquent de forts taux de pluie (50-60 dBZ). L'évolution de l'orage dans l'heure qui suit montre une baisse de l'intensité de pluie dans la partie nord-ouest et une désorganisation de sa partie sud. La ligne convective laisse place à une succession de cellules convectives séparées par des zones de réflectivité autour de 25 à 30 dBZ. La zone stratiforme se développe tandis que le taux d'éclair baisse et le nombre d'éclairs +CG de forte intensité augmente. Vers 2130 TU le système a développé une structure avec une ligne convective à l'avant et une zone stratiforme à l'arrière sur une distance d'environ 70 km dans la direction du déplacement et sur une distance transversale beaucoup plus importante. Les sprites observés sont produits autour de la période où le système présentait cette structure. La partie convective est alors constituée de plusieurs cœurs qui évoluent séparément et sur des dirée assez proches de l'ordre de 30 minutes. L'évolution et la position de chaque cœur dans le système sont décrites dans cette partie. Les sprites sont produits par des éclairs positifs que l'on peut failement associer à un cœur convectif par sa proximité.

V- Etude de cas

Trois cas de sprites et d'éclairs associés sont considérés dans cette partie. Pour chaque cas, l'activité enregistrée par le système XDDE est analysée temporellement et spatialement. La position des points sources VHF sont superposés aux réflectivités radar et

aux lignes de direction des éléments de sprites vus depuis la caméra. Sur les mêmes graphes sont également reportés les localisations des éclairs identifiés par le système Linet comme des arcs de CG. L'activité d'éclair est également présentée sur des diagrammes temporels en superposant les trois types de détection: VHF (XDDE), VLF/LF (Linet) et MF (AM radio).

Un premier cas de sprite correspond à un double événement constitué de 2 éléments de type carotte séparés temporellement de 400 ms environ. Dans ce premier cas, l'activité VHF n'a pas été très importante. Un éclair positif avec un pic de courant assez élevé (46 kA) et identifié comme « parent » du sprite est localisé à proximité d'un cœur convectif dans la partie la plus au nord du système. Les sources VHF associées ont été localisées entre ce cœur et la ligne de direction du premier élément de sprite qui passe à environ 40 km plus au sud. Le deuxième élément de sprite est détecté après 2 signatures VLF reconnues comme des arcs positifs mais de très faible courant (6 et 7 kA) et quelques sources VHF. Dans ce cas, les émissions VLF pouvaient être dues à des composantes M pendant associées à un courant continu après le premier éclair. La ligne de direction de ce second élément de sprite correspond assez bien aux sources VHF et VLF mais toutefois la distance ne le place pas au-dessus directement. L'ensemble des sources détectées se lacent nettement dans la partie stratiforme du système.

Un deuxième cas de sprite se présente sous la forme d'un élément carotte et d'un élément colonne. Le sprite est détecté avec un délai important de l'ordre de 150 ms après un éclair +CG avec un pic de courant de 31 kA qui se trouve largement décalé par rapport à l'azimuth du sprite principal. Par contre, dans un délai très court un élément de sprite à peine visible est noté dans la direction de cet éclair. Dans la direction du sprite principal, une activité VHF et VLF est bien enregistrée pendant quelques dizièmes de seconde mais essentiellement après le sprite. L'activité d'éclair est globalement étalée et continue autour de l'événement sur une durée supérieure à 2 s. Cette activité débute dans un cœur convectif et se poursuit ensuite dans des zones de plus faible réflectivité qui sont aussi superposées aux lignes d'azimuth des éléments de sprite.

Le troisième cas de sprite a une structure beaucoup plus complexe et une durée plus importante. Un éclair +CG a bien été détecté et a produit un pic de courant de 78 kA estimé avec Linet. Le délai entre +CG et sprite est estimé inférieur à 17 ms. L'éclair +CG a été précédé de sources VHF dans la même zone proche d'un cœur convectif. Pendant la durée totale du sprite (80 ms) un grand nombre de souces VHF sont détectées dans la zone traversée par les directions des azimuths des sprites. Par contre, peu de détections VLF sont enregistrées sur toute cette période. La grande majorité des sources VHF est localisée dans une zone de faible réflectivité radar.

VI- Analyse de séquences d'éclairs associées ou non aux sprites

Dans cette partie les séquences d'éclairs associées aux sprites sont analysées (durée, type, étendue, nombre de sources, etc.) et comparées à des séquences non associées à des sprites.

VII- Conclusion et discussion

Les décharges associées à la présence de sprites produisent en moyenne 7 fois plus de sources VHF détectées par le système interferrométrique XDDE. De même, les séquences de sources VHF détectées ont une durée et une étendue horizontale (dans la direction perpendiculaire à la ligne convective) plus importantes dans les cas associés aux sprites. La taille médiane de l'extension horizontale des séquences de sources VHF associées aux sprites est de 43 km (37 km dans la direction perpendiculaire à la ligne convective). Ces observations sont les premières réalisées en Europe tandis qu'aux Etats-Unis le même type d'observation a été réalisé (Mazur et al., 1998 par exemple).

Le système XDDE ne détecte pas une production continue pendant les phases de l'éclair mais plutôt une production sous la forme de « burst » qui sont bien corrélés aux fortes émissions VLF (sférics). Ce sont notamment les éclairs +CG et en particulier ceux qui sont associés aux sprites observés, qui concentrent un grand nombre de sources VHF. Les processus de décharges pendant la composante continue de ces éclairs peuvent avoir un rôle dans ces émissions VHF. Certains sprites observés avec un délai important (plusieurs dizaines de ms) sont associés à une seconde séquence de sources VHF, ce qui peut aussi s'expliquer par un nouveau +CG non détecté ou une composante M pendant le courant continu de l'éclair. Ces observations sont discutées et mises en comparaison avec les travaux récents du même type.

Le système XDDE ne détecte pas une forte activité intranuage précédant les éclairs +CG associés aux sprites et une fois sur deux il n'en détecte pas du tout. Lorsqu'elle est détectée cette activité est localisée dans la zone convective ou très proche d'elle. Pour beaucoup de cas de sprites, le +CG parent est localisé à l'arrière et tout près d'un cœur convectif alors qu'un deuxième +CG peut être détecté plus loin dans la zone stratiforme tout en étant associé parfois à un second sprite. Le premier +CG peut aussi être détecté assez loin de la zone de l'activité intranuage au cœur de la zone stratiforme. L'activité (VHF + VLF) de la décharge peut se poursuivre plusieurs centaines de ms après le sprite. Pendant cette période, des éclairs –CG peuvent être détectés, ce qui signifie que la disparition de charge positive peut aussi entrainer des décharges négatives suite à une intensification de champ électrique. La même observation a été faite par Soula et al. (2009, 2010).

La production de sprites semble suivre le cycle de formation et développement de cœurs convectifs de façon à ce que la charge positive de la zone stratiforme est liée à l'activité convective. D'une façon générale, les directions des lignes de visée des sprites correspondent bien aux activités intranuageuses détectées.

5.2 Article

Spatial and temporal evolution of horizontally extensive lightning discharges associated with sprite-producing positive cloud-to-ground flashes in northeastern Spain

Oscar A. van der Velde,[1] Joan Montanyà,[1] Serge Soula,[2] Nicolau Pineda,[3] and Joan Bech[3]

Received 30 August 2009; revised 21 April 2010; accepted 26 April 2010; published 28 September 2010

[1] During the evening of 6 August 2008, a small mesoscale convective system (MCS) entered the area of radar and 2-D interferometric lightning detection system coverage in northeastern Spain and produced 17 sprites recorded by a camera at only 95–180 km distance. This study presents an analysis of the in-cloud component of the sprite-associated lightning flashes and those of other flashes. The analysis focuses on the horizontal development of sprite-producing lightning by discussing three examples, divided into the periods before the positive cloud-to-ground flash (+CG), between +CG and the end of the sprite, and the period after the sprite. Location and horizontal size of sprites appear to be well explained by the temporal and spatial development of the lightning path. The majority of sprite-producing discharges started directly at the rear side of developing and mature convective cores within the decaying MCS, either with the +CG or with preceding negative leaders. The +CG started a burst of VHF sources during which the sprite developed. Delayed carrot sprites developed after a secondary, smaller burst and were well collocated with the burst toward the rear of the MCS. The order of development of elements in a grouped sprite followed the direction of lightning propagation during the burst stage. The second part of the analysis concentrates on the metrics of sequences of VHF sources and shows that sprites are indeed produced by the largest, longest lasting discharges with particularly large line-perpendicular dimensions (37 km median compared with 11 km for −CG >25 kA).

Citation: van der Velde, O. A., J. Montanyà, S. Soula, N. Pineda, and J. Bech (2010), Spatial and temporal evolution of horizontally extensive lightning discharges associated with sprite-producing positive cloud-to-ground flashes in northeastern Spain, *J. Geophys. Res.*, *115*, A00E56, doi:10.1029/2009JA014773

1. Introduction

[2] It has been 20 years since peculiar optical flashes in the clear sky above thunderstorms were recorded and confirmed for the first time [*Franz et al.*, 1990]. Sprites, as they were called 5 years after their discovery, occur at altitudes between 40 and 90 km in the mesosphere [*Sentman et al.*, 1995] a few milliseconds to tens of milliseconds after intense positive cloud-to-ground flashes (+CG) [*Boccippio et al.*, 1995; *Lyons et al.*, 2003]. Only very few −CG-triggered sprites have been reported [*Barrington-Leigh et al.*, 1999; *Williams et al.*, 2007]. +CG flashes support continuing currents up to a few kiloamperes (kA) which can last a few hundred milliseconds [e.g., *Rust et al.*, 1985; *Bell et al.*, 1998; *Cummer and Füllekrug*, 2001; *Füllekrug et al.*, 2006; *Campos et al.*, 2009], so that large amounts of charge can be drained from the cloud. In response to the charge removal, a transient electric field develops between the cloud and the ionosphere. *Pasko et al.* [1996] explained that the effect of a sudden removal of positive charge from the thunder cloud is equivalent to inserting negative charge of the same magnitude, so that the resulting quasi-electrostatic field in the mesosphere causes streamers of positive polarity to grow downward and negative streamers to grow upward. Details of sprite development are currently being unraveled by analysis of high-speed camera recordings [e.g., *Cummer et al.*, 2006; *McHarg et al.*, 2007; *Montanyà et al.*, 2010].

[3] So far the only way to approximate the strength of the quasi-electrostatic field has been via remote recordings of extremely low frequency radio (ELF) waves by calculating the impulse charge moment change [e.g., *Huang et al.*, 1999; *Hu et al.*, 2002; *Cummer and Lyons*, 2005; *Greenberg et al.*, 2007, 2009]. For longer lasting discharges, the dielectric relaxation due to conductivity of air significantly counteracts the effects of ongoing charge removal. The total charge moment change values can then become very large, but the corresponding electric fields become just large enough to trigger a long-delayed sprite [*Li et al.*, 2008; *Hu et al.*, 2007]. Most sprites are delayed up to 10–20 ms to their associated

[1] Lightning Research Group, Electrical Engineering Department, Technical University of Catalonia, Terrassa, Spain.
[2] Université de Toulouse, Laboratoire d'Aérologie, CNRS, Observatoire midi Pyrenees, Toulouse, France.
[3] Meteorological Service of Catalonia, Barcelona, Spain.

0148-0227/10/2009JA014773

+CG, with relatively few sprites delayed longer than 40 ms [*São Sabbas et al.*, 2003]. However, *Mika et al.* [2005] found 35% of sprites to be long-delayed (30–280 ms), and there are studies which have found much longer average delays for winter sprites over maritime storms [65–85 ms, *Greenberg et al.*, 2007; 45–90 ms depending on geographic region, *Matsudo et al.*, 2009]. Generally, delays of 200–400 ms can be considered exceptional. The horizontal displacement of the sprite to the triggering +CG can be greater than 50 km, consistent with previous studies by *Lyons* [1996] and *Wescott et al.* [2001]. This horizontal displacement could be partially due to charge removal by horizontally extensive in-cloud lightning channels away from the +CG stroke, which was tentatively confirmed by our initial case study [*Neubert et al.*, 2008, section 2.2] and partially due to other factors determining ionization in the mesosphere. Occasionally, displaced sprites have their lower tendrils apparently aligned with the electrical field lines from the region of charge removal [*Neubert et al.*, 2005]. Also, *Vadislavsky et al.* [2009] described the occurrence of ringlike grouping regularly observed in columniform sprites, and *Stanley* [2000] noted that the elements of grouped sprites appeared to occur at the perimeter of the associated mapped lightning flashes. It has been speculated that radiated electric fields of the in-cloud discharge or electromagnetic interference patterns cause important ionization [*Valdivia et al.*, 1997; *Cho and Rycroft*, 2001] on top of the quasi-electrostatic fields, but also gravity waves [e.g., *Pasko et al.*, 1997; *Sentman et al.*, 2003] or any other preexisting ionization patterns (sometimes visible as structured sprite halos [*Moudry et al.*, 2003]) have been considered to influence the spacing of sprite elements. Furthermore, *Yashunin et al.* [2007] calculated that surges in continuing current in vertical lightning channels enhance the quasi-electrostatic field laterally.

[4] Very low frequency (VLF) radio sferic clusters suggest that strong in-cloud lightning activity is indeed associated with sprites [*Ohkubo et al.*, 2005; *van der Velde et al.*, 2006]. The first direct mapping of in-cloud lightning channels associated with sprite producing CG flashes was provided by *Stanley* [2000] and *Lyons et al.* [2003]. *Marshall et al.* [2007] confirmed VLF sferic clusters to correlate strongly with directly detected in-cloud lightning channels, which were confirmed to be an important component of sprite-producing discharges, but the VLF sferic cluster signature is not unique to sprites.

[5] The type of thunderstorm most commonly associated with sprites is the Mesoscale Convective System (MCS) during the mature to decaying stage [*Lyons*, 1996]. During these stages, a wide area of light to moderate "stratiform" precipitation has developed adjacent to the more intense convective cores, which are often arranged linearly. The stratiform region contains extensive layers of alternating charge polarity at different altitudes [e.g., *MacGorman and Rust*, 1998]. This part of the MCS has lower CG flash rates than the cores, of predominately positive polarity, and produces large horizontal discharges known as spider lightning [e.g., *Mazur et al.*, 1998; *Lang et al.*, 2004], which often are directed from the higher altitudes of convective regions toward lower altitudes in the stratiform region, supposedly following trajectories of ice particles toward the rear of the storm system [*Carey et al.*, 2005; *Ely et al.*, 2008]. These horizontally extensive lightning flashes can have multiple connections to ground of different polarity [*Lang et al.*, 2004]. *Soula et al.* [2009] described sequences of several CGs in particular for sprite-producing flashes in France, and it was suspected they were either connected by long horizontal lightning channels or triggered indirectly by electric field changes, much like independent storm cells can exhibit "communicating" lightning flashes [*Fuir et al.*, 2006, 2009].

[6] *Mazur* [2002] summarized the development and different processes of lightning flashes. It is widely believed that lightning (with the exception of upward discharges from objects connected to the ground) develops as a bidirectional leader [*Kasemir*, 1960] in a region of the cloud where the electric field strength has been observed to surpass the runaway breakdown threshold [*Stolzenburg et al.*, 2007], commonly between two charged areas in the cloud. The negative leader end builds in the direction of positive charge and usually displays a stepped behavior. The positive leader end grows toward negative charge and usually does not step. Recoil streamers, now called recoil leaders [*Mazur*, 2002], are of negative polarity and connect repetitively to the positive leader end, extending the channel retrogressively at speeds of 2×10^4 m s^{-1} [*Proctor et al.*, 1988; *Shao and Krehbiel*, 1996]. The positive leader itself moves commonly at speeds between $0.3–6 \times 10^5$ m s^{-1} (vertically [*Saba et al.*, 2008, *Kong et al.*, 2008]). Negative leaders propagate at similar speeds, on average 2×10^5 m s^{-1} [e.g., *Mazur et al.*, 1998; *Morimoto et al.*, 2005]. Recoil leaders are very fast processes with minimum observed speeds of 4×10^6 m s^{-1} [*Saba et al.*, 2008] to several 10^7 m s^{-1} [e.g., *Richard et al.*, 1986; *Rhodes et al.*, 1994].

[7] In this article, we demonstrate the development of lightning discharges that produced +CG flashes which triggered sprites by means of an interferometer network which provides two-dimensional maps of VHF sources. Additionally, we demonstrate by means of a statistical study the extent to which the sprite-producing flashes are different from other flashes.

2. Data

[8] The storm chosen for this work occurred during the evening of 6 August 2008 and produced 17 sprites when it was within range of the interferometric lightning detection system operated by the Meteorological Service of Catalonia in northeastern Spain [*Montanyà et al.*, 2006]. This system consisted of two SAFIR (Système d'Alerte Foudre par Interférométrie Radioélectrique [*Richard and Lojou*, 1996]) and two upgraded sensors (LS8000), processed by a more recent CP8000 central processor (Vaisala, Inc.). This system computes azimuthal (two-dimensional) directions from each antenna site to sections of a lightning flash by analyzing phase differences between antenna pairs of bursts of very high frequency (VHF) radio pulse trains and provides locations and times of all located radio sources. The time resolution is 10^{-4} second. Triangulation from the four sensor sites (marked in Figure 1) is possible if at least two sensors were able to detect and correlate the radio emissions from the lightning flash. The detection range extends ~250 km from the center of the network, but low altitudes in the storm at shorter distances may be blocked by the local horizon at the sensor locations. The azimuthal precision of the sensors is specified as 0.5° RMS. For this storm, most sources were

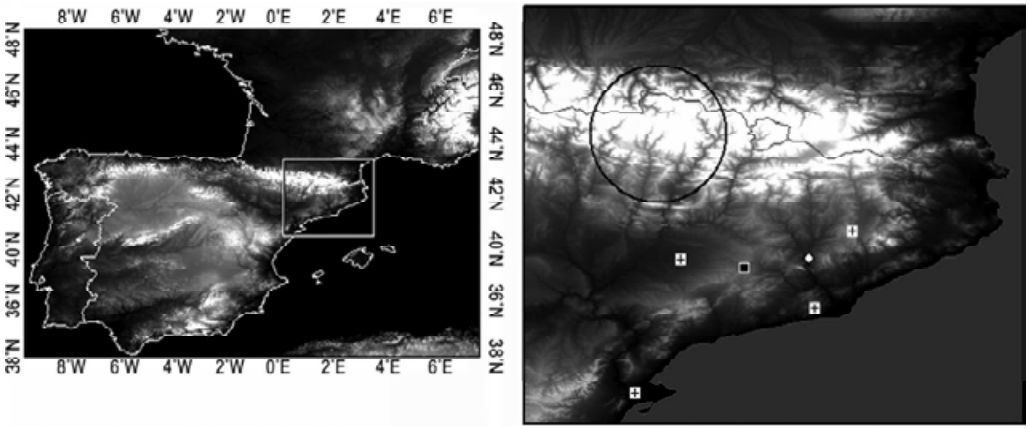

Figure 1. Map of Spain and the region concerned in this study. The radar is plotted as a black square. XDDE (Xarxa de Detecció de Descàrregues Elèctriques) stations as crosses, and the camera as a diamond, with the region of interest in a black circle.

located only by two sensors. For this study, the CG information from the system was not used, only the VHF sources. Since the configuration of the system and the resulting detection efficiency characteristics may be particular to this region, we refer to the data as XDDE (Xarxa de Detecció de Descàrregues Elèctriques), the abbreviation in use by the regional weather service.

[9] CG stroke locations, times, and peak current information were provided by the LINET network (Lightning Network), which utilizes direction finding and time of arrival in very low to low radiofrequency range [*Betz et al.*, 2004] and which has in recent years expanded to southern France and northern Spain. LINET detects a greater number of CGs related to sprite-producing flash sequences than the EUCLID (European Cooperation for Lightning Detection) network for the region surrounding the Pyrenees. In EUCLID, several Vaisala-manufactured national networks are joined, such as Météorage in France, used in *van der Velde et al.* [2006]). It is the European equivalent of the North American Lightning Detection Network (NALDN). An estimate of detection efficiency (DE) for sprite-triggering +CG flashes for nine recent storms in northeastern Spain and southern France including 188 sprites yielded for LINET a DE of 93%, whereas EUCLID obtained a DE of 76%. The peak current values of LINET are usually quite close to those of EUCLID (within 5%–15%).

[10] C-band radar 0.6° Plan Position Indicator (PPI) scans from the radar of Panadella (marked in Figure 1) in central Catalonia, available at 6-minute intervals, were used to describe the structure and development of the thunderstorm system. Radar images were georeferenced, allowing comparisons with lightning locations.

[11] Sprites were observed using a Watec 902H2 Ultimate camera operated in Sant Vicenç de Castellet (41.67°N, 1.86°E, marked in Figure 1) with a manual gain setting and a CBC Computar 12 mm F0.8 lens with a horizontal field of view of 31°. Its interlaced video fields provided a time resolution of 20 ms (PAL standard). The capturing of events was done with UFOCapture software. In the audio track of the video clips, the sferics received by two AM (amplitude modulation) radios, tuned to approximately 150 kHz and 1650 kHz, were recorded. Although this data is unsuitable for quantitative purposes (polarity cannot be retrieved, gain and filtering are unknown), it lends itself well to a qualitative comparison of the lightning detection systems and the sferic bursts, particularly with respect to the continuity and duration of lightning discharge processes. The presented waveform comes from the radio tuned to approximately 1650 kHz (medium wave, MW), with a passband of 4.5 kHz. Noise reduction was applied.

[12] Initially, a target storm was over southwestern France, but the thunderstorm system described in this study traveled between the observer and the French storm. The first sprite was recorded over this storm at 2056 UT in the top left corner of the image, requiring adjustment of the camera's view. The sprites were then successfully followed during more than an hour, with distances from the observing site of only 95–180 kilometers. Owing to the short distance, the semitransparent anvil cloud of the storm interfered with the observations, in particular between 2130 and 2145 UT, and it is possible that sprites occurring over the far end of the storm were invisible. From the stars visible in the images, accurate azimuths and elevations were retrieved by means of star catalog software which allows fitting the stars to a background image of the sprite after rescaling the PAL 720 × 576 pixels images to a 4:3 aspect ratio. The great circle paths from the camera to the sprite elements (the features marked by crosses in Figure 2) have been plotted to a maximum distance corresponding to an altitude of ~85 km. Sprites are commonly reported to initiate between 70 and 85 km altitude [e.g., *Cummer et al.*, 2006; *McHarg et al.*, 2007], which is also roughly the altitude of the visually identifiable transition region between downward streamers and diffuse upper parts [*Pasko et al.*, 1998]. If we take 70 km as the altitude for a reasonable lower bound on the

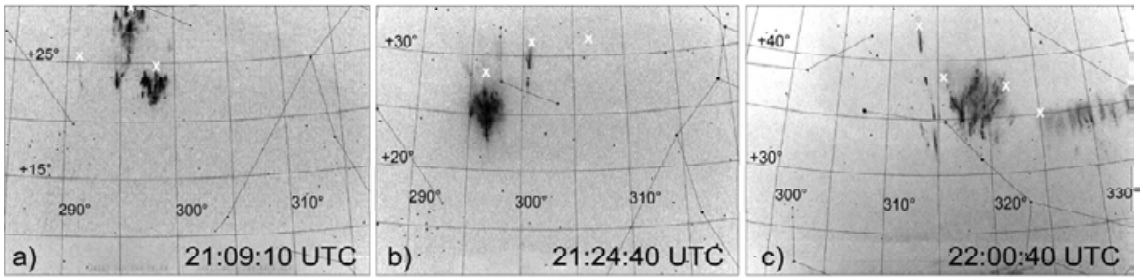

Figure 2. Inverted images of the three example sprite events of 2109:10, 2124:40, and 2200:40 UTC with a grid overlay of azimuth and elevation, based on matching stars in the image and software. The sprite features marked by white crosses are indicated by great circle paths mapped in Figure 3, 4, and 5, respectively. (a) The double carrot sprite event of 2109:10. The lower marked column and carrot, including the column between them, occurred between 101–141 ms, while the carrot near the top edge of the image occurred between 501–541 ms. (b) The carrot sprite event of 2124:40. The two small elements at the right were weakly luminous between 032–178 ms, while the carrot near the top edge of the image occurred after a long delay, between 178–198 ms. (c) The sprite event of 2200:40. The sprite started at the right side of the image in the first frame (40.976–41.016 s), then developed the central part during subsequent frames (40.996–41.036 s), followed by its decay, while the columniform filaments at the left side developed slightly later (41.036–076 s) and decayed very slowly, with upward-moving luminous parts.

distance, the resulting locations would be ~20 km closer to the camera as an indication of the location precision.

3. Methods

[13] The original XDDE source locations per flash can look rather incoherent and often appear in radial patterns caused by random noise and azimuthal digitization. This is worse at larger distances from the baselines between sensors and when the angle of a lightning VHF emission to the baseline between two sensors is small. The system itself provides confidence ellipses on the basis of the azimuthal errors of the sensors. The mean dimension of the longest ellipse axis for 95% probability is 19.5 km with a standard deviation of 13.8 km. For the shortest ellipse dimension, these numbers are 6 km and 2.2 km, respectively. The mean ellipse axis orientation is 127° with a standard deviation of 27°. So, the position error is most severe in a direction along the linear MCS, which is oriented on average along 150°.

[14] While plotting the data, time-coloring the sources allows one to follow the progress of the discharge, even when subsequent sources show erratic behavior in the spatial domain. For the statistical study, a moving average (running mean) with a window of six subsequent sources was performed on latitude and longitude data, which resulted in much more consistent patterns which are less dispersed radially. The window size was essentially an arbitrary choice. Visually, the moving average of six worked best. An assessment of the spatial scatter before and after the moving average procedure has been done on the basis of the source-to-source distance within groups of sources with intersource time interval of <0.2 ms, close to the resolution of the XDDE system. The data show that 95% of raw source-to-source distances are <24 km, whereas the moving average with a window of six results in 95% of source-to-source distances <3.3 km. The resulting cluster size of sources is reduced from 95% <37 km to <15 km. Using a wider window for the moving average does not decrease this further. At the same time, the median speed between sources separated in time by at most 300 ms is 1.1×10^7 m s^{-1} in the raw data, which is reduced to 2.4×10^5 m s^{-1} after the moving average in space and time domains (standard deviation 5×10^4 m s^{-1} to 4×10^6 m s^{-1}), corresponding to common values quoted for negative leaders. The choice of a window of 5 or 7 points leads to ~20% larger or 10% lower source-to-source distances and speeds, respectively, and similar differences in sequence size. Although the propagation speeds are in correspondence with reported values, we must remember that they are not a result of real measured leader propagation or other process velocity, because these cannot be inferred from the data. For this reason, apparent propagation speeds are not considered.

[15] In particular for the statistical part of this study, XDDE data were organized into "sequences" (a proxy for flashes) on the basis of a time criterion that groups original VHF sources if they occur within 300 ms of each other. The threshold is close to the typical criterion for CG lightning detection networks to group strokes belonging to flashes. Video observations of interstroke intervals show that this criterion is very suitable [e.g., *Valine and Krider*, 2002; *Saba et al.*, 2006]. However, this interval is a trade-off between including sources which could belong to the same flash and excluding sources which belong to different flashes. This is mostly (but not exclusively) a problem at high flash rates. A distance criterion was not applied because the individual raw source locations, ordered by time of occurrence, were too noisy. An advanced grouping algorithm would be required to deal with this, which would have made the procedure (and hence the results of the statistical analysis) less transparent and no less dependent on the choice of grouping criteria.

[16] Finally, the word *burst* is used throughout the text. It is loosely defined as a series of VHF sources, usually >10, with typically submillisecond time intervals between sour-

Table 1. Time Evolution of Convective Cores of the MCS After Breakup of the Original Convective Line, and the Sprite Events Which Were Triggered by Lightning Initiating at the Corresponding Cores

Core	Start time	Time of maximum reflectivity	End time	Related Sprites
A	2106	2124	2136	2109, 2112, 2115
B	2054	2112	2142	2056, 2059, 2100, 2110, 2111, 2117
C	2124	2142	2154	2131, 2146
D	2118	2130	2142	2119, 2124
E	2136	2142	2200	2156, 2200, 2203

ces, in contrast with more isolated VHF sources with much longer intervals (tens of milliseconds).

4. Evolution of the Mesoscale Convective System

[17] At 2000 UT, the radar network of the Catalonian weather service scanned a 67-km-long and 14-km-wide northwest-southeast-oriented linear multicell thunderstorm with strong precipitation intensity values (50–60 dBZ radar reflectivity) entering the region. The storm developed in the afternoon over central Spain and moved in a north-northeasterly direction. Surrounding weaker precipitation became visible near the northwestern end of the line. After 2024 UT, the northwestern half of the line started to lose intensity (from >50 dBZ to 35–45 dBZ), followed shortly by a weakening and disorganization of the southern half of the line, especially after 2048 UT. After the convective line broke up and during the expansion of stratiform precipitation, the total flash rates detected by XDDE decreased steadily while the number of +CG flashes with high peak currents increased.

[18] The system assumed a weak (broken) leading line-trailing stratiform structure, which measured a maximum 70 km front to rear ~2130 UT. The convective line became interrupted by areas of reflectivity of 25–35 dBZ after 2100 UT. The first sprite was recorded during this stage at 2056 UT, although earlier sprites may have occurred when the camera was still observing the larger, more distant MCS over southwestern France. The fragmented convective region contained several persistent maxima of higher reflectivity, labeled as core A, B, C, D, and E by order of direction (NW to SE). These cores were actually *not* just remains of the convective line, but were growing and decaying in an independent fashion.

[19] Core A developed in advance of the stratiform precipitation NW of the original line, and reached the strongest reflectivity at 2124 UT. It was near the limit of the radar range. Core B at first sight appeared as a surviving group of cells from the northwestern part of the line, but closer inspection revealed it developed newly ahead of the line, which then decayed behind it. This core was the largest and longest lasting. It started to weaken after 2118 UT while a small new core C grew directly at its east flank, which obtained its strongest reflectivity at 2142 UT and then decreased. Behind core B and C, the widest and most intense stratiform precipitation region (moderate, relatively uniform precipitation) developed. The southeastern half of the original line fragmented at 2118 UT, with core D developing in advance of the further decaying line. Core D still increased in intensity until 2130 UT and was overtaken by a newly developed core E just to its east at 2142 UT. Core E retained reflectivity values over 35 dBZ until 2200 UT. The rest of the line segment to the southeast disappeared in the meantime. The extent of the stratiform precipitation area directly behind cores D and E was not much wider than the original convective line, at least at low altitudes.

[20] These cores appeared to be a starting point of sprite-producing discharges, as the examples in the following section show. Table 1 summarizes the life cycles of the convective cores and the associated sprites, of which the lightning discharge or +CG initiated at the corresponding core. The occurrence of sprites in space and time appeared closely tied to the presence of these cores, and the period before the maximum precipitation intensity of the core at the ground is the prime time for initiating sprite-producing discharges (except for core E). So, the decay of large parts of convective areas with simultaneous expansion of stratiform precipitation area introduces a period of sprites, which were triggered by lightning flashes initiating in or near convective cores in their growing stage.

5. Examples of Lightning Sequences Associated With Sprites

[21] We now discuss three examples of the lightning flashes detected by the XDDE and LINET and differentiate between the period before the +CG return stroke, the period between the +CG and the end of the sprite, and the period after the sprite. The examples show the typical characteristics of the discharges but also the limitations of the present XDDE lightning detection system.

5.1. Example 1: 2109:10 UT

[22] This event was the fourth recorded sprite over this thunderstorm and occurred at 2109:10 UT. It consisted of two carrot sprites (Figure 2a) widely separated in time (101–141 and 501–541 milliseconds). Figures 3 shows the spatial and temporal evolution of the sequence of lightning detections. An initial +CG of 70 kA was detected at 2109:09.907 UT but resulted in only three detected sources and did not (or not immediately) produce the sprite. The +CG that produced the first sprite was detected at 2109:10.111 ms and had a peak current of 46 kA. The location was within 5–10 km of the first +CG. Figure 3 shows the location of sources and the great circle paths to the main sprite elements. The +CG flash producing the sprite occurred at the northern extent of the discharge. At the time of this +CG, a burst of 16 VHF sources was detected, located southwest of the +CG, lasting a few milliseconds. The first sprite was delayed by at most 9 ms. The carrot sprite element did not occur directly over this in-cloud activity but was displaced laterally by at least 19 kilometers from the +CG and by 7 km from the southwestern-most detected in-cloud activity. However, two other simultaneous, smaller elements were even more displaced to the southwest, up to 40 km from the +CG. Lightning activity also occurred directly under the area of the sprites, but this activity was detected *after* the sprite had already decayed, during the period leading to the second sprite 400 ms later.

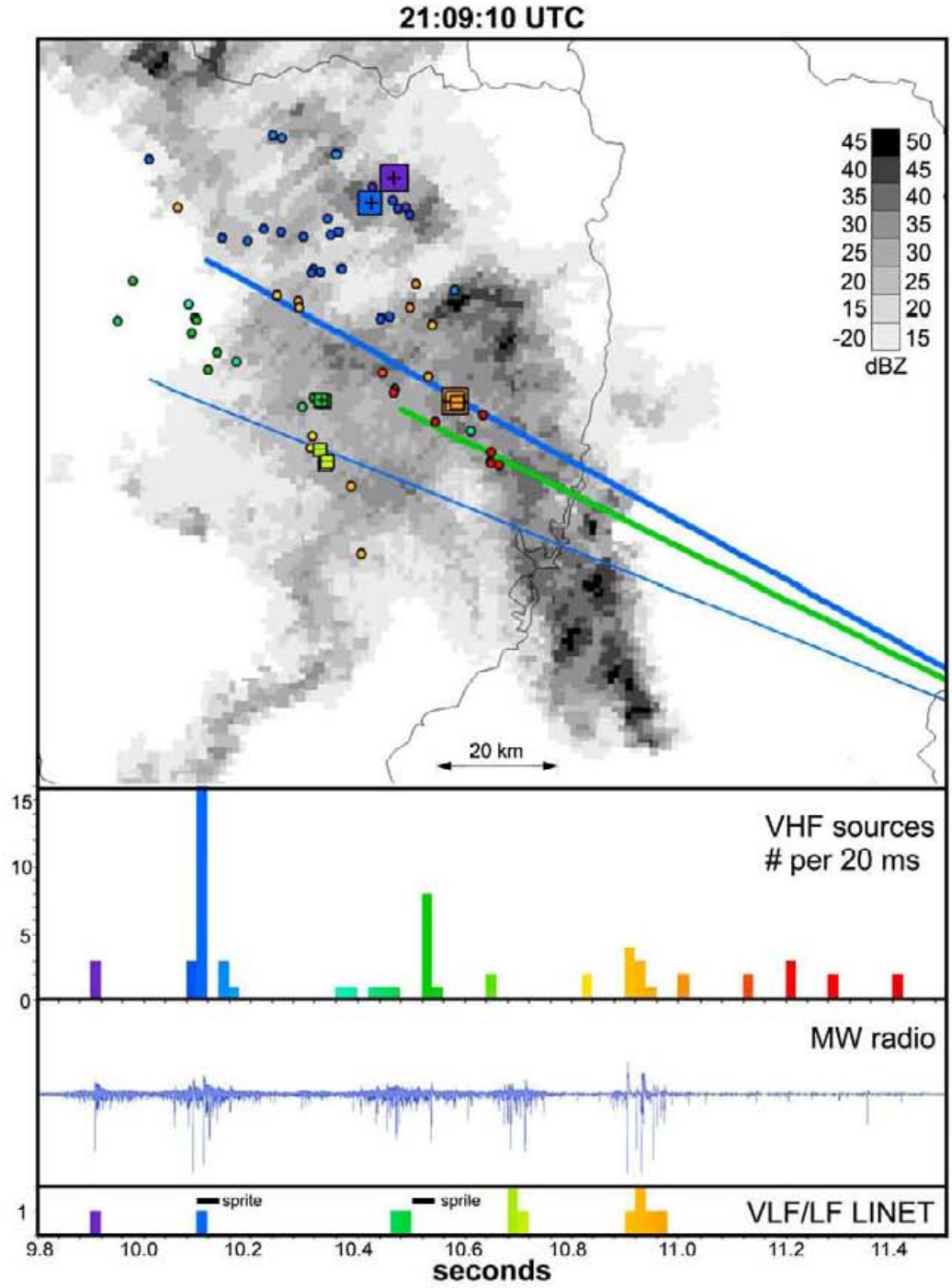

Figure 3. Spatiotemporal representation of detected lightning sources and sprites for the event of 2109:10 UTC. The background is the radar reflectivity image of 2106 UTC. The time evolution of XDDE very high frequency (VHF) sources (circles) and the LINET network (Lightning Network) positive cloud-to-ground flash (+CG) and −CG (+ and − squares) is indicated by symbol color according to the lower images, with a resolution of 20 ms. Square size scales with peak current (see section 5.1 for details). Lines indicate the great circle paths from the camera to the sprite features marked in Figure 2a. The line ends correspond to an assumed sprite feature altitude of 83–87 km. The medium wave radio sferic shows the continuity of the lightning flash as reference. The period covered by this graph spans 1.7 sec with ticks spaced every 40 ms.

[25] Two possible +CGs were detected at 21:09:10.471 and 21:09:10.483 by LINET before the second sprite with peak currents of only 7 and 6 kA with the sprite occurring at a delay of 18–51 ms. However, these weak detections might have been related to M-components (a peak of current superimposed on continuing current as described in +CG flashes, for example, by *Campos et al.* [2009] and *Li et al.* [2008]). So, it is possible that continuing current lasted for more than 400 ms after the first sprite-producing +CG. A second small burst of 9 VHF sources occurred during the progress of the second sprite (at 535 ms, lagging the small +CGs detected by LINET). While the second carrot occurred in the direction of this activity (at a greater elevation in the image), it is impossible that it occurred directly over it because a plausible altitude of the measured sprite initiation point elevation results in a location more to the east. This places the sprite at least 30 km closer to the camera than the VHF sources that occurred around the time of this sprite. After the second sprite, VHF sources occurred scattered over the stratiform area during the following 600 ms. During this period, LINET detected a low peak current −CG with three strokes in the west side of the stratiform region, and a 5-stroke −CG flash at 21:09:10.903–21:09:10.969 with a peak current of −65 kA. The in-cloud detected VHF activity was spatially poorly correlated to these CGs. Finally, the medium wave radio sferic shows that XDDE detections match with several sferic maxima, but reveals also that VHF sources are missing during weaker sferic activity.

[26] Peculiarly, both the first and the second sprite of this event occurred horizontally offset from preceding or simultaneous VHF sources, to the southwest and southeast, respectively. We offer a possible explanation in section 7.

[27] Comparison of the propagation of the lightning sources with the radar image (Figure 3) shows initiation near convective core A at the front side of the system, more to the northwest than the sprites of 2056 and 2059 UT. The sprites occurred over a wide area with more intense moderate (stratiform) reflectivity behind core A and B, and the average path of the flash (not shown) apparently circled the region of weak reflectivity between core A and the second sprite.

[28] In summary, the detected activity can explain the horizontal displacement of the sprite with respect to the triggering +CG, and bursts occur during the sprite appearance and can explain the delay.

5.2. Example 2: 2124:40 UT

[29] The eleventh sprite consisted of a carrot and a long narrow element (Figure 2b), between 21:24:40.178–21:24:40.198 ms. However, at second inspection, one can find a few marginally visible small sprite elements to the right which started at 0.032 and stayed weakly luminous until the carrot sprite appeared. Figure 4 shows the spatial and temporal evolution of the sequence of lightning detections. The +CG that produced the sprite was detected at 21:24:40.020 ms and had a peak current of 31 kA. The carrot sprite was long delayed to this +CG by 158–178 ms. Lightning was detected by the XDDE system 2 sec before the sprite and can be considered as part of the same flash, since the typical intervals between lightning flashes were very long and the radio sferic also shows no interruption longer than 10–20 ms for the entire 2.8 sec displayed in Figure 4. The initial activity was located in a cluster of sources centered on convective core C. At the beginning of the discharge, LINET detected a −15 kA CG (or IC) at 38.695 corresponding well with the location of in-cloud sources. More than 300 ms later, a VHF burst occurred at 39.028–39.033 sec and occurred simultaneously with an optical flash in the video. The burst itself was located 12 km to the west of the initial LINET detection. Some subsequent VHF detections corresponded with weak fluctuations of brightness in the video, after which a second distinct burst at 39.669 sec coincided again with a brighter flash in the video. The detected in-cloud activity then moved to the west, where the sprite-triggering +CG struck in weaker precipitation intensity (the transition region of the MCS). Thirty-four sources followed directly within 10 ms. The activity discharged a region behind convective cell B (in the sense of storm motion), then moving on into the stratiform region toward the rear of the area with reflectivity values >30 dBZ, where six VHF sources were detected during the development of the carrot sprite. From the perspective of the camera and the plausibility of the altitude of the sprite corresponding to that distance, the sprite appears well collocated with the VHF activity. Starting 120 ms after the sprite, LINET also detected five low peak current flashes in the same area of negative polarity over the course of 600 ms. These were marked as "intracloud," at altitudes of 10–15 km (we cannot confirm whether these high values are correct). This activity occurred either as a continuation of the in-cloud leaders or in response to electric field changes resulting from the charge removal that caused the sprite. XDDE also produced a number of sources in this region at that time. Medium wave radio sferics also clearly showed a continuing sferic after the sprite, supporting the continuing leader activity.

5.3. Example 3: 2200:40 UT

[28] The sixteenth sprite occurred at 22:00:40 and consisted of a curtain-like feature at the right side of the image (Figure 2c), visible between 976–1036 ms, followed by a closer appearing, more complex part to the left between 996–1056 ms, slowly decaying. Figure 5 shows the spatial and temporal evolution of the sequence of lightning detections. Note that the graph has been plotted with a fine time resolution 2 ms instead of 20 ms as in the previous two cases. The +CG that produced the sprite was detected at 22:00:40.979 ms and had a peak current of 78 kA (92 kA in EUCLID). The onset of the sprite was delayed by at most 17 ms. VHF sources were first registered by XDDE 62 ms before the +CG (40.916 sec, blue in the color graph), simultaneous with a subtle increase of brightness visible in the video. LINET (but not EUCLID) shows a coincident detection marked as "intracloud" but having a peak current of −19 kA, 2 km south of the later +CG. The radio sferic also shows a marked spike. The initial burst detected by XDDE occurred near core D, well away from the larger region of moderate reflectivity which produced earlier sprites. Note that the northwest-southeast alignment of sources is likely the result of the asymmetric location accuracy as discussed in section 3. The radio sferic actually reveals that a lightning process was going on between the initial detection and the +CG. At the time of the +CG, a

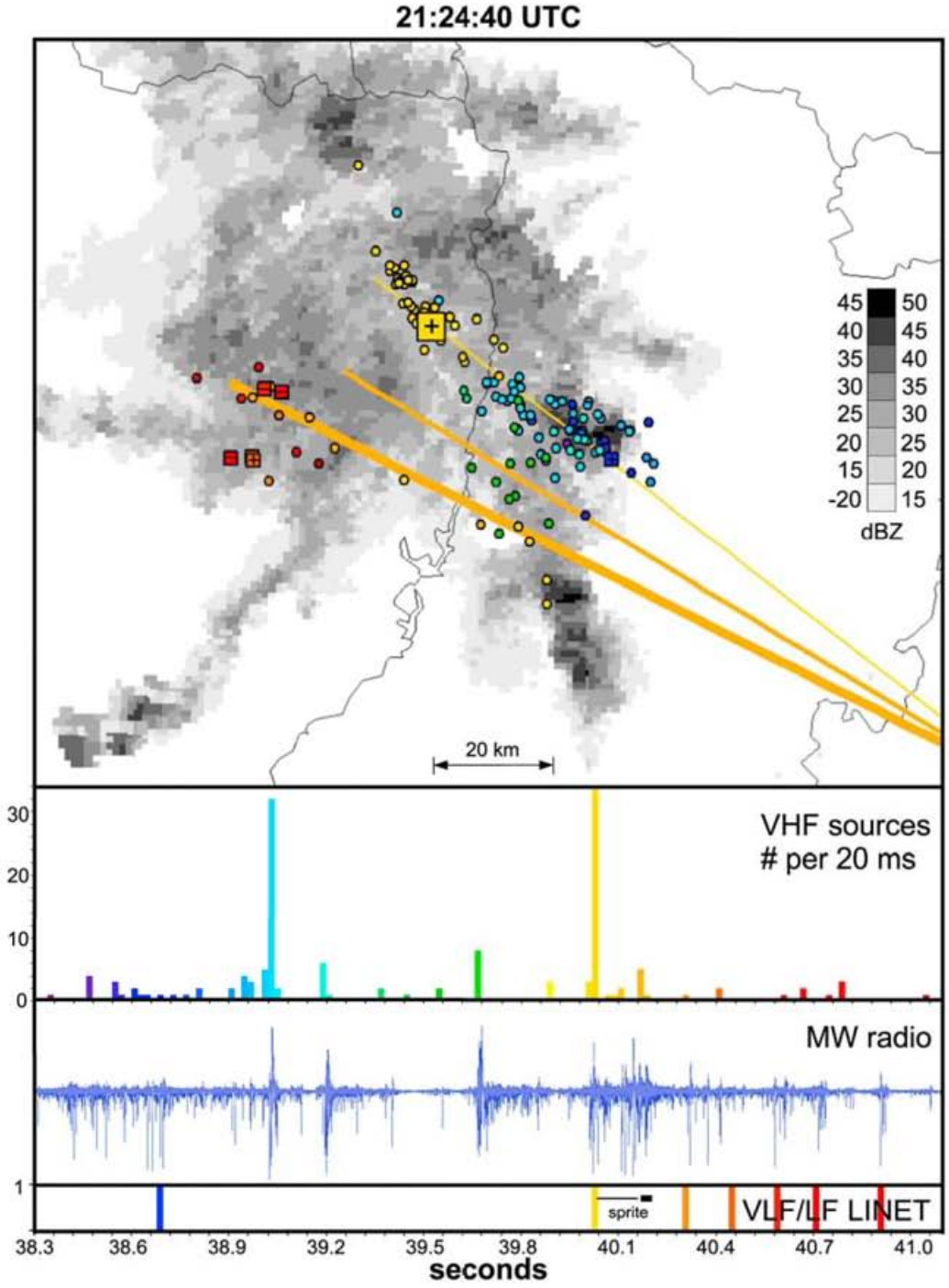

Figure 4. Spatiotemporal representation of detected lightning sources and sprites for the event of 2124:40 UTC. The background is the radar reflectivity image of 2124 UTC. The time evolution of XDDE VHF sources (circles) and LINET +CG and −CG (+ and − squares) is indicated by symbol color according to the lower images, with a resolution of 20 ms. Square size scales with peak current (see section 5.2 for details). Lines indicate the great circle paths from the camera to the sprite features marked in Figure 2b. The line ends correspond to an assumed sprite feature altitude of 83–87 km. The medium wave radio sferic shows the continuity of the lightning flash as a reference. The period covered by this graph spans 2.8 sec with ticks spaced every 60 ms.

burst was detected of 298 VHF sources, lasting until 41.032 sec (52 ms long). This is the largest and most consistent VHF cluster observed, stretching over an area of 27 km, to the southeast and southwest of the +CG. The high number of sources over a large area is likely the result of improved detection efficiency at closer range to the XDDE system (the sprite/lightning event occurred more than 1° longitude to the east of the first events). The VHF burst

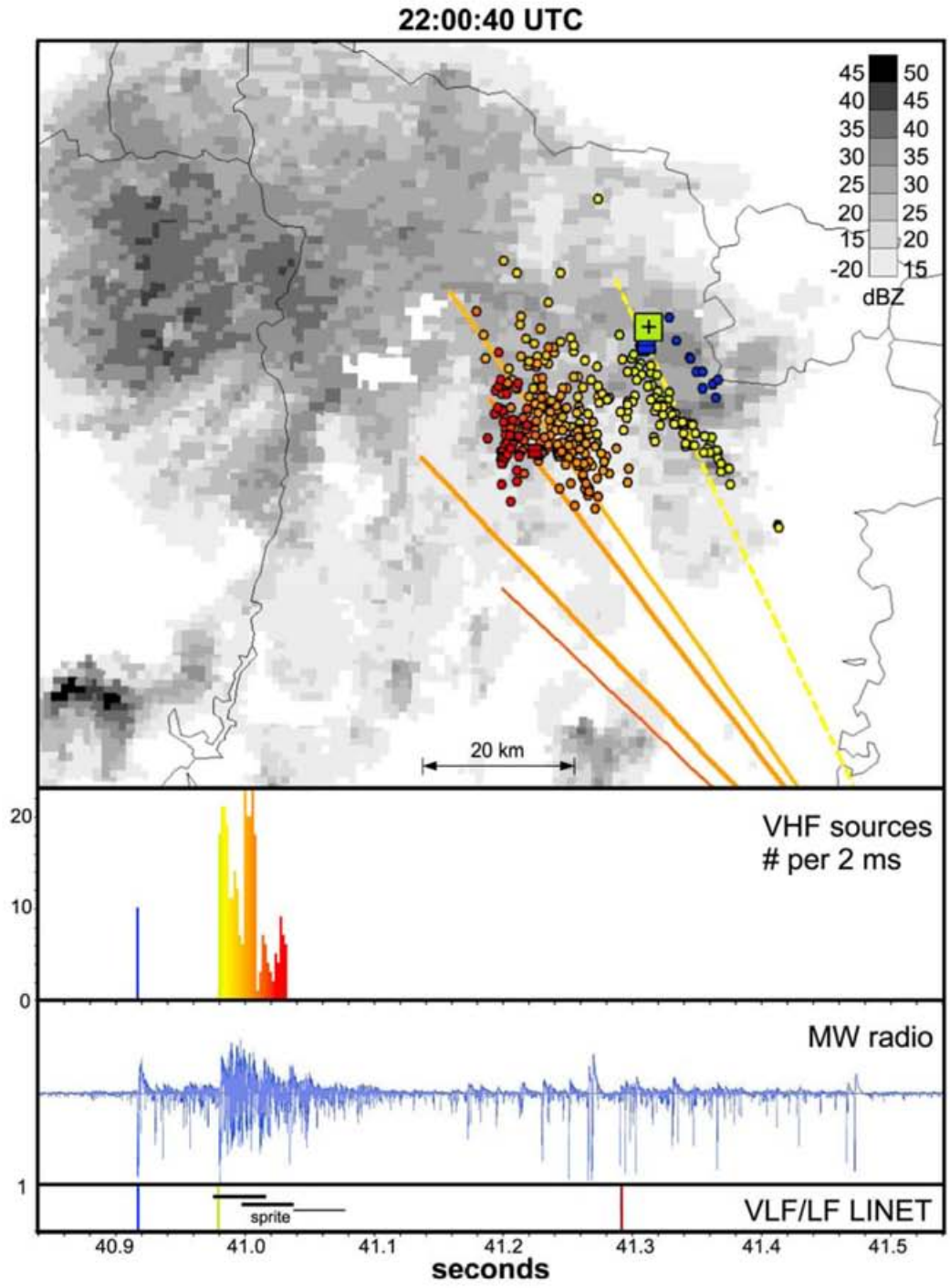

Figure 5. Spatiotemporal representation of detected lightning sources and sprites for the event of 2200:40 UTC. The background is the radar reflectivity image of 2200 UTC. The time evolution of XDDE VHF sources (circles) and LINET +CG and −CG (+ and − squares) are indicated by symbol color according to the lower images, with a resolution of 2 ms. Square size scales with peak current (see section 5.3 for details). Lines indicate the great circle paths from the camera to the sprite features marked in Figure 2c. The line ends correspond to an assumed sprite feature altitude of 83–87 km. The rightmost sprite azimuth has been drawn with a hatched line, since it is possible that more elements occurred outside view. The medium wave radio sferic shows the continuity of the lightning flash as a reference. The period covered by this graph spans 0.7 sec with ticks spaced every 20 ms.

Table 2. Characteristics of XDDE-Detected Sequences During the Period 2030–2230 UTC Grouped by the Peak Current of the Most Intense Stroke as Detected by LINET[a]

		Number of sequences in each category								
		Positive (kA)			Negative (kA)				
Sources	Sprite	0–10	10–25	>25	0–10	10–25	>25	IC	CG
dt = 300 ms									
≤6	2	76	16	16	82	29	4	390	183
>6	15	110	33	18	64	32	10	203	233
>6 (%)	88%	59%	67%	53%	55%	52%	71%	20%	56%
dt = 700 ms:									
≤6	2	88	21	12	41	21	3	522	136
>6	15	133	40	21	22	42	10	270	267
>6 (%)	88%	69%	78%	64%	64%	67%	77%	25%	66%

[a]The sequences in the sprite category are unique (i.e., do not occur in the peak current classes), whereas a sequence producing both positive and negative CG strokes occurs in the category according to the highest positive and negative polarity of these strokes.

fluctuations and their corresponding locations appear to coincide with the development of new sprites progressively to the southwest. It has to be noted that the complex second part of the sprite developed more to the southwest than the simultaneously detected activity, and also the following smaller columniform elements to the left of it. In this respect, there is a resemblance to the example of 21:09:10 UTC.

[29] The distances of the two parts of the sprite are not inconsistent with the corresponding lightning pattern in time. The altitude of the sprite, when considered to occur directly over the detected lightning path, is 72 km for the curtain-like feature at the right side and 76 km for the complex feature at the left side. This appears somewhat low. If we consider 82 km and 86 km instead (10 km higher), the sprite should have occurred between 5 and 10 km farther away than the edge of the detected lightning pattern, which is plausible. If a sprite were to surround the extensive lightning channels, as suggested by the observations of *Stanley* [2000], then closer sprite elements may have occurred as well which would have been out of the view of the camera (too high elevation angle) if they were closer than 60 km from the camera, assuming the lower part of such element reaching 60 km at 45° in the top of the image. This would imply a distance >20 km from the discharge edge nearest to the camera, which is not likely. However, a smaller element at greater altitude may have been missed even if closer to the detected VHF cluster location.

[30] The VHF cluster producing the sprite occurred in weak reflectivity, 20–35 dBZ, and no activity was detected in the region of moderate intensities to the west that produced the lightning activity for most of the earlier sprites, which seems related to the disappearance of the convective cells at the leading edge of the stratiform region. The rightmost extension of the sprite is not known (out of view), but the total visible width, assuming the distance of the sprite to be that of the underlying discharge, was 33 km. The leftmost extension was ~37 km from the center of the detected cluster. The orientation of the complex western part of the sprite is along the vertical, suggesting the triggering discharge must have been directly below the sprite, but it was not detected. Additional clues that detection was incomplete are the short total duration of the flash compared with those of the earlier events, and the much longer lasting sferic activity in the simultaneous long-medium wave radio recording which lasted certainly >500 ms after the triggering +CG. A −6 kA −CG or intracloud flash was detected after the end of the detected in-cloud activity at 41.292 sec near the southwestern tip of the discharge, without any subsequent detections.

6. Characteristics of Lightning Sequences Associated With Sprites Compared With Other Sequences

[31] The example events confirmed that the in-cloud lightning processes associated with sprite-producing +CG flashes are large and long lasting. Another characteristic is the occurrence of large bursts of VHF sources between +CG and sprites. This study would not be complete without answering the question how unique such properties are among other lightning flashes in the storm.

6.1. Procedure

[32] The basic procedure is summarized as follows.

[33] 1. Apply a moving average filter with a window of six to all sources (location).

[34] 2. Group raw data into "sequences" with intersource time interval less than threshold (300 ms).

[35] 3. Remove the first five moving-averaged sources of each sequence.

[36] 4. Calculate geometric properties of the sequences (needs two or more "averaged sources"; in other words, seven or more raw sources, except for the metrics "total number of sources" and "sequence duration").

[37] 5. Associate sequences to detected CG flashes and sprites and divide into categories.

[38] 6. Calculate statistics of geometric properties of sequences for each category.

[39] The moving average processing and their effects (step 1) and grouping XDDE data into "sequences" (step 2) were explained in detail earlier. Step 3 ensures that all moving-averaged sources belong indeed to the same sequence (does not include interpolation in space between separate sequences). The time interval used for the analysis was 2030–2230 UT, excluding the most active period of the storm to reduce the number of undesired combinations of independent flashes into one sequence. Geometric properties were calculated for each sequence, and the XDDE sequences were then associated to the data of LINET and classified by the highest peak current positive and negative CG occurring during a XDDE sequence. So, even if several CGs occurred during a sequence, for example, 51 kA, 23 kA, −7 kA, and −12 kA, the sequence was included in the highest peak current CG categories (e.g. >25 kA and −10 to −25 kA). The same sequence was excluded from the lower peak current CG categories (10–25 kA and 0 to −10 kA in this example). If a sequence contained a sprite, it was not included in any other category. XDDE sequences during which there was no LINET detection were listed as "IC" (intracloud), and the union of all sequences containing CG sequences of any polarity, including those associated with sprites, represents the "CG" category.

Table 3. Number of Sources

	Positive (kA)				Negative (kA)				
	Sprite	0–10	10–25	>25	0–10	10–25	>25	IC	CG
Median	63	8	10	7	7.5	8	13.5	3	8
95% CI Mean	43–128	21–47	23–31	10–25	13–22	20–25	6.1–34	4.2–4.9	14–20
St.Dev	82	29	31	31	24	29	24	5.5	30

[40] Tables 2–7 show a summary of characteristics by sequence category (sprite, +CG of 0–10, 10–25, >25 kA, −CG of 0–10, 10–25, >25 kA, IC, and all CGs: all CGs combined). The absolute values of the metrics in Tables 2–7 depend on the performance of the XDDE system, the distance of the lightning to the sensors, and the selected sequence time criterion (dt), but nevertheless there are significant differences between some of the categories. The choice of moving average window size affects all sequences equally (uniformly) and cannot cause shifts between categories. The time criterion can cause similar shifts as the moving average in our tests, which appear to be rather small, but these shifts may not be uniform across the different categories. Whenever the statistical significance of differences between categories appears to be marginal (<99% or small overlap between confidence intervals), a double check was done with dt = 700 ms.

6.2. Category Population Size

[41] The number of sequences in each category is displayed in Table 2. The top row indicates the number of sequences that had six or fewer sources, which are excluded from the statistics which required the moving average. In particular, the category of −CG sequences with a peak current of 25 kA or higher is small (only 10 sequences) and will probably not yield reliable statistics. The sprite category contains 27 sequences, 15 of them large enough to calculate geometric properties. While this is a small number as well, the statistics show this category to be consistently different from the other classes.

[42] Table 2 also lists the percentage of sequences with more than six sources of the total detected for that category. Here, on average, ~56% of CG sequences without sprites were large enough to be considered for the statistics involving the moving average. For sprites this was 88%, and for intracloud sequences only 20%, which indicates that XDDE typically displays just a few sources for the majority of IC sequences. Note that the cases with a total absence of sources are not displayed.

[43] To get an idea how large the influence is of the chosen sequence criterion (dt) on the number of sequences, the numbers have been calculated both for dt = 300 ms and dt = 700 ms. For most categories, the absolute number of sequences greater than six sources increases by some 15%–20% when increasing dt, with the exception being the category of IC sequences (+16%), of which the sources apparently become part of a sequence containing CG flashes. Listed P values (two-tailed) were obtained using the nonparametric Mann-Whitney (Wilcoxon) statistical significance test, also known as the rank sum test, while 95% confidence intervals for the mean assumed a Student's t-distribution.

6.3. Number of Sources Per Sequence

[44] This simple statistic includes all sequences with one or more sources (Table 3). The median value for all CG-containing sequences (rightmost column) is eight sources. IC sequences are much smaller with a median of three sources and a six times smaller standard deviation. This difference is extremely statistically significant (P = 0). Sequences with sprites contain a remarkably high number of sources (median of 63), even when compared with sequences that contain one or more +CG strokes. The median is about seven times higher than for other +CG categories. This difference is extremely statistically significant (P = 0.0000206). Using an alternative dt of 700 ms, the medians increase by three sources for most CG categories while the standard deviations stay the same.

6.4. Linear Dimensions

[45] We calculated the maxima and minima of moving-averaged source locations for latitude and longitude, marking a bounding box of the sequence. The diagonal of this box (Table 4) is the largest diameter the sequence could have been. Sprite-producing sequences are the largest horizontally extended sequences with medians more than twice the median for all CGs: 43 km versus 17 km. The difference between sprite and +CG 10–25 kA categories is statistically significant (P = 0.00152), but between sprite and +CG >25 kA is not significant (P = 0.148, P = 0.056 for dt = 700 ms). This does not imply that the nonsprite sequences cannot be large. The 95th percentile value for the combined CG category is 68 km, for IC 34 km, and for sprite-associated sequences 86 km. The maximum size is constrained by the size of the stratiform precipitation area. No significant differences are found between the +CG and −CG group and peak currents. Note that this metric is rather sensitive to dt with all values increasing by 2–4 km for dt = 700 ms, the largest difference is the median for +CG 10–25 kA going from 12 to 24 km, and the sprite category median, which increases to 57 km.

Table 4. Diagonal of Bounding Latitude-Longitude Box (km)

	Positive (kA)				Negative (kA)				
	Sprite	0–10	10–25	>25	0–10	10–25	>25	IC	CG
Median	43	18	12	30	19	20	15	9.5	17
95% CI Mean	35–59	19–26	15–32	19–46	22–33	16–31	7.5–32	11–13	21–26
St.Dev	22	18	24	28	22	22	17	10	21

Table 5. Dimension Perpendicular to the Convective Line (km)[a]

	Positive (kA)				Negative (kA)				
	Sprite	0–10	10–25	>25	0–10	10–25	>25	IC	CG
Median	37	8.5	8.1	11	9.4	8.2	11	4.5	7.9
95% CI Mean	26–44	9.0–13	7.1–21	7.2–23	11–16	6.4–19	3.6–21	5.6–7.3	11–14
St.Dev	16	9.4	19	16	13	18	13	6.1	14

[46] Note also the interesting fact that the IC category differs statistically very significantly from sequences associated with low peak current positive and negative CG flashes, as detected by LINET, not only in size but also in number of sources (IC are twice as small).

6.5. Line Perpendicular Dimension

[47] The thunderstorm convective line was oriented approximately along a 150° (or −30°) angle with the meridians. Sprite sequences propagated under a median angle of 65° to the line, compared with 28° for the category of all CGs (data not shown). This was determined from the difference in location of the beginning of a sequence and the averaged (central) location of the sequence. Since virtually all sprite-producing sequences started at the convective line, it is more interesting to compare the size of the sequence in the direction perpendicular to the convective line, best reflecting the convective-to-stratiform distance of propagation. To do this, a simple rotation of the coordinate system was performed after converting latitude and longitude to a kilometer-based grid. The y-axis was taken as the direction perpendicular to the line. Table 5 shows the result ($y_{max} - y_{min}$ per sequence). It is immediately apparent that the sprite category of sequences has indeed the largest dimension perpendicular to the line with a median of 37 km (maximum 56 km). The all-CG category has a median of only 8 km, so the difference is more pronounced than for the box diagonal. While the medians of the >25 kA categories are slightly larger (11 km) than for weaker CG categories, the differences are by far not statistically significant, as is already obvious from the confidence intervals.

6.6. Duration

[48] Table 6 shows the duration computed as the time between the first and the last source of the sequence. Table 7 shows the interquartile range (IQR) of VHF source times per sequence, "IQR-time," as an alternative representation: the time interval in which 50% of the sources of the sequence occurred. Sequences with six or fewer sources are included as well. Keeping in mind the criterion that defines a sequence (300 ms maximum interval) and the imperfect detection efficiency, the sequences in the IC category clearly last the shortest with a median of 84 ms, whereas the sequences of the CG category last almost four times as long with 302 ms and the sequences with sprites last the longest with a median of 539 ms. The longest lasting sprite-associated sequence had a duration of 2.7 sec, and the longest nonsprite CG sequence lasted 1.7 sec (95th percentile of 1.3 sec). IC sequences lasted up to 989 ms (95th percentile of 564 ms).

[49] However, the differences in duration between the sprite category and +CG categories are not significant at the 95% level ($P = 0.19$). For $dt = 700$ ms, median durations increased by a factor of 2 to 3 for all categories, but significance remained low ($P = 0.07$). Apparently, this is due to the large standard deviation within the sprite category, which is twice as large as the value for all CG combined (782 ms versus 386 ms).

[50] Although not immediately obvious from Tables 6 and 7, the difference between positive and negative CG sequences with peak current >10 kA (241 and 450 ms median durations and 61 and 150 ms median IQR-time, respectively, are statistically significant at the 95% level ($P = 0.011$; $P = 0.021$)). At $dt = 700$ ms, the differences become totally insignificant, mainly due to the much larger increase for −CG-containing sequences. The multistroked behavior of −CG flashes appears responsible for the difference at <300 ms time scales [see *Valine and Krider*, 2002].

7. Conclusions and Discussion

[51] This study considered the in-cloud lightning component associated with the lightning flashes of a small leading line trailing stratiform thunderstorm system that produced 17 detected sprites.

7.1. Spatial and Temporal Dimensions of Sprite-Producing Flashes

[52] Sprite-triggering discharges emitted on average (median) seven times more VHF sources, detected by the interferometer system in northeastern Spain, lasted longer, and were horizontally twice as extensive as the average CG sequence, in particular in the direction perpendicular to the linear convective region (four times as extensive). The variation in duration of sequences was rather large and overlapping for most CG categories. Sprite-associated sequences and negative CG sequences tended to have twice as long median durations as sequences with positive CGs (>10 kA). Intracloud sequences were the smallest, on

Table 6. Sequence Duration (ms)[a]

	Positive (kA)				Negative (kA)				
	Sprite	0–10	10–25	>25	0–10	10–25	>25	IC	CG
Median	539	336	238	244	396	414	512	84	302
95% CI Mean	308–1112	277–477	264–503	286–542	383–543	366–588	337–842	126–164	377–450
St.Dev	782	334	398	468	407	385	397	189	386

Table 7. Sequence Duration (IQR of Source Times) (ms)

	Positive (kA)				Negative (kA)				
	Sprite	0–10	10–25	>25	0–10	10–25	>25	IC	CG
Median	215	111	59	79	142	167	159	68	106
95% CI Mean	83–492	136–188	80–196	68–232	151–227	138–241	98–327	87–116	147–192
St.Dev	369	137	162	167	152	243	160	107	171

average about half the size and duration of CG sequences. The median horizontal size of sprite-producing sequences was 43 km, with a median propagation distance of 37 km perpendicular to the convective line, where the discharges usually initiated. Convective-to-stratiform lightning propagation has also been reported with time of arrival lightning mapping systems by *Lang et al.* [2004], *Carey et al.* [2005], and *Ely et al.* [2008]. This appears to be the first time that discharges of this remarkable size are documented in Europe. In the United States, such observations date back to 1956 [*Ligda*, 1956] and have become known as "spider lightning" [*Mazur et al.*, 1998]. Note that the term *spider lightning* is usually applied to large horizontal lightning channels under the base of the cloud which are visible to an observer on the ground. In case of horizontally extensive flashes detected by a mapping system these may also occur inside the cloud, hidden from view. The flashes producing sprites in our storm were of a similar size to those reported by *Lyons et al.* [2003], but half the size of the average horizontally extensive lightning flash in the MCS studied by *Lang et al.* [2004].

7.2. Characteristics of Detection of Sprite-Associated Lightning by the XDDE Interferometer System

[54] Comparison of VHF sources with sferics as in the examples shown reveals that the XDDE system does not detect lightning processes continuously, as a VHF time of arrival lightning mapping array would, but instead shows intermittent VHF pulses. The XDDE bursts tended to be correlated with the stronger sferics instead of the weaker periods of sferics. An important finding is that +CGs, particularly those that trigger sprites, do initiate bursts of many VHF sources, which apparently are associated with the discharging process supplying a continuing current to the grounded channel [*van der Velde et al.*, 2006]. The system is apparently most sensitive to this particular form of lightning process. The bursts are the major contributor to the larger total number of sources for sprite sequences compared with other sequences in the statistical results. The duration of such bursts tended to be short, generally 2–10 ms, but was longer for the sprite-producing flashes that occurred closer to the detection system. Compared with data from a French SAFIR interferometer system analyzed by *van der Velde et al.* [2006], the later-generation (LS8000/CP8000) XDDE interferometer system showed many more VHF sources during the period between the +CG stroke and the sprite, although it is likely that a significant part of the post-+CG activity is still not located by the central processor due to the spatiotemporal complexity of the discharge with many simultaneous processes [*Mazur et al.*, 1997, 1998]. *Mazur et al.* [1997] showed that it is characteristic for an interferometric system such as the XDDE (SAFIR) to miss a large part of the negative leader activity, compared to short baseline time-of-arrival systems, which record leader activity continuously. Positive leaders are even more difficult to detect, also for time-of-arrival systems, because their radio emissions are much weaker [*Shao and Krehbiel*, 1996, p. 26,663; *Shao et al.*, 1999].

[55] In a number of cases, the XDDE system detected a second (sometimes first), usually less intense burst of sources after some delay to the +CG, which corresponded with a long-delayed carrot sprite in space and time. In this study, this was the only demonstrable difference between detected sequences producing carrots (which tend to be delayed longer compared to columns [*van der Velde et al.*, 2006]) and those producing other types of sprites, which were mostly groups of weak but closely spaced "grassy"-looking elements. It is possible that the secondary burst was produced by a missed +CG, or instead by enhanced in-cloud activity leading to an M-component (current maximum) during the continuing current stage of the +CG flash as documented by high-speed video measurements of natural +CG flashes by *Campos et al.* [2009] and by remote ELF/VLF radio measurements of lightning flashes associated with long-delayed sprites by *Li et al.* [2008]. The bursts explain well why a long-delayed sprite occurred, but not all bursts were associated with detected +CG flashes or sprites, an example of which was shown (2124:40 UT event). The possibility exists that secondary bursts after +CGs are a result of a short blackout in the detection of a continuous cluster of VHF sources and that their detection was resumed if the activity continued for long enough (which can be reason in itself to produce a delayed sprite).

7.3. Storm-Relative Location of Leading In-Cloud Activity and +CG Strokes in Sprite-Producing Flashes

[56] The typical sprite-producing lightning discharge as detected by the XDDE system showed relatively little leading (pre-CG) in-cloud activity, in part due to failure to detect leaders. Pre-+CG VHF sources were absent in 8 of the 17 sprite cases and started in or close to the convective region in the remaining 9 sprite cases. In this storm system, +CG discharges that triggered sprites were often (11 of 17 cases) located at the rear side of a convective core, sometimes followed by another +CG striking deeper inside the stratiform precipitation area which may trigger a second sprite. In other cases, leading in-cloud activity started inside the convective region, and the first +CG struck well inside the stratiform region. These occurred mainly between 2117–2146, when the stratiform region was largest and the transition zone of lower reflectivity behind the convection was most pronounced. Our observations are in line with those of *Lang et al.* [2004], who also found comparatively few +CG flashes (9 of 39) which originated inside the stratiform region.

[56] In 9 of the 17 cases, VHF sources continued to be detected after the sprites in the center and southwest (rear) side of the stratiform region for several hundred milliseconds. During this period, detections of low peak current (~6 kA) of predominantly negative polarity were indicated by LINET. In a few cases such as 2109 (example 1), 2111, and 2115, a strong (>60 kA) or long multiple-stroked (10–13 strokes) deep stratiform −CG occurred during the late stages of the sequence. It is possible that these discharges, tapping stratiform negative charge layers, occur in response to enhanced electric fields between cloud and ground after the removal of large amounts of positive charge which caused the sprite. LINET often showed more detections than EUCLID during the part of the sequences after the sprites, and the XDDE showed VHF sources close to these CG. Simultaneous audio records of medium wave radio sferics (in Figures 3–5) also show these CGs (or strong in-cloud lightning) to be part of ongoing sferic activity. *Soula et al.* [2009, 2010], using *Météorage* (EUCLID) lightning detection data, documented similar sequences of −CG and +CG flashes throughout the stratiform region close to the times of sprites.

[57] Not only did sprite-associated VHF sequences start at the convective region, such as those reported by *Lang et al.* [2004], *Carey et al.* [2005], and *Ely et al.* [2008], but we also observed that the temporal and spatial occurrence of sprite-producing discharges followed the cycles of convective cores, generators of charge, in the MCS. The flashes showed a preference for the developing stage of these cores from which they originated (Table 1). It has to be noted that this occurred during the larger-scale decay of sections of the convective region. Additionally, we observed that despite there being a large, moderate reflectivity stratiform precipitation area still present after 2150 UTC, no sprites were triggered over this section after core C disappeared, the last core adjacent to this area. In fact, the sprite-producing discharges of 2156, 2200, and 2203 UTC occurred in a weaker and narrower part of stratiform rain, triggered from core E at the east side of the cell (as in Figure 5). A related observation is that of *Shufer et al.* [2006], who noted that CG lightning flash rates in convective and stratiform regions of an MCS exhibited simultaneous trends, suggesting a close link. A pronounced isolated "sprite +CG producing convective cell" also occurred in the parallel stratiform MCS on 28–29 August 2003 over France during EuroSprite (using MCS morphological definitions of *Parker and Johnson* [2000]). So, it can be concluded that the presence of a convective cell is beneficial for triggering of horizontally extensive sprite-producing lightning flashes.

[58] There could be several reasons for the connection between sprite-producing discharges and active convective cores. First, the discharge needs a strong local electric field for its initiation, which may be most easily attained in a growing or mature convective cell of the storm. Second, the discharge (if not triggered from a ground-based object, e.g., *Rakov and Uman* [2003], chapter 6) most likely develops in a bidirectional way (zero net charge, equipotential channel [*Mazur and Ruhnke*, 1993, 1998]) with a positive leader branch and a negative leader branch, each propagating into pockets of opposite charge in the storm (potential wells, *Coleman et al.* [2003]). This implies that besides the negative leader finding its way into the stratiform positive charge layer, the positive leader needs an equal body of negative charge for the entire flash to expand to large dimensions. This negative charge may be most easily accessed in the convective region itself. Furthermore, charge is consumed in the process, so that rapid regeneration of charge, both positive and negative, is necessary to reproduce large discharges with reasonable frequency. This is most probable in updraft regions, and indeed the observation that sprite-associated sequences occur during the growing and mature stage of convective cells points to this requirement.

[59] Also, the placement of +CG strokes inside or not far from the convective region may be explained by the bidirectional development of lightning discharges in light of what happens when positive and negative charges are not in balance [*Krehbiel et al.*, 2008]. An imbalance may be assumed because the stratiform positive charge reservoir is usually a vertically narrow layer (<1 km) of very large horizontal dimensions, several tens of kilometers wide, containing charge densities about equal to those found in convective cells (e.g., 2–4 nC m^{-3} [*Hunter et al.*, 1992; *Marshall and Rust*, 1993]). On the other hand, charge in the convective cells is typically found over a depth of 1–3 km, but having smaller horizontal dimensions (usually <10 km as can also be assumed to be the case in this storm, based on the area with radar reflectivity >40 dBZ). So, when a large, contiguous negative convective charge region is lacking, an imbalance exists between positive and negative charge for discharges that can tap into both reservoirs. During bidirectional development, the positive leaders can then consume most of the negative charge and subsequently grow to ground in the vicinity of the convective core forming a +CG while the negative leaders encounter a sufficiently high potential gradient in their surroundings to keep expanding deeper into stratiform positive charge. This is analogous to the concept exploited by *Krehbiel et al.* [2008] to explain the escape of lightning discharges from a cloud in the form of CG flashes, bolts from the blue, cloud to air discharges, and even gigantic jets, which is supported by their modeling results.

[60] For the majority of our sprite-associated discharges, VHF activity was detected only in and near the convective region and after a +CG occurred, so negative leaders venturing deep into the stratiform region before the +CG were not detected. As soon as a +CG connection to ground occurs, the conductive ground becomes the supplier of opposite charge, allowing negative leaders to discharge an extensive layer of positive charge more effectively than by virgin bileader breakdown. Examples from the STEPS 2000 campaign, shown by *Lyons et al.* [2006] and *Marshall et al.* [2007], using a time-of-arrival lightning mapping array, which is more sensitive to individual pulses emitted by leaders than the XDDE system, also demonstrated a single uniform expansion of lightning channels after the +CG stroke in a dendritic fashion.

[61] A consequence of the bidirectional nature of propagation could be that when the amount of accessible negative charge is larger, the longer it may take until the +CG occurs (after its consumption), the deeper the initial negative leader branch can enter into the stratiform region, and the more effective charge removal following a +CG could proceed.

starting from a more developed initial set of negative leader branches.

7.4. Positioning and Size of Sprites Relative to the In-Cloud Lightning Component

[62] An important conclusion is that in case of sprites displaced from the +CG by tens of kilometers (including the examples in Figure 3 and 4), the sprite azimuth occurred over VHF sources occurring after the +CG. In other cases, such as the case presented in Figure 5, the horizontal sprite size and direction of development matched well with the size and development of the in-cloud lightning underneath. So, it confirms the location of in-cloud discharge processes as the main factor of sprite positioning, at least the larger structure. The obvious reason is that the branches in the cloud gather charge and supply it as a continuing current to the grounded +CG channel [e.g., *Lyons et al.*, 2003; *van der Velde et al.*, 2006; *Marshall et al.*, 2007], so this must also be the location above which the largest quasi-electrostatic field due to the charge moment change is felt.

[63] Note that for a few of the sprite producing discharges, such as examples 1 and 3, sprites also occurred laterally displaced from the simultaneously detected in-cloud discharge activity. This is most probably the result of the system's failure to detect a part of the lightning discharge. However, *Stanley* [2000] noted that the elements of grouped sprites appeared to occur at the perimeter of the associated mapped lightning flashes, not directly above the largest charge removal. This is a topic that deserves more attention and requires multistation simultaneous observations to pinpoint the sprite element locations, as well as high time resolution to compare to lightning development.

[64] Large stratiform lightning flashes are very complex, and more research is necessary to explain their full behavior with respect to bidirectional development, the role of convective cores in their initiation, positive and negative charge layers and internal irregularities, and different types of associated ground strokes, including those that initiate from tall structures at the ground or from mountains.

[65] **Acknowledgments.** This study was conducted with the support of the Spanish Ministry of Science and Innovation under grant ESP2007-66542-C04-02.

[66] Z. Pu thanks the reviewers for their assistance in evaluating this paper.

References

Barrington-Leigh, C. P., U. S. Inan, M. Stanley, and S. A. Cummer (1999), Sprites triggered by negative lightning discharges, *Geophys. Res. Lett.*, *26*(24), 3605–3608, doi:10.1029/1999GL010692.

Bell, T. F., S. C. Reising, and U. S. Inan (1998), Intense continuing currents following positive cloud-to-ground lightning associated with red sprites, *Geophys. Res. Lett.*, *25*(8), 1285–1288, doi:10.1029/98GL00734.

Betz, H. D., K. Schmidt, P. Oettinger, and M. Wirz (2004), Lightning detection with 3-D discrimination of intracloud and cloud-to-ground discharges, *Geophys. Res. Lett.*, *31*, L11108, doi:10.1029/2004GL019821.

Boccippio, D. J., E. R. Williams, S. J. Heckman, W. A. Lyons, I. T. Baker, and R. Boldi (1995), Sprites, ELF transients, and positive ground strokes, *Science*, *269*, 1088–1091.

Campos, L. Z. S., M. M. F. Saba, O. Pinto Jr., and M. G. Ballarotti (2009), Waveshapes of continuing currents and properties of M-components in natural positive cloud to ground lightning, *Atmos. Res.*, *91*, 415–424, doi:10.1016/j.atmosres.2008.02.020.

Carey, L. D., M. J. Murphy, T. L. McCormick, and N. W. S. Demetriades (2005), Lightning location relative to storm structure in a leading-line trailing-stratiform mesoscale convective system, *J. Geophys. Res.*, *110*, D03105, doi:10.1029/2003JD003941.

Cho, M., and M. J. Rycroft (2001), Non-uniform ionisation of the upper atmosphere due to the electromagnetic pulse from a horizontal lightning discharge, *J. Atmos. Solar Terr. Phys.*, *63*, 559–580.

Coleman, L. M., T. C. Marshall, M. Stolzenburg, T. Hamlin, P. R. Krehbiel, W. Rison, and R. J. Thomas (2003), Effects of charge and electrostatic potential on lightning propagation, *J. Geophys. Res.*, *108*(D9), 4298, doi:10.1029/2002JD002718.

Cummer, S., and M. Füllekrug (2001), Unusually intense continuing current in lightning produces delayed mesospheric breakdown, *Geophys. Res. Lett.*, *28*(3), 495–498, doi:10.1029/2000GL012214.

Cummer, S. A., and W. A. Lyons (2005), Implications of lightning charge moment changes for sprite initiation, *J. Geophys. Res.*, *110*, A04304, doi:10.1029/2004JA010812.

Cummer, S. A., N. Jaugey, J. Li, W. A. Lyons, T. E. Nelson, and E. A. Gerken (2006), Submillisecond imaging of sprite development and structure, *Geophys. Res. Lett.*, *33*, L04104, doi:10.1029/2005GL024969.

Ely, B. J., R. E. Orville, L. D. Carey, and C. J. Hodapp (2008), Evolution of the total lightning structure in a leading-line, trailing-stratiform mesoscale convective system over Houston, Texas, *J. Geophys. Res.*, *113*, D08124, doi:10.1029/2007JD008445.

Füllekrug, M., M. Ignaccolo, and A. Kavshinov (2006), Stratospheric Joule heating by lightning continuing current inferred from radio remote sensing, *Radio Sci.*, *41*, RS2S19, doi:10.1029/2006RS003472.

Fuquay, R. C., R. J. Nemzek, and J. R. Winckler (1980), Television image of a large upward electrical discharge above a thunderstorm system, *Science*, *249*, 48–51.

Greenberg, E., C. Price, Y. Yair, M. Granot, J. Bor, and G. Satori (2007), ELF transients associated with sprites and elves in eastern Mediterranean winter thunderstorms, *J. Atmos. Solar Terr. Phys.*, *69*(13), 1569–1586.

Greenberg, E., C. Price, Y. Yair, O. Chanrion, and T. Neubert (2009), ELF/VLF signatures of sprite-producing lightning discharges observed during the 2005 EuroSprite campaign, *J. Atmos. Solar-Terr. Phys.*, *71*(12), 1254–1266, doi:10.1016/j.jastp.2009.05.005.

Hu, W., S. Cummer, W. A. Lyons, and T. Nelson (2002), Lightning charge moment changes for the initiation of sprites, *Geophys. Res. Lett.*, *29*(8), 1279, doi:10.1029/2001GL014593.

Hu, W., S. A. Cummer, and W. A. Lyons (2007), Testing sprite initiation theory using lightning measurements and modeled electromagnetic fields, *J. Geophys. Res.*, *112*, D13115, doi:10.1029/2006JD007939.

Huang, E., E. Williams, R. Boldi, S. Heckman, W. Lyons, M. Taylor, T. Nelson, and C. Wong (1999), Criteria for sprites and elves based on Schumann resonance observations, *J. Geophys. Res.*, *104*(D14), 16,943–16,964, doi:10.1029/1999JD900139.

Hunter, S. M., T. J. Schaar, T. C. Marshall, and W. D. Rust, (1992) Electric and kinematic structure of the Oklahoma mesoscale convective systems of 7 June 1989, *Mon. Weather Rev.*, *120*, 2226–2239.

Kasemir, H. (1960), A contribution to the electrostatic theory of a lightning discharge, *J. Geophys. Res.*, *65*(7), 1873–1878, doi:10.1029/JZ065i007p01873.

Kong, X., X. Qie, and Y. Zhao (2008), Characteristics of downward leader in a positive cloud-to-ground lightning flash observed by high-speed video camera and electric field changes, *Geophys. Res. Lett.*, *35*, L05816, doi:10.1029/2007GL032764.

Krehbiel, P. R., J. A. Riousset, V. P. Pasko, R. J. Thomas, W. Rison, M. A. Stanley, and H. E. Edens (2008), Upward electrical discharges from thunderstorms, *Nat. Geosci.*, *1*(4), 233–237, doi:10.1038/ngeo162.

Lang, T. J., S. A. Rutledge, and K. C. Wiens (2004), Origins of positive cloud-to-ground lightning flashes in the stratiform region of a mesoscale convective system, *Geophys. Res. Lett.*, *31*, L10105, doi:10.1029/2004GL019823.

Li, J., S. A. Cummer, W. A. Lyons, and T. E. Nelson (2008), Coordinated analysis of delayed sprites with high-speed images and remote electromagnetic fields, *J. Geophys. Res.*, *113*, D20268, doi:10.1029/2008JD010008.

Lugeon, M. G. H., (1956), The radar observations of lightning, *J. Atmos. Terr. Phys.*, *9*, 329–346, doi:10.1016/0021-9169(56)90052-0.

Lyons, W. A. (1996), Sprite observations above the U.S. High Plains in relation to their parent thunderstorm systems, *J. Geophys. Res.*, *101*(D23), 29,641–29,652, doi:10.1029/96JD00866.

Lyons, W. A., T. E. Nelson, E. R. Williams, S. A. Cummer, and M. A. Stanley (2003), Characteristics of sprite-producing positive cloud-to-ground lightning during the 19 July 2000 STEPS mesoscale convective systems, *Mon. Weather Rev.*, *131*(10), 2417–2427.

Lyons, W. A., L. M. Andersen, T. E. Nelson, and G. R. Huffines (2006), Characteristics of sprite-producing electrical storms in the STEPS 2000

domain. Online summary and CD, 2nd Conf. on Meteorological Applications of Lightning Data, American Meteorological Society, Atlanta, GA, USA, 19 pp.

MacGorman, D. R., and W. D. Rust (1998), *The Electrical Nature of Storms*, pp. 258–286, Oxford University Press, New York.

Marshall, R. A., U. S. Inan, and W. A. Lyons (2007), Very low frequency sferic bursts, sprites, and their association with lightning activity, *J. Geophys. Res.*, *112*, D22105, doi:10.1029/2007JD008857.

Marshall, T. C., and W. D. Rust (1993), Two types of vertical electrical structures in stratiform precipitation regions of mesoscale convective systems, *Bull. Am. Meteorol. Soc.*, *74*, 2159–2170.

Matsudo, Y., T. Suzuki, K. Michimoto, K. Myokei, and M. Hayakawa (2009), Comparison of time delays of sprites induced by winter lightning flashes in the Japan Sea with those in the Pacific Ocean, *J. Atmos. Sol. Terr. Phys.*, *71*, 101–111, doi:10.1016/j.jastp.2008.09.040.

Mazur, V. (2002), Physical processes during development of lightning flashes, *Comptes Rendus Phys.*, *3*, 1393–1409.

Mazur, V., and L. Ruhnke (1993), Common physical processes in natural and artificially triggered lightning, *J. Geophys. Res.*, *98*(D7), 12,913–12,930, doi:10.1029/93JD00626.

Mazur, V., and L. Ruhnke (1998), Model of electric charges in thunderstorms and associated lightning, *J. Geophys. Res.*, *103*(D18), 23,299–23,308, doi:10.1029/98JD02120.

Mazur, V., E. Williams, R. Boldi, L. Maier, and D. E. Proctor (1997), Initial comparison of lightning mapping with operational time-of-arrival and interferometric systems, *J. Geophys. Res.*, *102*(D10), 11,071–11,086, doi:10.1029/97JD00174.

Mazur, V., X. Shao, and P. R. Krehbiel (1998), "Spider" lightning in intracloud and positive cloud-to-ground flashes, *J. Geophys. Res.*, *103*(D14), 19,811–19,822, doi:10.1029/98JD02003.

McHarg, M. G., H. C. Stenbaek-Nielsen, and T. Kammae (2007), Observations of streamer formation in sprites, *Geophys. Res. Lett.*, *34*, L06804, doi:10.1029/2006GL027854.

Mika, Á., C. Haldoupis, R. A. Marshall, T. Neubert, and U. S. Inan (2005), Subionospheric VLF signatures and their association with sprites observed during EuroSprite-2003, *J. Atmos. Sol. Terr. Phys.*, *67*, 1580–1597, doi:10.1016/j.jastp.2005.08.011.

Montanyà, J., N. Pineda, V. March, A. Illa, D. Romero, and G. Solà (2006), Experimental evaluation of the Catalan Lightning Detection Network, paper presented at *19th International Lightning Detection Conference*, Tucson, AZ, USA.

Montanyà, J., O. van der Velde, D. Romero, V. March, G. Solà, N. Pineda, M. Arrayas, J. L. Trueba, V. Reglero, and S. Soula (2010), High-speed intensified video recordings of sprites and elves over the western Mediterranean Sea during winter thunderstorms, *J. Geophys. Res.*, *115*, A00E18, doi:10.1029/2009JA014508.

Morimoto, T., Z. Kawasaki, and T. Ushio (2005), Lightning observations and consideration of positive charge distribution inside thunderclouds using VHF broadband digital interferometry, *Atmos. Res.*, *76*, 445–454, doi:10.1016/j.atmosres.2004.11.024.

Moudry, D. R., H. C. Stenbaek-Nielsen, D. D. Sentman, and E. M. Wescott (2003), Imaging of elves, halos and sprite initiation at 1 ms time resolution, *J. Atmos. Sol. Terr. Phys.*, *65*, 509–518, doi:10.1016/S1364-6826(02)00323-1.

Neubert, T., et al. (2005), Co-ordinated observations of transient luminous events during the EuroSprite2003 campaign, *J. Atm. Sol.-Terr. Phys.*, *67*, 807–820, doi:10.1016/j.jastp.2005.02.004.

Neubert, T., et al. (2008), Recent results from studies of electric discharges in the mesosphere, *Surv. Geophys.*, *29*, 71–137, doi:10.1007/s10712-008-9043-1.

Ohkubo, A., H. Fukunishi, Y. Takahashi, and T. Adachi (2005), VLF/ELF sferic evidence for in-cloud discharge activity producing sprites, *Geophys. Res. Lett.*, *32*, L04812, doi:10.1029/2004GL022043.

Parker, M. D., and R. H. Johnson (2000), Organizational modes of midlatitude mesoscale convective systems, *Mon. Weather Rev.*, *128*, 3413–3436.

Pasko, V. P., U. S. Inan, and T. F. Bell (1996), Sprites as luminous columns of ionization produced by quasi-electrostatic thundercloud fields, *Geophys. Res. Lett.*, *23*(6), 649–652, doi:10.1029/96GL00475.

Pasko, V. P., U. S. Inan, and T. F. Bell (1997), Sprites as evidence of vertical gravity wave structures above mesoscale thunderstorms, *Geophys. Res. Lett.*, *24*(14), 1735–1738, doi:10.1029/97GL01687.

Pasko, V. P., U. S. Inan, and T. F. Bell (1998), Spatial structure of sprites, *Geophys. Res. Lett.*, *25*(12), 2123–2126, doi:10.1029/98GL01242.

Proctor, D., R. Uytenbogaardt, and B. Meredith (1988), VHF radio pictures of lightning flashes to ground, *J. Geophys. Res.*, *93*(D10), 12,683–12,727, doi:10.1029/JD093iD10p12683.

Rakov, V. A., and M. A. Uman (2003), *Lightning: Physics and Effects*, Cambridge Univ. Press, New York.

Rhodes, C., X. Shao, P. Krehbiel, R. Thomas, and C. Hayenga (1994), Observations of lightning phenomena using radio interferometry, *J. Geophys. Res.*, *99*(D6), 13,059–13,082, doi:10.1029/94JD00518.

Richard, P., and J. Y. Lojou (1996), Assessment of application of storm cell electrical activity monitoring to intense precipitation forecast, paper presented at 10th International Conference on Atmospheric Electricity, June 10–14, Osaka, Japan, pp. 284–287.

Richard, P., A. Delannoy, G. Labaune, and P. Laroche (1986), Results of spatial and temporal characterization of the VHF-UHF radiation of lightning, *J. Geophys. Res.*, *91*, 1248–1260, doi:10.1029/JD091iD01p01248.

Rust, W. D., D. R. MacGorman, and W. L. Taylor (1985), Photographic verification of continuing current in positive cloud-to-ground flashes, *J. Geophys. Res.*, *90*, 6144–6146, doi:10.1029/JD090iD04p06144.

Saba, M. M. F., M. G. Ballarotti, and O. Pinto Jr. (2006), Negative cloud-to-ground lightning properties from high-speed video observations, *J. Geophys. Res.*, *111*, D03101, doi:10.1029/2005JD006415.

Saba, M. M. F., K. L. Cummins, T. A. Warner, E. P. Krider, L. Z. S. Campos, M. G. Ballarotti, O. Pinto Jr., and S. A. Fleenor (2008), Positive leader characteristics from high-speed video observations, *Geophys. Res. Lett.*, *35*, L07802, doi:10.1029/2007GL033000.

São Sabbas, F. T., D. D. Sentman, E. M. Wescott, O. Pinto Jr., O. Mendes Jr., and M. J. Taylor (2003), Statistical analysis of space–time relationships between sprites and lightning, *J. Atmos. Sol.-Terr. Phys.*, *65*(5), 525–535.

Sentman, D. D., E. M. Wescott, D. L. Osborne, D. L. Hampton, and M. J. Heavner (1995), Preliminary results from the Sprites94 aircraft campaign: 1. Red sprites, *Geophys. Res. Lett.*, *22*(10), 1205–1208, doi:10.1029/95GL00583.

Sentman, D. D., E. M. Wescott, R. H. Picard, J. R. Winick, H. C. Stenbaek-Nielsen, E. M. Dewan, D. R. Moudry, and J. Merrill (2003), Simultaneous observations of mesospheric gravity waves and sprites generated by a midwestern thunderstorm, *J. Atmos. Solar-Terr. Phys.*, *65*(5), 537–550, doi:10.1016/S1364-6826(02)00328-0.

Shaffer, M. A., D. R. MacGorman, and S. B. Carr (2000), Cloud-to-ground lightning throughout the lifetime of a severe storm system in Oklahoma, *Mon. Weather Rev.*, *128*, 1798–1816, doi:10.1175/1520-0493(2000)128<1798:CTGLTT>2.0.CO;2.

Shao, X., and P. Krehbiel (1996), The spatial and temporal development of intracloud lightning, *J. Geophys. Res.*, *101*(D21), 26,641–26,668, doi:10.1029/96JD01803.

Shao, X., C. Rhodes, and D. Holden (1999), RF radiation observations of positive cloud-to-ground flashes, *J. Geophys. Res.*, *104*(D8), 9601–9608, doi:10.1029/1999JD900056.

Soula, S., O. van der Velde, J. Montanyà, T. Neubert, O. Chanrion, and M. Ganot (2009), Analysis of thunderstorm and lightning activity associated with sprites observed during the EuroSprite campaigns: Two case studies, *Atmos. Res.*, *91*(2–4), 514–528, doi:10.1016/j.atmosres.2008.06.017.

Soula, S., O. van der Velde, J. Palmieri, J. Montanyà, O. Chanrion, T. Neubert, F. Gingneron, Y. Meyerfeld, F. Lefeuvre, and G. Loiatier (2010), Characteristics and conditions of production of transient luminous events observed over a maritime storm, *J. Geophys. Res.*, *115*, D16118, doi:10.1029/2009JD012600.

Stanley, M. A. (2000), Sprites and their parent discharges, Ph.D. dissertation, 163 pp., New Mexico Institute of Mining and Technology, Socorro, NM, USA.

Stolzenburg, M., T. C. Marshall, W. D. Rust, E. Bruning, D. R. MacGorman, and T. Hamlin (2007), Electric field values observed near lightning flash initiations, *Geophys. Res. Lett.*, *34*, L04804, doi:10.1029/2006GL028777.

Vadislavsky, E., Y. Yair, C. Erlick, C. Price, E. Greenberg, R. Yaniv, B. Ziv, N. Reicher, and A. Devir (2009), Indication for circular organization of column sprite elements associated with Eastern Mediterranean winter thunderstorms, *J. Atmos. Solar-Terr. Phys.*, *71*, 1835–1839, doi:10.1016/j.jastp.2009.07.001.

Valdivia, J. G., Milikh, and K. Papadopoulos (1997), Red sprites: Lightning as a fractal antenna, *Geophys. Res. Lett.*, *24*(24), 3169–3172, doi:10.1029/97GL03188.

Valine, W. C., and E. P. Krider (2002), Statistics and characteristics of cloud-to-ground lightning with multiple ground contacts, *J. Geophys. Res.*, *107*(D20), 4441, doi:10.1029/2001JD001506.

Van der Velde, O. A., A. Mika, S. Soula, C. Haldoupis, T. Neubert, and U. S. Inan (2006), Observations of the relationship between sprite morphology and in-cloud lightning processes, *J. Geophys. Res.*, *111*, D15203, doi:10.1029/2005JD006879.

Wescott, E. M., H. C. Stenbaek-Nielsen, D. D. Sentman, M. J. Heavner, D. R. Moudry, and F. T. S. Sabbas (2001), Triangulation of sprites, associated halos and their possible relation to causative lightning and micrometeors, *J. Geophys. Res.*, *106*(A6), 10,467–10,478, doi:10.1029/2000JA000082.

Williams, E., E. Downes, R. Boldi, W. Lyons, and S. Heckman (2007), Polarity asymmetry of sprite-producing lightning: A paradox?, *Radio Sci.*, *42*, RS2S17, doi:10.1029/2006RS003488.

Yair, Y., R. Aviv, G. Ravid, R. Yaniv, B. Zis, and C. Price (2006), Evidence for synchronicity of lightning activity in networks of spatially remote thunderstorms, *J. Atmos. Sol. Terr. Phys.*, *68*, 1407–1415.

Yair, Y., R. Aviv, and G. Ravid (2009), Clustering and synchronization of lightning flashes in adjacent thunderstorm cells from lightning location networks data, *J. Geophys. Res.*, *114*, D09210, doi:10.1029/2008JD010738.

Yashunin, S. A., E. A. Mareev, and V. A. Rakov (2007), Are lightning M components capable of initiating sprites and sprite halos?, *J. Geophys. Res.*, *112*, D10109, doi:10.1029/2006JD007651.

J. Bech and N. Pineda, Meteorological Service of Catalonia, Barcelona 08029, Spain.

J. Montanyà and O. A. van der Velde, Lightning Research Group, Electrical Engineering Department, Technical University of Catalonia (Colom 1, Terrassa, Barcelona 08222, Spain. (oscar.van.der.velde@upc.edu)

S. Soula, Université de Toulouse, Laboratoire d'Aérologie, CNRS, OMP 14 ave. Edouard Belin, 31400 Toulouse, France

6 Etudes statistiques des relations entre sprites et leur morphologie, éclair et précipitation

6.1 Résumé

Ce chapitre reprend une étude qui a fait l'objet d'un article soumis dans la revue Journal of Geophysical Research:

- Van der Velde, O. A., S. Soula, and T. Neubert (2008), Statistical Studies of the Relations of Sprites and their Morphology to Lightning and Precipitation

L'article inclus dans cette thèse a été améliorée sur la base des commentaires des examinateurs. Par ailleurs, une partie de ce travail a fait l'objet d'une communication lors de la Conférence Internationale d'Electricité Atmosphérique (ICAE 2007) et la Conférence Europeenne d'Orages Violents (ECSS 2007):

- O. van der Velde, S. Soula, T. Neubert, Analysis of thunderstorm systems and lightning activity associated with sprites observed during the Eurosprite campaigns: 1- Statistical studies, International Conference of Atmospheric Electricity, Pékin, Chine, August 13th-17th, 2007.

- O. van der Velde, S. Soula, T. Neubert, Statistical Studies of the relationship between Sprites, Lightning and Thunderstorm Precipitation during the EUROSPRITE campaigns. 4th European Conference on Severe Storms, Trieste, Italy, 10-14 September 2007.

L'article est inséré dans le chapitre après une synthèse qui en fait une présentation en décrivant la démarche de l'article, et en résumant chaque partie de l'article.

I- Contexte de l'étude

Dans de nombreuses études, les sprites ont été classés par type en fonction de leur morphologie et éventuellement associés à d'autres observations pour en étudier les relations possibles. Les chapitres précédents contiennent des descriptions sur cet aspect du contexte général de la recherche sur les sprites. Ces classements ou ces études de relation ne faisaient intervenir aucun aspect quantitatif sur la taille, le développement, les éléments le cas échéant, les proportions entre diverses parties des sprites. De même, les

caractéristiques microphysiques ou les taux de précipitation des zones génératrices des sprites dans les systèmes orageux concernés, n'ont pas été décrits de façon exhaustive. Pour finir, l'activité d'éclair nuage-sol associée à la production de sprites n'a pas non plus été analysée en détail afin d'être comparée à celle qui n'est pas accompagnée de sprites pour les mêmes systèmes orageux. Ainsi dans cette étude, nous abordons d'une part un aspect quantitatif des relations entre différents paramètres caractéristiques de la morphologie des sprites (taille, extensions horizontale et verticale, proportion des différentes parties, nombre d'éléments…) et certains paramètres décrivant l'activité d'éclair associée à la production des sprites. D'autre part nous développons une étude des conditions de précipitation (taux, homogénéité…) dans les régions où sont localisés les éclairs nuage-sol qui précèdent les sprites. Différentes catégories d'éclairs nuage-sol sont considérées dans cette étude statistique, puisque nous distinguons les éclairs non associés aux sprites, ceux qui les génèrent, ceux qui leur sont associés sans en être les générateurs mais qui appartiennent à des séries d'éclairs qui peuvent avoir un lien entre eux. Le support à cette étude reste les événements enregistrés lors de campagnes EuroSprite en France au cours des étés 2003, 2005 et 2006 pour un nombre de jours d'observations de 7.

Les données utilisées pour cette étude proviennent de plusieurs caméras vidéo à haute sensibilité pour l'observation des sprites et de deux réseaux de mesure pour la description de l'activité orageuse. Tous ces systèmes ont été décrits dans les chapitres précédents. Les deux caméras qui ont fourni des images de sprites ont été décrites dans les chapitres 2.6.1, 3 et 4. Les deux réseaux de mesure évoqués sont le réseau Météorage pour les données d'activité d'éclair nuage-sol et du réseau français Aramis de radars météorologiques pour les données sur la structure des systèmes précipitants qui produisent les sprites. Ils ont été decrits également dans le chapitre 3 et de façon plus exhaustive dans le chapitre 2.6.

II- Statistiques sur les relations entre activité d'éclairs et précipitation

L'article est structuré en deux parties pour la présentation de la méthodologie et des résultats. Ainsi, cette partie présente l'analyse de relations entre les éclairs nuage-sol, leurs caractéristiques et leur type selon une classification proposée d'une part, et les caractéristiques des précipitations dans le milieu nuageux où ils sont produits d'autre part.

Les caractéristiques des précipitations sont essentiellement le taux calculé à partir de la réflectivité radar fourni par les radars météorologiques qui font des explorations à altitude constante. Cette réflectivité est représentative des précipitations dans la mesure où elles constituent les réflecteurs du faisceau radar dans le milieu nuageux et elle est mesurée avec une résolution spatiale de 1×1 km^2 et une résolution temporelle de 5 minutes. Cette réflectivité est fournie en dBZ qui est un logarithme de la réflectivité en unité physique (mm^6 m^{-3}) et la restitution de cette nouvelle réflectivité – qui est proportionnelle au diamètre élevé à la puissance 6 et à la concentration en gouttes – est liée au taux de pluie par une relation dite Z-R où R est le taux de pluie en mm h^{-1}. La relation Z-R utilisée est celle de Marshall et Palmer bien connue des hydrologues radar et qui représente assez

bien la relation pour des précipitations pas trop convectives comme c'est le cas dans les zones où sont produits les sprites. Pour analyser les zones concernées, nous avons calculé le taux de pluie moyen dans des cercles autour des localisations 2D d'éclairs nuage-sol, de rayons 5 et 10 km, respectivement. Ainsi la comparaison de ces réflectivités permet de quantifier l'homogénéité de ces zones en terme de précipitation.

Pour les éclairs, nous avons classé les arcs (strokes en anglais) en 4 classes avec des symboles associés. Ainsi nous avons les arcs qui apparaissent avant les périodes de production de sprites positifs et négatifs (P+ et P-), les arcs produits pendant les périodes de sprites mais pas reliés à ces sprites, c'est-à-dire se produisant en dehors de la seconde environ autour du sprite (+ et -), les arcs positifs générateurs des sprites (ST+) et le cas échéant les arcs subséquents au ST+ (S+ et S-) mais qui peuvent être relativement éloignés en distance (quelques dizaines de km) pouvant faire penser à un éclair différent au sens habituel des groupements faits par les systèmes de détection du type NLDN ou Météorage pour nous en France. D'autres catégories sont également considérées lorsque plusieurs arcs sont détectés dans un temps très court mais à des distances supérieures à 5 km, constituant ainsi des séquences d'éclairs avec pour les premiers S1+ et 1+ s'ils sont associés à un sprite ou pas, respectivement, avec pour les suivants S2+ et 2+. Il faut bien sûr garder en mémoire tout au long de l'étude que l'efficacité de détection d'éclairs n'est pas de 100% et de même la caméra ne voit probablement pas tous les sprites pour diverses raisons dont l'une est le seuil de déclenchement nécessaire pour l'enregistrement des films vidéo.

Une première analyse a été consacrée à la distribution des arcs en considérant leur pic de courant en fonction du taux de pluie moyenné dans un cercle de 5 km autour de la localisation de l'impact. La distribution est faite pour les arcs positifs et pour les arcs négatifs. Les arcs positifs de type ST+ sont distingués dans cette distribution. Ainsi, on voit que les forts pics de courant sont essentiellement produits dans les zones de faible taux de pluie et cette tendance est beaucoup plus nette pour les positifs. Tous les ST+, même si leur pic de courant n'est pas très élevé, sont issus de zone à faible taux de pluie. Un autre aspect a été de montrer la distribution de les mêmes pics de courant d'arcs positifs et négatifs en fonction de la différence entre les taux de pluie moyens dans deux cercles de rayon 5 et 10 km autour de la localisation de l'arc. Dans ce cas on voit que les forts pics de courant sont uniquement associés aux zones de pluie uniforme donc stratiformes. Cette observation s'applique aux deux polarités d'éclairs. La forme de la distribution montre bien que la grande majorité des éclairs privilégient les zones de fortes différences de taux de pluie entre les 2 cercles et donc à proximité des cœurs de précipitation (zones convectives).

Les éclairs ont ensuite été séparés suivant les catégories définies précédemment et leurs distributions en fonction des valeurs de pics de courant et des taux de pluie ont été analysées au moyen de graphes présentant les distributions par percentile (25%, 50% et 75%). Ces graphes permettent de comparer les différentes catégories d'éclairs et d'analyser quantitativement les caractéristiques de chaque catégorie d'éclair. Les résultats sont aussi présentés par événement orageux plutôt que globalement. En effet, les systèmes orageux de type MCS peuvent être de plusieurs types selon la configuration de la partie stratiforme par rapport au déplacement du système et il est important d'étudier les propriétés

séparément. Il ressort de ces études que les pics de courant des éclairs positifs déclenchant (ST+) sont nettement plus élevés en moyenne que tous les autres éclairs tout en ayant une variabilité très grande. Cette distinction est plus importante dans les cas de MCS de type à zone stratiforme parallèle. Pour les distributions des éclairs en fonction du taux de pluie local dans un rayon de 10 km, la plupart des cas donnent des taux plus faibles aux éclairs de type S+, c'est-à-dire les positifs associés aux sprites. Les éclairs de la catégorie + se distribuent dans une gamme de taux de pluie plus importante. Plusieurs observations conduisent à montrer des localisations privilégiées pour chaque catégorie d'éclairs. L'aspect uniformité du taux de pluie de la zone de l'éclair a été considéré également. Le paramètre utilisé est la gamme de valeurs de l'interquartile (25%-75%) qui est appelé IQR dans le texte et qui peut représenter un certain aspect d'uniformité de la pluie. La principale observation est que les éclairs associés aux sprites sont dans des zones de précipitation plus uniforme que les autres éclairs. Dans le cas de séquences d'éclairs (plusieurs arcs séparés spatialement), les premiers éclairs ont tendance à se produire dans les zones moins uniformes que les suivants, d'où une "propagation" de la partie convective vers la partie stratiforme. Les résultats de ces distributions par rapport l'IQR sont également présentés de façon globale par un graphe 2D avec des isolignes différenciées pour plusieurs catégories d'éclairs. Ce mode de représentation permet de quantifier les valeurs d'IQR et de montrer dans quelles gammes de valeurs les concentrations d'éclairs sont plus importantes. On y voit que les éclairs –CG sont dans les gammes d'IQR plus larges et des valeurs de réflectivité plus grandes également avec des valeurs préférentielles autour de 35-47 dBZ pour les 25èmes % et 75èmes %, respectivement. Ce sont les catégories S+ qui sont les plus proches de l'uniformité absolue (même réflectivité moyenne dans les cercles de 5 et 10 km). D'autres caractéristiques peuvent être tirées de ce dernier graphe.

III- Statistiques sur les relations entre morphologie des sprites et activité d'éclairs/précipitation

Dans ce volet de l'étude, nous abordons l'aspect de la morphologie des sprites en considérant plusieurs paramètres ce cette morphologie. Ces paramètres sont tous quantitatifs et caractérisent le développement vertical et/ou horizontal, des rapports entre différentes parties du sprite, le nombre d'éléments distincts, l'altitude approximative. Les corrélations entre certains de ces paramètres sont d'une part analysées, et celles avec des paramètres relatifs à la précipitation dans la zone du sprite et les caractéristiques de l'éclair à l'origine du sprite (pic de courant, décalage temporel) sont également envisagées. Il faut noter l'existence d'une certaine incertitude sur les dimensions du sprite car la distance d'observation n'est pas connue exactement. Aucun des sprites considérés n'a pu être triangulé car toujours vu avec une seule caméra. Certains aspects de la morphologie comme le nombre d'éléments ou la limite des parties streamers et corps du sprite sont sujets à appréciation donc quelque peu sujectifs. Toutefois, les tendances ne seront

considérées que si elles apparaissent très nettement. D'autre part le nombre d'événements est suffisamment important pour que la statistique soit révélatrice de certaines tendances.

Parmi les tendances qui ressortent de cette étude, on peut citer une tendance à l'augmentation pour la longueur des streamers ascendants en fonction du délai entre le ST+ et le sprite et donc d'une façon générale un développement de la partie supérieure plus important si le délai est long. On peut voir une très nette relation entre le nombre d'éléments et le délai avec des délais toujours très courts pour les sprites avec un nombre important d'éléments et un nombre d'éléments très fable pour les sprites avec un délai très long. Les sprites avec un rapport vertical de taille élevé sont produits par des ST+ de faible pic de courant et les forts pics de courant sont toujours associés à des sprites avec un faible rapport vertical de la taille. Les sprites avec un nombre important d'éléments sont situés dans des zones de précipitation très stratiforme alors que les zones peu uniforme en précipitation sont associées à des sprites avec des faibles nombres d'éléments. D'autres tendances ou particularités semblent se dessiner entre différentes caractéristiques de la morphologie des sprites, dont certaines sont interdépendantes. Ainsi, l'altitude du sommet du corps du sprite semble augmenter lorsque le rapport vertical de taille augmente ou encore le nombre d'éléments semble augmenter avec l'altitude du sommet du corps du sprite. De même, le nombre d'éléments semble diminuer lorsque la largeur du corps du sprite augmente. Enfin, l'altitude du sommet du corps du sprite semble augmenter avec le délai entre le ST+ et le sprite.

IV Discussion

Les observations étant nombreuses, dont certaines se recoupant, et le nombre de paramètres considérés particulièrement élevé, il est nécessaire de faire une synthèse pour faire ressortir les faits marquants et pour les relier à des explications physiques par rapport à la décharge que constitue le sprite et les mécanismes qui en sont à l'origine. La discussion résume donc les observations en essayant déjà de trouver des liens entre elles. Quelques statistiques sur les taux de production de sprites par les +CG sont données. On remarquera que ces taux dépendent des cas de MCS en étant liés à la taille respective de la partie convective. La gamme de pic de courant des ST+ est telle que ce paramètre ne peut constituer un critère de production de sprites et est sans doute peu corrélé à la variation du moment de charge. Les éclairs qui produisent des sprites sont en général localisés dans les régions stratiformes et de plutôt faible réflectivité, et souvent associés à d'autres éclairs dans une même séquence. Les premiers éclairs de ces séquences sont plus souvent proches de parties convectives (ou anciennement convectives) que les éclairs subséquents de ces séquences. Cette apparente propagation confirme des observations par d'autres auteurs qui expliquent la correspondance de ces trajectoires avec celles de chutes de particules de neige vers la zone stratiforme près du niveau de congélation dans le nuage. La présence de charge positive dans ces zones stratiformes peut s'expliquer aussi par celle de cœurs convectifs en phase de disparition, une discussion sur ce point est développée.

Pour la partie d'analyse sur la morphologie des sprites, on y retrouve un trait déjà décrit dans le chapitre 3 et confirmé ici avec un grand nombre de cas, c'est l'augmentation du nombre d'éléments d'un sprite avec la diminution du délai entre sprite et ST+. Pour des délais on a tendance à avoir des sprites avec peu d'élément mais pouvant être de grande taille. Les ST+ de fort pic de courant ont tendance à être associés à des délais courts et des sprites avec des filaments inférieurs plus développés que les supérieurs. Dans le même sens, les sprites avec un faible délai ont des corps plus petits. On peut trouver des liens entre les deux parties de l'analyse, par exemple plus la précipitation est uniforme plus les pics de courant sont élevés et plus les sprites qui en sont issus auront tendance à être multi-élément. Ainsi, lorsque le délai est court après le ST+, il semble que les conditions de déclenchement sont atteintes en plusieurs points et a propagation du sprite se fait essentiellement vers le bas. Lorsque le délai est plus long, la décharge du nuage est plus progressive sous forme de composante continue et le seuil de déclenchement est atteint préférentiellement en un point d'où le déclenchement préférentiel du sprite en un point. Cet aspect de la discussion est aussi développé de façon exhaustive dans l'article.

6.2 Article

Statistical Studies of the Relations of Sprites and their Morphology to Lightning and Precipitation

Oscar van der Velde[1], *Serge Soula*[1], *Torsten Neubert*[2]

[1]Laboratoire d'Aérologie, Observatoire Midi-Pyrénées, Université de Toulouse, Toulouse, France (oscarvdvelde@yahoo.com, sous@aero.obs-mip.fr)

[2]Danish National Space Center, Copenhagen, Denmark (neubert@space.dtu.dk)

Abstract

During the *EuroSprite* campaigns of 2003-2006 in France, 145 sprites obtained in seven nights occurred in an area covered by radar and cloud-to-ground (CG) lightning detection networks, providing sufficient basis for two statistical analyses: 1) Positioning of sprite-triggering and other lightning flashes relative to precipitation characteristics in mesoscale convective systems (MCS), and 2) Relations between sprite morphological features and their causative lightning. Radar reflectivity distributions were automatically analyzed within 10 km around every CG flash, and features of sprites such as dimensions and number of elements were measured.

The results show that sprite-triggering positive CG (ST+) flashes occur in a more limited range of stratiform precipitation than other +CG flashes, but the range of overlap is significant. The ST+ itself tends to occur in less uniform (more convective) precipitation than accompanying +CG flashes. Sequences of +CG are identified spanning tens of kilometers and lasting usually less than a second. First +CGs in such sequences statistically occur near more intense, less homogeneous precipitation than subsequent +CGs, suggesting propagation into the stratiform area. On average 33% of such sequences produced sprites, against 9% of all +CGs during sprite-producing periods.

The results of the sprite morphology study (of 91 sprites) show that clustered sprites are short-delayed and generally have shorter upper branches, thin bodies and a higher peak current +CG in very stratiform precipitation, while more singular sprites see a much wider range of delays and +CG precipitation conditions, and tend to have longer upward streamers (often carrot type).

1. Introduction

Sprites are large but short-lasting electrical streamer discharges in the mesosphere, triggered by lightning flashes. They were predicted by *Wilson (1925)* on basis of Coulomb's Law and the decrease of the electric breakdown threshold with height, but have only been seriously considered after having been recorded serendipitously in 1989 *(Franz et al., 1990).*

Modelling (e.g. *Pasko et al, 1997*) suggest that sprites initiate by electric breakdown at heights usually between 70-90 km, a result of quasi-electrostatic (QE) fields that occur suddenly when vast amounts of positive charge are removed from the cloud by a subset of usually positive cloud-to-ground (+CG) flashes, a relation established by *Boccippio et al. (1995).* The strength of the QE field in the mesosphere is proportional to the *charge moment change* of the lightning discharge: charge times the altitude from which it is removed (units Coulomb times kilometer, *C km*). This quantity can be estimated remotely from electromagnetical measurements. *Huang et al. (1999)* and *Hu et al. (2002)* demonstrated that sprites are caused by +CG flashes with charge moment changes of at least a few hundred C km. *Cummer and Lyons (2005)* additionally demonstrated that the CG flashes that did not produce sprites had charge moment change values below a sharp threshold, which varied from night to night. By a simple superposition of electric field components from a series of point charges, using Coulomb's Law, the horizontal shape of the QE field at such altitudes resulting from an instantaneous charge removal can be shown to be a uniformly circular disk with the largest values in the center, irrespective of the pathway of lightning channels through a charge distribution in the cloud (as explained in more detail by *Moudry et al., 2003*).

The direct relation between charge moment change and QE field in the mesosphere is valid only if charge would be removed instantaneously. In reality, lightning can remove charge more gradually from different areas of the cloud via long continuing currents (e.g. *Bell et al., 1998*; *Cummer and Füllekrug, 2001*) and QE fields are restored by ion fluxes at the time scale of the dielectric relaxation time, ranging from 100 ms in the lower mesosphere to 1 ms near 80 km altitude where sprites usually initiate. So, lightning discharge processes (e.g. *Stanley 2000, Lyons et al., 2003, van der Velde et al. 2006, Marshall et al, 2007*), interference patterns of their emitted radiation (*Valdivia et al., 1997; Cho and Rycroft, 2001*) and local ion density distributions *(e.g. Moudry et al., 2003; Sentman et al., 2003)* add complexity and allow for different shapes as well as significant delays and horizontal displacements of sprites relative to the detected triggering +CG return stroke (*Lyons, 1996; Wescott et al., 2001; São Sabbas et al., 2003*).

Sprites have been documented to occur mostly over mesoscale convective systems (MCS) with diameters of usually 100 km and larger, in the later stages of their lives. Winter thunderstorms over sea also produce sprites, and have been observed mainly in Japan (e.g. *Hayakawa et al.*, *2004*; *Matsudo et al., 2007*) and Israel (*Ganot et al., 2007; Greenberg et al., 2007*). Our *EuroSprite* region of study features both types of storms, the

MCS occurring mostly in summer over France and Spain and during the early fall over the western Mediterranean Sea, transitioning to smaller, lower topped storms when depressions associated with cold air aloft settle over the warm sea in late fall and winter. The sprite-producing storms included in this study can all be considered of MCS type.

MCSs consist of clusters or lines of convective cores with similar updraft speeds and microphysics as normal thunderstorms, and an adjacent region of weaker precipitation. However, not this convective region with high intracloud and cloud-to-ground flash rates but the later developing adjacent extensive areas of generally uniform weak to moderate precipitation rates, known as the stratiform region, host the discharges that produce sprites (*Lyons, 1994; Williams, 1998; Lyons et al., 2003*). It seems that convective cores typically do not accumulate a large enough amount of charge to create flashes with sufficiently high charge moment changes, because of their frequent discharging. *Rutledge and MacGorman (1988)* found that +CG lightning tended to occur mainly in the stratiform region, with +CG flash rates increasing as stratiform precipitation mass expanded. Analogously, *Soula et al. (2009)* found sprite occurrence in two *EuroSprite* case studies to be tied to periods of growth of the stratiform precipitation mass, after convective precipitation mass started decreasing. These observations suggest that charge inside the stratiform region needs to be in net growth mode in order to sustain repeated discharges, and that the charge configuration is such that discharges can indeed connect to the ground from a charge layer (or the reverse).

Extensive horizontal flashes, studied by means of lightning mapping systems, are an important component of the +CG flashes triggering sprites (*Lyons et al., 2003, 2006, Stanley 2000*) and +CG flashes in general (*Mazur et al., 1998; Lang et al., 2004*). Often such flashes can be seen crawling the cloud base, and are often called 'spider lightning'.

Spider lightning often originates in the convective region and descends while it expands into the stratiform region *(Lyons et al. 2003, Carey et al., 2005)*. The downward slope appears to follow (charged) ice particle trajectories, in accordance with the simulations of *Rutledge and MacGorman (1988)*. *Ely et al. (2008)* found that in earlier stages of a leading line-trailing stratiform MCS this pathway is nearly horizontal for 40 km long at about 9 km altitude. The descent of the pathway occurred within an hour and suggested growth of heavier particles above the freezing level in response to an intensifying mesoscale updraft. This observation is in support of the modelling results of *Schuur and Rutledge (2000)* who tested several different charging modes and found that significant charge densities inside the stratiform region could only be explained well by the non-inductive ice-ice charging mechanism in low cloud liquid water content working on particles produced inside the mesoscale updraft. 30% of charge arrived by advection from the convective region. However, our understanding of the mechanisms of the development of many layers of alternating charge polarities (e.g. *Stolzenburg et al., 1998*) and their small depth especially near the melting level (<300 m, *Marshall and Rust, 1993; Shepherd et al., 1996*) is still far from complete. *Marshall and Rust (1993)* discovered that electric field profiles through stratiform regions could usually be divided into type A and type B. Type B has two main charge layers near the 0°C level, while type A has more

layers and contains the main positive charge layer at higher altitudes. Charge at higher altitudes in a storm, if discharged, cause stronger QE fields in the mesosphere for a constant amount of charge.

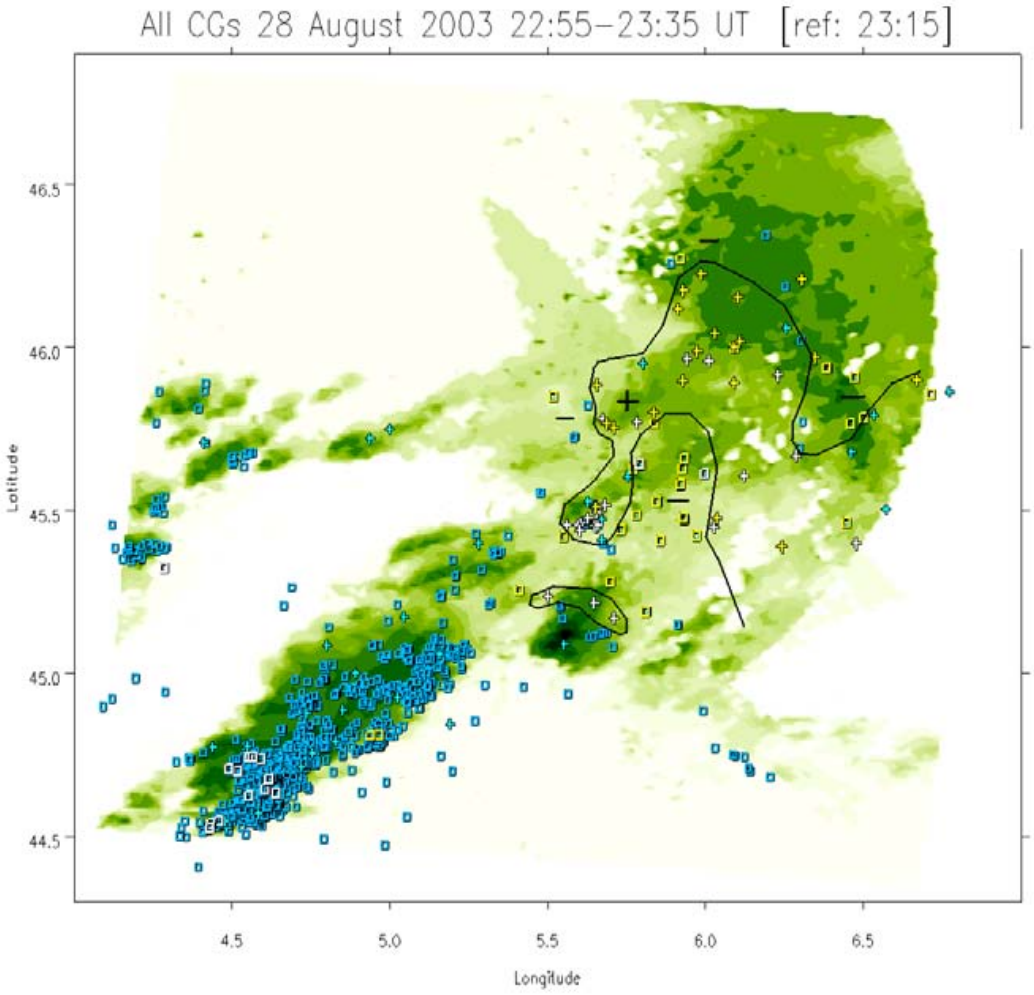

Figure 1. Accumulated 40-minute lightning activity using Lagrangian correction for plotting relative to the radar reflectivity features of a moving storm system. Yellow are all CGs occurring within one second of a sprite, white are those which triggered sprites (ST+), square symbols are negative and plus symbols positive CGs.

In the first part of this article we look into the relation between precipitation conditions, measured by radar, and CG flashes which do or do not trigger sprites. It may provide insight on how conditions in thunderstorms become favorable for production of sprites and strong +CG flashes. Also the characteristics of sequences of CG flashes (not strokes), first noticed by *Lyons (1996)* and *Soula et al. (2009)*, are investigated. This study was inspired by the clustering of sprite-triggering +CG flashes around certain precipitation features in some mesoscale convective systems, of which an example of 28-29 August 2003 (over southeastern France) is shown in Figure 1. Remarkable are the small areas of enhanced reflectivity which appear to be the preferred location of sprite-triggering +CG flashes.

The second part of this article is a statistical study of objectively determined morphological features of 91 sprites in relation to their triggering lightning and precipitation characteristics. Several studies have listed some morphological characteristics of sprites and an indication of the size of the event (e.g. *Lyons 1996; Lyons et al. 2003)* but no conclusions have been drawn regarding correlations between morphology and variables as peak current, delay time, charge moment changes or radar reflectivity. *Lyons et al. (2006)* found that the relative occurrence of brighter sprites increases towards the weaker reflectivity values in stratiform regions (~30 dBZ). *Van der Velde et al. (2006)* analyzed sprites during one thunderstorm system and reported that carrot sprites were significantly longer delayed than columniform sprites and that the delay corresponded with a Very Low Frequency (VLF) sferic cluster after the +CG return stroke. This sferic activity was attributed to ongoing in-cloud lightning activity acting to remove charge from the cloud via the +CG channel, which is now confirmed by *Marshall et al. (2007). Greenberg et al.* (2007) confirmed for Israelian winter sprites the longer delay for carrots compared to columns.

The characterization of sprite morphology, however, has so far been mostly subjective. In the present work common morphological features of sprites are measured and compared to lightning and precipitation quantities.

2. Data

In the framework of the European Union research training network CAL (Coupling of Atmospheric Layers), observation campaigns have been conducted under the name *EuroSprite* starting in the summer of 2003 (*Neubert et al., 2005*). Low-light unintensified video cameras were operated from several locations in southern France. Lenses of either 22° or 31° horizontal field of view were used and the PAL video standard results in fields of 20 ms duration. The cases of 2003 and 2005 observed by the camera at Pic du Midi used real-time detection algorithms described in *Füllekrug et al.* (2006, chapter 5), storing the images with file names containing the GPS time. The cases of 2006 were recorded as AVI movies using UFOCapture software by SonotaCo and the KIWI-OSD GPS time inserter from PFD Systems, LLC. The *EuroSprite* image database over 2003-2006 we used contains 250 sprites occurring over southern to central France, northern Spain and the western Mediterranean Sea. Although this number is small compared to typical numbers observed during campaigns in the United States, this database provides sufficient basis for statistical studies, supplemented by basic radar, lightning detection and satellite data.

CG lightning data is used from the French network of Météorage, which is equivalent to the National Lightning Detection Network used in the United States (*Cummins et al., 1998*) It localizes CG lightning by both time-of-arrival (TOA) and magnetic direction finding (MDF) in the Low Frequency (LF) band, and provides the peak current and polarity of each stroke. In this study, only first strokes of -CG are used and termed flash.

The criterium we used for identifying subsequent strokes is the same as used by NLDN: <500 ms and 10 km between strokes (*Cummins et al. 1998*). For positive flashes it is very rare to have a multiplicity greater than one, and all strokes are simply taken as flashes. We did not filter out small Météorage-detected +CGs with peak currents less than 10 kA, which are most likely intracloud (IC) discharges (*Cummins et al., 1998; Biagi et al., 2007*), but these should not significantly influence our results.

Precipitation data comes from the French national network of C-band weather radars (ARAMIS), providing composites (mosaics) of base reflectivity (Plan Position Indicator) every 5 minutes at a pixel size of 1.5 km in 2003 and 1 km for 2005 and later. The radar and lightning detection systems did not sufficiently cover Spain and the Mediterranean Sea, so we excluded this subset of sprite events, reducing the number to 147 included sprites for the lightning-precipitation study.

The sprite morphology analysis required sufficiently clear images to make out the features to be measured, and accurate time stamps to determine the delay to parent +CG flashes. A more limited dataset is employed for this analysis, including most sprites of 20/21, 23/24 July 2003, 28/29 August 2003, 11/12 September 2006 and 17/18 November 2006, a total of 91 sprites.

3. Part I: Statistics of CG lightning in relation to precipitation

3.1 Methods

As the sprites collected during *EuroSprite 2003-2006* have not been observed simultaneously by two or more cameras, their true geographic positions could not be determined. For this reason the sprites cannot not be related directly to precipitation characteristics, but instead this can be done for the +CG flashes that occurred near the time of the sprite. Sprites are quite commonly displaced to the triggering +CG by several tens of kilometers and a +CG does not necessarily reflect the origin of the charge removed from the cloud system, so this is strictly taken a study of different types of CG flashes.

Distributions of radar reflectivity (precipitation rates) have been summarized within circles of 5 and 10 km radius around every CG flash of a thunderstorm. The number of included radar pixels may vary somewhat according to the placing of a CG flash relative to the radar pixel grid, but this issue was mitigated by dividing each pixel into four subpixels of the same value. Radar reflectivity Z, typically expressed in dBZ, is related to a factor Z_0 by a logarithm law: $Z = 10 \log Z_0$. Z_0 (in $mm^6\ m^{-3}$) is proportional to the density of particles n and their diameter D ($Z_0 \sim n\ D^6$) in the scanned radar beam volume. For non-critical use as in this study, reflectivity Z_0 can be conveniently converted to the rainfall rate R by the commonly used empirical Z-R relationship stemming from the *Marshall-Palmer (1948)* drop size distribution: $Z_0 = 200\ R^{1.6}$ (Z_0 in $mm^6\ m^{-3}$ and R in mm/hr). For

every CG flash detected by Météorage, the minimum, 25th percentile, median, 75th percentile and maximum reflectivity values (dBZ) within the predefined distance were stored, as well as the reflectivity sum (Z_0) converted to average rainfall rate (mm/hr). Radar pixels with a reflectivity lower than 9 dBZ ('dry') in the circle have been excluded. We have determined also the uniformity (or variability) of precipitation around a CG flash, expressed by the interquartile range (IQR), the difference between the 75th and 25th percentile values of the distribution of precipitation intensity within the circle. A larger IQR means a wider distribution and thus less horizontally uniform precipitation. Because there is a large linear dependency on precipitation rate, we found it most useful to normalize the IQR by the average between the 75th and 25th percentile rain rates. This can be considered a measure of relative uniformity of precipitation, with increasing values indicating less uniform conditions.

Minimum and maximum Meteosat (12.8 μm) IR cloud top brightness temperature values near each CG flash and the coldest storm top value were stored as well, but due to 30-minute intervals it was necessary to perform interpolation, which may affect the results. This interpolation was done linearly in time between two images to obtain the value at the location of the CG.

Next, flashes were grouped into four basic classes: flashes occurring before the start of the period of sprites (abbreviated as P+, P-), flashes occurring during the period of sprites, but not related (abbreviated as +, -), the apparent triggering flash, (ST+) which occurs the shortest time before the sprite, and any accessory CGs that appeared very close to the sprite in time and space (S+, S-). These classes are summarized in Table 1.

The latter group S+/S- occurred usually within 1 second before or after the sprite and in areas with sparse lightning activity, giving the appearance that they are part of the same lightning flash or a sequence of charge redistributing flashes, possibly connected by extensive horizontal 'spider lightning'. *Lang et al. (2004)* provide strong support for this assertion, and photographic evidence and detections of large intracloud lightning flashes (*van der Velde et al. 2010*) suggest spider lightning is common also in European thunderstorm systems. There was also one sprite triggered by a -CG confirmed by Extremely Low Frequency radio observations from Israel and Hungary to have a charge moment change of -800 C km. It has been treated here as if it were a ST+.

We then defined a *flash sequence* as a series of subsequent +CGs happening within tens to hundreds of milliseconds of each other with distances between flashes of up to several tens of kilometers. Although –CGs can be part of these sequences, for automatic sequence identification purposes we confined it to +CGs only, because their generally low numbers decrease the chance that unrelated flashes would be grouped under one sequence. Figure 2 is a histogram of time interval (logarithmic x-axis) between subsequent +CG flashes during periods of storms when sprites occurred, showing clearly two modes of occurrence: return times of roughly 20-90 seconds, as well as return times shorter than one second, which we identify as sequences.

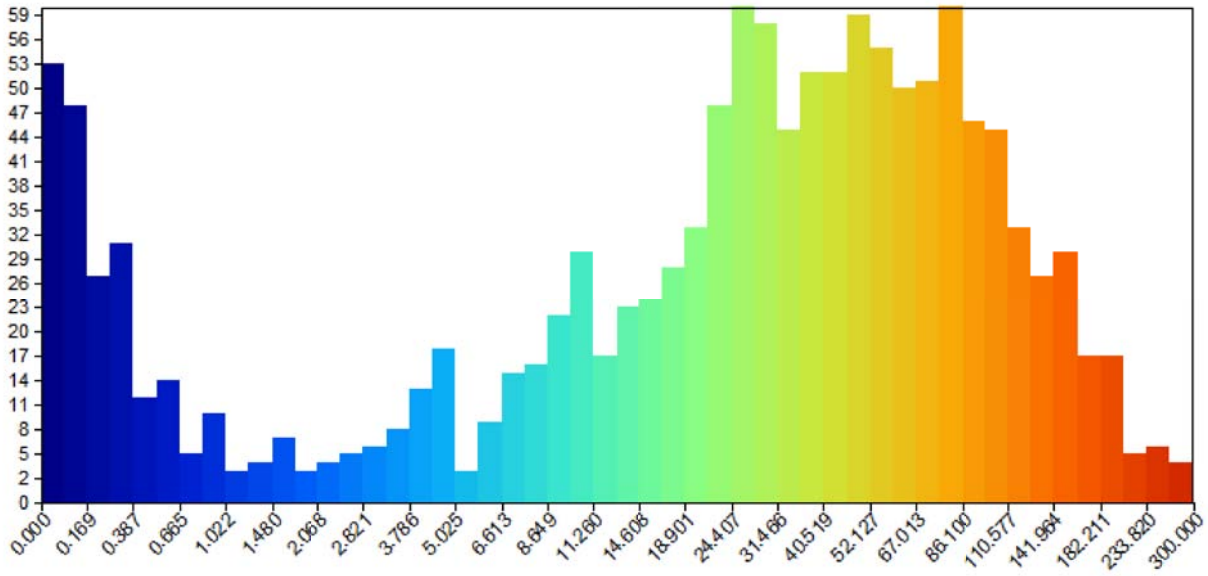

Figure 2. Histogram of time interval between subsequent +CG flashes during sprite-active periods for all the storms included in this study, with arbitrarily defined logarithmically increasing time bins in seconds.

Most of the sequence +CGs occurred with spatial and temporal intervals that fit the typical range of horizontal leader propagation speeds (10^4-10^6 m s^{-1}, e.g. *Mazur et al., 1998*), which we have used to automatically identify possible sequences, which were then manually checked for extreme values of apparent speed, distance and time. For sprites, CG activity within 1 second before and after the event was plotted on a radar image together with the azimuths of the sprites. Such plots commonly show 1-5 additional +CGs and often also a few -CGs, all inside the stratiform precipitation or old convective cores. This provided visual confirmation that automatically identified flash sequences were plausible. Based upon flash sequences, additional categories were included: single +CG (0+, S0+, not followed by subsequent flashes), sequence-starting +CG flashes (1+, S1+) and subsequent +CG flashes of a sequence (2+, S2+). This latter category contains also any third, fourth, or later subsequent flashes if present.

Histograms of +CG within sequences (*figure 3*) show that the median time between subsequent flashes of sprite-producing sequences is 166 ms (242 ms for non-sprite +CG sequences) and that there is a long tail of outliers starting from about 500 ms (or about 1000 ms for non-sprite sequences) up to approximately 1650 ms (both types of sequences). The median distance between subsequent +CG flashes of a sprite-producing sequence is 30 km (24 km, non-sprite) and outliers beyond 77 km (89 km, non-sprite). Note that the stratiform -CG flashes that fit in the sequences were not included.

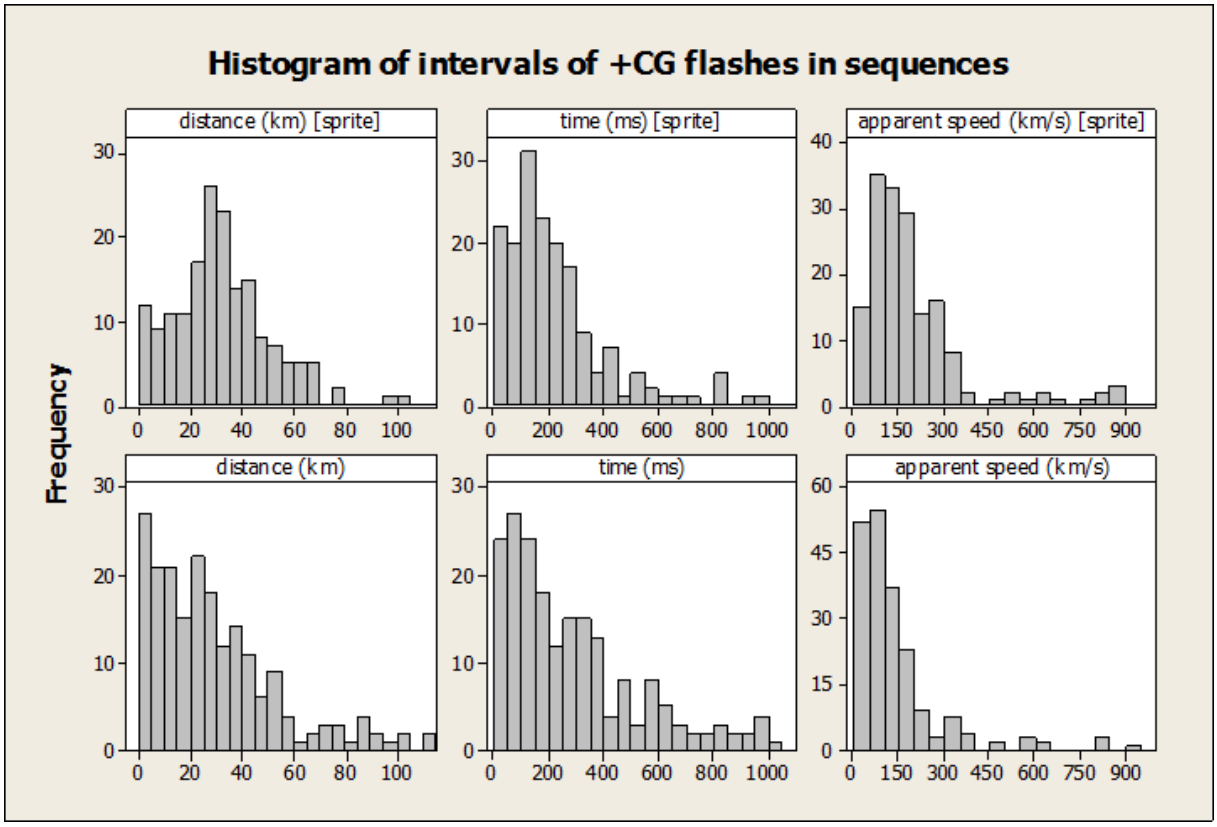

Figure 3. Histograms of time, distance and apparent speed between subsequent +CG flashes within sequences. Top row : sequences which contained a sprite-triggering +CG (ST+). Bottom row : other +CG sequences.

For interpretation of the results we have to keep in mind that the lightning detection network has a detection rate of 80-90% for +CG flashes. Also, the camera system (combined with factors as cloudiness) is unlikely to detect 100% of sprites. This would muffle the separation in characteristics between sprite- and non-sprite producing flashes to some extent.

The results of the flash categories are presented in the form of box-and-whiskers plots defined by *Tukey (1977)*. The box stretches to the 25th and 75th percentile values (i.e. 1st and 3rd quartile), thus containing fifty percent of the observations in the category, while the whiskers extend outward to 1.5 times the box length, or to the data extremities if those are reached first. The points beyond the whiskers are by definition outliers, and are not displayed here.

Table 1. Abbreviations used for flash categories used in this study.

P+, P-	Pre-sprite period CG. The sprite period starts just before the first sprite has been observed (<10 min). CG categories below refer to the sprite period only.
+	+CG not associated with a sprite
-	-CG first stroke
ST+	+CG shortest before a sprite, considered the trigger (SP+CG in other works)
S+, S-	+CG or -CG occurring within -500 ms to +1 s of sprite, as part of a +CG sequence
S0+, 0+	+CG not belonging to a sequence (not followed by other +CG in 1 s), associated with sprite / without sprite
S1+, 1+	First +CG of a sequence during which a sprite occurred / no sprite occurred
S2+, 2+	Second or later +CG of a sequence during which a sprite occurred / no sprite occurred

3.2 Results

3.2.1 CG peak currents and precipitation: general relations

Before going into results of the flash categories, we present the general relation between peak current of all lightning flashes, and precipitation. *Figure 4* shows a scatterplot of positive and negative peak currents against the average precipitation rate within 10 km distance of the flash. The graph shows that the highest precipitation rates (>50 mm/hr) associate with only low peak current +CGs (mostly <30 kA). The strongest positive discharges (>50 kA) are produced in weak to moderate precipitation, mostly below 15 mm hr^{-1}, but also many weak discharges occur in weak precipitation. This distribution was very obvious for every storm we included.

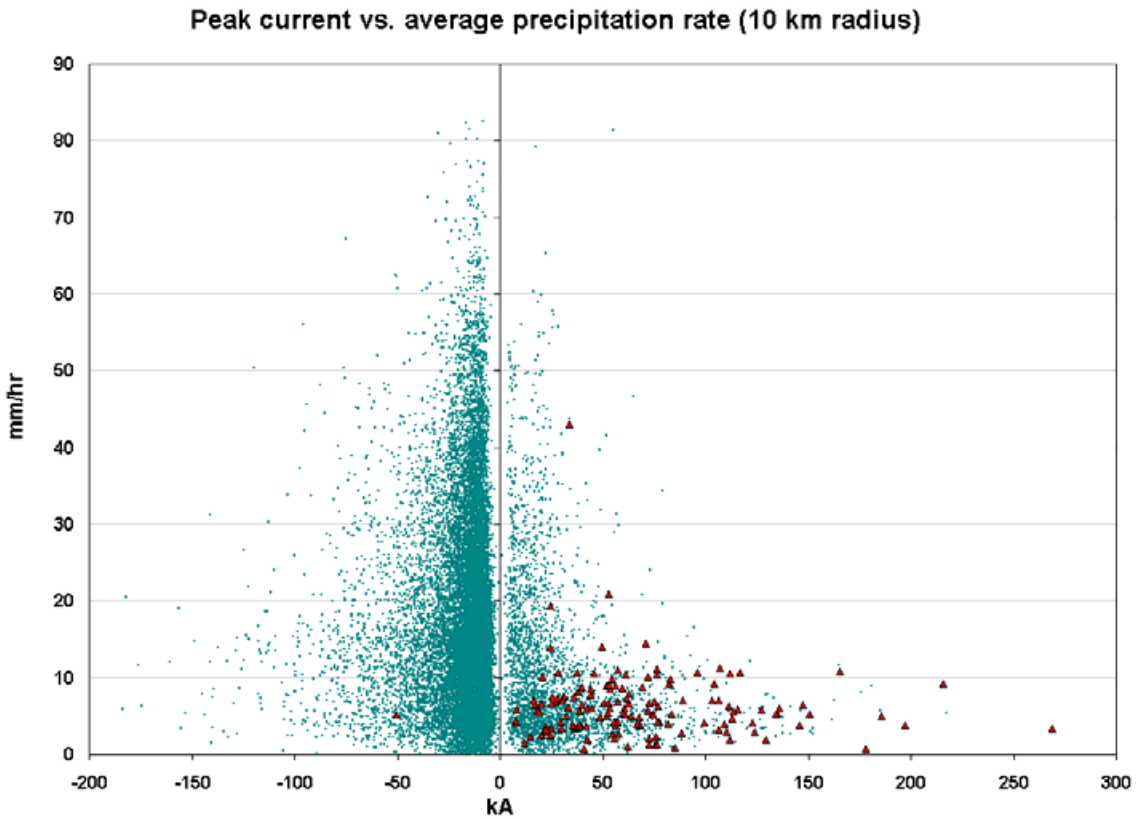

Figure 4. Distribution of cloud-to-ground lightning flash (first stroke) peak currents measured by the Météorage lightning detection network, versus radar-derived precipitation intensity averaged over circles of 10 km radius around each flash. Red triangles indicate sprite-triggering CG flashes. The same distribution is found for a circle of 5 km around each stroke, but with different values of precipitation rate. Note also the sprite-triggering -CG, which was confirmed to have a charge moment change of -800 C m by measurements in Hungary (J. Bór) and Israel (E. Greenberg).

For –CGs, the maximum observed peak currents increase more gradually with decreasing average precipitation rates. Another remarkable feature is that very low peak current –CGs (<7 kA) also become more likely with weaker precipitation. This is also true for small +CGs. Both are likely intracloud discharges.

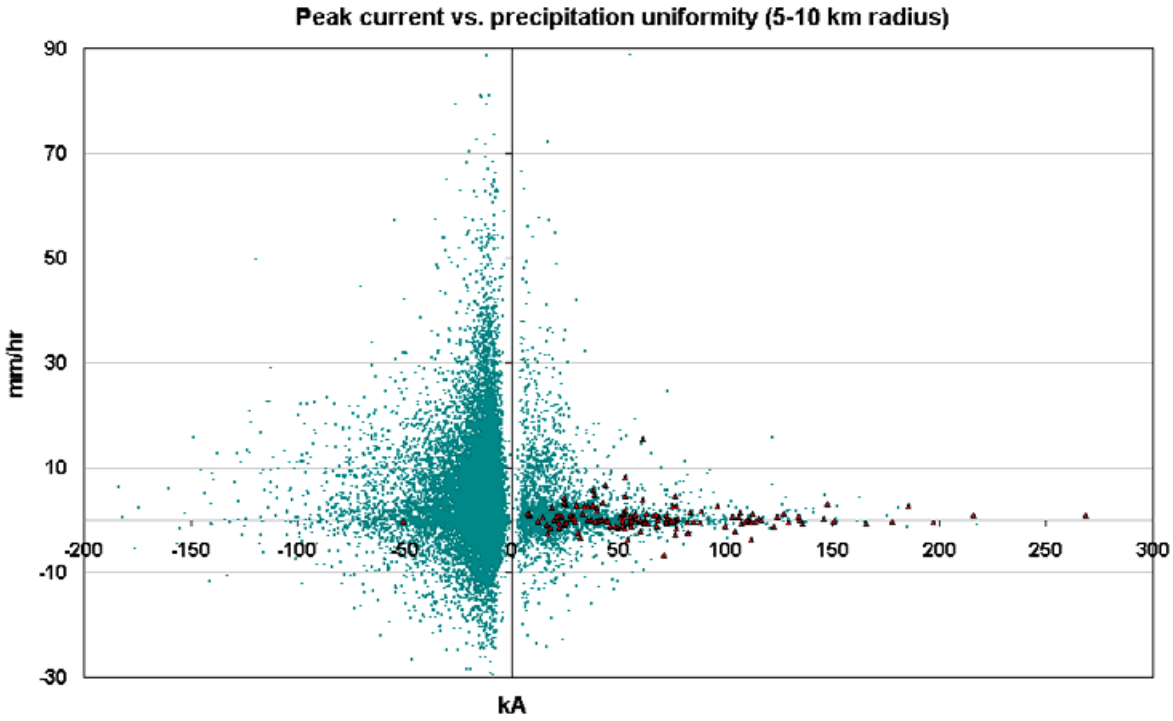

Figure 5. As Figure 4, but for the difference in average precipitation rate between the circles of 5 and 10 km radius around any flash.

The difference between the average precipitation rates of the 5 and 10 km circles for individual CGs is an indication of the uniformity of precipitation (*Figure 4*). Especially for +CGs, the distribution has its greatest weight towards the most uniform precipitation. The greatest positive peak currents occur with the most uniform precipitation, for example, >100 kA is almost exclusively found with an absolute difference of under 5 mm/hr between the 5 and 10 km radius average precipitation. For –CGs >100 kA, the range is wider: mostly less than 20 mm/hr absolute difference. The asymmetric distribution around 0 mm/hr difference reflects a preference for lightning of both polarities to occur closer to cores of precipitation (positive values in the graph mean that the 5 km radius circle has a stronger average precipitation than the larger 10 km radius circle). The smallest peak current flashes (<7 kA) are again found to occur most frequently in the more uniform precipitation regions. It is possible that the lightning detection system picked up pulses from intracloud discharges occurring in stratiform precipitation regions.

3.2.2 Flash counts in each CG group

From the last column of *Table 2* can be derived that there are on average 1.0 additional +CG and 0.8 –CG flashes for every ST+. Additionally, a flash sequence producing a long-lasting sprite event may contain more than one ST+.

During the sprite-producing stages of the included storm systems, an average of 9% of all +CG flashes or 1% of all CG flashes in the entire MCS triggered a sprite. If the accessory flashes in sprite-producing sequences are included (S+ and S-), 18% of +CGs and

3.5% of all flashes (any polarity) belonged to sequences that caused sprites. When all the cases are combined, of all flashes greater than 20 kA occurring in average precipitation rates under 15 mm/hr (within 10 km radius), 14% of +CG flashes triggered a sprite, and 25% of +CG flashes were part of a sprite-producing sequence, at 90% detection rate of sprite-triggering flashes. At more strict thresholds of 35 kA and 10 mm/hr the probability of detection decreases more rapidly than the false alarm rate: still only 20% of +CG flashes triggered a sprite, 31.5% of +CG flashes were part of a sprite-producing sequence, at 66% detection rate of sprite-triggering flashes. So, even within the precipitation intensity range favored by ST+, the majority of +CG do not produce sprites.

Only 14% of all the non-producing +CGs during sprite-producing stages of storms were part of sequences of several flashes as opposed to single-flash, while for sprite-producing flashes this was on average 67%. The average number of subsequent flashes to first flashes in a flash sequence is 1.2 for non-sprite sequences, and 2.0 for sprite-sequences. 33% of all +CG sequences (S1+ versus 1+) produced sprites, while only 4% of all isolated +CGs (not in a sequence, 0+ and S0+) produced sprites.

Table 2. Mesoscale convective system properties and lightning counts per category.

CASE		1	2	3	4	5	6	7	SUM/ AVG
DATE		20-21 July 2003	23-24 July 2003	25-26 August 2003	28-29 August 2003	28-29 July 2005	11-12 September 2006	17-18 November 2006	
OBS PERIOD (UTC)		0200-0315	2100-2340	1950-2300	2245-0347	0125-0300	2015-0245	1900-2130	
TYPE MCS		Trailing	Amorphous	Leading	Parallel	Trailing	Trailing	Parallel	
MAX SPRITE RATE (30 min)		14	6	5	11	8	6	8	**8.3**
COLDEST CLOUD TOP T at beginning of OBS PERIOD ℃		-61.5	-57	n/a	-65.5	-63	-65	-53	**-59.3**
AVG CLOUD TOP T at ST+ ℃		-56.1	-50.5	n/a	-59.8	-44.9	-60.5	-44.7	**-52.8**
HEIGHT 0℃ (km)		3.7-4.1	3.7-4.4	3.9	4.1	3.8-4.5	3.6	2.7	**4**
NUMBER DURING SPRITE OBS PERIOD*	+	123	202	162	299	48	367	190	**1391**
	-	519	1476	1880	3818	89	1657	673	**10112**
	ST+	**26**	**13**	**9**	**29**	**15**	**31**	**23**	**146**
	S+	32	6	11	36	22	28	17	**152**
	S-	20	2	7	29	17	36	8	**119**
	0+	88	147	124	232	29	255	139	**1014**
	1+	16	24	17	29	7	50	27	**170**
	2+	19	31	21	37	12	62	24	**206**
	S0+	9	7	5	3	3	10	4	**41**
	S1+	18	5	5	19	9	17	12	**85**
	S2+	31	7	10	43	25	32	24	**172**

** See category explanation, section 3.1. + and – are not totals but comprise only flashes not associated with sprites.*

3.2.3 Peak current

For all thunderstorm cases, the group of ST+ discharges had the highest average (as well as 25th and 75th percentile) peak currents, but the overlap between peak currents of regular and sprite-triggering +CGs varied among the cases. Typically, the 25th percentile of the ST+ group and the 75th percentile of the + group peak currents are close to each other, usually in the 30-50 kA range. This generally means a 50% overlap of peak current range for the two groups.

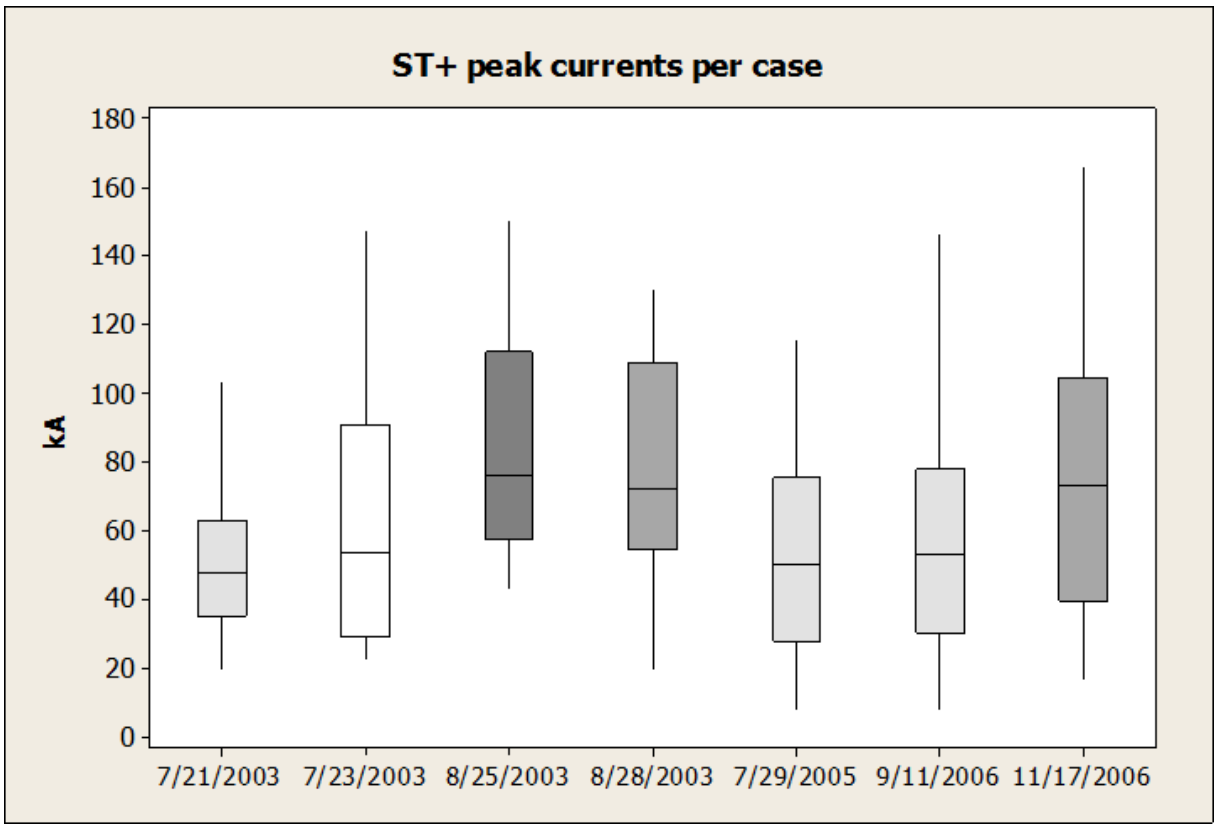

Figure 6. Peak currents of ST+ for all considered storm systems.

Following the classification by *Parker and Johnson (2000)* for typical configurations of mesoscale convective systems, *Figure 6* reveals that the highest ST+ peak currents occur for the parallel-stratiform (PS) MCS cases (median 70-80 kA), while the lowest ST+ peak currents (and most overlap with ordinary +CG) occur for the trailing-stratiform (TS) MCS cases (median 45-55 kA). Only for the case of 25-26 August 2003, the only leading-stratiform (LS) MCS in our study, the ST+ flashes had larger peak currents than any other +CG. If these differences would prove to be consistent in a study of a larger set of cases, they must result from the differences in storm dynamics and the role of a mesoscale updraft in generating stratiform charge structures, in particular the heights and charge densities of the charge layers relevant to the sprite-producing lightning discharges.

3.2.4 Radar reflectivity

3.2.4.1 Sprite -related CG and other CG flashes

Of all radar distribution parameters, the *maximum reflectivity* found within a radius of 10 km around a CG shows the clearest systematic differences among the CG flash categories (*Figure 7*), but the ranges overlap by a large amount. The median values of maximum reflectivity for all cases together are, respectively, 43 dBZ (S+), 45 dBZ (ST+) and 49 dBZ (+). The histogram shows that the + category generally shows the largest range of values and has two modes: a convective (53 dBZ) and a stratiform (43 dBZ) mode. During the pre-sprite periods, +CG occurrence extended to higher reflectivity values and there were fewer flashes in stratiform precipitation. –CGs in sprite-producing sequences (S-) are usually found within the same narrow range of moderate reflectivity values as their positive equivalents with an equal median: 42 dBZ. This is in strong contrast to normal –CGs which occur typically in and near the most convective areas, with medians of 54 dBZ.

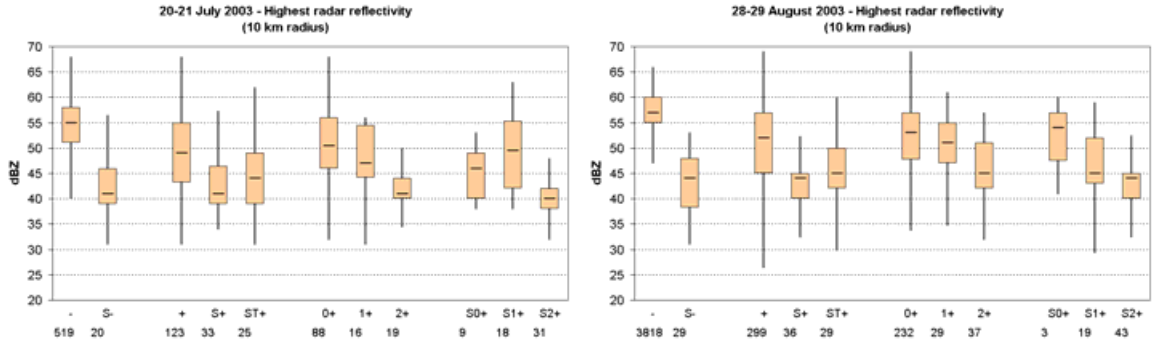

Figure 7. Two very similar examples of distributions per flash category of the highest radar reflectivity found within 10 km of a flash.

The strongest reflectivity values found anywhere in the system during sprites ranged between a minimum of 50 and a maximum of 68 dBZ, with a median of 61 dBZ. Compared to the findings of *Lyons et al. (2006)*, these values are 5 dBZ lower in France, but still confirm their suggestion that a minimum of strong convection must still be present, fulfilling a role in the charging of the stratiform region and/or the lightning triggering process.

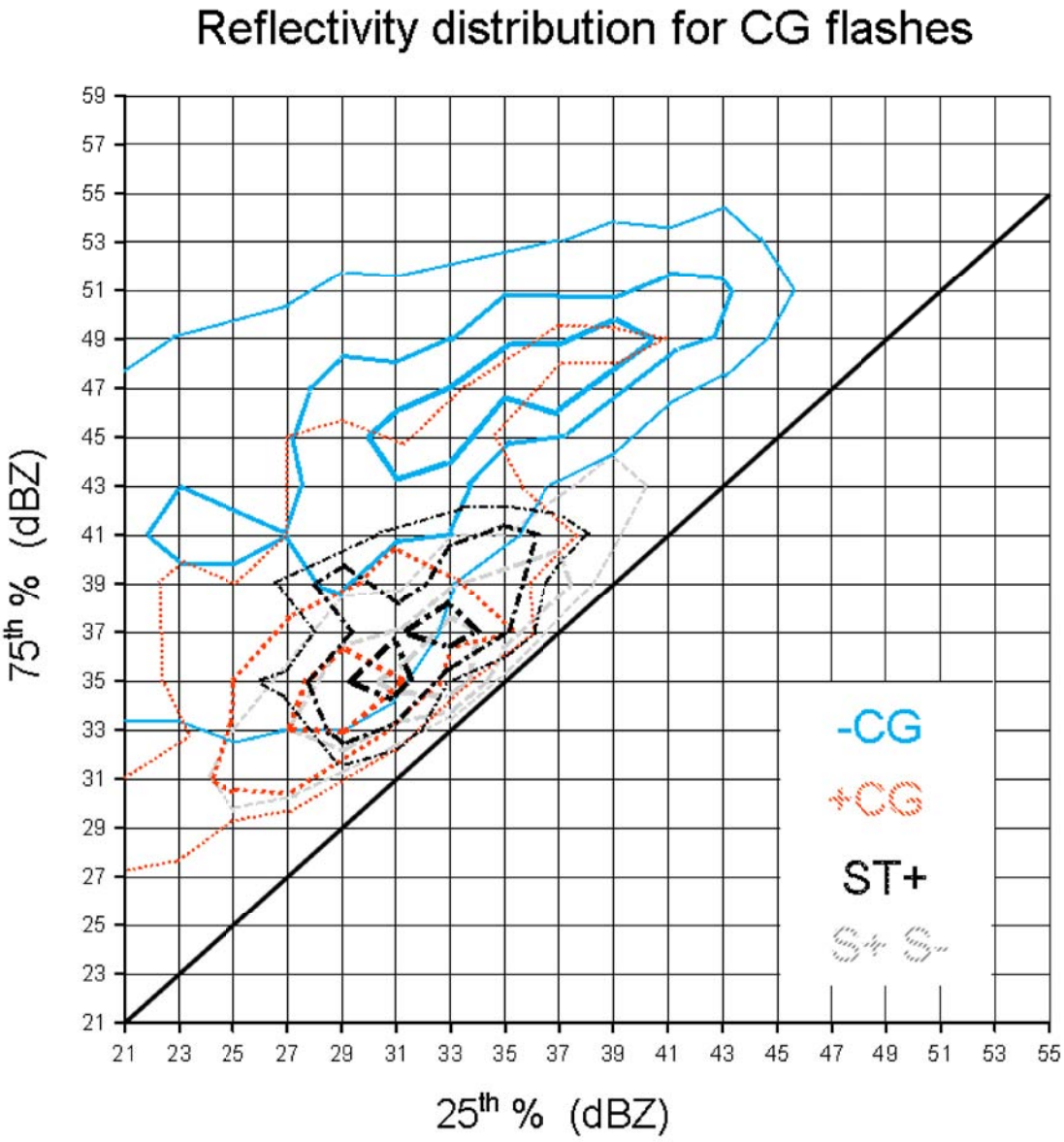

Figure 8 : The reflectivity distribution (within 10 km distance) parameter space for different categories of flashes. The diagonal line indicates the most uniform precipitation possible for a given intensity (interquartile range of zero) while uniformity decreases perpendicular the line (wider distribution). The lines show qualitatively the relative density per events category. Outliers may occur outside the lines. See Table 1 for total numbers.

Figure 8 shows the distribution of flashes in the parameter space of 25th and 75th percentiles of the reflectivity distributions around all flashes of all storms together. This figure allows a more specific conclusion about the intensity and uniformity modes for the different flash categories. Precipitation intensity near a flash increases along the vertical axis, while precipitation uniformity is greatest close to the diagonal line where 75th and 25th percentile reflectivity values are nearly equal. We see that:

- -CGs occur in a broad reflectivity range with the highest concentration around the 75/25th percentile line 41/23 – 45/32 – 49/39 dBZ. They become relatively scarce for 75th percentile values under 39 dBZ, in other words, away from convective cores.
- +CGs (non-sprite) also occur in a wide reflectivity range reaching out into the same values as –CGs, but are much more concentrated between 33/27 – 36/30 dBZ (stratiform precipitation). When considering only data from periods of the MCSs *before* sprites occurred (not shown), the distribution features an already present stratiform mode and a convective mode along 41/31 – 47/39 dBZ: the same region as negative flashes.
- The relative occurrence of S- is similar to that of S+, shifted to slightly weaker precipitation: 31/25 – 39/37 dBZ (the S+ and S- categories are combined in figure 6)
- Most ST+ concentrate between a 25th percentile reflectivity value of 28 dBZ and a 75th percentile reflectivity value of 42 dBZ, with a modal value of 35/31 – 37/33 dBZ.

Keep in mind that these ranges are derived for all cases together, so that possible storm to storm differences are obscured.

3.2.4.2 Flash sequences

Systematic differences are also found between first flashes and subsequent flashes of a sequence (as defined before). The first +CG flashes (S1+ and 1+) are associated with maximum reflectivity values (10 km radius) with medians about 5 dBZ higher than those for subsequent +CG flashes (S2+ and 2+) in this dataset: 48 dBZ versus 44.5 dBZ for non-sprite +CG sequences, and 47 dBZ versus 42 dBZ for sprite +CG sequences. This is also found for individual pairs of first and second flashes of each sequence: for sprite flash sequences, the interquartile range of the difference of the highest reflectivity from 0 to 9 dBZ (median: 4 dBZ), for non-sprite sequences this is 0 to 7 dBZ (median: 1 dBZ). The positive values indicate an apparent propagation of flashes within a sequence from higher to lower precipitation intensities, and is probably a manifestation of convective-to-stratiform spider lightning propagation as observed by *Lyons et al. (2003), Lang et al., (2004), Carey et al. (2005), and Ely et al. (2007).* Combining the 67% of sequences that produce sprites with the 75% of sequences that involved core-to-stratiform propagation, then at least 50% of all sprites in this study are triggered by this type of lightning.

The 0+ and S0+ categories of flashes are associated with about the same median and quartile values for maximum reflectivity as 1+ and S1+, respectively (when data from all cases are combined).

Second and later +CGs of sequences (S2+, 2+) generally occur also in more uniform precipitation than first +CGs (S1+, 1+). The S2+ occur in significantly more uniform precipitation than 2+, best noticed in 5 km circle normalized IQR values (not shown): S2+ have the smallest IQR range at a median of 0.43, versus 0.69 for 2+ (95% confidence intervals do not overlap). S1+ and 1+ occur through a range of values very similar to each

other. S-, the negative flashes occurring during sprite-producing sequences, occur in the same range as S2+.
Finally, also the median distance from the location with the highest reflectivity in the storm system (*figure 9*) is greatest for S2+, at a median 109 km. The ST+ median value is 97 km while the + and – flashes occur at medians of 75 and 63 km distance from the strongest core. Note that the strongest core may be tens of kilometers away from the convective cells closest to the flash. The S2+ flashes also propagate farther away from the strongest core when directly compared to their preceding S1+: a median of 19 km, compared to a 2+/1+ median of 1 km. Thus, there is evidence that sprite-producing flash sequences tend to propagate farther away and into more uniform precipitation than other flash sequences.

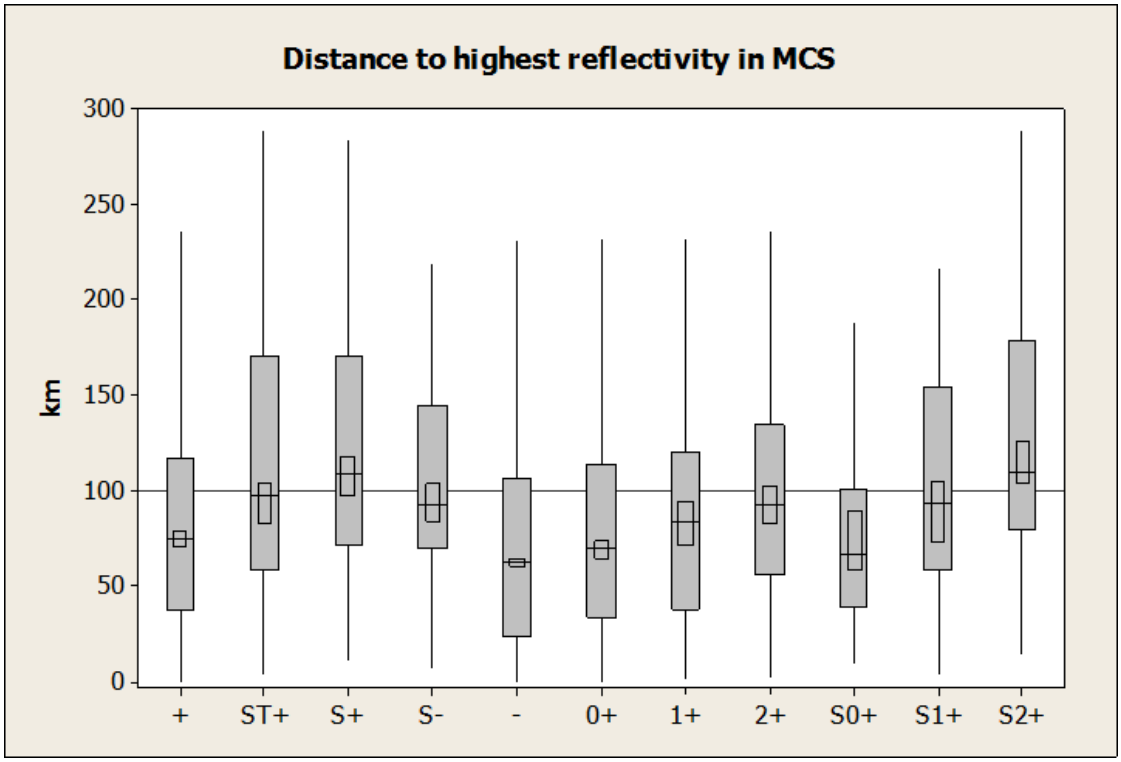

Figure 9. Distance of CG lightning categories to the highest reflectivity location in the storm.

3.2.7 Cloud top temperatures

Cloud top temperatures and their gradients exhibit only little differences among the flash categories and the graphs are therefore omitted. We describe here the bulk results for all cases: The categories + and – show a wider interquartile (IQR) range of occurrence of cloud top temperatures (-60.1/-44.2 °C and -60.7/-43.7 °C respectively) than S+, S- and ST+ (-58.2/-47.4 °C). During the sprites, coldest cloud tops of the storm systems ranged between -65.5 and -53.4 °C IQR. All these values are 10-15 °C warmer than the typical values for Great Plains storms (*Lyons et al., 2006; São Sabbas and Sentman, 2003*) but tens of degrees colder than for Israelian and Japanese winter storms producing sprites (*Ganot*

et al., 2007; Takahashi et al., 2003). These differences result from the tropopause height climatology for these regions. *Soula et al. (2009)* showed the expansion in time of the -45 °C to -55 °C cloud top temperature range (just below the tropopause level) to correspond best with the time of sprite production. *Lyons et al. (2006)* found that ST+ occur under several degrees warmer cloud tops than the coldest top in the storm system, and *São Sabbas and Sentman (2003)* found ST+ to occur under 2-3° warmer cloud tops than other +CGs in a large MCS. Our results show indeed the ST+ to occur under about 6° warmer cloud tops than the coldest top of the storm, but the same is found for other +CGs, so there is no discriminating value.
The observed number of sprites per storm seems proportional to the temperature of the cloud tops under which the ST+ occurred (Table 1), but this is influenced largely by observing conditions such as cloudiness over the camera causing lower total sprite counts. When considering the perhaps more robust largest rate of sprite production per case, measured over half an hour, compared to cloud tops over the ST+ during these periods, no clear tendencies found in our limited set of cases.

3.3 Conclusions and Discussion (Part I)

The first study was based on data from seven EuroSprite storms, including 145 observed sprites (Table 2). The objective was to quantitatively identify the precipitation regime in which +CG flashes occur, with respect to high peak currents or sprite production. Radar reflectivity characteristics from the French network of weather radars have been summarized with 5 and 10 km distance to CG flashes detected by the Météorage lightning detection network. CG flashes were divided into several classes based on the relation of CG flashes with sprites or their order in flash sequences (Table 1). The results are summarized below:

1. Sequences of +CG flashes can be identified, with flashes separated a median 166 ms and 24 km from the preceding flash (outliers beyond 500 ms and 77 km). Visual inspection of lightning activity in the area and time frame around sprites shows that also -CG flashes occur in stratiform parts of MCSs during these sequences.
2. During sprite-productive periods of mesoscale convective systems, on average about 9% of +CG trigger sprites, 33% of +CG flash sequences trigger 67% of sprites, while sequences associated with sprites consist of more +CG (and commonly also –CG) flashes. These percentages vary between different MCSs.
3. Peak currents >50 kA of +CG flashes in MCSs are greatly confined to precipitation of lower intensity (<15 mm/hr) and greater uniformity. The weaker flashes occur both in stratiform and intense convective precipitation. -CG peak currents show a slight increase towards the more uniform precipitation as well. This conclusion is similar to earlier studies (e.g. *Rutledge and Petersen, 1994; MacGorman and Morgenstern, 1998*).

4. The typical reflectivity range (within 10 km radius) for ST+ lies between lower quartile values of 28 dBZ or higher, and upper quartile reflectivity values of 42 dBZ and lower. These are not hard limits, though. Other +CGs (especially below 40 kA) occur in a much wider range, but the overlap is such that for every sprite, 7 other +CG occur in the same precipitation region, not counting S+.
5. +CG and –CG flashes accompanying the triggering flash in sprite-producing flash sequences occur in the most uniform stratiform precipitation of all flashes, while the actual reflectivity range is relatively wide (27-41 dBZ medians).
6. First +CG flashes of a sequence (1+ and S1+) strike near more convective precipitation than subsequent +CG flashes (2+ and S2+), suggesting they are connected by horizontal lightning propagating from convective cores into stratiform regions. Subsequent +CG flashes in sprite-associated sequences occur in more uniform precipitation and at greater distances to convective core regions than those in sequences not associated with sprites.

It proved problematic to make a distinction between sprite and no-sprite producing +CG flashes based on precipitation characteristics. ST+ do occur within a narrower range of precipitation characteristics: the moderate to high intensity zones of stratiform regions and decaying parts of the convective region. Both the strongest peak currents and the larger sprites, though uncorrelated, occur more frequently towards the most uniform precipitation.

50% of sprites in this study are associated with flash sequences traveling from higher to lower precipitation intensities. This behavior has recently been observed in detail for intracloud lightning by means of total lightning mapping systems (*Lang et al. 2004, Carey et al. 2005, Lyons et al., 2003*). It was suggested that these flashes descend along snow trajectories from convective cores into the stratiform region near the freezing level. Our individual sprite observations suggest that many sprite triggering +CG flashes strike at the stratiform-facing side of convective precipitation in trailing-stratiform MCSs, or less uniform areas like local reflectivity maxima bordering or embedded in stratiform precipitation in parallel-stratiform MCSs. In radar sequences these maxima can often be identified as remnants of convective cells, producing -CGs in earlier stages, which was also noted by *Parker et al. (2001)* to occur regularly in parallel-stratiform MCSs. We hypothesize that old convective cells cause disruptions or enhancements of the local electric fields necessary to trigger lightning discharges propagating into the stratiform region. Old cells may also deposit high concentrations of frozen hydrometeors into the stratiform region, and aid non-inductive charging in the mesoscale updraft (*Schuur et al. 2000*), perhaps more effectively than younger cells that transport frozen particles to higher regions inside their stronger, more upright updrafts. Evidence for this comes from the lightning mapping observations of *Ely et al. (2008)* showing front-to-rear intracloud lightning pathways in a trailing-stratiform MCS to slope downward over time as the mesoscale updraft intensifies. Several of our case studies (*Soula et al., 2009)* suggest that decreases of convective precipitation mass, coincident with decreasing –CG rates and

increasing stratiform precipitation mass in the MCS, often corresponds with the start or increase of sprite production.

4. Part II: Sprite morphology in relation to cloud-to-ground lightning and precipitation

4.1 Methods

Sprites have often been classified as carrots, columns, jellyfishes, angels or other subjective terms. In our earlier work, *Van der Velde et al. (2006),* the sprites could rather easily be classified as carrot or column. However, this proved more difficult for many other cases. This inspired us to take a different approach. We measured for each event the altitudes and length of the different features identifiable for the majority of sprites, eliminating much of the subjectivity:

- upper streamers (diffuse flaring structure, in the shape of branches or a plume)
- body (or core, the brightest, longest-lasting part: a column or densely clustered section)
- lower streamers (fine structure, tendrils)
- body width
- number of elements
- total horizontal and vertical dimensions
- ratios of different parts

To keep consistency with *Van der Velde et al. (2006)* and many other studies, and for convenience, we have also classified sprites also the conventional way - to the best of our judgement - by counting the number of carrots, columns, and intermediate sprites present in each event. In this study, each of these types is counted as an element. The most simple of sprite shapes is the classic columniform sprite, often occurring in groups (*Wescott et al., 1998*). This type lacks any upper branches, the column itself is considered as the body. Their tendrils are usually straight and very dim. If tendrils were not visible, they were excluded from the analysis, as well as features that include it, such as total length. Carrot sprites are fully featured with tendrils and upward branches, compared to the standard column, and have a clustered appearance of the body. Angel sprites could be considered as an intermediate form or as slender carrots.

There remain some limits to this morphological model: Some events contain no obvious main body or well-separable elements needed to make sensible feature distinctions, these were excluded from the analysis. In case clouds obscured just a small part of the event, the indeterminable attributes were not included in the analysis. For example, a cloud covering the center parts of three carrots still allows determinations of top and bottom height and the number of elements, in case of doubt the event was entirely excluded.

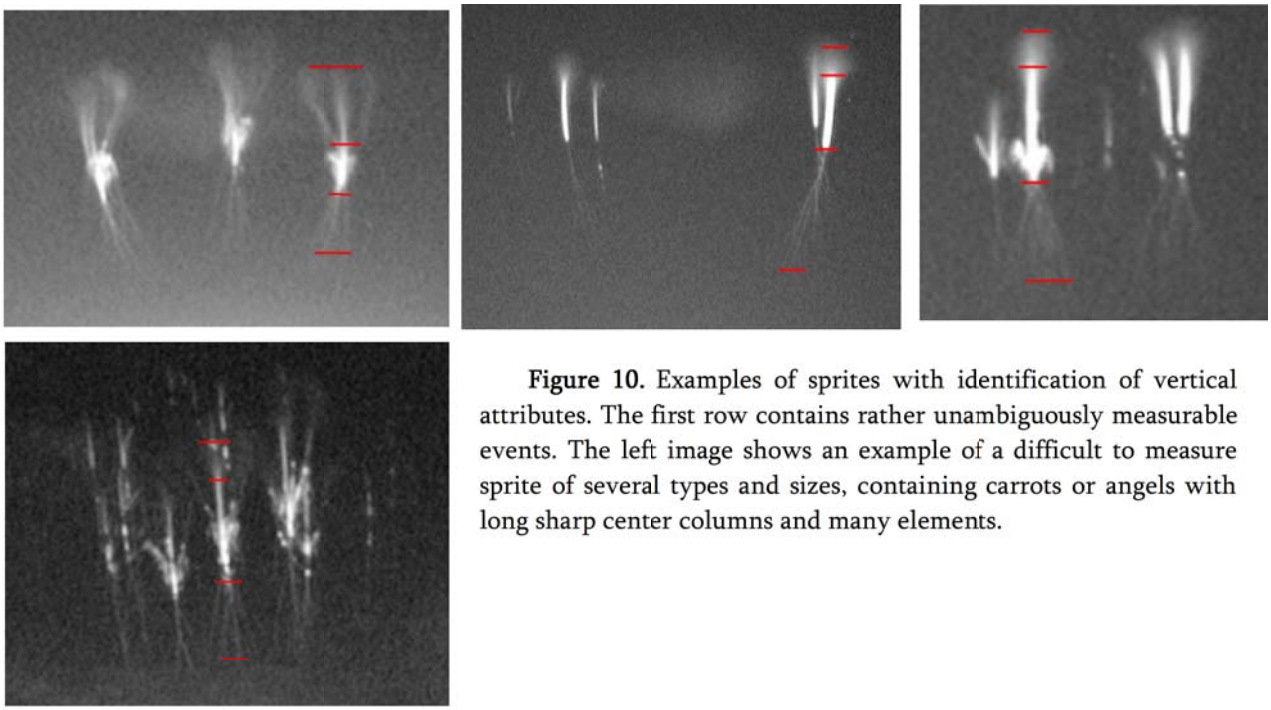

Figure 10. Examples of sprites with identification of vertical attributes. The first row contains rather unambiguously measurable events. The left image shows an example of a difficult to measure sprite of several types and sizes, containing carrots or angels with long sharp center columns and many elements.

The estimated number of elements in an event becomes less accurate in cases where the elements are difficult to be visually separated from each other: underestimation is larger at greater distances, for brighter sprites, and for larger groups. The elements in overexposed sprites can still be counted by the afterglow in the subsequent video frame. Events are characterized by the feature lengths and body width of the most developed element, while the count reflects the total number of discernible elements. This is obviously an arbitrary choice, the alternative is to take the mean of all elements in an event.

Altitude calculations of the vertical features are based on the measured elevations in the software Sky Charts v2.76, with the stars in the images matched to those in the program. The Earth's curvature was taken into account when calculating the altitude of the sprite features above the surface, assuming the orientation of sprite is perpendicular to the Earth's surface at the position of the sprite.

Because sprites in the dataset were observed by only one camera, the position of the sprite and individual elements could not be triangulated. The great circle distance from the camera to the triggering +CG (ST+) was used for altitude and width calculations. This of course leads to considerable errors in altitudes and absolute dimensions. Percentages or ratios of certain features to another, are associated with much smaller errors than those of absolute measures of size and altitude, because they depend hardly on the distance. We calculated the percentage of upper and lower streamers of the total length of the sprite, as well as the "vertical ratio" of the upper part of the sprite to the total length, using the center of the body as division line. A vertical ratio greater than 50% indicates that the upper part of the sprite (above the body center) is more developed than the lower part of the sprite, which is often the case for carrot sprites, whereas a smaller vertical ratio

indicates a mostly downward development of streamers, common for columniform and jellyfish sprites.

The delay of a sprite to its ST+ was determined from time-stamped PAL video fields, lasting 20 ms. For one night (24 sprites) images were recorded with only 40 ms accuracy, these have been excluded from the statistics, but most of the time do show the same correlations. The delays are the difference between the time of the ST+ and the end of the video field containing the first appearance of the sprite, as explained by *São Sabbas et al., (2003)*. Note the difference with *Van der Velde et al. (2006)* in which the start of the video frame was used, so the delay times in the present work are 20 ms longer. Note that if the real ST+ was missed by the network, an earlier +CG detected within reasonable time before the sprite may have been assumed as the ST+, which would render a longer delay. As *São Sabbas et al. (2003)* explained, the issue arises whether sprites occurring in several consecutive fields are independent from each other. We considered a sprite independent if in the video field of the new sprite the earlier one was decaying or already gone. Usually the new sprite was significantly displaced from the earlier activity as well, or had a different appearance. However, it is obvious that such sprites are not completely independent in the physical sense, the more so if the time and space between them is smaller. The number of occasions in the dataset was small, however. The issue will also have to be dealt with when high-speed cameras are used, resolving individual elements.

Table 3 summarizes the mean morphological variations per storm. They are discussed in the next section.

4.2 Results

This section discusses the correlations between morphology parameters and their relation to their causative +CG (ST+) in terms of delay, peak current and position relative to precipitation. *Figure 11* offers an overview of scatterplots, of which we discuss only the stronger correlations in detail in the following sections.

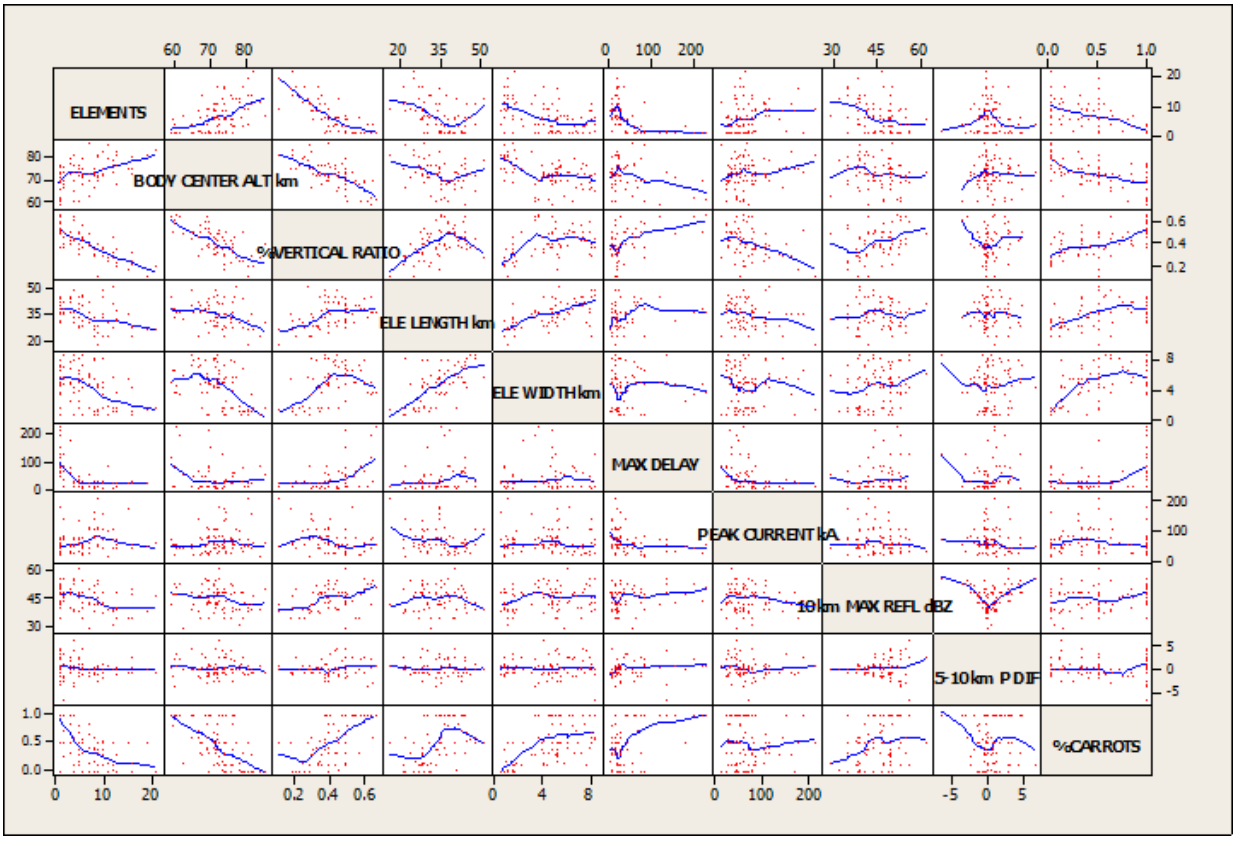

Figure 11. Overview of relations between a selection of morphological attributes (first five rows and columns) and parameters related to lightning and precipitation.

The coefficient of determination (R^2) is calculated for linear regressions. It is the percentage of variation of the y variable explained by variation of the x variable. Following *Cohen (1988)*, correlations are termed weak, moderate or strong (or small, medium, large) based on intervals of the Pearson correlation coefficient, R (not squared): 0.1-0.3, 0.3-0.5, and >0.5, respectively. P-values were calculated by software (Minitab), values smaller than 0.05 indicate the correlation is significant at the 95% level.

4.2.1 General morphology of carrots and columns

We determined the fraction of carrots of the total number of elements, giving the "intermediate" group half the weight of a true carrot. For example, a group of 2 column sprites, 2 carrot sprites and 1 intermediate sprite (6 elements) yield a fraction of 0.583 carrots (58.3%). The pure column and carrot events (no mixtures) can be identified easily by their values of 0 and 1, respectively. Using the fraction of carrots, our data (some of which are shown in *Figure 11*) shows that the most discriminating morphological parameters between carrots and columns are: element width, upper branch length, body and tendril bottom altitudes, and total vertical length. Qualitatively, carrots have thicker bodies, extend to lower altitudes and have larger upper branches.

4.2.2 Delay and number of elements , carrots and columns

A strong linear correlation (R^2 = 0.47, p-value 0.000) is found for delay and the total number of elements (*figure 12*), using the logarithm of both variables. However, there is no correlation when considering events with more than three elements. In principle it is not possible to tell whether increasingly larger sprites are also shorter delayed, because of the 20 ms resolution of standard video fields. In fact, the larger events do not converge to delays within one video field. So, typically, groups of sprites are virtually always delayed to within two PAL video fields (one frame, 40 ms) whereas any longer delayed sprites have only few elements (three or less in this dataset).

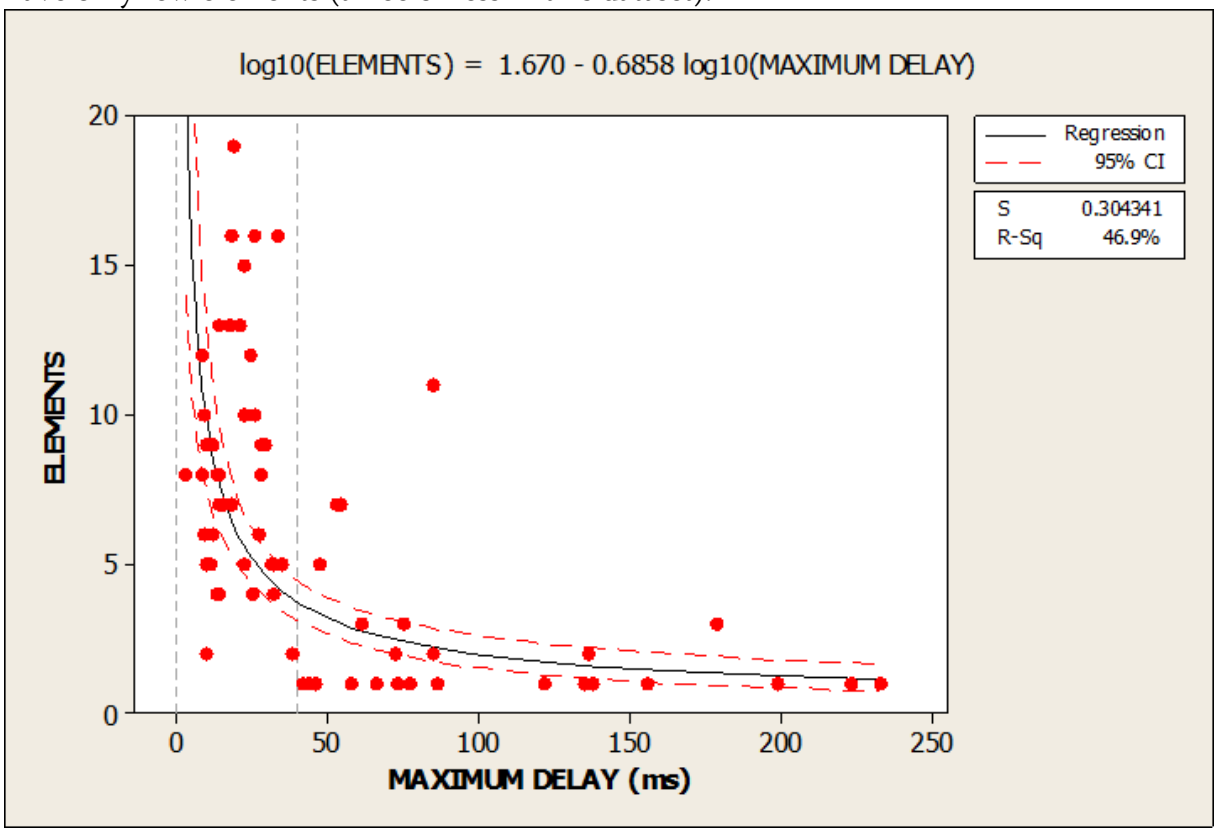

Figure 12. Number of elements versus maximum delay to the triggering +CG.

Repeating what was done in *van der Velde et al. (2006)* with the present, much larger dataset, we find for 12 pure columniform events a median delay of 26.5 ms, and for 19 pure carrot events a median delay of 85 ms. The 21 July 2003 sprites were excluded because of the larger time uncertainty, but of the five carrots excluded, four had delays over 100 ms. So, with respect to the earlier study, after correcting for the 20 ms difference resulting from the different definitions of delay time (start or end of video field), we find the delays for columns to be nearly equal while the delays for carrots in this study are 15-20 ms longer. In more detail, *Figure 13* shows the delay for the number of columniform, intermediate and carrot elements. We see that almost all columns occur within 35 ms

delay. For events containing zero columns, the delay range is significantly larger. The same is seen for intermediate events. This leaves almost solely the carrot events associated with the long delays, in particular events with carrots = 1 (bottom left graph in *figure 13*). For events containing a single carrot among other elements, the bottom right graph shows the number of extra elements (columns or intermediate) that occur by its side. The graph illustrates that events with a single carrot and nothing else (value of 0) are the most delayed of all, with a minimum of 42 ms, whereas the carrot events with several additional elements are just as short-delayed as columns and intermediate sprites.

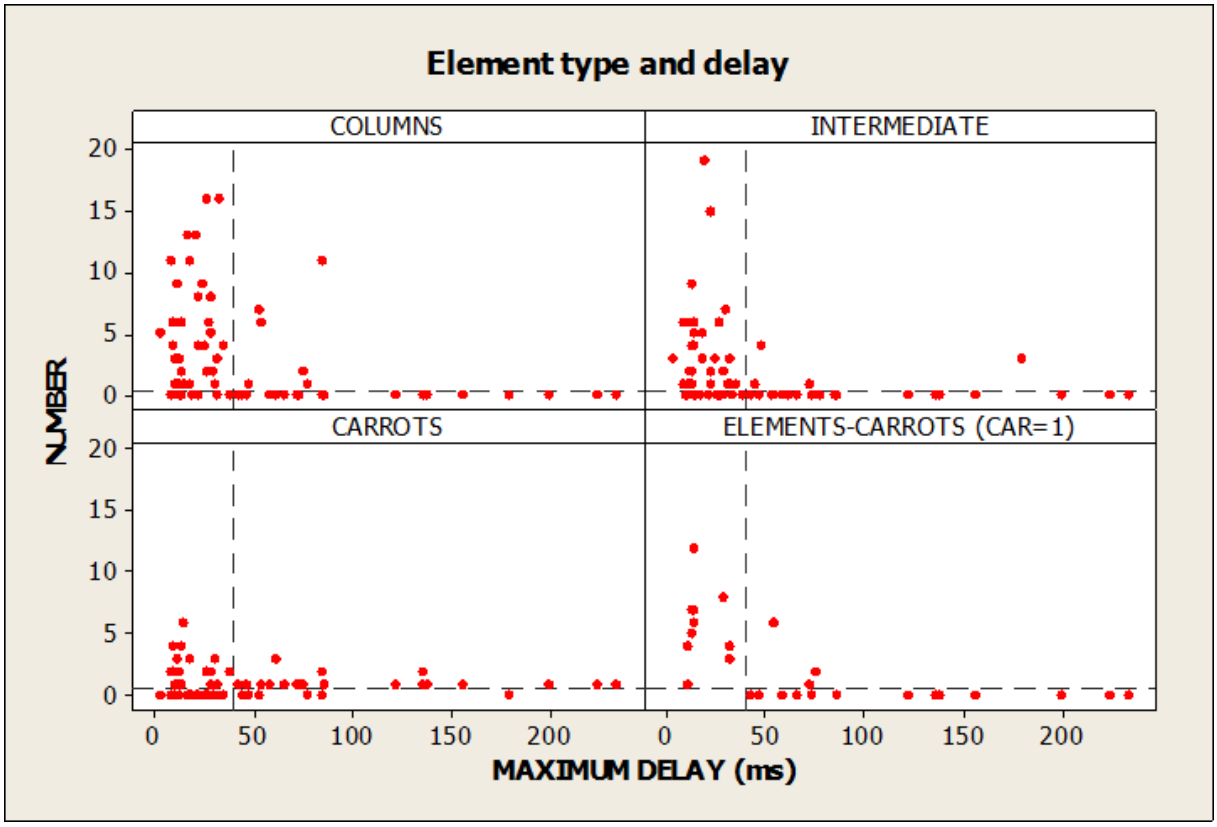

Figure 13. Maximum delay to the triggering +CG sorted by the number of columniform, intermediate and carrot elements in each sprite event. The zero value in the carrots panel, for example, indicates all events which did not contain any carrots. The last panel shows the total number of elements minus the carrots for each event that contained one carrot sprite.

4.2.3 Peak current

There is no correlation in the data between peak current and total length or width of sprite elements. Also, the number of elements, even if we consider only pure columniform events, is completely randomly distributed against peak current, in contrast with the results of *Adachi et al. (2004)* which were based on a small sample size of 12 columniform events with only 1, 2 or 3 elements (except one). *Greenberg et al. (2007)* found for a larger range of columns but the same limited sample size that the number of columns increases with charge moment changes. It is important to use a dataset large enough to identify the distribution.

While ST+ peak currents >100 kA always gave short-delayed sprites (see panel in *figure 11*), the data show no correlation within the large group of ST+ <100 kA and delay. This result is in line with figure 14 in *Lyons et al. (2006)* showing peak current versus delay.

4.2.5 Precipitation

Surprisingly, a correlation arises between the precipitation characteristics around a ST+ (not necessarily under the sprite itself) and the morphology of sprites. The most obvious is the cone-shaped scatter centered along the zero line of the difference of average precipitation rate between the circles of 5 and 10 km around the ST+ (the most uniform values) in the P DIF column in *Figure 11*. We have seen in section 3.2.1 that the highest +CG peak currents also cluster around the same zero line. The ST+ of almost all sprites with more than six elements occurred in very uniform precipitation (<2 mm/hr differences), whereas those of sprites with fewer elements occur over a wider range up to 7 mm/hr difference. A moderate statistically significant correlation is found with number of elements if we consider the absolute of precipitation difference (R^2 = 0.16, p-value = 0.000). Similar distributions are found for other measures of uniformity.

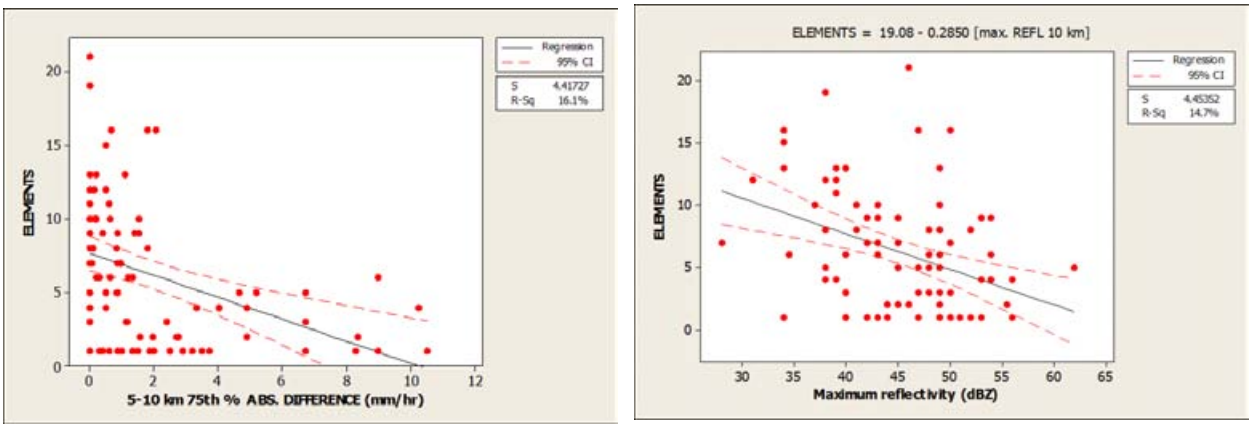

Figure 14. Sprites with more elements tend to be triggered by a +CG discharge striking in more uniform and weaker precipitation. Left: difference of 75th percentile precipitation rate between circles of 5 and 10 km radius around the ST+. Right: Maximum reflectivity found within 10 km around a ST+.

Similarly, a moderate statistically significant correlation (R^2 = 0.14, p-value = 0.000, *figure 14*) is found for the highest reflectivity within 10 km range of a ST+ and number of elements: lower reflectivity values favor sprites with more elements.

Lyons et al. (2006) found that the relative brightness of sprites increased for decreasing reflectivity, here we find an equivalent conclusion for the horizontal development of sprites.

Note, finally, that delay times do not increase for sprites triggered by more convective (less stratiform) +CG flashes.

4.2.7 Morphology interrelations

A remarkable negative correlation is found between two independent parameters: vertical ratio and number of elements (R^2 = 0.50). A slightly different formulation of the vertical ratio, obtained by dividing the upper part of the sprite (upper branches + ½ body) by the total length of the sprite, yields a straight line with a higher correlation (R^2 = 0.62, p-value = 0.000, *figure 15*). Unlike the case of delay and elements, in which delay times do not become shorter for events larger than three elements, the vertical ratio decreases uniformly with increasing number of elements. This result was not anticipated and suggests there is a yet unexplained physical relation. Note also that a vertical ratio greater than 1 (or >50%) almost only occurs for single elements (carrots).

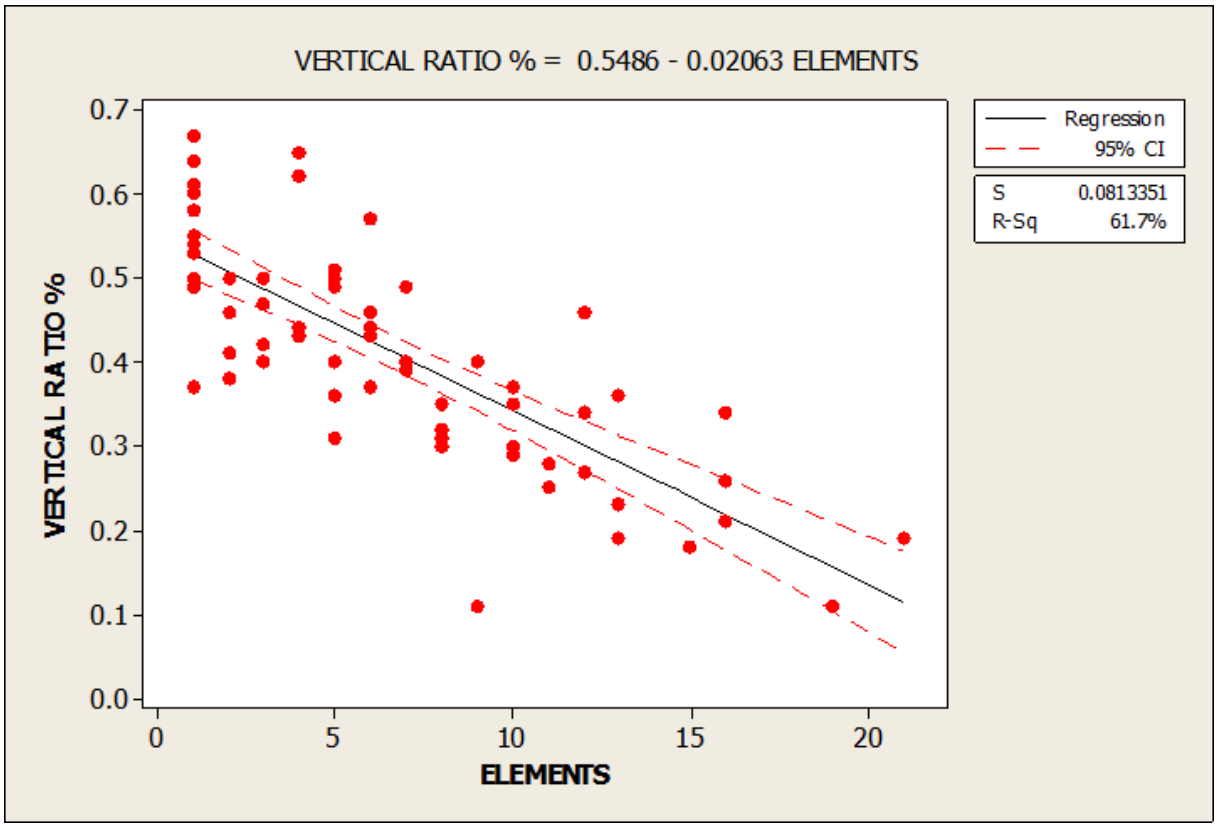

Figure 15. The relation between the vertical ratio ((upper + ½ body)/total length) and the number of elements in sprite events.

Figure 16 displays the lengths of upper and lower streamers versus elements, confirming that the tendency toward shorter upward branches (R^2 = 0.44) and longer downward tendrils (R^2 = 0.18) with larger numbers of elements is found also in the absolute dimensions. The length of the body itself does not show any correlation with number of elements. The total length of the element decreases slightly with the number of elements (R^2 = 0.17).

Vertical ratio correlates negatively with body center altitude (R^2 = 0.47, see panel in *Figure 11*), indicating that the body in general indeed occurs at lower altitudes for sprites with a high vertical ratio. Body altitude correlates negatively with the length of the upper streamers (R^2 = 0.42) and slightly positively with the length of tendrils (R^2 = 0.17, both p-value = 0.000). Because a much smaller positive correlation exists between top altitude and upper branch length (R^2 = 0.13, p-value 0.000, graph not shown), it can be concluded that the length of the upper streamers depends in the first place on the varying altitude of the body (its source) while the upper boundary remains relatively constant at the base of the ionosphere. Body center altitude correlates moderately with the number of elements (R^2 = 0.24).

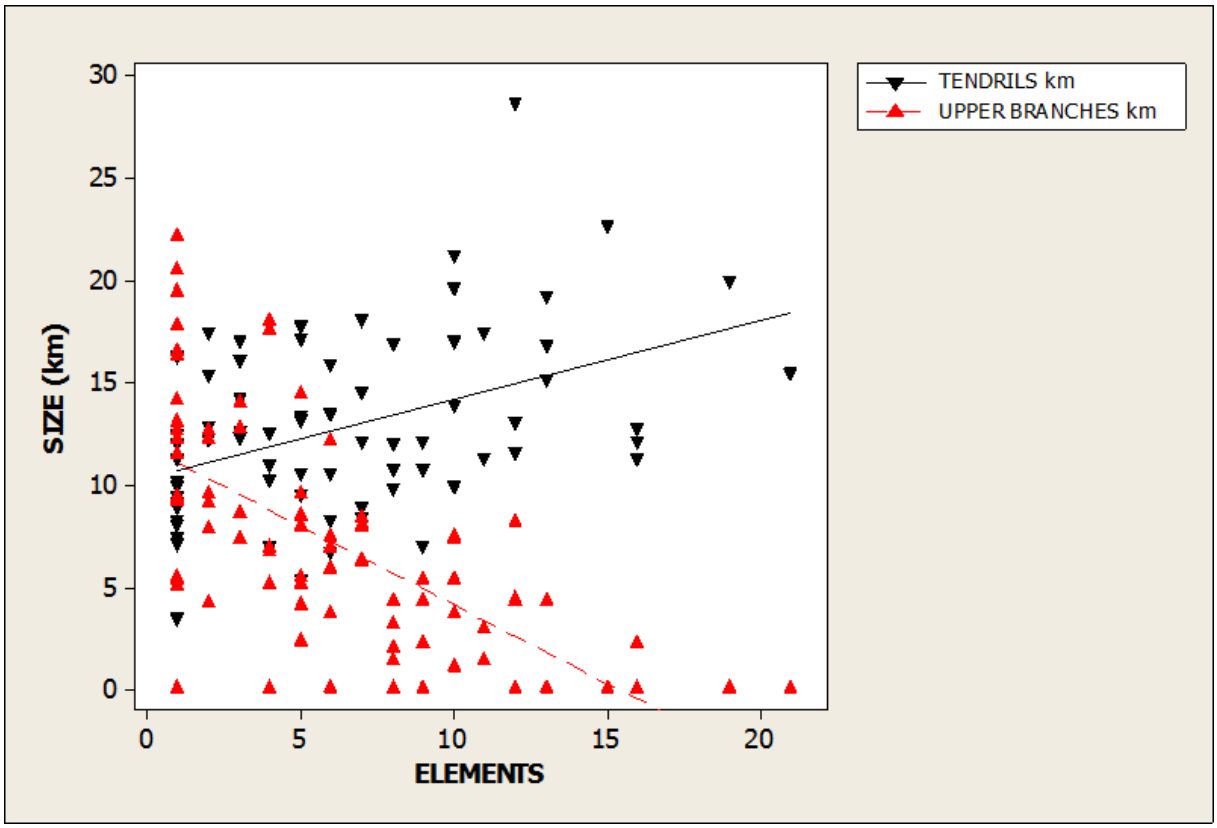

Figure 16. Length of upper streamers (red triangles) and lower streamers (black triangles) compared with the number of elements in a sprite.

Finally, elements become narrower with increasing number of elements (R^2 = 0.22, p-value 0.000) and thicker if tendrils reach to lower altitudes (R^2 = 0.36, p-value 0.000).

It is likely that element width, vertical ratio and total length would turn out smaller for large events containing a mix of different types of sprites, if these would be calculated as the average of all elements instead of only the most developed element. This would improve the correlations.

4.2.8 Storm to storm variation of average morphology

Table 3 presents an overview of average morphological features of sprites observed for the different storms, and the corresponding interquartile ranges. For example, the night of 11 September 2006 yielded many columniform sprites with a high average number of narrow elements (8), whereas 23 July 2003 was more carrot-productive with a much lower average number of elements (3.5) which are thicker with taller upper streamers. Consistent with the individual sprite results, the average delay for the latter case was twice as long.

When considering the average altitudes of sprite features it should be noted that systematic errors are possible per case, related to the orientation of the stratiform region of each MCS to the camera viewing direction. Because spider lightning (and +CG sequences) associated with sprites often propagate away from convective precipitation and the ST+, a sprite is likely to occur closer than its ST+ if the stratiform region is closer to the camera than the convective region, and vice versa. In trailing-stratiform MCS cases of 21 July 2003 and in particular 11-12 September 2006, sprites can be expected to have occurred at smaller distances, on average, which would decrease their calculated altitudes and dimensions, while for the parallel-stratiform MCS case of 28 August 2003 the sprites are expected to have occurred at greater distances. If we suppose that - under a constant ion density ledge altitude - a relative measure as the ratio of [distance top-bottom of sprite]/[distance sprite bottom-ground] ideally correlates linearly with the bottom altitude of the sprite, then the residuals to a fit correspond to the error of altitude resulting from the use of the distance of the ST+ as estimation of the true sprite distance. Indeed, it was confirmed clearly that different nights had either mostly positive or negative residuals (not shown here).

Table 3. Average values and interquartile range (in brackets) for morphological sprite features per case.

CASE*	1	2	4	6	7	AVG [25-75%]	
DATE	20-21 July 2003	23-24 July 2003	28-29 August 2003	11-12 September 2006	17-18 November 2006		
AVG DISTANCE ST+	423	477	571	398	290	**422**	km
SPRITES ANALYZED [COMPLETE]	**24 [16]**	**13 [10]**	**15 [12]**	**20 [14]**	**19 [16]**	**91 [68] TOTAL**	
AVG ST+ PEAK CURRENT	**60** [35-63]	**58** [42-63]	**73** [59-95]	**70** [39-70]	**71** [53-83]	**66 [39-77]**	kA
MAX DELAY	-	**78** [38-72]	**50** [18-70]	**39** [17-58]	**44** [11-34]	**50 [15-64]**	ms
ST+ 10 km MAX REFLECTIVITY	**45** [40-49]	**44** [43-46]	**43** [40-45]	**43** [38-48]	**50** [47-53]	**45 [40-49]**	dBZ
ST+ 10 km MEDIAN REFLECTIVITY	**34** [33-37]	**33** [30-36]	**31** [27-35]	**32** [31-34]	**35** [33-37]	**33 [31-36]**	dBZ
ELEMENTS	**5.6** [2-7]	**3.5** [1-5]	**5.9** [2-9]	**8.1** [5-12]	**6.8** [3-9]	**6.1 [2-9]**	
HORIZONTAL SIZE	**27** [12-39]	**16** [5-26]	**30** [13-40]	**33** [24-45]	**28** [15-42]	**27 [10-40]**	km
VERTICAL SIZE	**38** [34-43]	**38** [32-43]	**37** [32-45]	**30** [26-34]	**32** [28-36]	**35 [29-41]**	km
BODY WIDTH	**5** [4-7]	**5** [5-6]	**6** [5-8]	**3** [1-5]	**4** [2-5]	**4 [2-6]**	km
VERTICAL RATIO-%	**41** [34-49]	**44** [39-50]	**40** [32-45]	**34** [26-44]	**47** [37-59]	**41 [33-50]**	%
SPRITE TOP ALTITUDE	**87** [86-91]	**89** [86-91]	**84** [82-87]	**87** [83-91]	**83** [81-85]	**86 [83-89]**	km
BODY TOP ALTITUDE	**82** [79-85]	**80** [77-83]	**77** [73-80]	**82** [80-85]	**74** [70-79]	**79 [77-83]**	km
BODY BOTTOM ALTITUDE	**64** [60-68]	**65** [62-69]	**61** [59-64]	**71** [66-77]	**62** [58-65]	**65 [61-69]**	km
SPRITE BOTTOM ALTITUDE	**51** [46-56]	**53** [50-55]	**46** [43-48]	**57** [53-61]	**52** [48-56]	**52 [46-56]**	km

* Statistics only over the sprites considered measurable for morphological features. Not all features could be measured of all sprites.

4.3 Conclusions and Discussion (Part II)

The second study considered the different aspects of the morphology of sprites, as measured from video images of 91 sprites from five storms, and their relation to the delay, peak current and location of the parent lightning flash relative to precipitation. Measurements of charge moment changes were unavailable for this study, but are planned to be incorporated in a future study. In spite of the limitations resulting from the lack of triangulation, four conclusions arise unambiguously from the dataset:

1. Long-delayed sprites (>40 ms) tend to consist of three or less elements. The large majority of these are isolated carrots. Large events (many elements) occur with short delays, but do not converge to within 1 video field of delay (20 ms).
2. The ratio of upper branches to tendrils becomes smaller as the number of elements of a sprite increases. This effect is observed through the full range of sprite types. Larger vertical ratio and longer upward streamers correlate with a lower body (brighest part of the sprite) altitude.
3. The ST+ of the larger events (>6 elements) occur in highly uniform precipitation.
4. While peak currents of ST+ are higher than other +CG, peak current is not relevant to any of the morphological features.

São Sabbas et al. (2003) found no relation between "visual size and brightness" of a sprite and sprite-lightning delay times. However, their sample contained only two events delayed longer than 40 ms, not allowing a robust conclusion about long-delayed sprites. Our current study employed objective measures of different dimensions, and agrees with their results that there is no difference in sizes for sprites delayed within 40 ms from their parent +CG. Remarkably, delay times for a sample of columniform sprites as observed from Israel in winter (*Greenberg et al., 2007*) were much longer than either in the United States or in France: on average 65 ms. So, there appear to be differences between sprite-producing lightning in winter storms and summer storms, or in the properties of the lower ionosphere between seasons (or both). In our previous study (*van der Velde et al., 2006*) it was observed that VLF (Very Low Frequency) sferic clusters associated with lightning triggering carrot sprites, which were longer-delayed, lasted longer than for column sprites. The current study confirms again that long-delayed sprites were virtually all carrots, dominated by upper streamers which correlated well with lower body altitudes ($R^2 = 0.41$), despite the error from the lack of triangulation. Our observations agree with the calculations by *Pasko et al. (1996)* and *Li et al. (2008),* predicting that a longer lasting, gradual removal of charge from the cloud will result in a long-delayed sprite developing at lower altitudes, because of the slower dielectric recovery at lower altitudes. The body of the sprite appears to correspond with the altitude of the strongest quasi-electrostatic field. However, it must be kept in mind that our results did not directly show a correlation

between body altitude (or any other measured altitude) and delay time from the dataset of not triangulated sprites. The data actually show a better correlation between vertical ratio and the number of sprite elements, instead of delay time. This calls for a physical explanation. If we assume the body section of the sprite (the brightest part) to correspond with the strongest electric fields, and the top of the sprite to be limited to a fixed altitude, then a sprite with a low vertical ratio (as defined in this study) is indication that the strongest electric field occurred close to the ionospheric D-region conductivity ledge, whereas a high vertical ratio is indication for stronger electric fields at lower altitudes. Following the simulations by *Pasko et al. (1996)* and *Li et al. (2008)*, a stronger electric field at a higher altitude is occurs for more impulsive charge removal by lightning, whereas weaker but longer lasting fields will exist at lower altitudes during long continuing current lightning discharges. At altitudes just below the lower ledge of the ionospheric D-region, electric fields relax faster, dissociative attachment takes longer, and streamers develop more slowly from electron avalanches *(Pasko et al., 1998; Pasko and Stenbaek-Nielsen, 2002).* The stronger electric field creates a larger local electron density and may create more numerous electron avalanches turning into streamers (sprite elements) as they reach lower altitudes. The short time scale creates simple columniform bodies without upward streamers, while tendril growth can become as long as the lightning charge removal duration and dielectric relaxation allow. Lower-initiated sprites will be fewer in number of elements, as a result of lower electron density, and can develop more convoluted structures because the ambient electric fields last for a longer time. Upward branches have headroom to grow to similar altitudes as the tops of high-initiated sprites, while the tendrils can reach similar or lower altitudes as the more impulsively initiated sprites.

Interestingly, because impulse charge moment changes would determine both the horizontal and the vertical extents of sufficient electric fields, the lowest altitude the body and tendrils reach and the total width of a sprite would show a correlation, but this is not the case. It was already noticed by *Cummer and Stanley (1999)* that charge moment changes show no correlation with tendril altitude.

Our results show that sprites consisting of more than six elements are triggered by +CG occurring virtually always in highly uniform precipitation. The same sprites are short-delayed to within 40 ms. This could indicate that such +CG flashes draw charge from their near surroundings, from the narrow but extensive layers of charge in the stratiform region. These +CG are likely to cause greater impulse charge moment changes, because larger amounts of charge can be tapped in short time after the return stroke. The higher number of elements might alternatively be a result from the effects of radiated electric fields generated by horizontal channels of lightning flashes and their resonances (*Valdivia et al., 1997; Cho and Rycroft, 2001*), producing a finer ionization pattern above more complex lightning structures in the charge layers in the most stratiform part of the storm. The lightning mapping data in *Stanley (2000)* and *Stanley et al. (2007)* suggest that the distribution of horizontal lightning branches influences the horizontal distribution of sprite elements. Since electric fields at sprite altitudes are, despite the details in the

underlying lightning channels, circular or oval and devoid of structure, sequential/progressively discharging of horizontally separated lightning branches could position sprites in an event from a quasi-electrostatic perspective. But sprite elements are often so closely spaced that this is unlikely to be the only mechanism, so the radiation mechanisms remain viable as possible explanations.

4.4 Summary

Our results show: 1) the importance of sequences of positive lightning flashes in the sprite triggering lightning process, often exhibiting convective-to-stratiform propagation similar to spider lightning discharges. 2) The importance of uniform precipitation for high peak currents (relevant to elves) and the largest sprites in terms of elements. 3) Further support for the relation between long-delayed sprites and their altitude, often being of the carrot type and of few elements. 4) An inverse linear relation between ratio of upper to lower streamers in sprites and their number of elements, providing strong indications that the initiation altitude of a sprite controls how many elements will form.

Acknowledgments

We wish to express our gratitude for the company Météorage for providing us the cloud-to-ground lightning detection data. We also acknowledge the great deal of work done by Thomas Allin and Olivier Chanrion on the programming and documentation of the camera systems and sprite records at Pic du Midi. This study has been performed as part of the European Union research training network "Coupling of Atmospheric Layers" (CAL), sponsored by the FP5 program under contract no. HPRN-CT-2002-00216 and was completed with funds of the "Gamma-ray Imaging" project from the Spanish Ministery of Science and Education (principal investigator: Joan Montanyà).

References

Adachi, T., H. Fukunishi, Y. Takahashi and M. Sato, 2004: Roles of the EMP and QE field in the generation of columniform sprites. Geophys. Res. Lett., 31, L04107, doi: 10.1029/2003GL019081, 2004.

Bell, T.F., Reising, S.C. and Inan, U.S., 1998. Intense continuing currents following positive cloud-to-ground lightning associated with red sprites. *Geophys. Res. Lett.,* 25, p. 1285.

Boccippio, D. J., E. R. Williams, S. J. Heckman, W. A. Lyons, I. T. Baker, and R. Boldi, Sprites, ELF transients, and positive ground strokes, ***Science,*** 269, 1088, 1995.

Carey, L. D., M. J. Murphy, T. L. McCormick, and N. W. S. Demetriades (2005), Lightning location relative to storm structure in a leading-line, trailing-stratiform mesoscale convective system, *J. Geophys. Res.*, 110, D03105, doi:10.1029/2003JD004371.

Cummer, S. A. (2003), Current moment in sprite-producing lightning, *J. Atm. and Sol.-Terr. Phys.*, 65, 499

Cummer, S.A. and W.A. Lyons, 2005: Implications of lightning charge moment changes for sprite initiation. J. Geophys. Res., 110, A04304, doi:10.1029/2004JA010812.

Cummer, S. A., and M. Stanley (1999), Submillisecond Resolution Lightning Currents and Sprite Development: Observations and Implications, *Geophys. Res. Lett.*, 26(20), 3205–3208.

Cummer, S. A., N. Jaugey, J. Li, W. A. Lyons, T. E. Nelson, and E. A. Gerken (2006), Submillisecond imaging of sprite development and structure, *Geophys. Res. Lett.*, 33, L04104, doi:10.1029/2005GL024969.

Cummins, K. L., M. J. Murphy, E. A. Bardo, W. L. Hiscox, R. B. Pyle, and A. E. Pifer (1998), A Combined TOA/MDF Technology Upgrade of the U.S. National Lightning Detection Network, *J. Geophys. Res., 103*(D8), 9035–9044.

Greenberg, E., C. Price, Y. Yair, M. Ganot, J. Bór, and G. Sátori, (2007), ELF transients associated with sprites and elves in eastern Mediterranean winter thunderstorms. J. Atm. And Sol.-Terr. Phys., 69, 1569-1586, doi:10.1016/j.jastp.2007.06.002

Hu, W., S. A. Cummer, W. A. Lyons and T. E. Nelson, 2002, Lightning charge moment changes for the initiation of sprites, *Geophys. Res. Lett.*, 29 (8), 1279.

Johnson, M. P., and U. S. Inan, 2000, Sferic clusters associated with Early/Fast VLF Events, *Geophys. Res. Lett.*, 27, 1391–1394.

Lang, T. J., S. A. Rutledge, and K. C. Wiens, 2004, Origins of positive cloud-to-ground lightning flashes in the stratiform region of a mesoscale convective system, *Geophys. Res. Lett.*, 31, L10105, doi:10.1029/2004GL019823.

Füllekrug, M., Mareev, E. A. and Rycroft, M. J. (Eds.), 2006 , "Sprites, Elves and Intense Lightning Discharges", NATO Science Series II: Mathematics, Physics and Chemistry, Vol. 225, 2006, XVI, Springer, 398 p.

Li, J., S. A. Cummer, W. A. Lyons, and T. E. Nelson (2008), Coordinated analysis of delayed sprites with high-speed images and remote electromagnetic fields, J. Geophys. Res., 113, D20206, doi:10.1029/2008JD010008.

Lyons, W. A. (1994), Characteristics of luminous structures in the stratosphere above thunderstorms as imaged by low-light video, *Geophys. Res. Lett.*, 21(10), 875–878.

Lyons, W. A. (1996), Sprite observations above the U.S. High Plains in relation to their parent thunderstorm systems, *J. Geophys. Res.*, 101(D23), 29,641–29,652.

Lyons, W. A., L.M. Andersen, T.E. Nelson and G.R. Huffines, (2006), Characteristics of sprite-producing electrical storms in the STEPS 2000 domain. On line summary and CD, ***2nd Conf. on Meteorological Applications of Lightning Data***, AMS, Atlanta, 19 pp.

Lyons, W. A., E. R. Williams, S. A. Cummer, and M. A. Stanley, (2003), Characteristics of sprite-producing positive cloud-to-ground lightning during the 19 July 2000 STEPS mesoscale convective systems, *Mon. Weather Rev.*, 131, 2417–2427.

MacGorman, D. R., and C. D. Morgenstern (1998), Some characteristics of cloud-to-ground lightning in mesoscale convective systems, *J. Geophys. Res.*, 103(D12), 14,011–14,024.

Marshall, J. S. and W. M. Palmer, 1948, The distribution of raindrops with size. J. Meteor., 5, 165-166.

Marshall, R. A., U. S. Inan, and W. A. Lyons (2007), Very low frequency sferic bursts, sprites, and their association with lightning activity, *J. Geophys. Res.*, 112, D22105, doi:10.1029/2007JD008857.

McHarg, M. G., R. K. Haaland, D. Moudry, and H. C. Stenbaek-Nielsen (2002), Altitude-time development of sprites, *J. Geophys. Res.*, 107(A11), 1364, doi:10.1029/2001JA000283.

McHarg, M. G., H. C. Stenbaek-Nielsen, and T. Kammae (2007), Observations of streamer formation in sprites, Geophys. Res. Lett., 34, L06804, doi:10.1029/2006GL027854.

Moudry, D., H. Stenbaek-Nielsen, D. Sentman, and E. Wescott (2003) Imaging of elves, halos and sprite initiation at 1 ms time resolution, *J. Atmos. Solar-Terr. Phys., 65*, 509-518.

Neubert T., et al., (2005), Co-ordinated observations of transient luminous events during the EuroSprite2003 campaign, J. Atm. and Sol.-Terr. Phys., 67, 807-820.

Ohkubo A., H. Fukunishi, Y. Takahashi, and T. Adachi, 2005, VLF/ELF sferic evidence for in-cloud discharge activity producing sprites, *Geophys. Res. Lett.*, 32, L04812, doi:10.1029/2004GL021943.

Parker, M.D., and R.H. Johnson (2000), Organizational Modes of Midlatitude Mesoscale Convective Systems. *Mon. Wea. Rev.*, **128**, 3413–3436.

Parker, M.D., S.A. Rutledge, and R.H. Johnson (2001), Cloud-to-Ground Lightning in Linear Mesoscale Convective Systems. *Mon. Wea. Rev.*, **129**, 1232–1242.

Pasko, V. P., and H. C. Stenbaek-Nielsen (2002), Diffuse and streamer regions of sprites, *Geophys. Res. Lett.*, 29(10), 1440, doi:10.1029/2001GL014241.

Pasko, V. P., U. S. Inan, and T. F. Bell (1996), Sprites as luminous columns of ionization produced by quasi-electrostatic thundercloud fields, *Geophys. Res. Lett.*, 23(6), 649–652.

Pasko, V. P., U. S. Inan, T. F. Bell, and Y. N. Taranenko (1997), Sprites produced by quasi-electrostatic heating and ionization in the lower ionosphere, *J. Geophys. Res.*, 102(A3), 4529–4562.

Rutledge, S.A., and D.R. MacGorman, 1988: Cloud-to-Ground Lightning Activity in the 10–11 June 1985 Mesoscale Convective System Observed during the Oklahoma–Kansas PRE-STORM Project. *Mon. Wea. Rev.*, **116**, 1393–1408.

Rutledge, S.A., and W.A. Petersen, (1994), Vertical Radar Reflectivity Structure and Cloud-to-Ground Lightning in the Stratiform Region of MCSs: Further Evidence for In Situ Charging in the Stratiform Region. *Mon. Wea. Rev.*, **122**, 1760–1776.

São Sabbas, F. T., D. D. Sentman, E. M. Wescott, O. Pinto, Jr. Odim Mendes, Jr. and M. J. Taylor, 2003, Statistical analysis of space–time relationships between sprites and lightning, *J. Atm. and Sol.-Terr. Phys.*, 65, 5, 525-535.

Soula, S., O. van der Velde, J. Montanya, T. Neubert, O. Chanrion, and M. Ganot (2009), Analysis of thunderstorm and lightning activity associated with sprites observed during the EuroSprite campaigns: Two case studies, *Atmos. Res.* 91, 514-528, doi:10.1016/j.atmosres.2008.06.017

Stanley, M.A., 2000: Sprites and their parent discharges. PhD. Dissertation, New Mexico Institute of Mining and Technology, Socorro, NM, 163 pp.

Stanley, M., P. Krehbiel, M. Brook, C. Moore, W. Rison, and B. Abrahams (1999), High speed video of initial sprite development, *Geophys. Res. Lett.*, 26(20), 3201–3204.

Stanley, M. A., W. A. Lyons, T.E. Nelson, P. R. Krehbiel, W. Rison, and R. J. Thomas (2007): Comparison of Sprite Locations With Lightning Channel Structure *Eos Trans. AGU, 88*(52), Fall Meet. Suppl., Abstract E41A-07

Stenbaek-Nielsen, H. C., D. R. Moudry, E. M. Wescott, D. D. Sentman, and F. T. Sâo Sabbas (2000), Sprites and possible mesospheric effects, *Geophys. Res. Lett.*, 27(23), 3829–3832.

Tukey, J. W. (1977), Exploratory Data Analysis. Addison-Wesley, Reading, MA, 39-43

Valdivia, J. A., G. Milkh, and K. Papadopoulos, 1997, Red sprites: Lightning as a fractal antenna, *Geophys. Res. Lett.*, 24, 3169–3172.

Van der Velde, O. A., Á. Mika, S. Soula, C. Haldoupis,T. Neubert and U. S. Inan (2006), Observations of the relationship between sprite morphology and in-cloud lightning processes. J. Geophys. Res., 111, D15203, doi:10.1029/2005JD006879.

Wescott, E.M., D. D. Sentman, M. J. Heavner, D. L. Hampton, W. A. Lyons and T. Nelson, (1998), Observations of `Columniform' sprites, *J. Atm. and Sol.-Terr. Phys.*, 60, 733-740.

Wescott, E.M., Stenbaek-Nielsen, H.C., Sentman, D.D., Heavner, M.J. and São Sabbas, F.T., 2001. Triangulation of sprites, associated halos and their possible relation to causative lightning and micro-meteors. *J. Geophys. Res.*, 106, A6, pp. 10467–10477.

Williams, E. R., 1998, The positive charge reservoir for sprite-producing lightning, J. Atm. and Sol.-Terr. Phys., 60, 689-692.

7 Analyse du premier Jet Géant observé au-dessus du continent Nord-Américain

7.1 Résumé

Ce chapitre reprend une étude qui a fait l'objet d'un article publié dans la revue Journal of Geophysical Research:

- Van der Velde, O. A., W. A. Lyons, T. E. Nelson, S. A. Cummer, J. Li, and J. Bunnell (2007), Analysis of the first gigantic jet recorded over continental North America, *J. Geophys. Res., 112,* D20104, doi:10.1029/2007JD008575.

L'article est inséré dans le chapitre après une synthèse qui en fait une présentation en décrivant la démarche de l'article, et en résumant chaque partie de l'article. Par ailleurs, une partie de ce travail a fait l'objet d'une communication orale lors de la Conférence d'Union Géophysique Americain:

- Van der Velde, O. A., W. A. Lyons, S. A. Cummer, T. Nelson: Analysis of the First Gigantic Jet Recorded From the Continental United States. American Geophysical Union, Fall Meeting, San Francisco, 11-15 December 2006, abstract AE41A-07

Une analyse similaire d'un cas avec deux Jets Géants observés en août 2007 à été présenté par W. Lyons:

- Van der Velde, O. A., W. A. Lyons, S. A. Cummer, M. B. Cohen, D. D. Sentman, N. Jaugey, T. E. Nelson, R. Smedley (2007), Electromagnetical, Visual and Meteorological Analyses of two Gigantic Jets Observed Over Missouri, USA, Eos Trans. AGU, 88(52), Fall Meet. Suppl., Abstract AE23A-0895

I- Contexte de l'étude

Il n'existe que très peu de cas d'observations de ces membres de la famille des TLEs que sont les Jets géants. Deux cas ont été publiés à ce jour dans la revue Nature en 2002 et 2003, avec 1 événement dans un cas et 5 événements dans l'autre. C'est donc un phénomène rare par rapport à ses "petits frères" que sont les blue jets et ses "petits cousins" que sont les sprites et les elves. Ainsi ils démarrent du sommet du nuage et peuvent atteindre environ 90 km d'altitude par des développements de branchement vers la base

de l'ionosphère. C'est cette altitude atteinte et ce développement caractéristique qui les distinguent des autres TLEs qui démarrent aussi du nuage tels que les "blue jets", les "palm trees". Comme les simples jets, les gigantic jets sont produits au-dessus de la zone convective d'orages à fort développement vertical. Cette étude a été consacrée au premier cas de gigantic jet observé directement au-dessus d'un orage sur le continent américain.

II- Méthode d'observation

Le Jet géant (GJ) analysé dans cette étude a été observé avec 2 caméras identiques à une faible distance l'une de l'autre, 2,35 km, et localisées dans le Sud-Ouest du Texas près de Marfa aux Etats-Unis. Ces deux caméras étaient des Watec 120N équipées d'optique procurant un champ de 30° de focale 12mm et d'ouverture f/0,8. Elles étaient orientées vers le Sud-Est dans la nuit du 13 Mai 2005 lorsque l'observation du Jet a été faite vers 0423 UTC. Le mode d'acquisition à travers un enregistreur vidéo fournissait des images intégrées sur une durée de 4,27 secondes. De ce fait, l'événement lumineux n'était présent que sur une image pour chaque caméra ce qui ne permet d'appréhender ni la vitesse de développement vertical ni la durée approximative. Une méthode reposant sur la comparaison des temps de sprites observés après le Jet et des temps d'éclairs nuage-sol a permis de faire une estimation de la probable fourchette temporelle de production du Jet d'une durée de 5 secondes environ. D'autre part, l'utilisation d'un logiciel de carte du ciel superposée à l'image a permis de déterminer très précisément l'azimuth du Jet à 122,25°. Dans cette direction, 2 orages potentiellement générateurs étaient localisés, l'un à 230 km environ et l'autre à 305 km. La triangulation à partir des 2 caméras ne permet de lever l'ambiguité sur les 2 orages candidats à l'origine du Jet mais une observation pertinente telle que l'altitude du sommet du nuage et l'altitude maximale du jet (par rapport aux observations de Pasko et al. 2002 et Su et al. 2003) renforce la probabilité pour l'orage le plus éloigné.

III- Analyse

L'analyse des observations porte tout d'abord sur les caractéristiques du Jet. Dans sa morphologie, dans la répartition de la luminosité et dans sa structure branchée, ce Jet a plus de similitudes avec les cas de GJ déjà observés par d'autres auteurs qu'avec les cas de blue jets. Une comparaison avec les sprites observés dans les mêmes conditions dans la même nuit avec les caméras montre que la partie supérieure du GJ sous forme de branches ascendantes reste moins lumineuse que dans les cas de GJ observés auparavant. Pour ce qui est du développement vertical, plusieurs possibilités sont envisagées en fonction de l'intersection de la direction du GJ et d'un amas nuageux d'altitude élevée. En fonction des distances correspondantes, l'altitude du sommet de la partie lumineuse du GJ est calculée et le résultat le plus probable par rapport à sa forme donnerait une altitude de 70 (80) km, ce qui déterminerait l'orage générateur. Dans ces conditions la largeur de la parti fourchée du GJ serait d'environ 4 (5) km. (position sur la partie intense d'orage loin la plus probable)

Dans la période probable de production du GJ de 5 secondes, des signaux électromagnétiques ont été enregistrés dans plusieurs gammes de fréquence. Ainsi, le réseau NLDN américain a enregistré quelques éclairs nuage-sol dans la direction du GJ. Un système de détection en ELF/ULF (3-3000 Hz) a également enregistré des signaux sous forme de sférics au nombre de 3 et de polarité positive. Comme le NLDN n'a pas enregistré des éclairs nuage-sol positifs correspondant à tous les sférics, on en déduit qu'il a peut-être des difficultés de détection de signaux particuliers relatifs à ces GJ. (Dans le cas d'un décharge intra-nuageux, il est probable que NLDN ne les détecte pas, mais une displacement de grande charge pourrait être détecte en ELF). Les variations de moment de charge relevées dans les enregistrements ne sont pas du tout du même ordre de grandeur de celles trouvées dans les cas de GJ publiés. Il est donc difficile d'associer un des signaux au GJ.

Les orages se trouvant dans la direction du GJ ont été analysés sur la base des observations radar issues du réseau américain NEXRAD et sur la base d'observations satellitaires issues de GOES. Le système le plus proche des caméras était de nature multicellulaire tandis que l'orage le plus probable pour avoir produit le jet était plutôt de nature supercellulaire. Les données radar ont signalé une forte probabilité de grêle dans les deux systèmes mais toutefois, aucune observation pertinente n'a permis de dire si les orages étaient classés comme sévère ou pas. Le développement vertical d'un cœur convectif dans l'orage le plus éloigné des caméras avait atteint au moins 17 km, dépassant largement l'altitude locale de la tropopause. Mais la direction du GJ ne passe pas directement dans cette région. La position probable du GJ serait donc dans une région correspondant à l'enclume qui atteint une altitude de 10 à 12 km et qui donne des réflectivités de moins de 25 dBZ (la position des trois candidats le plus loin) ou une région plus proche characterisée par forte precipitation et un sommet de 14-15 km d'altitude.

L'activité d'éclair nuage-sol a été analysée pour l'orage supercellulaire qui a probablement produit le GJ. Le taux d'éclair nuage-sol n'a pas été élevé globalement avec un taux de l'ordre de 4 min^{-1} sur une période d'une heure entourant l'instant de production le jet. On a pu remarquer un zone active sous forme d'un cluster d'éclairs dans la direction du GJ avec une majorité d'éclairs positifs et un fort taux dans les secondes précédant la production du GJ. Ce "saut" d'éclairs nuage-sol positifs a duré quelques 20 secondes avec un taux de production d'1 éclair toutes les 5 secondes. Par contre après le jet dans cette zone peu d'éclairs des 2 signes étaient produits. On a pu voir également une forte production d'éclairs nuage-sol positifs de faible pic de courant 2 minutes avant le GJ, ces éclairs pouvant être en fait des éclairs intra-nuage mal classés par le système. Un calcul d'énergie a permis d'établir le rôle du GJ dans la continuité de l'activité de l'orage.

30 sprites étaient observés dans la région de l'orage considéré comme le producteur du GJ et sur une durée de 3h 30 environ. Le premier sprite était détecté 28 minutes après le jet.

IV- Discussion

Le GJ étudié est un cas rare observé au-dessus d'un orage continental et non maritime. Un certain nombre de similitudes à d'autres GJ nous a permis d'identifier l'orage qui en était à l'origine. Nous montrons que ce phénomène peut être produit à une certaine distance du cœur de l'orage avec un très fort développement vertical, en l'occurrence à quelques 30 km et dans la direction sous le vent. L'activité d'éclair juste avant le GJ était probablement fortement dominée par des nuage-sol positifs ce qui laisse penser à une structure de charge tripolaire inversée avec une charge positive à des altitudes moyennes dans le nuage. Cette caractéristique d'orages sévères est pour le moins courante dans cette région des Etats-Unis. Les éclairs nuage-sol déclenchés dans la partie intermédiaire de l'orage pourrait avoir un rôle dans le déclenchement du GJ produit par des charges de la zone élevée de l'orage. La comparaison des activités de notre orage et des orages ayant produit des GJ documentés par d'autres auteurs, le notre était peu actif mais le déroulement des phases d'activité montre certaines similitudes. Le processus le plus probable, si la charge électrique était supposé de provenir de la région de charge plus haute dans le nuage, était donc un GJ negatif avec des charges négatives drainées vers la partie supérieure de l'atmosphère. Toutefois, l'activité complexe des éclairs, la localisation incertaine du GJ par rapport au nuage, et l'absence d'un signal ELF clairement attribuable au cet GJ rend la conclusion de la charge électrique déplacée incertaine.

7.2 Article

JOURNAL OF GEOPHYSICAL RESEARCH, VOL. 112, D20104, doi:10.1029/2007JD008575, 2007

Analysis of the first gigantic jet recorded over continental North America

Oscar A. van der Velde,[1] Walter A. Lyons,[2] Thomas E. Nelson,[2] Steven A. Cummer,[3] Jingbo Li,[3] and James Bunnell[4]

Received 22 February 2007; revised 30 April 2007; accepted 20 June 2007; published 17 October 2007.

[1] Two low-light cameras near Marfa, Texas, recorded a gigantic jet over northern Mexico on 13 May 2005 at approximately 0423:50 UTC. Assuming that the farthest of two candidate storm systems was its source, the bright lower channel ended in a fork at around 50–59 km height with the very dim upper branches extended to 69–80 km altitude. During the time window containing the jet, extremely low frequency magnetic field recordings show that there was no fast charge moment change larger than 50 coulomb times kilometers (C km) but there was a larger and slower charge moment change of 520 C km over 70 ms. The likely parent thunderstorm was a high-precipitation supercell cluster containing a persistent mesocyclone, with radar echo tops of at least 17 km. However, photogrammetric analysis suggests that the gigantic jet occurred over the forward flank downdraft region with echo tops of 14 km. This part of the supercell may have had an inverted-polarity charge configuration as evidenced by positive cloud-to-ground lightning flashes (+CG) dominating over negative flashes (−CG), while −CGs occurred under the downwind anvil. Four minutes before the gigantic jet, −CG activity practically ceased in this area, while +CG rates increased, culminating during the 20 s leading up to the gigantic jet with four National Lightning Detection Network–detected +CGs. A relative lull in lightning activity of both polarities was observed for up to 1.5 min after the gigantic jet. The maturing storm subsequently produced 30 sprites between 0454 and 0820 UTC, some associated with extremely large impulse charge moment change values.

Citation: van der Velde, O. A., W. A. Lyons, T. E. Nelson, S. A. Cummer, J. Li, and J. Bunnell (2007), Analysis of the first gigantic jet recorded over continental North America, *J. Geophys. Res.*, *112*, D20104, doi:10.1029/2007JD008575.

1. Introduction

[2] The discovery of gigantic jets by *Pasko et al.* [2002] from Puerto Rico and by *Su et al.* [2003] from Taiwan enlarged the family of documented types of middle atmospheric transient luminous events (TLEs). While red sprites and elves are common over large thunderstorm complexes [*Lyons et al.*, 2003a] and oceanic winter thunderstorms [*Takahashi et al.*, 2003], both ground-based and space-based observations of the jet-like phenomena in the TLE family have been comparatively sporadic.

[3] Jet-like TLEs (upward lightning, blue starters, blue jets, gigantic jets, and palm tree events) share the common characteristic that they emerge from the top of a thunderstorm [*Lyons et al.*, 2003b], as opposed to sprites and elves, which initiate in the mesosphere [*Sentman et al.*, 1995]. The few available observations have shown the stratospheric jets to be blue [*Wescott*, 1996; *Wescott et al.*, 1995, 1998, 2001], but palm tree events have been observed as red [*Heavner*, 2000]. The gigantic jets reported by *Pasko et al.* [2002] and *Su et al.* [2003] reached higher altitudes than blue jets, 70–90 km instead of 40 km, and did not exhibit a simple cone shape but exhibited one or more collimated rising channels, branching out into altitudes where sprites normally occur, at 50–90 km. The five events of *Su et al.* [2003] could be grouped in "tree" and "carrot" type jets and the upward speed (1000 km s^{-1}) was an order of magnitude faster than that of *Pasko et al.* [2002]. A characteristic found in both observations, as well as by *Tsai et al.* [2006], was a long-lasting afterglow of the transition zone and lower part of the gigantic jet. Note that palm tree or troll events (occurring during horizontally extensive sprites) bear considerable resemblance to gigantic jets by their appearance, with lower top altitudes ranging from 32 to 61 km. They can appear as grouped jets. *Marshall and Inan* [2007] recorded 12 palm tree events during two observing seasons in New Mexico. They proposed that these secondary TLEs develop in response to the enhanced vertical electric field when ionospheric potential is brought closer to the cloud top via the body of sprites. They also occur in Europe: Two such events

[1] Laboratoire d'Aérologie, CNRS, Université de Toulouse, Toulouse, France.
[2] FMA Research, Inc., Fort Collins, Colorado, USA.
[3] Electrical and Computer Engineering Department, Duke University, Durham, North Carolina, USA.
[4] Benbrook, Texas, USA.

0148-0227/07/2007JD008575$09.00

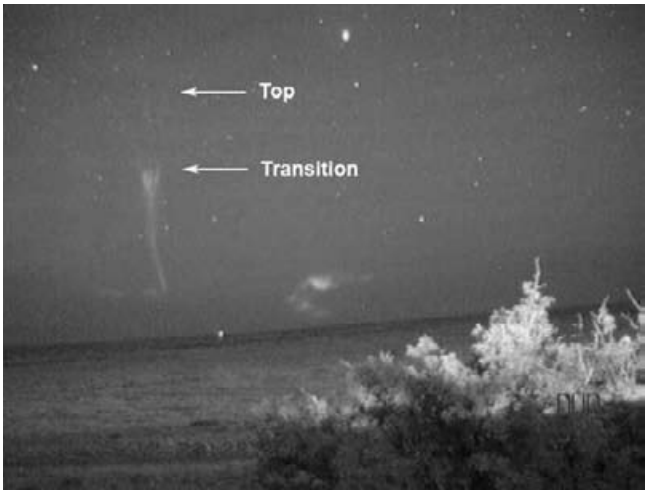

Figure 1. Low-light TV camera 4-s stacked image of the gigantic jet, seen in southeasterly direction from Marfa, Texas, 13 May 2005 at approximately 0423:50 UTC (corrected time). The horizontal field of view is 30°. Image is printed with permission (J. Bunnell).

were found by one of the authors (O. van der Velde) over the western Mediterranean Sea during Eurosprite 2005.

[4] Many jets appear to emanate from cores of thunderstorms with cloud tops reaching 16 km or more, unlike sprites, which typically occur over the stratiform region of thunderstorms. Previous studies have not found any triggering cloud-to-ground lightning activity, but the cases of *Pasko et al.* [2002] and *Su et al.* [2003] had associated large extremely low frequency (ELF) electromagnetic signals indicative of a large upward transfer of negative charge. In this paper we discuss a new observation of a gigantic jet, the first one to be recorded from the continental United States, with available meteorological data allowing the first in-depth analysis of a thunderstorm that produced cloud top TLEs since the analyses by *Wescott et al.* [1998] and *Lyons et al.* [2003b].

2. Observing Method

[5] Two Astrovid Stellacam II (Watec 120N) low-light monochrome surveillance cameras were installed by coauthor J. Bunnell near Marfa, in southwestern Texas. They were fitted with Cosmicar/Pentax 12 mm f/0.8 lenses, used at their widest aperture, that give a horizontal field of view of 30°. Both had a view to the southeast with a baseline of 2.35 km, oriented NNW-SSE, not perpendicular to the direction of the gigantic jet. To allow for longer unmanned operation, the cameras were set to frame integration mode, producing stacked images, each spanning 4.27 s. The images were each stored by a digital video recorder (DVR), which overlays a time stamp from its uncontrolled clock and varies according to where the DVR paused during the 4-s frame. For the camera that produced the image of Figure 1, gamma was set to "high" (0.35), and the manual gain dial was set to 3 ticks out of 15 (12 dB).

[6] Before local midnight on 13 May 2005, around 0423 UTC, both cameras imaged what appears to be a gigantic jet (Figure 1). The camera integration mode generated only a single image for each camera, not a video sequence, so that we cannot infer upward velocities or the total duration from the footage. The DVR time stamp could not resolve the gigantic jet time to within 4 s and had an unknown drift. However, the rich star field of the image, the presence of a distant mercury vapor light with known coordinates, and an astronomical program with the capability to overlay stars over an image made it possible to obtain a more precise estimate of the gigantic jet time and azimuth. Following the gigantic jet, 30 sprites were observed. Because sprites can be linked to a positive cloud-to-ground lightning strike [*Boccippio et al.*, 1995], a successful comparison of the drifting DVR time stamps with the times of positive cloud-to-ground lightning flashes (+CG) strikes resulted in a high confidence estimate that the gigantic jet occurred in the time window 0423:47–0423:52 UTC, 13 May 2005 (4 s of play in the time stamp and a rounding error of 1 s).

[7] The azimuth of the event was determined to be 122.25°. The great circle path crosses two thunderstorm cores at about 230 and 305 km distance, both over extreme northern Mexico. To ascertain which storm produced the gigantic jet, triangulation was attempted using the azimuths found by the star fixes of the two cameras. The parallax was only 15–20′, so the resulting intersection point was very sensitive to small errors. The errors of star fixing, pixel width, and cursor readout of the angles, as well as comparing distances of sprite +CGs with triangulated distances, made it clear that both storms remained potential gigantic jet-producing candidates. However, we postulate that the

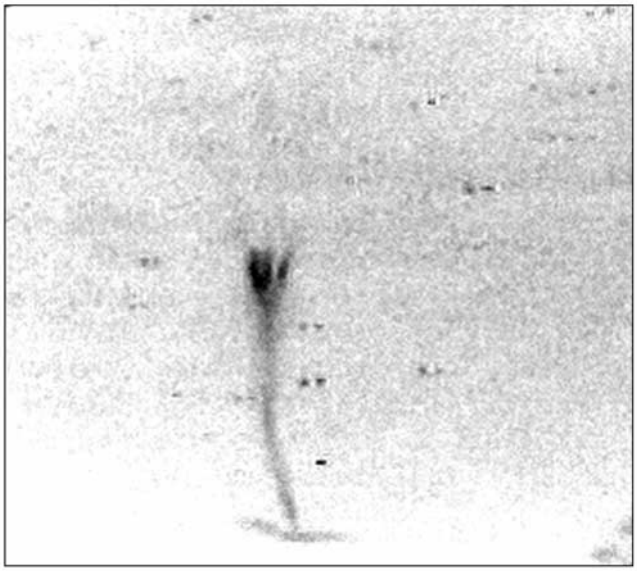

Figure 2. Contrast-enhanced inverted image of the gigantic jet, obtained by overlaying the jet in the images from the two cameras. The dots are stars displaying a parallax of 15–20 arc min. Discernable branches stretch upward from the bright transition zone.

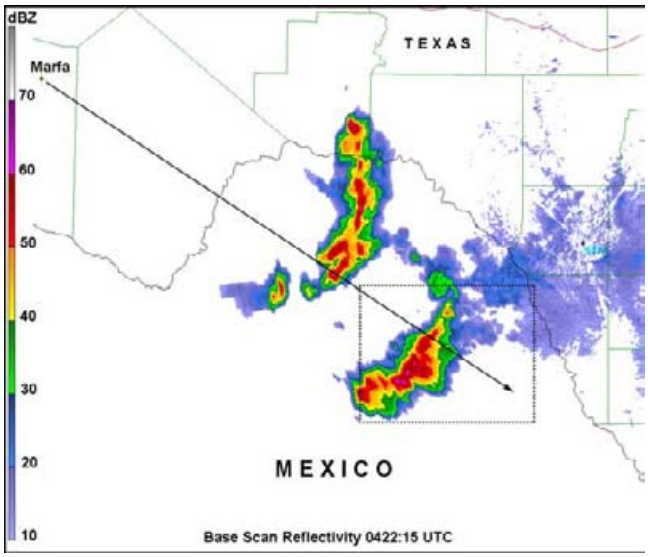

Figure 3. Base scan radar reflectivity at 0422 UTC from the Laughlin AFB, Texas, radar. The line of sight to the gigantic jet is indicated by an arrow. The box indicates the area of lightning activity plotted in Figure 6.

probability is greater that the more distant storm produced the gigantic jet, as also suggested by the storm top and altitude estimates shown in section 3.

3. Gigantic Jet Features

[8] The event appears as a collimated, slightly bent jet with a forked top. However, in both images, there are discernable dim branches extending upward half the height of the main channel (Figure 2). The branches look similar in the images from both cameras so that image noise patterns can be ruled out. The bright forked transition zone makes for a different appearance than that of blue jets, which have been observed as diverging cone shapes with gradually decreasing brightness. The gigantic jets of *Pasko et al.* [2002] and *Su et al.* [2003] show a long-lasting, relatively bright transition zone from which upward branches emerge. This similarity is the reason we believe this jet is a gigantic jet instead of a large blue jet as in the work of *Wescott et al.* [2001].

[9] No lower side streamers as in the work of *Pasko et al.* [2002] or *Wescott et al.* [2001] are visible. The lower tendrils of the recorded sprites (known to appear typically in only a few normal video frames) provided a reference in the assessment of brightness of the features in the 4-s accumulated frames. While the bottom gigantic jet channel appeared of similar brightness as the brightest of tendrils of the subsequent sprites, the wispy top part appears much less luminous. Even if we assume a duration for the upper branched part of one normal video frame (~20 ms) with a longer-lasting lower channel, we must conclude that the brightness of the upper branches must have been less than most sprites. This marks a difference with the gigantic jets studied by *Pasko et al.* [2002] and *Su et al.* [2003], where the top parts appear as bright as sprites.

[10] The estimated gigantic jet altitudes depend on the choice of distance (Figures 3 and 4 and Table 1). The triangulation showed that the gigantic jet somewhat more likely occurred over the far storm. The great circle path runs over both the secondary storm top and part of the downwind anvil that produced National Lightning Detection Network (NLDN) detected lightning discharges within the time interval of the gigantic jet video image, at approximately 305 and 348 km from the camera baseline. Heights calculated using these distances mark lower and upper bounds for the gigantic jet features. Also listed in Table 1 are the heights if the close storm at 233 km had produced the gigantic jet. These are considerably lower than previously documented cases [*Pasko et al.*, 2002; *Su et al.*, 2003; *Hsu et al.*, 2004], so assuming that the present gigantic jet reached similar altitudes of 70–90 km, the far storm must have been the more likely producer of the event. The channel width calculated from these distances cannot be reliably calculated since it barely exceeds the pixel width of stars, which have an infinitely small angular size in reality. The wider fork feature varies from 3 to 5 km according to the choice of near or far storm, respectively.

4. Electromagnetic Signals

[11] The NLDN detected the storm's cloud-to-ground discharges. During the 0423:47–0423:52 UTC time period bounding the gigantic jet image, only a few flashes were reported close to the direction of the gigantic jet. We also use the Duke University extremely low/ultralow frequency (ELF/ULF, 3–3000 Hz) radio sensor in North Carolina [*Cummer and Lyons*, 2004] to detect any lightning sferics from the direction of the jet. Figure 5 shows the continuously

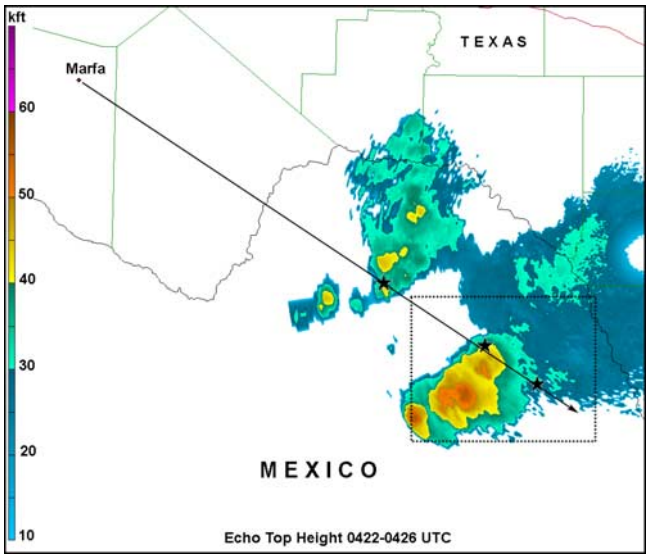

Figure 4. Radar echo top heights at 0422–0426 UTC (smoothed). Box and arrow are as in Figure 3. Stars indicate areas along the gigantic jet line of sight with lightning flashes during the gigantic jet time frame. The maximum top reaches about 17 km, while the highest tops under the gigantic jet azimuth are around 14 km.

Table 1. Altitudes Over the Spherical Surface of the Globe Corresponding to Possible Positions of the Gigantic Jet[a]

Elevation	Altitude, km at Distance of 233 km	at Distance of 305 km	at Distance of 348 km
Top of branches ~11°	51	69	80
Top of fork 7.75°	37	51	59
Width of fork ~46′	3.1	4.1	4.7

[a]Not corrected for atmospheric refraction of light.

measured azimuthal magnetic field at Duke University during the 5-s jet window. The system detected three clear sferics (shown as A, B, and C in Figure 3) that originated in the direction of the jet, all of which are positive polarity. Signal C is from a flash classified as two simultaneous −CG strokes by the NLDN that occurred at 0423:50.945 UTC in the anvil east of the far storm core. This waveform is unambiguously positive, which suggests that the NLDN must have had difficulty classifying this unusual discharge signal. The other two were not detected by NLDN. All three of these pulses were produced by impulsive charge moment changes between 40 and 50 coulomb times kilometers (C km). Signal B also contains a larger but slower charge moment change of an additional 450 C km over 70-ms duration. This waveform is not unlike a sprite-producing +CG, which can contain a modest return stroke and significant continuing current. These magnetic field recordings are continuous, not triggered, and therefore signals from all lightning and related processes are part of this analysis. Whether any of these signals were produced by or in association with the gigantic jet cannot be determined, given the uncertainty of the image time. However, even the largest total charge moment change (520 C km) is less than the charge moment changes possibly associated with jets reported by *Su et al.* [2003] (1000–2000 C km).

5. Thunderstorm Analysis

[12] Next Generation Weather Radar (NEXRAD) radar data from Laughlin Air Force Base in Texas were examined to understand the characteristics and organization of convection which occurred in the Big Bend region of Texas and the Serranías del Burro region of northeastern Mexico. GOES geostationary satellite and radar imagery initially revealed two distinct areas of convection (see Figure 3) that shared one large anvil canopy downstream at their northeast side. The western storm was a linearly organized multicell. The southern end of this line was composed of rapidly evolving multicellular convective elements. No cells within the line showed any supercellular characteristics. The cells over which the great circle path passes developed at the southern end of the line about 30 min before the gigantic jet and were decreasing in intensity shortly after the event. These cells reached echo tops of approximately 14 km (Figure 4), while values of 40 *dBZ* (decibels *Z*) (moderate precipitation intensity) in the reflectivity column were estimated to reach 10–12 km.

[13] The storm more likely associated with the gigantic jet was a "high-precipitation" (HP) supercell [*Moller et al.*, 1994]. This cell was part of a NNE-SSW oriented broken line of storms. Although we have no reports of severe weather from this sparsely populated area, large hail is common to this type of storm, and even a tornado could have occurred [*Edwards*, 2006]. The NEXRAD Level III hail indicator marked both this storm and the closer storm as hail producers.

[14] The embryonic cell that eventually developed into the storm of interest formed at about 0157 UTC and split

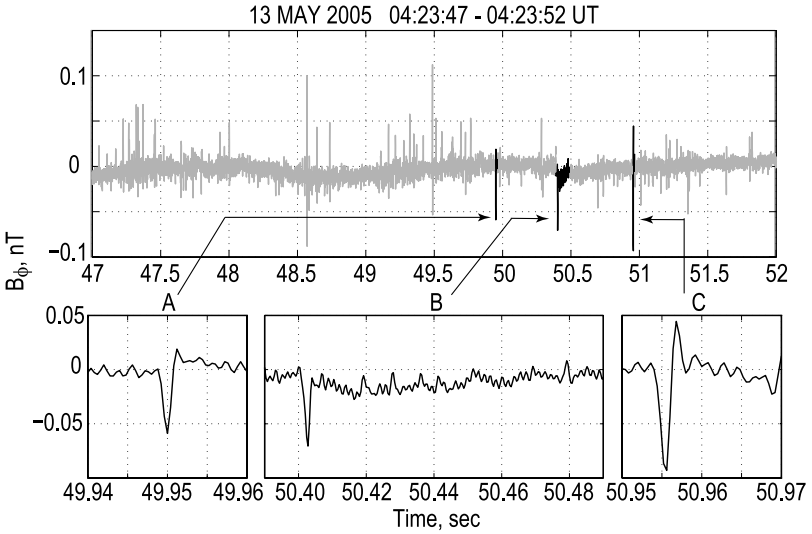

Figure 5. (top) Measured ELF/ULF magnetic field during the 5-s jet window. The three biggest sferics (A, B, and C) from the geographic direction of the gigantic jet are highlighted as dark. All other significant signals in the gray background are from other geographic directions. (bottom) Waveform of these three pulses, all of which are produced by impulsive charge moment changes between 40 and 50 C km. Signal B is also followed by a slow current containing an additional charge moment change of 450 C km over 70 ms.

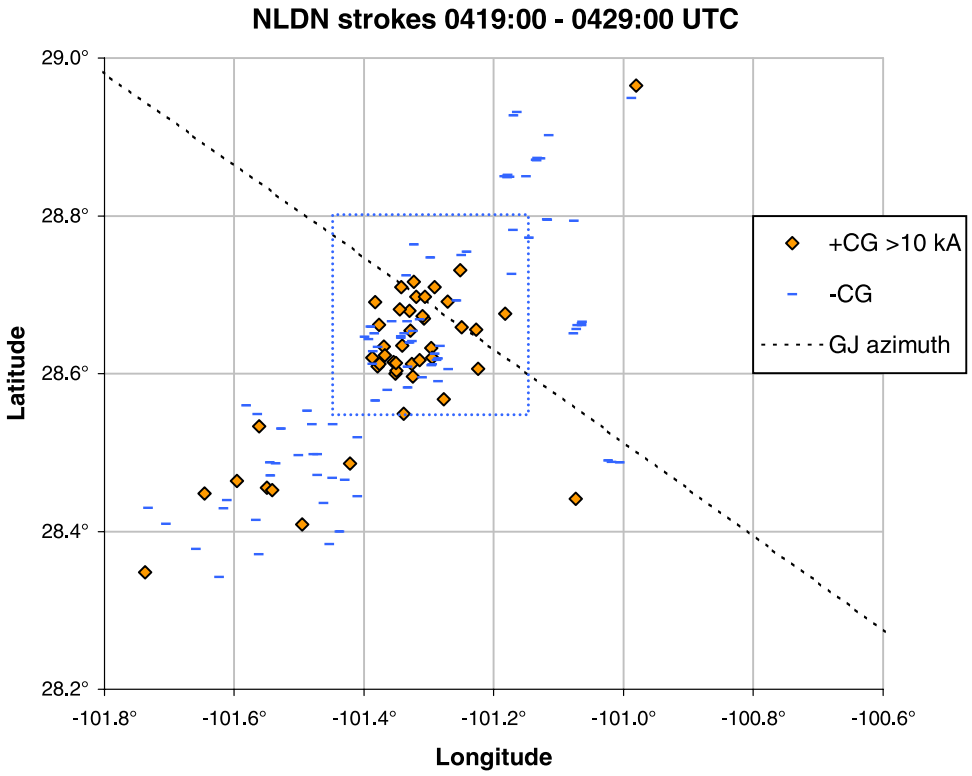

Figure 6. Plot of +CG and −CG strokes between 0419 and 0429 UTC. This domain is shown as a box in Figures 3 and 4. The portion over which the gigantic jet has occurred was dominated by +CGs, with −CGs occurring in the downwind anvil, suggesting a possible inverted polarity charge structure. The box marks the region used for the cumulative flash rate graph of Figure 7.

into left and right members at 0241 UTC. The right member became dominant and evolved into a HP supercell that displayed an inflow notch or hook echo radar reflectivity structure from 0325 to 0450 UTC. This notch was widest around the time of the gigantic jet and started to occlude 7 min later. Analysis of Level II reflectivity data using three-dimensional display software revealed that the maximum supercell echo top at the time of the gigantic jet was at least 17 km and possibly up to 20 km (uncertainty caused by the radar beam width), with a well-defined overshooting top penetrating the local tropopause of 12.7 km. However, the great circle path from the cameras near Marfa to the gigantic jet did not pass over the highest top and mesocyclone (rotating updraft) of the supercell but rather over the forward flank downdraft region [*Lemon and Doswell*, 1979] about 30 km to the northeast. This part of the storm also displayed very strong precipitation (>55 *dBZ* echoes) but had lower echo top heights of around 14 km. It may have been a separate convective cell, as there is a distinct separation in high reflectivities between the supercell main core and this area, and the echo tops indicate two maxima. In this supercell cluster, reflectivities of 40 *dBZ* were found at very high levels of 12–15 km.

[15] Infrared satellite images indicated the vigor of the supercell complex as the anvil of this storm was rapidly expanding against the direction of the upper winds. This may have caused convergence of the upper charge which may have been an additional factor in the initiation of the gigantic jet, although there is no certainty as to where exactly over the forward flank downdraft region the gigantic jet occurred. The largest possible distance of the gigantic jet (Figure 4) is associated with a part of the anvil away from precipitation at the surface, with radar echo tops of 10–12 km and reflectivities aloft of less than 25 *dBZ*. Almost no lightning activity was present in this part of the storm, except a sequence of a few NLDN-detected strokes occurring during the time window of the event, seen in Figure 6 near −101°, as described earlier.

[16] The storms formed in an environment sampled at 0000 UTC by the Del Rio, Texas, sounding, believed to be still roughly representative of the conditions near 0400 UTC on 13 May. Strong conditional instability with convective available potential energy values about 3000 J kg^{-1} and a lifted index of −9 may have actually been enhanced by higher dew point temperatures advecting into the Rio Grande Valley after 0000 UTC as indicated by the NOAA/National Centers for Environmental Prediction Rapid Update Cycle (version II) mesoscale model analysis for 0400 UTC. The HP supercell's overshooting top penetrating the tropopause by more than 4 km suggests very intense updrafts. The vertical wind profile was marginally favorable for supercell storms. Winds between 800 and 700 hPa levels displayed veering with height from southeast to southwest, while vertical wind shear and storm-relative flow were just at the lower margins common for supercells. The nearly stationary movement of the line of cells at the east side of the Serranías del Burro mountain range seems to indicate

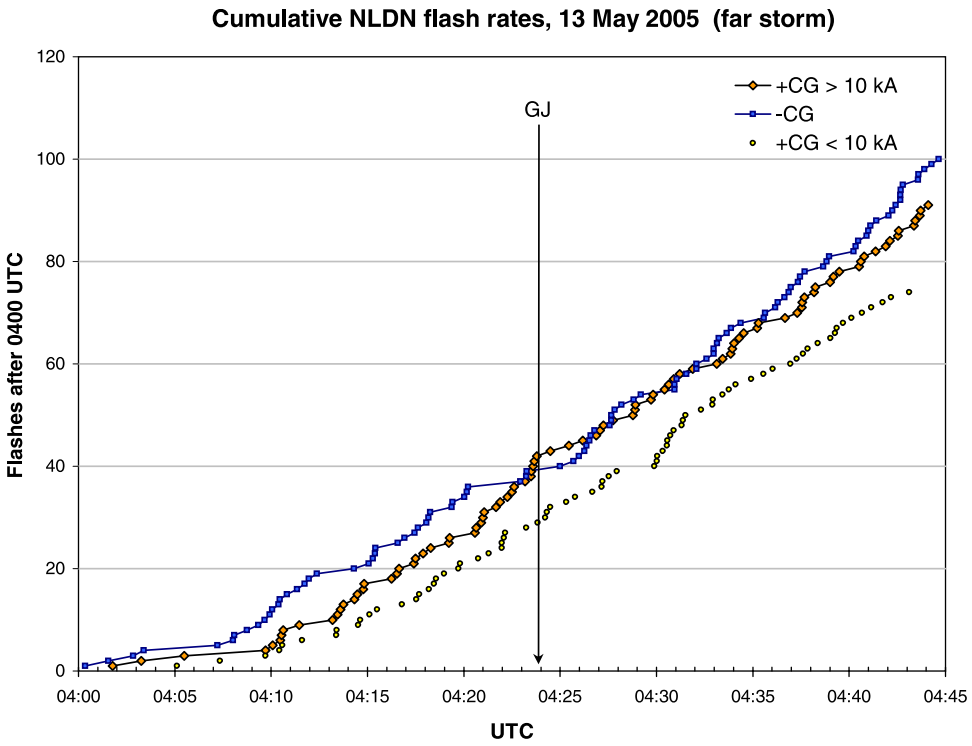

Figure 7. Cumulative flash rates (by NLDN) for the portion of the far storm near the direction of the gigantic jet, indicated by a box in Figure 4. A rapid rise of +CG flash rates occurs before the gigantic jet, during a 5-min period of almost absent −CG flashes, followed by a relative pause in +CG rates. NLDN +CG flashes <10 kA are considered a subset of intracloud flashes.

that orographic lift associated with southeasterly low-level flow was triggering the convection.

6. Lightning Activity

[17] We segregated +CG strokes with peak currents less than 10 kA, which are likely to be intracloud flashes falsely identified by the NLDN system [*Cummins et al.*, 1998]. Series of strokes occurring within 10 km and 1 s from each other were grouped as flashes.

[18] The HP supercell did not exhibit the highest cloud-to-ground flash rates of the storm cells in the region on this night. At the time of the gigantic jet, the HP supercell exhibited a low density of negative and positive CG flashes throughout the main core/mesocyclone region near 28.4°N and 101.45°W: only 26 −CGs and 8 +CGs during the period of 0419–0429 UTC (see lightning plots, Figure 6). Just 5 min prior to this period, −CG flash rates increased temporarily together with the intensification of rear flank downdraft reflectivites and widening of the inflow notch. The highest −CG flash rates occurred around 0433 and 0441 UTC.

[19] A separate more concentrated cluster of CG flashes occurred northeast of the main core/mesocyclone region in the forward flank downdraft over which the gigantic jet azimuth passes. This portion of the storm was dominated by positive CGs: 28 +CG flashes and 22 −CG flashes occurred during the above 10-min period (19 excluded +CGs had peak currents less than 10 kA), and only 11% of the peak currents of both polarities were over 20 kA. Farther northeast, around an extension of weaker precipitation, −CG strokes occurred in similar densities as in the main core region.

[20] In the part of the far storm over which the gigantic jet direction ran (depicted by a box in Figure 6), positive flash rates increased to a small "jump" of one flash every 5 s during the 20-s period before the gigantic jet (see the cumulative flash rate graph in Figure 7). A relative lull of more than 1.5 min followed, with only +CGs at 0424:30 and 0425:27 UTC, after which previous flash rates (2–3 min^{-1}) were regained. Negative CG flashes almost ceased during a long period (0420:13–0425:00 UTC), while positive flashes occurred frequently: 4 −CG flashes to 17 +CG flashes. Such a sequence appeared only once to this extent.

[21] Note that the chance of NLDN falsely categorizing intracloud (IC) flashes as CGs decreases gradually with increasing peak current, especially for +CG flashes. Several flashes that made up the jump were classified by NLDN as +CG of 12–16 kA and might have been IC. For >15 kA +CGs, rates did not change around the time of the gigantic jet (1 min^{-1}), while for weak +CGs <10 kA (most likely intracloud flashes), a small activity jump occurred 2 min before the gigantic jet.

[22] Following the method used by *Wescott at al.* [1998], an energy estimation can be obtained. While four +CG flashes are normally expected to occur during the 1.5-min lull, on the basis of previous average rates of 2.5 flashes per minute, only two occurred. The two missing +CG flashes would have had relatively low peak currents and a single stroke, so we assume that the ones in this storm are comparable in energy to normal −CG first strokes [*Cooray*,

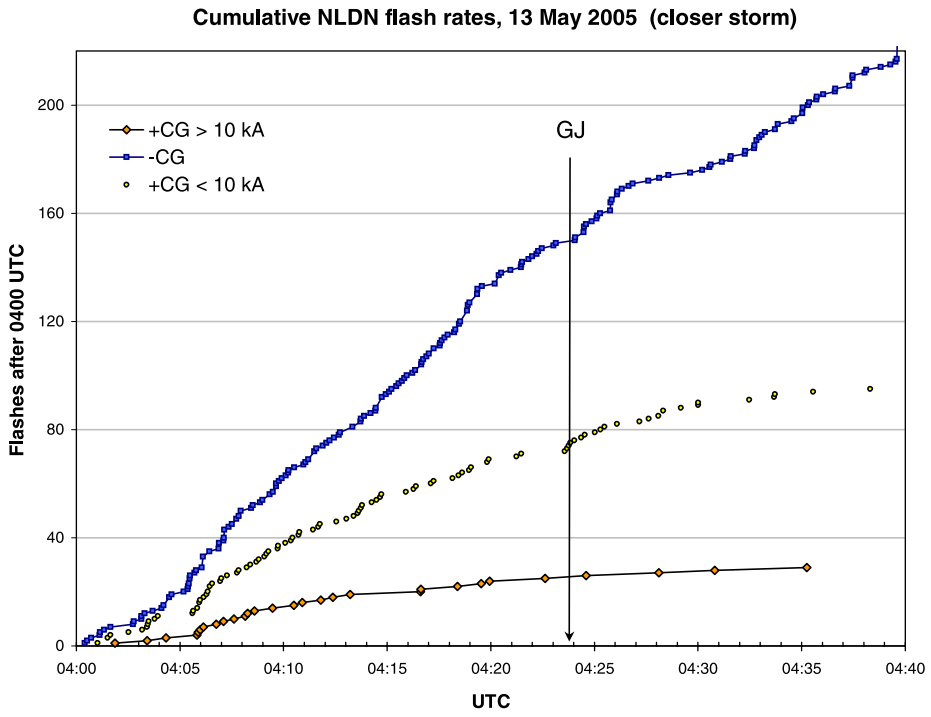

Figure 8. Cumulative flash rates (by NLDN) for the portion of the close storm near the direction of the gigantic jet. This storm produced about six −CG flashes per minute, with low +CG flash rates. Just before the time of the gigantic jet, a lull of −CG flashes occurred, with NLDN +CG <10 kA (intracloud flashes) starting to become active just before the time of occurrence of the gigantic jet (GJ), after an absence of 2 min.

1997]. This equates to an energy deficit of about 1.25×10^9 J that we suggest could be attributed to the gigantic jet. If we consider instead the four flashes per minute occurring during the few minutes before the gigantic jet, we arrive at twice the amount of energy, although the storm did not regain such flash rates.

[23] The same flash rate analysis was performed for the closer candidate storm, which was dominated by −CG activity. Figure 8 shows the cumulative flash rates for the southern cells of the linear multicell storm over which the gigantic jet path ran. It shows −CG flash rates of on average 6 min^{-1}. A short lull of about 45 s in −CG rates occurs before the time of the gigantic jet. Shortly before the gigantic jet, four weak NLDN +CGs, likely intracloud flashes, started occurring with a rate of one every 5 s, after a lull of 2 min. These rates slowed gradually after the event.

7. Sprites

[24] Thirty sprites were recorded from this storm, the first (0454 UTC) occurring 28 min after the gigantic jet with the last at 0820 UTC. The more frequent sprite rates were recorded after the two convective regions of the storm system coagulated, (forming a mostly parallel stratiform multichannel seismic profile [*Parker and Johnson*, 2000]) and developed a substantial stratiform precipitation region such as described by *Lyons et al.* [2003a]. Many sprites were quite bright and were associated with large impulse charge moment change values [*Cummer and Lyons*, 2004]. The 0606 UTC sprite parent +CG produced an exceptionally large value of 1908 C km. Imagery showed a group of bright columniform elements with long tendrils. Most sprites occurred a few tens of kilometers northeast of the cross section of the earlier gigantic jet azimuth and the far storm.

8. Discussion and Conclusions

[25] A gigantic jet occurred just east of the Serranías del Burro mountain range in northern Mexico. It is the first recorded over continental North America. At 28.7°N, this gigantic jet is the most distant from the equator documented so far. The event did not occur over sea (it occurred 440 km inland), which *Su et al.* [2003] previously speculated to be an important factor. One other gigantic jet [*Hsu et al.*, 2004] also occurred over land (but perhaps it also occurred in a maritime tropical air mass).

[26] A bright transition zone and dim upward branches correspond with the previously observed morphology of gigantic jets rather than blue jets, although we could not confirm upward propagation speed, color, and an accurate location of the event. We made the assumption that this gigantic jet reached similar altitudes as previously observed, thus placing it above the far storm with a top height of 69–80 km, consistent with those of *Pasko et al.* [2002] and *Su et al.* [2003]. The dimness of the upper part leads us speculate that this jet did not complete the electrical pathway to the ionosphere, lacking a return current as indicated by *Pasko et al.* [2002] and *Su et al.* [2003] as a rebrightening after the full height has been reached. This

may perhaps explain the weaker or absent ULF/ELF signal compared to the positive findings of *Pasko et al.* [2002] and *Su et al.* [2003], whose images also showed much brighter top parts.

[27] Our case shows that an exceptionally high thunderstorm cloud top directly beneath the gigantic jet is not the only determining factor for producing this phenomenon nor is the presence of a mesocyclonic updraft. Assuming the far storm system as the producing system, the gigantic jet occurred 30 km downwind (northeast) of a supercell core, from lower tops, where NLDN-detected lightning activity was predominantly positive at rates of 4 min^{-1} during the minutes before the gigantic jet. Although supercell charge configurations can be complex and are currently subject to intense study [e.g., *Stolzenburg et al.*, 1998; *Wiens et al.*, 2005; *Rust et al.*, 2005], the observed pattern of lightning may be indicative of an inverted polarity tripole charge configuration [*Rust and MacGorman*, 2002] with a main positive charge in the midlevel mixed-phase temperature region and significant negative charge in the anvil, away from the main core. Predominantly positive lightning activity is rare for normal thunderstorms but fairly common to supercells over the Great Plains of the United States [*Carey et al.*, 2003]. Despite having a view covering this area, more than 10 years of TLE observations from Colorado have not yielded any video observations of blue jets and gigantic jets.

[28] The vigor of convection in the far storm system can also be illustrated by comparing observed vertical reflectivity profiles to the climatology of *Zipser and Lutz* [1994]. With our storm displaying 40 *dBZ* echoes reaching into altitudes of 12–15 km, this reflectivity column is 3–6 km higher than the average for midlatitude continental thunderstorms. The anvil containing the farthest candidate position displays only reflectivities below 25 *dBZ*. Interestingly, in tropical continental and oceanic storms the 40 *dBZ* reflectivity column typically does not reach higher than 6 km, with oceanic storms exhibiting the weakest storm tops of less than 15 *dBZ* at altitudes beyond 9 km, due to weaker updrafts.

[29] If the closer linear multicell storm system with echo tops of about 14 km produced the event, the branches would extend to 51 km and the fork-shaped end of the bright channel to 37 km altitude. Predominantly negative flash rates of 6 min^{-1} were present (total rates more frequent than in the other candidate storm), and the cells were only 30 min old at the time of the event. The 40 *dBZ* column is less tall than that of the other candidate storm, 10–12 km, but is still much taller than for the average tropical storm of *Zipser and Lutz* [1994]. It is slightly above the average for midlatitude continental storms. Contrary to *Wescott et al.*'s [1998] observations, negative flash rates showed a lull before and during the event, while only NLDN-detected intracloud discharge rates showed a short increase just before the event.

[30] The far storm, however, displayed a rapid rise in cloud-to-ground lightning activity, followed by a lull that occurred around the time of the event, similar to the blue jet and starter events described by *Wescott* [1996] and *Wescott et al.* [1998]. In our case, this concerned positive flash rates (in the temporary absence of negative flashes), compared to the *Wescott et al.* [1998] case's negative flash rates. This is consistent with the different CG polarity dominance in the storms. There is a remarkable difference in the timescale, partly caused by the much lower flash rates in our storm (2.5–4 min^{-1}) compared to their storm (30 min^{-1}): about 1.5 min from start of the increase to the end of the lull, compared to a few seconds in the analysis of *Wescott et al.* [1998]. From our calculation we find a 2–4 times larger energy deficit than for *Wescott*'s *et al.* [1998] blue jets, or about $1.25–2.5 \times 10^9$ J using CG flash energy estimates by *Cooray* [1997]. Note that it is currently unknown how common such "rise-and-lull" flash rate features are and how often they are accompanied by jet-like TLE.

[31] If the association of the gigantic jet with the far storm is correct, it, together with *Wescott*'s *et al.* [1998] results, supports the thinking that (relative) removal of lower charge by numerous CG flashes may trigger jet events from the upper charge reservoir if a sufficiently high amount of charge has accumulated there. Besides this, *Tong et al.* [2005] found that their model preferred to initiate an upward discharge if a large vertical charge separation (one at 7 km and the other at 15 km) was used, which may also fit with our flash rate observations and the elevated charge hypothesis of *MacGorman et al.* [1989].

[32] *Pasko et al.* [1996] and *Pasko and George* [2002] simulated jets using the classic positive over negative charge dipole configuration from which they removed the lower negative charge. Extremely low frequency (ELF) signals in the work of *Pasko et al.* [2002] and *Su et al.* [2003], however, have suggested upward motion of negative charge. Our lightning observations also hint at an inverted-polarity charge configuration with an upper negative charge center. We therefore suggest reconsidering the negative streamer option for some of the jet phenomena (as modeled by *Sukhorukov et al.* [1996]) growing out of inverted polarity storms. The observed transition zone and the occurrence or absence of a return current appear equally worthy of modeling efforts.

[33] **Acknowledgments.** This work was funded in part by NSF grants ATM-0221512 and ATM-0221968 and by the EU Research Training Network "Coupling of Atmospheric Layers" (CAL), sponsored by the FP5 program under contract HPRN-CT-2002-00216. We wish to thank Bruce Lee and Cathy Finley for their helpful insights into the evolution of the convective structures in this case.

References

Boccippio, D. J., E. R. Williams, W. A. Lyons, I. Baker, and R. Boldi (1995), Sprites, ELF transients and positive ground strokes, *Science*, *269*, 1088–1091, doi:10.1126/science.269.5227.1088.

Carey, L. D., S. A. Rutledge, and W. A. Peterson (2003), The relationship between severe storm reports and cloud-to-ground lightning polarity in the contiguous United States from 1989 to 1998, *Mon. Weather Rev.*, *131*, 1211–1228, doi:10.1175/1520-0493 (2003)131<1211:TRBSSR>2.0.CO;2.

Cooray, V. (1997), Energy dissipation in lightning flashes, *J. Geophys. Res.*, *102*(D17), 21,401–21,410.

Cummer, S. A., and W. A. Lyons (2004), Lightning charge moment changes in U. S. High Plains thunderstorms, *Geophys. Res. Lett.*, *31*, L05114, doi:10.1029/2003GL019043.

Cummins, K. L., M. J. Murphy, E. A. Bardo, W. L. Hiscox, R. B. Pyle, and A. E. Pifer (1998), A combined TOA/MDF technology upgrade of the U. S. National Lightning Detection Network, *J. Geophys. Res.*, *103*(D8), 9035–9044.

Edwards, R. (2006), Supercells of the Serranias del Burro (Mexico), paper presented at 23rd Conference on Severe Local Storms, Am. Meteorol. Soc., St. Louis, Mo.

Heavner, M. J. (2000), Optical spectroscopic observations of sprites, blue jets, and elves: Inferred microphysical processes and their macrophysical implications, Ph.D. thesis, Univ. of Alaska Fairbanks, Fairbanks.

Hsu, R., et al. (2004), Transient luminous jets recorded in the Taiwan 2004 TLE campaign, *Eos Trans. AGU*, *85*(47), Fall Meet. Suppl., Abstract AE31A-0151.

Lemon, L. R., and C. A. Doswell III (1979), Severe thunderstorm evolution and mesocyclone structure as related to tornadogenesis, *Mon. Weather Rev.*, *107*, 1184–1197, doi:10.1175/1520-0493 (1979)107<1184:STEAMS>2.0.CO;2.

Lyons, W. A., T. E. Nelson, E. R. Williams, S. A. Cummer, and M. A. Stanley (2003a), Characteristics of sprite-producing positive cloud-to-ground lightning during the 19 July STEPS mesoscale convective systems, *Mon. Weather Rev.*, *131*, 2417–2427, doi:10.1175/1520-0493 (2003)131<2417:COSPCL>2.0.CO;2.

Lyons, W. A., T. E. Nelson, R. A. Armstrong, V. P. Pasko, and M. A. Stanley (2003b), Upward electrical discharges from thunderstorm tops, *Bull. Am. Meteorol. Soc.*, *84*, 445–454, doi:10.1175/BAMS-84-4-445.

MacGorman, D. R., D. W. Burgess, V. Mazur, W. D. Rust, W. L. Taylor, and B. C. Johnson (1989), Lightning rates relative to tornadic storm evolution on 22 May 1981, *J. Atmos. Sci.*, *46*(2), 221–251, doi:10.1175/1520-0469 (1989)046<0221:LRRTTS>2.0.CO;2.

Marshall, R. A., and U. S. Inan (2007), Possible direct cloud-to-ionosphere current evidenced by sprite-initiated secondary TLEs, *Geophys. Res. Lett.*, *34*, L05806, doi:10.1029/2006GL028511.

Moller, A. R., C. A. Doswell III, M. P. Foster, and G. R. Woodall (1994), The operational recognition of supercell thunderstorm environments and storm structures, *Weather Forecasting*, *9*(3), 327–347, doi:10.1175/1520-0434 (1994)009<0327:TOROST>2.0.CO;2.

Parker, M. D., and R. H. Johnson (2000), Organizational modes of midlatitude mesoscale convective systems, *Mon. Weather Rev.*, *128*, 3413–3436, doi:10.1175/1520-0493 (2001)129<3413:OMOMMC>2.0.CO;2.

Pasko, V. P., and J. J. George (2002), Three-dimensional modeling of blue jet and blue starters, *J. Geophys. Res.*, *107*(A12), 1458, doi:10.1029/2002JA009473.

Pasko, V. P., U. S. Inan, and T. F. Bell (1996), Blue jets produced by quasi-electrostatic pre-discharge thundercloud fields, *Geophys. Res. Lett.*, *23*(3), 301–304.

Pasko, V. P., M. A. Stanley, J. D. Mathews, U. S. Inan, and T. G. Wood (2002), Electrical discharge from a thundercloud top to the lower ionosphere, *Nature*, *416*, 152–154, doi:10.1038/416152.

Rust, W. D., and D. R. MacGorman (2002), Possibly inverted-polarity electrical structures in thunderstorms during STEPS, *Geophys. Res. Lett.*, *29*(12), 1571, doi:10.1029/2001GL014303.

Rust, W. D., D. R. MacGorman, E. C. Bruning, S. A. Weiss, P. R. Krehbiel, R. J. Thomas, W. Rison, T. Hamlin, and J. Harlin (2005), Inverted-polarity electrical structures in thunderstorms in the Severe Thunderstorm Electrification and Precipitation Study (STEPS), *Atmos. Res.*, *76*, 247–271, doi:10.1016/j.atmosres.2004.11.029.

Sentman, D. D., E. M. Wescott, D. L. Osborne, D. L. Hampton, and M. J. Heavner (1995), Preliminary results from the Sprites 94 aircraft campaign: 1. Red sprites, *Geophys. Res. Lett.*, *22*(10), 1205–1208.

Stolzenburg, M., W. D. Rust, and T. C. Marshall (1998), Electrical structure in thunderstorm convective regions: . Synthesis, *J. Geophys. Res.*, *103*(D12), 14,097–14,108.

Su, H. T., et al. (2003), Gigantic jets between a thundercloud and the ionosphere, *Nature*, *423*, 974–976, doi:10.1038/nature01759.

Sukhorukov, A. I., E. V. Mishin, P. Stubbe, and M. J. Rycroft (1996), On blue jet dynamics, *Geophys. Res. Lett.*, *23*(13), 1625–1628.

Takahashi, Y., R. Miyasato, T. Adachi, K. Adachi, M. Sera, A. Uchida, and H. Fukunishi (2003), Activities of sprites and elves in the winter season, Japan, *J. Atmos. Sol. Terr. Phys.*, *65*(5), 551–560, doi:10.1016/S1364-6826 (02)00330-9.

Tong, L., K. Nanbu, and H. Fukinishi (2005), Randomly stepped model for upward electrical discharge from top of thundercloud, *J. Phys. Soc. Jpn.*, *74*(4), 1093–1095, doi:10.1143/JPSJ.74.1093.

Tsai, L., et al. (2006), Taiwan TLE campaign, *Eos Trans. AGU*, *87*(52), Fall Meet. Suppl., Abstract AE41A-02.

Wescott, E. M., Jr. (1996), Blue starters: Brief upward discharges from an intense Arkansas thunderstorm, *Geophys. Res. Lett.*, *23*(16), 2153–2156.

Wescott, E. M., D. Sentman, D. Osborne, D. Hampton, and M. Heavner (1995), Preliminary results from the Sprites94 aircraft campaign: 2. Blue jets, *Geophys. Res. Lett.*, *22*(10), 1209–1212.

Wescott, E. M., D. D. Sentman, M. J. Heavner, D. L. Hampton, and O. H. Vaughan Jr. (1998), Blue Jets: Their relationship to lightning and very large hailfall, and physical mechanisms for their production, *J. Atmos. Sol. Terr. Phys.*, *60*(7–9), 713–714, doi:10.1016/S1364-6826 (98)00018-2.

Wescott, E. M., D. D. Sentman, H. C. Stenbaek-Nielsen, P. Huet, M. J. Heavner, and D. R. Moudry (2001), New evidence for the brightness and ionization of blue starters and blue jets, *J. Geophys. Res.*, *106*(A10), 21,549–21,554.

Wiens, K. C., S. A. Rutledge, and S. A. Tessendorf (2005), The 29 June 2000 supercell observed during STEPS. part II: Lightning and charge structure, *J. Atmos. Sci.*, *62*, 4151–4177, doi:10.1175/JAS3615.1.

Zipser, E. J., and K. Lutz (1994), The vertical profile of radar reflectivity of convective cells: A strong indicator of storm intensity and lightning probability?, *Mon. Weather Rev.*, *122*, 1751–1759, doi:10.1175/1520-0493 (1994)122<1751:TVPORR>2.0.CO;2.

J. Bunnell, Benbrook, TX 76132, USA.

S. A. Cummer and J. Li, Electrical and Computer Engineering Department, Duke University, Hudson Hall Room 130, Box 90291, Durham, NC 27708, USA.

W. A. Lyons and T. E. Nelson, FMA Research, Unit X-9, 46050 Weld County Road 13, Fort Collins, CO 80524, USA.

O. A. van der Velde, Laboratoire d'Aérologie, CNRS, Université de Toulouse, 14 Avenue Edouard Belin, Toulouse F-31400, France. (vdvo@aero.obs-mip.fr)

8 Conclusions et perspectives

Ce travail avait pour but d'analyser les conditions de production des TLEs, en particulier celles des sprites, d'une part en caractérisant les orages qui les produisent et d'autre part en analysant l'activité d'éclair associée à plusieurs échelles de temps et en considérant plusieurs systèmes de détection de cette activité. Le cadre de l'analyse a été le projet européen CAL et les données des campagnes d'observation associées EuroSprite au cours des étés et automnes 2003 à 2006. Ce projet permettait d'étudier pour la première fois de façon systématique la production de TLEs par les orages en Europe et d'en analyser les caractéristiques. C'est donc dans les objectifs scientifiques du WP 5 de CAL que s'inscrivaient ceux de mon travail de thèse. Il s'agissait de déterminer la nature et les structures d'orages pouvant produire des TLEs en Europe afin de contribuer à l'évaluation des taux de production de ces phénomènes à l'échelle globale. Un intérêt de cette caractérisation était aussi l'acquisition d'une expérience dans la prévision de ces phénomènes pour les futures observations spatiales en déterminant les outils les mieux adaptés à cette prévision. Afin de contribuer à la compréhension des processus qui conduisent à la production des TLEs, un accent particulier allait être mis sur l'analyse fine de l'activité d'éclair associée aux sprites et notamment en développant particulièrement celle de l'activité intranuage à l'échelle de temps de l'éclair. Enfin, un aspect rarement abordé dans les études antérieures sur les sprites dans d'autres régions a été ici particulièrement développé, il s'agit des corrélations entre plusieurs paramètres de leur morphologie et les paramètres caractéristiques des éclairs associés. Les données sur lesquelles pouvaient s'appuyer mes études étaient tout d'abord les images radar issues des réseaux opérationnels de radars météorologiques en France (ARAMIS) et dans le Nord de l'Espagne (MeteoCat) sous la forme de champ de réflectivité. J'ai pu ensuite utiliser les données canal infrarouge du satellite Météosat 1ère et 2ème génération pour les altitudes des sommets de nuage. Pour tous les cas d'observation j'ai pu disposer des données de détection de foudre (éclairs nuage-sol) issues des réseaux nationaux français (Météorage) et espagnol (SLDN et LINET). Dans certains cas, j'ai pu avoir les données de l'activité d'éclair intranuage fournie par des systèmes SAFIR comme celui du Sud-Est opérationnel en 2003, celui du Centre d'Essai des Landes (CEL) ou celui du service météorologique catalan (MeteoCat), tout deux opérationnels en permanence mais avec des capacités de détection locale. J'ai introduit aussi l'analyse de signaux produits par les éclairs dans la gamme VLF pour compléter l'analyse de l'activité de certains processus d'éclairs générant des sprites.

Les campagnes d'observation des étés 2003, 2005 et 2006 ont fourni un nombre important d'événements, avec 102, 65 et 123 sprites, respectivement. Les TLEs détectés sont donc des sprites et le travail d'analyse a été principalement orienté sur ces événements. Mis à part un nombre très limité de sprites vus par 2 caméras simultanément (2 au cours de ces 3 campagnes), tous ces sprites ne pouvaient être localisés précisément par rapport à l'éclair associé ou par rapport au système orageux qui en était à l'origine. Une

méthode utilisant la carte du ciel au moment de la détection du sprite a été mise au point pour déterminer sa direction pouvant être par la suite superposée à l'image radar et située par rapport aux différents éclairs ou éléments d'éclairs détectés. Deux types d'analyse ont été élaborés, l'une avec des études de cas et l'autre avec une étude globale statistique sur un grand nombre d'événements produits par 7 orages différents. Les observations ont confirmé la plupart des connaissances établies à partir des observations faites sur d'autres continents. Ainsi, les sprites observés ont été produits par des systèmes convectifs de moyenne échelle (MCS) de taille certes limitée par rapport aux systèmes de type complexe convectif méso-échelle (MCC) reconnus comme les plus efficaces pour produire des sprites. Ils ont été produits à la suite d'éclairs positifs localisés dans la partie stratiforme des orages en question et dans une période de faible activité d'éclair alors que la partie stratiforme était en pleine phase d'expansion. Les périodes de production ont été identifiées comme bien distinctes dans la vie de l'orage. Nos observations ont précisé les conditions de production de ces sprites. La comparaison entre plusieurs cas montre que le taux de production est d'autant plus important que le taux d'éclair produit par la région convective est élevé. Si le taux d'éclair global est faible dans les périodes de production des sprites, il est souvent observé plusieurs éclairs nuage-sol au moment du sprite, ce qui signifie un processus d'éclair complexe. L'analyse de l'activité intranuage montre une propagation horizontale importante dans ces cas-là, ce qui suppose que les éclairs de type "spider" peuvent être particulièrement efficaces pour la production de sprites. D'autre part, l'analyse de l'activité intranuage entre l'éclair positif qui est à l'origine du sprite et le sprite lui-même montre que la neutralisation de la charge positive nécessaire à la production d'une décharge d'altitude sous forme de sprite ne se limite pas à l'arc positif. L'analyse de la morphologie des sprites étudiés montre qu'il y a un lien entre le type de sprite et le délai après l'arc positif, dans le sens où les sprites de type colonne sont produits avec des courts délais alors que les types "carotte" sont produits avec des délais plus longs. En poussant l'analyse de la morphologie de façon plus détaillée, on voit qu'il y a également une forte corrélation entre le délai et le nombre d'éléments du sprite, et la morphologie des éléments. Nous avons pu expliquer en détail le phénomène de déplacement du sprite par rapport à l'éclair positif dans quelques cas observés dans le Nord de l'Espagne, en montrant que la propagation horizontale de l'éclair éloigne la zone déchargée dans le nuage de l'impact au sol alors que le sprite est produit plutôt au-dessus de la zone déchargée.

D'autre part, j'ai contribué à la première analyse des conditions météorologiques associées à la production d'un jet géant observé aux USA. Dans ce cas, il apparaît que la hauteur du sommet du nuage de la supercellule orageuse génératrice n'est qu'une pièce du puzzle alors que la configuration de charge et l'activité d'éclair associées doivent avoir un rôle et être explorées de façon plus exhaustive que cela a été fait jusqu'à maintenant.

Il apparaît que les observations sont la clef pour confirmer les explications théoriques sur les processus de production des sprites notamment. L'été et l'automne 2007 nous a permis de faire beaucoup plus d'observations dans la région de la France avec un certain nombre de cas de double détection et donc des possibilités de triangulation. Un gros travail d'analyse reste à faire sur ces situations là. Un certain nombre a concerné une région couverte par un système Safir pour l'activité intranuage.

Il sera nécessaire à l'avenir de considérer l'activité intranuage avec un système performant au niveau de la résolution temporelle. L'outil idéal pour cela serait le système de détection LMA (Lightning Mapping Array) avec des capacités de localisation en 3 dimensions. De même, il y a un manque de description du système orageux avec des moyens radar à exploration volumique et polarimétrique. La multiplication de caméras dans une région donnée pourra permettre de mieux couvrir des systèmes de grande échelle et de faire des localisations de sprite par triangulation. Aussi, l'utilisation d'une caméra rapide (10000 trames par seconde) permettrait d'améliorer la résolution temporelle de la connexion entre éclair et sprite. Dans le contexte des futurs projets spatiaux d'observation de ces TLEs tels que TARANIS, microsatellite préparé par le CNES ou ASIM, instrument prévu sur le module COLUMBUS de la station spatiale internationale, il est important de collecter des observations pour établir précisément les conditions de production et les techniques de prévision de ces conditions afin d'optimiser les périodes d'observation. Les mesures de champ électrique en altitude ou dans le nuage constituent également un point important pour confirmer les hypothèses faites sur les mécanismes possibles à l'origine des sprites. Enfin les modèles de nuage avec la prise en compte des phénomènes électriques pourraient également contribuer à une meilleure compréhension de l'établissement des conditions de production. Il s'agirait là de montrer les répartitions de charge dans le système nuageux au moment de la production de sprites.

Abstract

This thesis work is devoted to the analysis of meteorological data and lightning activity, in order to describe the conditions of production of sprites observed during EuroSprite campaigns, and those of one gigantic jet observed in Texas (USA). These data are issued from radar networks for thunderstorm structure and rainfall rates, from meteorological satellite for cloud top altitude, and detection systems for cloud-to-ground and intracloud lightning activity. The TLE images, obtained by high sensitivity black and white cameras, provided the time for each event, and the accurate direction thanks to a method based on the sky map. Also the the morphology, size and altitude of the events are determined from the images. The methodology included case studies and a statistical study over a large number of sprites produced by seven different storms. This work emphasized on aspects of the TLEs research little investigated so far, the detailed analysis of the lightning flash associated with the sprite and especially of its intracloud phase, the analysis of the sprite morphology and its correlations with some parameters of the associated lightning flash, and the analysis of the meteorological conditions associated with the production of a gigantic jet, of which only few have been observed worldwide.
The observed sprites were produced by mesoscale convective systems (MCS) of moderate size while the stratiform area was large and in expanding phase and the cloud-to-ground lightning flash rate had decreased. Several cloud-to-ground (CG) flashes were often observed near the moment of the sprite, and scattered over tens of kilometers, which indicates a complex lightning process. The analysis of the intracloud lightning component confirms a stronger horizontal propagation (convective-to-stratiform) compared to non-sprite producing flashes, which indicates that spider lightning can be an efficient mechanism for charge collection and the sprites can be significantly displaced relative to the parent positive CG flash location. "Column"-type sprites were produced with shorter delays than "carrot" sprites. In fact, the shorter the delay, the more elements, and their luminosity concentrates towards greater altitudes. In the case of the gigantic jet the height of the cloud top of the producing supercell storm alone is not a good explanation for its occurrence, the charge structure and the lightning activity associated must play a role.

Résumé

Ce travail de thèse est consacré à l'analyse de données météorologiques et d'activité d'éclairs afin de décrire les conditions de production de sprites observés lors des campagnes EuroSprite et d'un jet géant observé au Texas (USA). Ces données sont issues de réseaux radar pour la structure des orages et les taux précipitants, de satellites météorologiques pour l'altitude des sommets de nuage et de systèmes de détection pour les éclairs nuage-sol et intranuage. Les images des TLEs analysés, prises dans chaque cas par une seule caméra noir et blanc haute sensibilité, ont fourni la datation, la direction précise par une nouvelle méthode utilisant la carte du ciel, le type, la morphologie et la taille des événements. La méthodologie utilisée revêt deux volets avec des études de cas et une étude statistique sur un grand nombre de cas de sprites produits par 7 orages distincts. Ce travail a mis l'accent sur des aspects de la recherche sur les TLEs peu développés auparavant, l'analyse détaillée de l'éclair associé au sprite et en particulier de sa phase intranuage, l'analyse de la morphologie des sprites et de ses corrélations avec certains paramètres de l'éclair associé, et enfin l'analyse des conditions météorologiques associées à la production d'un jet géant, qui sont encore rarement observés dans le monde.

Les sprites observés ont été produits par des systèmes convectifs de moyenne échelle (MCS) de taille limitée alors que la partie stratiforme était en pleine phase d'expansion et que le taux d'éclair nuage-sol était faible. Par contre, il a été souvent observé plusieurs éclairs nuage-sol au moment du sprite, ce qui signifie un processus d'éclair complexe. L'analyse de l'activité intranuage confirme une propagation horizontale (convective-vers-stratiforme) plus développé que pour les éclairs sans sprite, ce qui montre que les éclairs de type spider peuvent être particulièrement efficaces pour la production des sprites et que les sprites peuvent être largement déplacés par rapport à l'éclair nuage-sol parent. Les sprites de type colonne sont produits avec des courts délais alors que les types "carotte" sont produits avec des délais plus longs. En fait, plus le délai est court plus le nombre d'éléments est grand et plus leur luminosité est concentrée à une altitude élevée. Dans le cas du jet géant, la hauteur du sommet du nuage de la supercellule orageuse génératrice n'est pas la seule explication possible de l'origine de la décharge, la configuration de charge et l'activité d'éclair associées doivent jouer un rôle.

AUTHOR : Oscar Arnoud VAN DER VELDE

TITLE : *Morphology of sprites and conditions of sprite and jet production in mesoscale thunderstorm systems*

LOCATION AND DATE: Toulouse, Thursday February 21st, 2008

This dissertation is devoted to the analysis of the conditions of production of transient luminous phenomena (sprites, jets, elves) in the mesosphere, which occur in response to energetic lightning discharges in thunderstorms underneath. During *EuroSprite* observation campaigns, a few hundred images of sprites have been obtained, providing information about event morphology, location and timing. Data from weather radar and satellite as well as two different types of lightning detection networks and a wide band radio receiver have been analyzed. The methodology includes case studies and a statistical study over a large number of sprites produced by seven different storms. The work focuses on the aspect of the intracloud lightning component associated with positive cloud-to-ground flashes, the link with the morphology of sprites, and the life cycle of thunderstorm systems. Additionally, a storm which produced a rare gigantic jet observed in the United States is analyzed in detail.

KEYWORDS

transient luminous events · sprites · gigantic jets · thunderstorms · lightning · mesosphere · atmospheric electricity · mesoscale convective systems

---

AUTEUR : Oscar Arnoud VAN DER VELDE

TITRE : *Morphologie de sprites et conditions de productions de sprites et de jets dans les systèmes orageux de méso-échelle*

DIRECTEUR DE THESE : Serge SOULA

LIEU ET DATE : Toulouse, jeudi 21 février 2008

RÉSUMÉ

Ce document décrit l'analyse des conditions de production de phénomènes lumineux transitoires (sprites, jets, elves) dans la mésosphère, produits en réponse à des décharges électriques énergétiques orageuses localisées au-dessous. Pendant les campagnes d'observation EuroSprite, quelques centaines d'images de sprites ont été obtenues, fournissant des informations sur la morphologie des événements, la localisation et le moment de leur production. Des données issues de radars météorologiques, de satellite météosat, de deux types de système de détection d'éclairs, et de récepteur radio large bande ont été analysées. La méthodologie inclut des études de cas et une étude statistique sur des sprites produits par différents orages. Le travail se concentre sur le rôle de la composante intranuage des éclairs nuage-sol positifs à l'origine des sprites et notamment le lien avec leur morphologie, ainsi que la relation avec le stade d'évolution des orages. Par ailleurs, un orage ayant produit un jet géant aux Etats-Unis est analysé en détail.

MOTS-CLÉS

phénomènes lumineux transitoires · sprites · jets géants · orages · éclairs · mésosphère · électricité atmosphérique · systèmes convectifs méso-échelle

---

DISCIPLINE: Physique de l'atmosphère

ADRESSE DU LABORATOIRE: Laboratoire d'Aérologie, UMR 5560 UPS/CNRS, Observatoire Midi-Pyrénées (OMP), 14 avenue Edouard Belin 31400 – Toulouse, France.